YEAR-END TECHNICAL REPORT
August 29, 2016 to September 29, 2017

Environmental Remediation Science and Technology

Date submitted:

November 3, 2017

Principal Investigator:

Leonel E. Lagos, Ph.D., PMP®

Florida International University Collaborators:

Yelena Katsenovich, Ph.D.
Ravi Gudavalli, Ph.D.
Angelique Lawrence, M.S., GISP
Vasileios Anagnostopoulos, Ph.D.
Hilary P. Emerson, Ph.D.
Mehrnoosh Mahmoudi, Ph.D.
Alberto Abarca, Graduate Research Assistant
DOE Fellows

Prepared for:

U.S. Department of Energy
Office of Environmental Management
Under Cooperative Agreement # DE-EM0000598

FIU | Applied Research Center
FLORIDA INTERNATIONAL UNIVERSITY

This document represents one (1) of four (4) reports that comprise the Year End Reports for the period of August 29, 2016 to September 28, 2017 prepared by the Applied Research Center at Florida International University for the U.S. Department of Energy Office of Environmental Management (DOE-EM) under Cooperative Agreement No. DE-EM0000598.

The complete set of FIU's Year End Reports for this reporting period includes the following documents:

Project 1: Chemical Process Alternatives for Radioactive Waste
Document number: FIU-ARC-2017-800006470-04b-255

Project 2: Environmental Remediation Science and Technology
Document number: FIU-ARC-2017-800006471-04b-254

Project 3: Waste and D&D Engineering and Technology Development
Document number: FIU-ARC-2017-800006472-04b-245

Project 4: DOE-FIU Science & Technology Workforce Development Initiative
Document number: FIU-ARC-2017-800006473-04b-253

Each document will be submitted to OSTI separately under the respective project title and document number as shown above.

TABLE OF CONTENTS

LIST OF FIGURES

LIST OF TABLES

PROJECT 2 OVERVIEW

Florida International University (FIU) is conducting applied research in collaboration with Pacific Northwest National Laboratory (PNNL), Savannah River National Laboratory (SRNL) and Savannah River Ecology Laboratory (SREL) scientists to support environmental remediation efforts at the Hanford Site and Savannah River Site (SRS), which are focused on cleanup technologies for contaminated soil and groundwater and the assessment of the fate and transport of contaminants in the environment. FIU is also teaming with scientists at Los Alamos National Laboratory (LANL) and the DOE Carlsbad Field Office (CBFO) to address potential contamination issues and update risk assessment models associated with the disposal of large quantities of defense-related, transuranic waste at the Waste Isolation Pilot Plant (WIPP). The aim of the Project 2 is to reduce the potential for contaminant mobility or toxicity in the surface and subsurface through the development and application of state-of-the-art scientific and environmental remediation technologies at DOE sites.

During FIU Performance Year 7 (2016-2017), FIU ARC worked on the following tasks:

Task 1: Remediation Research and Technical Support for the Hanford Site

Legacy waste from the development of atomic weapons at the Hanford Site has left significant radionuclide contamination in soil and groundwater. There is a need to further investigate the environmental fate of uranium and technetium under natural conditions and following remediation. For example, a significant residual mass of uranium still resides in the deep vadose zone (VZ) following release of over 200,000 kg of uranium from improper waste disposal and accidental spills (Szecsody et al. 2013).

During FIU Performance Year 7, ammonia gas and tripolyphosphate injection as a remediation strategy for uranium were investigated further with laboratory-scale experiments. Ammonia gas injection is currently being considered for uranium remediation at the pilot scale in the 200 Area of the Hanford Site. Previous work has shown that the injection of NH_3 gas to the vadose zone is a viable method to decrease uranium mobility in the contaminated subsurface via pH manipulation and co-precipitation processes (Szecsody et al. 2012a, Zhong et al. 2015). However, batch experiments focused on understanding the mechanisms leading to removal of uranium in the presence and absence of minerals and sediments as well as the mineral dissolution caused by weak base treatment. During FY 8, experiments will focus on solids characterization in order to confirm both mineral transformations and U association via adsorption and co-precipitation processes.

Pilot scale testing of tripolyphosphate injection for the formation of apatite and autunite minerals in the 300 Area subsurface was completed in 2009 (Vermeul et al. 2009). Although it was initially found to be an effective remediation technology, there was a rebound in aqueous uranium concentrations after several months. Therefore, there is a need to better understand the dissolution of autunite minerals especially through microbial pathways. Autunite and meta-autunite minerals, as $(X^m)_{2/m}[(UO_2)(PO_4)]_2 \cdot xH_2O$ where X is a monovalent or divalent cation, are an important group of uranyl minerals acting as a sink for dissolved U(VI) in soils. Even small quantities of phosphate present in groundwater can promote the formation of autunite group minerals that can persist over geologic periods (De Vivo et al. 1984).

Bacteria may dissolve uranyl-phosphate minerals in an effort to obtain phosphorous, thus liberating uranium from the solid phase. In addition to the biological activity, the presence of bicarbonate ions enhances the release of U(VI) into the aqueous phase (Gudavalli et al., 2013). Experiments in Year 7 focused on understanding of the effect of *Shewanella* cells on the biodissolution of syntetic Na-autunite minerals and microbial consortia on the dissolution of natural Ca-autunite. A subtask initiated with a PNNL during internship (DOE Fellow Alejandro Garcia) in spring of 2016 was continued. This task strives to utilize spectral induced polarization (SIP) geophysical measurements to detect the formation of microbial acitvities and biofilms based on their changes to the physical and electrical properties of the subsurface.

Four graduate students were involved in this research, including graduate research accistant, Alberto Abarca, and DOE Fellows Robert Lapierre and Alejandro Garcia, working towards their master's degrees and DOE Fellows Silvina Di Pietro and Claudia Cardona working towards their PhDs.The research was also supported by undergraduate student Sarah Solomon, working towards her bachelor degree.

Task 2. Remediation Research and Technical Support for Savannah River Site

The F/H Area Seepage Basins located in the center of SRS received approximately 1.8 billion gallons of acidic waste solutions (pH from 3.2 to 5.5) contaminated with a variety of radionuclides and dissolved metals. The acidic nature of the basin waste solutions caused the mobilization of metals and radionuclides, resulting in contaminated groundwater plumes. The primary focus of this investigation is uranium (VI), which is a key contaminant of concern in the basin's groundwater. During FIU Performance Year 7, the main objectives of this research was to identify the morphological and physico-chemical characteristics of sediments that are affected by chronic acid leaching (compared to clean background soil) and correlate the selected properties with the sorptive characteristics of the sediments for SRS contaminants of concern. The study also investigated via batch and column experiments humate substances abilities to affect the mobility of actinides in natural systems. Currently, four students are supporting this research including undergraduate research assistants DOE Fellows Alexis Smoot, Ripley Raubenolt, Awma Rana and a graduate student, Hansell Gonzalez, working towards his Ph.D.

Task 3: Surface Water Modeling of Tims Branch

The principal objective of this task is to develop an integrated hydrology/transport model as a tool to estimate flow and transport parameters and predict the spatial and temporal distribution of contaminants during extreme storm events. Results from this study are key to evaluating the effectiveness of tin(II)-based mercury treatment at the SRS site, and are also relevant to evaluating the potential of using water treatment and novel remediation technologies in other mercury-contaminated streams.

Task 5: Research and Technical Support for WIPP

FIU ARC collaborated with research scientist Donald Reed of the Actinide Chemistry and Repository Science (ACRSP) team in support of Los Alamos National Laboratory's field office located at the Carlsbad Environmental Monitoring and Research Center (CEMRC) in Carlsbad, New Mexico. The goal is to generate accurate sorption data for the actinides to minerals and under conditions relevant to the Waste Isolation Pilot Plant as previous risk assessment models are based on conservative assumptions. The project is currently supported by Fellow Frances Zengotita (B.S. Chemistry and English) who also spent ten weeks at LANL CEMRC conducting

experiments on the affect of bacteria on transport of relevant radionuclides in the WIPP. During FIU Performance Year 7, batch and mini column experiments were initiated to understand sorption of neodymium as an analog for the trivalent actinides at ionic strength from 0.1 - 5.0 M. DOE. FIU Performance Year 8 will focus on understanding ternary interactions of the trivalent and hexavalent oxidation states (Am, U, and lanthanide analogs) with relevant minerals in the presence of relevant ligands including but not limited to oxalate, EDTA, and isosaccharinic acid.

TASK 1: SEQUESTERING URANIUM AT THE HANFORD 200 AREA BY IN SITU SUBSURFACE PH MANIPULATION USING AMMONIA (NH_3) GAS

TASK 1: EXECUTIVE SUMMARY

During FIU Performance Year 7 for Subtask 1.3.1, batch experiments were finalized to understand the partitioning of uranium and dissolution of minerals following base treatment. This work is helping to understand the mechanisms controlling the fate of uranium during and after base treatment as a potential remediation technique. Silvina Di Pietro, a DOE Fellow and Ph.D. student within the chemistry department, successfully defended her original proposal and passed comprehensive exams moving her one step closer to a PhD. In addition, she earned 2nd place for her poster presentation at the Waste Management Symposia and a travel grant to participate in the Gilman Alumni Ambassador Workshop in Atlanta, GA. Throughout FY 7, three oral presentations and two poster presentations were given at conferences and one peer-reviewed publication was accepted to the Journal of Environmental Radioactivity entitled "Effect of Ammonia on Uranium Partitioning and Kaolinite Mineral Dissolution." In addition, an abstract based on this work was recently accepted for an oral presentation at the 2018 Waste Management Symposia. During FY 8, experiments will begin with a focus on solid phase characterization to understand the mineral phases forming and U association through adsorption and co-precipitation processes.

Oral Presentations between October 2016 and October 2017 (presenter is underlined):

Effects of ammonia and variable redox conditions on mineral dissolution, Silvina Di Pietro, Hilary P. Emerson, Yelena Katsenovich, and James Szecsody, ACS 253rd National Meeting, San Francisco, CA, Apr. 2, 2017.

Ammonia gas treatment for Uranium immobilization at DOE Hanford Site, Silvina Di Pietro, Hilary P. Emerson, and Yelena Katsenovich, Waste Management Symposia, Phoenix, AZ, Mar. 8, 2017 (Full paper in conference proceedings).

Removal of U(VI) in the Alkaline Conditions Created by NH_3 Gas, Claudia Cardona, Yelena Katsenovich, Jim Szecsody, Leonel Lagos, Waste Management Symposia, Phoenix, AZ, Mar. 8, 2017 (Full paper in conference proceedings).

Poster Presentations between October 2016 and October 2017 (presenter is underlined):

Subsurface Uranium Remediation via Base Treatment, Silvina Di Pietro and Hilary P. Emerson, Miami March for Science, Miami, FL, Apr. 22, 2017.

Fate of U and Mineral Dissolution upon Treatment with NaOH and NH_4OH, Silvina Di Pietro, Hilary P. Emerson, Yelena Katsenovich, Waste Management Symposia, Phoenix, AZ, Mar. 8, 2017. (2nd place poster)

This task also investigated autunite biodissolution by focusing on the bacterial strains of *Shewanella oneidensis* MR1 sp and microbial consortia isolated at PNNL. Sarah Solomon, A DOE Fellow undergraduate student presented her poster at WM symposia, "*Shewanella oneidensis*" MR1 Interaction with U(VI) in Bicarbonate Media". Alejandro Garcia, a graduate DOE Fellow students presented his poster at WM Symposia, " Laboratory analysis of the Spectral Induced Polarization response of biofilm formation within Hanford sediment."

Subtask 1.1: Sequestering Uranium at the Hanford 200 Area Vadose Zone by In Situ Subsurface pH Manipulation Using NH_3 Gas

Subtask 1.1: Introduction

Environmental remediation is of great importance to restore sites that have been heavily contaminated by nuclear waste. Uranium has been found to be one of the major pollutants of the Hanford Site 200 Area and represents a great risk to the water resources that are close to the site. Given its toxicity, long half-life (4.5×10^9 years), and high mobility in the subsurface, understanding the mechanisms of uranium migration from the DOE nuclear waste disposal sites is important to prevent further contamination and possible exposure hazard to the population of Washington State. pH manipulation via ammonia (NH_3) gas injection into the vadose zone has been shown to transform mobile uranium aqueous phases to lower solubility precipitates that are more stable in the natural environment (Szecsody et al., 2012). This type of in-situ remediation is of paramount significance since it will result in sequestration of U in the deep vadose zone conditions and prevent it from spreading to the natural water resources. This study is focusing on the stability of the relatively immobile U contained within the precipitates mimicking those created after NH_3 gas injections to the vadose zone (VZ). Specific objectives include (i) evaluation of uranium release from U-bearing precipitates via sequential extraction experiments and (ii) assessment of U precipitation/removal efficiencies from NH_3-treated synthetic pore water solutions at low Si concentrations.

The results of this study are expected to evaluate the effectiveness of the ammonia gas remediation method for the replicated environmental conditions.

Batch Experiments with Pure Minerals

Because a peer-reviewed publication is in process for this work, the full results will be attached as a separate appendix (Appendix A) of the draft. During FIU Year 7, experiments quantified partitioning of U and mineral dissolution up to 30 days in batch experiments prepared in the presence of 7.2 mM NaCl or synthetic groundwater of equivalent ionic strength with treatment via NaOH, NH_4OH, or 5% NH_3/95% N_2 gas in the presence of a suite of minerals (kaolinite, montmorillonite, illite, muscovite, calcite, or quartz) or Hanford sediments. These results show that base treatments generally result in greater U removal in the presence of synthetic groundwater although it cannot be concluded that one treatment was more effective than another. However, there is a more significant decrease in redox conditions with NH_3 gas treatment that could lead to a short term increase in U removal via reduction and precipitation. These data also show that greater U removal occurs in the presence of clays and in systems with aqueous Ca and carbonate. The greater removal in the presence of clays is likely due to mineral dissolution and secondary precipitate formation at elevated pH which may co-precipitate and coat U. The greater removal in the calcium carbonate system is likely due to co-precipitation with calcite as the pH increases and calcite solubility decreases.

Low Si/Al Experiment

Subtask 1.1: Methodology

1. Sample Preparation of U-bearing precipitates

For the purpose of this study, the pore water composition was simplified to have five major components in the solution matrix: uranium (U), bicarbonate (HCO_3), calcium (Ca^{2+}), silica (Si) and aluminum (Al). A low concentration of U (VI) (2 mg/L) and two different bicarbonate concentrations (3 mM and 50 mM) were tested. Three different calcium concentrations (0, 5 and 10 mM) were selected given past observation of 15 mM of Ca in 5% NH_3 treated Hanford sediments (Szecsody et al. 2012). The silica concentration used was 50 mM based on past experiments where concentrations reached up to 100 mM in 10% NH_3 treated sediments (Zhong et al, 2015). An aluminum concentration of 5 mM was tested based also on previous studies, which concluded that the concentration of Al released by 1 mol/L NaOH is relatively small, resulting in ~5.1 mM of Al in the soil solution (Qafoku et al. 2004). It is important to note that Si and Al concentrations are orders of magnitude greater than U which can lead to the potential U complexation as U-silicates in Si-rich solutions (Katsenovich et al, 2016). Table 1 summarizes the simplified pore water composition used to prepare the U-bearing precipitate samples.

Table 1. Target Concentrations in Synthetic Pore Water Solutions to Create U-Bearing Precipitate Samples

Sample ID	Si (mM)	Al (mM)	HCO_3 (mM)	Ca (mM)	U (mg/L)
1	50	5	3	0	2
2	50	5	3	10	2
3	50	5	3	15	2
4	50	5	50	0	2
5	50	5	50	10	2
6	50	5	50	15	2

a) Preparation of stock solutions

Stock solutions of HCO_3 (400 mM), Si (422 mM), and Al (50 mM) were first prepared in deionized water (DIW) from the salts $KHCO_3$, $Na_2SiO_3 \cdot 9H_2O$, and $Al(NO_3)_3 \cdot 9H_2O$, respectively, reaching the desired concentrations in 50 mL centrifuge tubes. Sodium metasilicate, $Na_2SiO_3 \cdot 9H_2O$, and potassium bicarbonate, $KHCO_3$, also served as a source of sodium and potassium in the mixture. The 200 µg/L stock solution of uranyl nitrate dissolved in DIW was prepared fresh from a uranyl nitrate hexahydrate (1000 µg/L) standard before use (Fisher Scientific). The subsequent Table 2 shows the type and amount of salts used to prepare the necessary stock solutions in 50 mL volumes.

Table 2. Type and Amount of Salts Used to Prepare Stock Solutions

Stock Solution	Salt Used	Molecular Weight of Salt (g/mol)	Stock Solution Concentration (mM)	Amount to prepare 50 mL (g)
Bicarbonate	$KHCO_3$	100.114	400	2.002
Metasilicate	$Na_2SiO_3 \cdot 9H_2O$	284.196	422.24	5.998
Aluminum	$Al(NO_3)_3 \cdot 9H_2O$	375.129	50	0.938
Calcium	$CaCl_2.H_2O$	219.08	500	5.447

b) Preparation of samples containing U-bearing precipitates

The general experimental procedure used to prepare 6 samples containing U-bearing precipitates was as follows:

1) Prepared two (2) test solutions in 50 mL centrifuge tubes by mixing measured aqueous volumes of Si and Al from the prepared stock solutions, given that Si/Al ratio concentration remains the same for all samples;
2) Measured volumes of the appropriate bicarbonate stock solution were added to the mixture to achieve the targeted concentration (3 or 50 mM). Deionized water (DIW) was added to each test solution to reach a final volume of 39 mL, leaving 1 mL of volume for pH adjustment.
3) The pH of the resulting solution was measured and adjusted to approximately 8 by titration with concentrated nitric acid (HNO_3), and DIW was added to end up with a final volume of 40 mL in each tube. This pH value is in line with values previously observed in the Hanford Site 200 Area vadose zone (Serne et al., 2008).
4) Next, 5% ammonia gas (NH_3) was injected into the mixture through a metal gas sparger (Mott Corporation, 20 µm pores) until the pH of the solution reached approximately 11 [0.063 mol/L (aq)]. This was followed by distribution of the mixture into six 10 ml centrifuge tubes consistent with the 6 different U-bearing precipitate test samples.
5) Finally, the corresponding amount of U and Ca were added to each tube. Control samples were prepared in DIW amended with U(VI) at a concentration of 2 mg/L to test more precisely for initial U(VI) concentration.

It is important to note that for confirmation purposes, duplicates were prepared for each test sample. In addition, a second set of six original and duplicate samples were prepared following an additional filtration step that will be explained later; therefore, the methodology was repeated four times. Tables 3 and 4 below show the amount of stock solutions and DIW used to prepare two 40 mL tubes of mixed samples, which were subsequently distributed into six tubes of 10 mL mixed samples amended with various concentrations of calcium solutions. The addition of calcium chloride solution caused precipitate formation in each sample.

Table 3. Amount of Stock Solution and DIW to Prepare 40 mL of Mixed Sample

Mixture	Si (µL)	Al (µL)	HCO_3 (µL)	DIW (mL)
1	4,737	4,000	300	30.963
2	4,737	4,000	5,000	26.263

Table 4. Amount of Mixed Sample, Ca and U to Prepare Six 10 mL Volume Containing U-Bearing Precipitate Samples

Sample ID	Sample Content	Ca (µL)	U(µL)	Mixed Sample (µL)	Total Sample V (µL)
1	3mM HCO_3, no Ca	0	200	9,800	10,000
2	3mM HCO_3, 5mM Ca	100	200	9,700	10,000
3	3mM HCO_3, 10mM Ca	200	200	9,600	10,000
4	50mM HCO_3, no Ca	0	200	9,800	10,000
5	50mM HCO_3, 5mM Ca	100	200	9,700	10,000
6	50mM HCO_3, 10mM Ca	200	200	9,600	10,000
Control	DIW: 9,800 mL	0	200	0	10,000

Unfiltered Samples

The first set of twelve samples (six samples prepared in duplicates) was selected to be the set of unfiltered samples. All control and experimental tubes were capped and placed in a shaker at 100 rpm at a temperature of 25°C. After letting solid particles within the solutions settle for approximately two days, the samples were centrifuged using a Thermo Scientific, Corvall ST 16R centrifuge for 15 minutes at a speed of 5,000 rpm. Following the centrifugation step, the supernatant solution from each sample was collected in different tubes for future analysis to determine the concentration of U left in the precipitates. The wet precipitates were set to dry in the oven at 35ºC for a period of approximately 2-3 weeks. Weights of precipitates were recorded until they were stable, which indicated that the solid particles were dried.

Filtered Samples

The second set of twelve samples (six samples prepared in duplicated) corresponded to the filtered set. The objective of this additional filtration step was to ensure the pore water accumulated inside the precipitates was removed before sample drying. The filtration process consisted of vacuum-filtering all the samples using micro sized pore (0.2µm) filters (Whatman™) and collecting the supernatant solutions in a similar method as the unfiltered samples. Figure 1 shows a Millipore 25mm Glass Microanalysis Vacuum Filtering set up as the one used for this experiment.

Figure 1.Vacuum-filtration set up.

A total of 24 U-bearing precipitate test samples were prepared following the methodology explained in the previous subsections.

2. Sequential Extraction Experiment

Though it is typically reserved for soil samples, sequential liquid extractions were conducted to evaluate U leaching potential from precipitates created in the previous steps to investigate for the stability of the U-bearing precipitate test samples. This process enabled the evaluation of the extractability of U(VI) associated with the solid particles. The sequential extraction experimental approach involved subjecting the solid particles to serial extraction using increasingly aggressive solutions, each intended to target specific uranium phases. Each extraction step utilized solutions and conditions chosen specifically to selectively target uranium associated with various phases within the precipitate sample.

A number of sequential extraction procedures have been reported using a wide variety of conditions. While some differences are simply adjustments to fit the sample composition and analyte being targeted, there are many variations for comparable extractions. As many as six different sequential extraction steps have been used to characterize U in different mineral phases of natural sediments (Smith and Szecsody 2011). For the scope of this study, a couple of weak extractants were used, such as deionized water, which would be easily to dissolve water soluble uranium species, and carbonate solution, which would remove adsorbed U species. In addition, a series of three sequential liquid extractions of increasing strength were employed to generally characterize U mobility (i.e. harder to extract phases are less mobile): an acetate solution, an acetic acid solution and finally a very strong extractant such as 8 M HNO_3, which would remove hard-to-extract U from uranium-bearing precipitate samples (Table 5).

Furthermore, the purpose of these 5 sequential extractions was to quantify the phases that are potentially able to interact with pore water (i.e., aqueous, adsorbed, associated with carbonates and in hydrous silicates) (Szecsody et al., 2012). Adapted from (Szecsody et al., 2012, Smith and Szecsody, 2011), the sequential extraction method, solutions, time of exposure, and target compounds for the experiment are presented in the following

Table 5. Sequential Extraction Experiment Steps

Step	Solution	Time (h)	Target Compounds
1	**Deionized Water (DIW)**	1	Aqueous U phases
2	**Carbonate solution:** 0.0144M $NaHCO_3$ + 0.0028M Na_2CO_3 (pH 9.3); 2 liters: 2.42 g $NaHCO_3$ + 0.592 g Na_2CO_3 + balance DI H_2O to 2.0 liters	1	Adsorbed U phases
3	**Acetate solution:** 2 liters: 136.1 g sodium acetate•$3H_2O$ + 30 mL glacial acetic acid (17.4 mol/L), pH 5.0, balance DI H_2O to 2.0 liters	1	Some dissolved U-Carbonates
4	**Acetic acid solution:** concentrated glacial acetic acid, pH 2.3; 2 liters: 50.66 mL glacial acetic acid (17.4 mol/L) + 47.2 g $Ca(NO_3)_2$*$4H_2O$, pH 2.3, balance DI H_2O to 2.0 liters	120	Most U-Carbonates and hydrated boltwoodite (uranyl silicate minerals)
5	**8 M Nitric Acid (HNO_3)** at 95°C	2	Harder-to-dissolve U phases

Additionally, after each extraction step, samples were rinsed with 5 mL of deionized water (DIW), which functioned to help remove any lingering extractant. For analytical purposes, this rinse solution was considered a part of the preceding extraction. For the purpose of this study, the extraction volume was selected using a 40:1 solid (mg) to solution (mL) ratio, which was used in a study on uranium extraction from Hanford sediment (Smith and Szecsody, 2011).

The extraction procedure began with the addition of the corresponding volume of extraction solution to the labeled vials containing the solid precipitates previously prepared. The mixture was briefly vortexed before being transferred to an orbital shaker where the vessel was agitated at 150 rpm for the duration of the extraction. After each extraction, samples were centrifuged at 5000 rpm for 30 minutes in order to separate the extractant and remaining precipitate. As mentioned before, the extraction was followed by a 10 minute DI water rinse, which was also accompanied with agitation and centrifugation steps. This process of extraction and rinse was repeated for extraction steps I through IV with each of their specified extraction times. The final extraction (Step V), intended to target hard-to-extract uranium species, differed in that its extraction solution used 8 M nitric acid (HNO_3) maintained at 95°C using a water bath.

Following the extractions protocol, all the collected supernatant from the test samples were analyzed for U using a kinetic phosphorescence analyzer (KPA-11, Chemchek Instruments, Richland, WA). For analysis with the KPA instrument, extracted aliquots from the supernatant of each test sample were diluted with 1% nitric acid between 5 and 20 times.

3. The Effect of Si Concentration on the Removal of Uranium

The objective of this experiment was to quantify the role of the major pore water constituent, Si, on uranium (VI) precipitation/removal from NH_3-treated synthetic pore water solutions and to find out what is a minimal silica concentration that could sustain U(VI) removal at different pore water compositions.

For the scope of this study and similar to the sequential extraction experiment, the large pore water composition was simplified to have the following major components in the sample

solutions: silica (Si), aluminum (Al), uranium (U), bicarbonate (HCO_3), calcium (Ca^{+2}); in addition, samples containing magnesium (Mg) and iron (Fe) instead of calcium were prepared to account for the effect of different pore water composition on U removal, if any. Silica concentrations tested were 7.5mM, 15mM and 25 mM. In addition, aluminum concentration of 5 mM, two different bicarbonate concentrations of 3 mM and 50 mM, two different calcium and magnesium concentrations of 5 and 10 mM, and finally two iron concentrations of 0.2 and 5 mM, based on concentrations observed in sediments from the Hanford Site (Szecsody, et al 2010), were tested in three different sets of samples. Table 6 to Table 8 summarize the simplified pore water composition used to prepare the U-bearing precipitate samples for this experiment.

Table 6. Target Concentrations in Synthetic Pore Water Solutions to Create U-Bearing Precipitate Samples Containing Ca

Sample	Si (mM)	Al (mM)	HCO_3 (mM)	Ca (mM)	U (mg/L)
1	7.5	5	3	0	2
2	7.5	5	3	5	2
3	7.5	5	3	10	2
4	7.5	5	50	0	2
5	7.5	5	50	5	2
6	7.5	5	50	10	2
7	15	5	3	0	2
8	15	5	3	5	2
9	15	5	3	10	2
10	15	5	50	0	2
11	15	5	50	5	2
12	15	5	50	10	2
13	25	5	3	0	2
14	25	5	3	5	2
15	25	5	3	10	2
16	25	5	50	0	2
17	25	5	50	5	2
18	25	5	50	10	2

Table 7. Target Concentrations in Synthetic Pore Water Solutions to Create U-Bearing Precipitate Samples Containing Mg

Sample	Si (mM)	Al (mM)	HCO_3 (mM)	Mg (mM)	U (mg/L)
1	15	5	3	5	2
2	15	5	3	10	2
3	15	5	50	5	2
4	15	5	50	10	2
5	25	5	3	5	2
6	25	5	3	10	2
7	25	5	50	5	2
8	25	5	50	10	2

Table 8. Target Concentrations in Synthetic Pore Water Solutions to Create U-Bearing Precipitate Samples Containing Fe

Sample	Si (mM)	Al (mM)	HCO_3 (mM)	Fe (mM)	U (mg/L)
1	15	5	3	0.2	2
2	15	5	3	5	2
3	15	5	50	0.2	2
4	15	5	50	5	2
5	25	5	3	0.2	2
6	25	5	3	5	2
7	25	5	50	0.2	2
8	25	5	50	5	2

a) Preparation of stock solutions

Similar to the Sequential Extraction experiment, stock solutions of HCO_3 (400 mM), Si (422 mM), Al (50 mM) were first prepared in deionized water (DIW) from the salts $KHCO_3$, $Na_2SiO_3 \cdot 9H_2O$, and $Al(NO_3)_3 \cdot 9H_2O$, respectively, reaching the desired concentrations in 50 mL volume. Likewise, stock solutions of Ca (219.08 mM), Mg (1250 mM) and Fe (100 mM) were prepared in deionized water (DIW) from the salts $CaCl_2.H_2O$, $H_{12}O_6MgCl_2$, and $FeCl_3.6H_2O$, respectively. The 200 µg/L stock solution of uranyl nitrate dissolved in DIW was prepared fresh from a uranyl nitrate hexahydrate (1000 µg/L) standard before use (Fisher Scientific). Table 9 shows the type and amount of salts used to prepare the necessary stock solutions in 50 mL volume.

Table 9. Type and amount of salts used to prepare Stock Solutions for Low Si Concentrations Experiment

Stock Solution	Salt Used	MW of Salt (g/mol)	Stock Solution Concentration (mM)	Amount to prepare 50 mL (g)
Bicarbonate	$KHCO_3$	100.114	400	2.002
Metasilicate	$Na_2SiO_3 \cdot 9H_2O$	284.196	422.24	5.998
Aluminum	$Al(NO_3)_3 \cdot 9H_2O$	375.129	50	0.938
Calcium	$CaCl_2.H_2O$	219.08	500	5.447
Magnesium	$H_{12}O_6MgCl_2$	203.3	1250	12.706
Iron	$FeCl_3.6H_2O$	270.32	100	1.3516

b) Preparation of U-bearing precipitate samples

Sample preparation procedures including steps to inject 5% ammonia gas were the same as for the sequential extraction experiment. A total of 34 samples and duplicated unfiltered samples were prepared following the protocol. After two days, the solutions were centrifuged for 15 minutes at 5000 rpm and supernatant solutions were withdrawn to analyze for U(VI). All the collected supernatant from the test samples were analyzed for U via a KPA-11 instrument (Katsenovich et al. 2016).

4. Flow-thru Uranium Leaching Experiment via Mini-Columns

The objective of this experiment was to evaluate the release of uranium from artificially prepared U-bearing precipitates in flow-through experiments. This test followed similar procedures as an experiment by (Smith and Szecsody, 2011). The experimental set-up included two mini columns with a volume of ~1 cm^3 that were filled with precipitates prepared with 3mM and 50mM of bicarbonate. Mini-columns were connected to the feed bottle containing synthetic groundwater solution (SGW) amended with 3mM HCO_3. A Tedlar bag filled with nitrogen gas was attached to the feeding bottle to prevent SGW solution from interferences caused by atmospheric carbon dioxide.

Figure 2. Experimental set-up with mini-columns (~1cm^3) filled with dried uranium-bearing precipitate.

SGW was prepared with nitrogen-purged DIW by combining three solutions A, B, and C (Table 10). 1 L of SGW was prepared by pipetting 10 mL each of solutions A and C and 20 mL of solution B into 900 mL deionized water and then diluted to 1 L with deionized water.

Table 10. Stock Solutions for SGW

	SGW Stock Solutions	Concentration (g/L)
A	$NaHCO_3$	12.1
	$KHCO_3$	1.6
B	$MgSO_4$	3.06
	$CaSO_4$	0.82
C	$Ca(NO_3)_2 \times 4H_2O$	5.43
	$CaCl_2 \times 2H_2O$	9.56

The process consisted of the continuous flow of SGW solutions into mini-columns at a constant flow rate of 1 mL/day and collecting discrete effluent samples over time. The protocol to prepare the precipitates was similar to the previous experiments. Table 11 provides information on the type and amount of salts used to prepare stock solutions that were further used to achieve the targeted concentrations in the samples.

Table 11. Amount of Salts to Prepare 50ml of Stock Solutions and Targeting Concentrations in Samples

Stock Solution	Salt Used	Molecular Weight of Salt (g/mol)	Stock Solution Concentration (mM)	Amount to prepare 50 mL (g)	Targeting Concentrations in Samples (mM)	
Bicarbonate	$KHCO_3$	100.114	400	2.002	3	50
Metasilicate	$Na_2SiO_3 \cdot 9H_2O$	284.196	422.24	5.998	50	
Aluminum	$Al(NO_3)_3 \cdot 9H_2O$	375.129	50	0.938	5	
Calcium	$CaCl_2.H_2O$	147.01	1250	9.188	10	
Uranium Nitrate	$UO_2(NO_3)_2$ $6H_2O$	238.03	1000			

The general procedure to prepare 4 samples containing the U-bearing precipitates was as follows: First, 4 tubes of 40 mL mixture were prepared containing measured volumes of Si and Al, then the corresponding amount of HCO_3 was added. Two mixed solutions contained 3 mM and the other two, 50 mM. The pH was then measured and adjusted to around pH 8 by adding small amounts (150-200 µL) of concentrated nitric acid (HNO_3), at which point would have made the pH in line with Hanford Site conditions. After this, 5% ammonia gas was injected to the mixture in order to increase pH to 11, followed by addition of the measured volumes of U and Ca. All the tubes were vortexed and kept on the bench for 1-2 days to let the precipitates settle. The last step was sample centrifugation for 30 minutes, followed by collection of supernatant solutions for further uranium analysis and setting of the precipitates to dry in the incubator at a temperature of 30° C. The table below shows amount of stock solution and DI water used to prepare the 4 mixed solutions.

Table 12. Number of Samples and Targeted Concentration in Each Sample

Amount of Stock Solution and DIW (µL) to prepare 50 mL of mixed sample					
	$Na_2SiO_3 \cdot 9H_2O$ (50mM)	5,921	uL	**$UO_2(NO_3)_2$ $6H_2O$**	1000 ppm
	Al(NO3)3·9H2O (5mM)	5,000	uL	**$CaCl_2.H_2O$**	1250 mM
# Sample	**Sample**	***$KHCO_3$ (µL)**	**DIW, mL**	****Ca (µL)**	**U(µL)**
1	3mM $KHCO_3$, 10mM Calcium	375	38.204	400	100
2	50mM $KHCO_3$, 10mM Calcium	6,250	32.329	400	100

It is important to note that four (4) centrifuge tubes for each sample composition were prepared to be able to obtain approximately 1 gram of dried solid precipitate. This resulted in a total of eight (8) mixed sample centrifuge tubes. The needed volume of 200mL was estimated based on

previous experimental experience to obtain about 1g of dried solid precipitate to fill each column.

5. Analytical Procedure

Samples were analyzed using a kinetic phosphorescence analyzer (KPA-11, Chemchek Instrument, Richland, WA) instrument to determine: a) U(VI) concentrations in the solution after preparation of U-bearing precipitates in both sequential extraction and Si concentration effect on uranium removal experiments, and b) U(VI) concentration after each sequential extraction and rinsing steps. For analysis with the KPA instrument, an aliquot was extracted from the supernatant of each test sample and diluted with 1% nitric acid between 5 and 100 times.

Subtask 1.1: Results and Discussion

1. Sequential Extraction on Unfiltered Samples

The KPA data collected from the analysis was graphed to display the mass of uranium removed with each extraction step based on the determined uranium concentrations and the volume that it was extracted into. Figure 3 displays the total mass of uranium removed, or in other words, the potential release of U from the unfiltered precipitate samples during sequential extraction experiments. These precipitates contained remaining pore water that was dried with the solids.

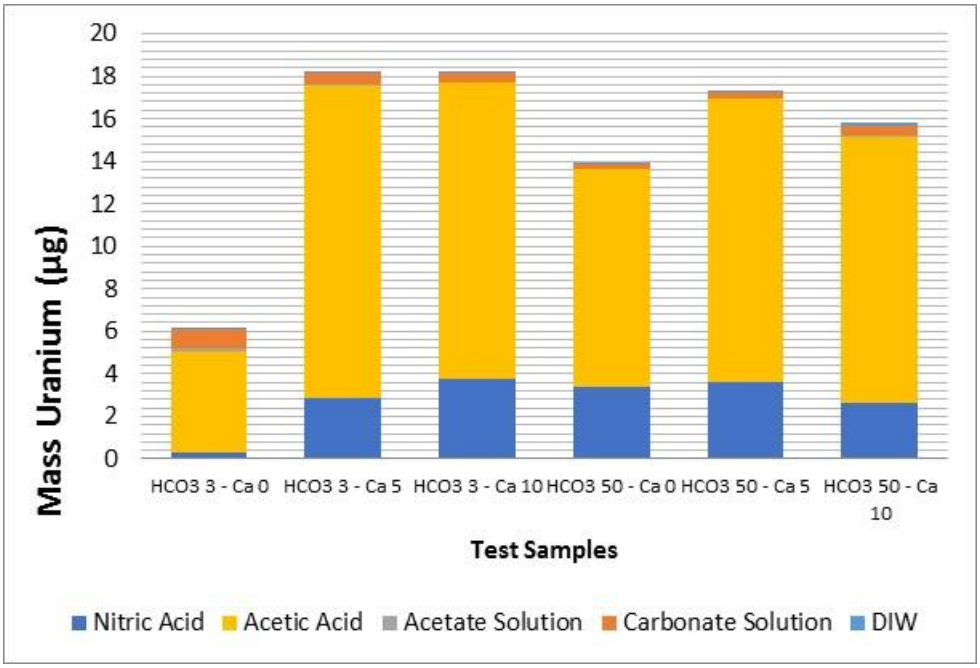

Figure 3. Sequential uranium extraction of unfiltered sample precipitates on mass basis.

Observing Figure 3, the total mass of uranium extracted shows that most of the U was extracted from the solid precipitates during the acetic acid extraction step, suggesting that most of the U was associated with uranyl silicate phases. Additionally, the samples containing Ca resulted in greater uranium removal compared to the Ca-free samples. Further, "high" bicarbonate samples showed, on average, a greater mass of U extracted compared to their "low" bicarbonate counterparts.

A comparison of the relative removal of uranium between the various extraction steps reveals how each extracting solution was favored in the different samples. This is useful for developing

an assumption of the types of uranium phases, which are most prevalent based on the "targeted" extraction phase (Refer to Table 5) and the relative mass of the analyte removed by its corresponding solution. Figure 4 and Figure 5 show U extraction distribution on a percentage basis for both "low" and "high" HCO_3 samples.

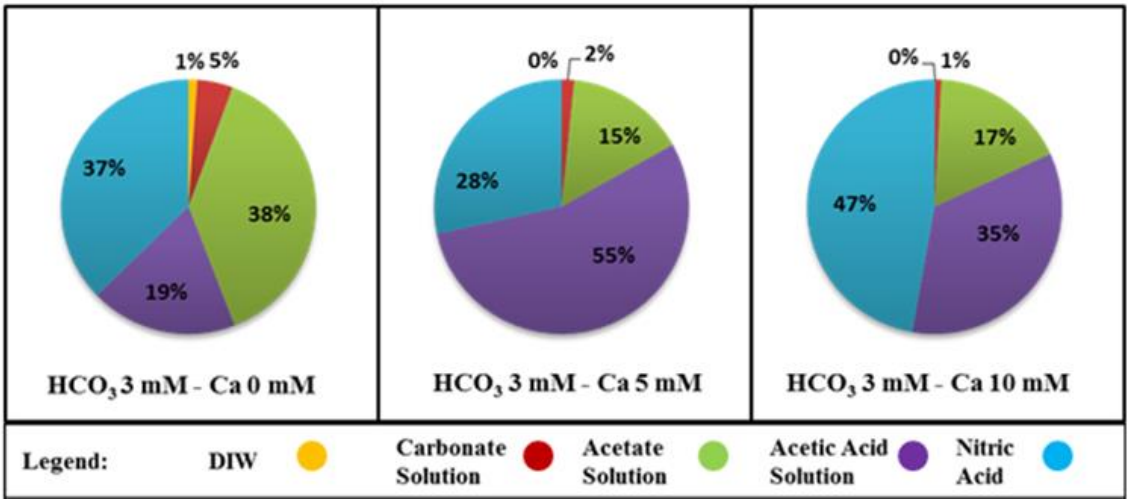

Figure 4. Uranium extraction distribution for unfiltered samples prepared with "low" bicarbonate concentration of 3mM.

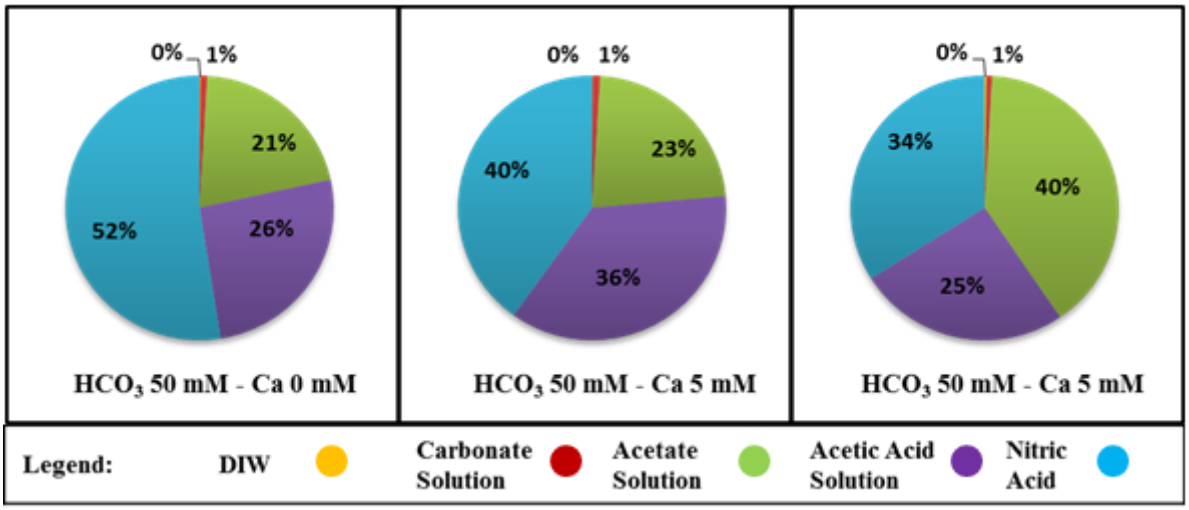

Figure 5. Uranium extraction distribution for unfiltered samples prepared with "high" bicarbonate concentration of 50mM.

The sequential extraction distribution charts reveal that there is a near insignificant uranium removal in the less aggressive DIW and carbonate solution extractions, suggesting uranium species were not present in the soluble phases. In addition, between equivalent "low" and "high" bicarbonate samples, the carbonate extraction, which targets the adsorbed species, had a decrease. The relative uranium removal decreased from 2-5% to 1% indicating less adsorbed U-phases formed at higher HCO_3 concentrations. Furthermore, it is clear that most uranium was removed in the acetate solution and nitric acid, step 3 and 4 respectively, suggesting that the uranyl carbonates and silicates make up the bulk of the extracted analyte.

2. Sequential Extraction on Filtered Samples

Similarly to the unfiltered set of samples, the KPA data collected from the analysis was graphed to display the mass of uranium removed with each extraction step based on the determined uranium concentration and the volume that it was extracted into. Figure 6 displays the total mass of uranium removed from the filtered test sample precipitates during the sequential extraction experiment.

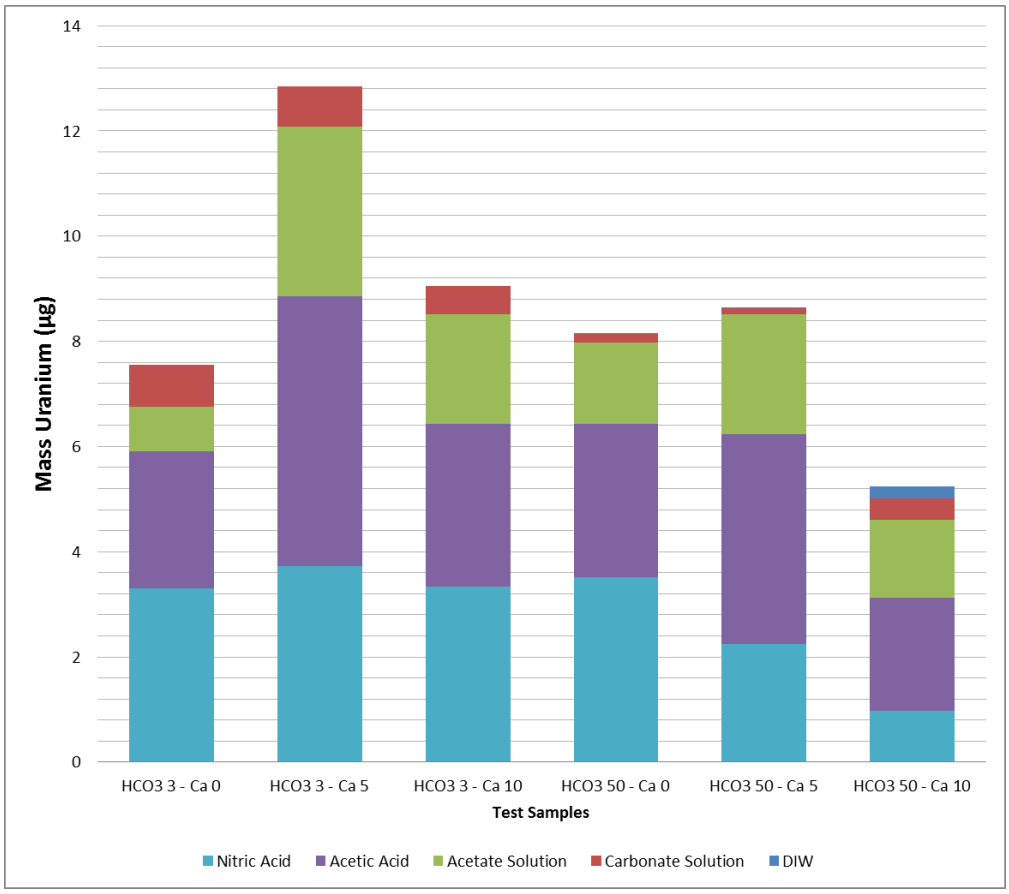

Figure 6. Sequential uranium extraction of filtered sample precipitates on mass basis.

The total mass of uranium extracted shows that, in general, "low" bicarbonate test samples had greater uranium removal than their "high" bicarbonate counterparts, except for the samples containing 5 mM of calcium. Additionally, the high bicarbonate sample containing 10 mM of calcium resulted in greater uranium removal during the first extraction than all of the samples previously tested. This could be explained by the fact that some solid uranium-bearing particles might have been inadvertently collected during sampling, consequently causing a higher supernatant uranium concentration result via KPA analysis.

Figures 9 and 10 below are presented im the same manner as the unfiltered samples, with the sole purpose of developing an assumption of the types of uranium phases which are most prevalent based on the "targeted" extraction phase and the relative mass of the analyte removed by its corresponding solution. Figure 7 and Figure 8 show the uranium extraction distributions on a percentage basis for unfiltered "low" and "high" HCO_3 samples.

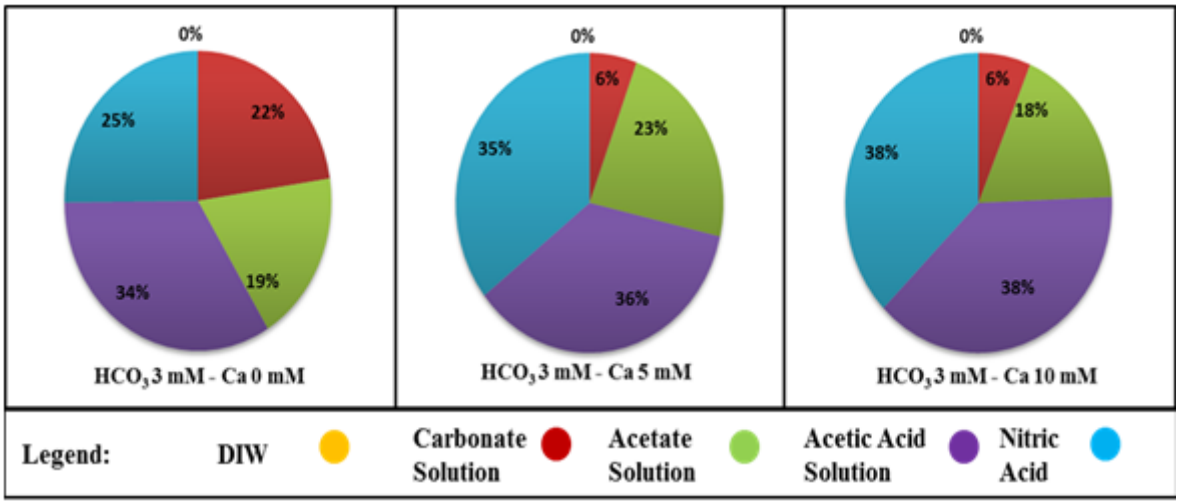

Figure 7. Uranium extraction distribution for filtered "low" HCO_3 samples.

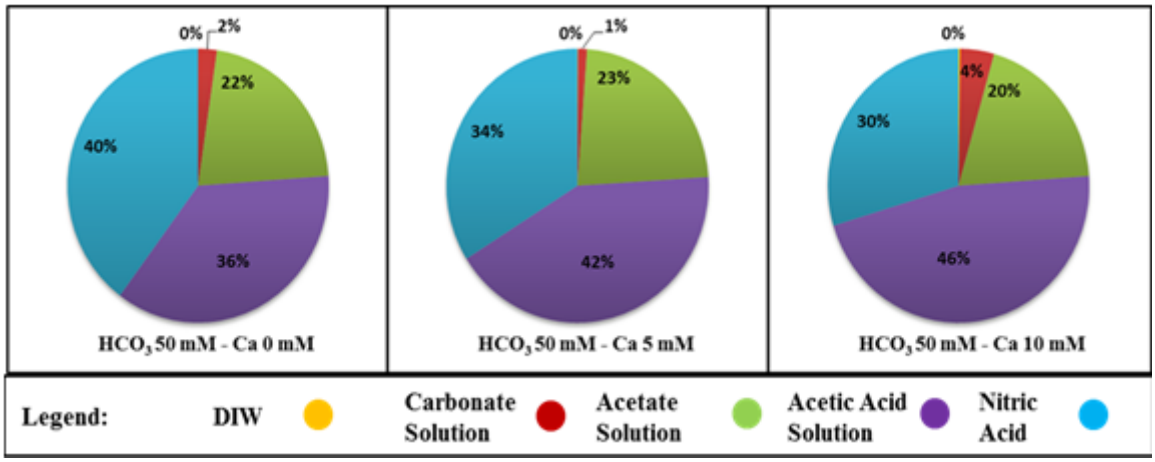

Figure 8. Uranium extraction distribution for filtered "high" HCO_3 samples.

The results obtained from the filtered test sample analysis, represented in the sequential extraction distribution charts, also reveal that there is a near insignificant uranium removal in the less aggressive DIW and carbonate solution extractions, suggesting uranium species were not present in the soluble phases. In addition, between equivalent "low" and "high" bicarbonate samples, the carbonate extraction, which targets the adsorbed species, had a significant decrease. The relative uranium removal decreased from 6-25% to 1-4%. Furthermore, it is clear that the majority of uranium was removed in the acetate solution and nitric acid, step 3 and 4 respectively, suggesting that the uranyl carbonates and silicates make up the bulk of the extracted analyte. Also, it should be noted that these filtered samples didn't contain pore water, only uranium that complexed with Si, adsorbed on the Si surface or incorporated inside the solid phases.

3. The Effect of Si Concentrations on the Removal of Uranium

Experimental results were calculated as percent removal of U (VI) from the supernatant solutions. The removal values for the contaminant were plotted on the y-axis against the initial concentration of Si on the x-axis (Figure 9). These graphs were used to compare results for each data set prepared with different HCO_3 concentrations (3mM as "low" and 50 mM as "high").

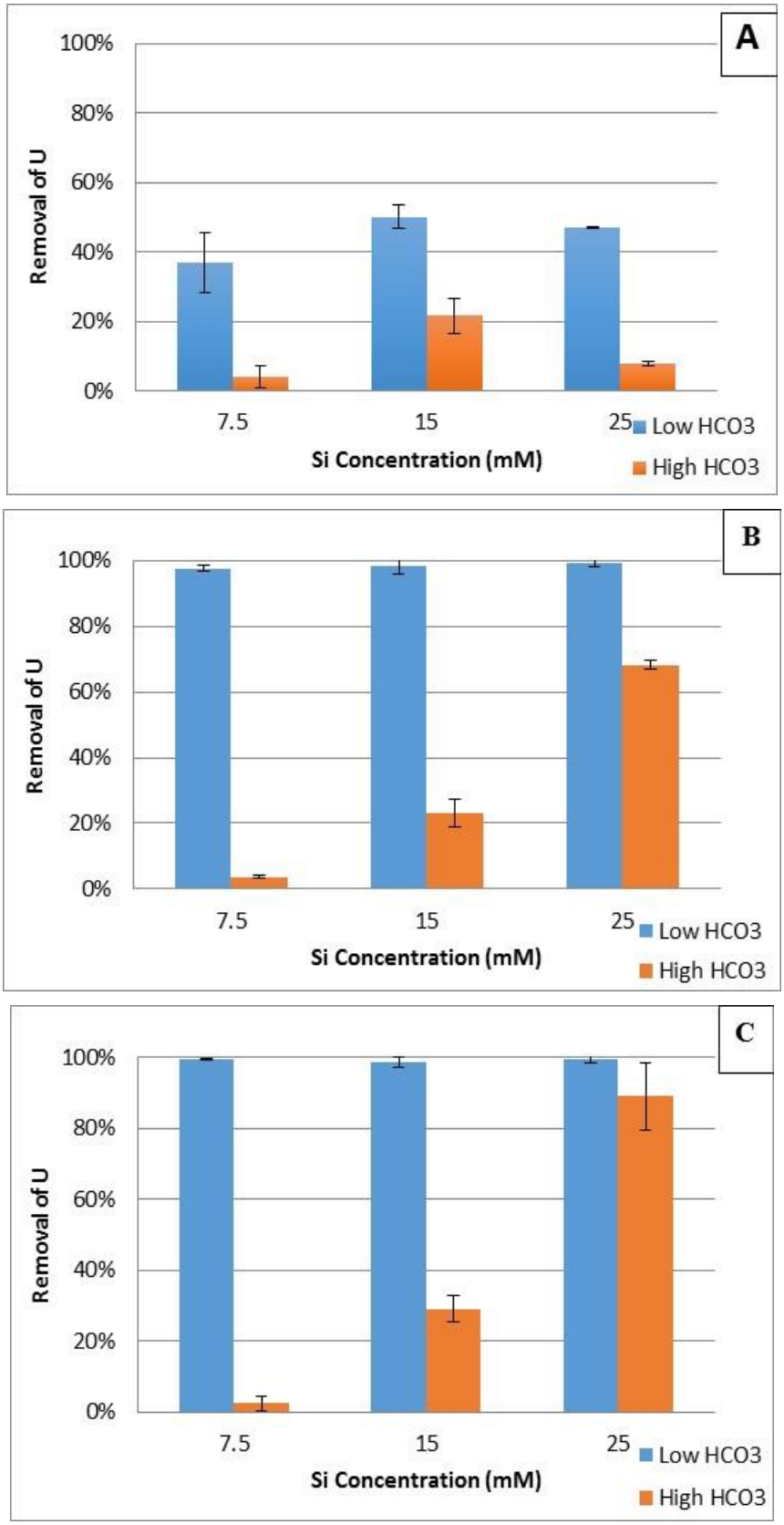

Figure 9. Percent removal of U (VI) tested at variable bicarbonate and silica concentrations in 5 mM Al amended solutions containing 2 mg/L U (VI) and (A) 0 mM; (B) 5 mM; and (C) 10 mM of Ca.

Generally, at Ca concentration of 0 mM and Si concentration of 15 mM, the removal efficiency of U resulted in the relatively low values, averaging less than 50% ± 20% including both "low" and "high" bicarbonate concentrations (Figure 9A). Also, the presence in the solution composition of "high" bicarbonate concentration (50 mM) appears to significantly reduce the removal efficiency of U at all Si concentrations. This can be explained by the formation of calcium carbonates or calcium silicates, which could provoke Si coagulation and precipitation reactions leading to co-precipitation of uranium. In the absence of Ca, the co-precipitation of U can only occur in the case of Si polymerization reactions that require much higher Si content on the level of Si solubility concentrations at alkaline conditions. Furthermore, it is evident that for the two Ca concentrations tested, at high bicarbonate concentrations, removal efficiency of U improves as concentration of Si increases (Figure 9B and Figure 9C). Moreover, the data collected suggests that at Si concentrations of 7.5, 15 and 25 mM, U(VI), removal efficiency reduces as the concentration of bicarbonate is increased; the gap in this reduction is smaller in the presence of higher Si concentrations of 25 mM (Figure 9B and Figure 9C). According to (Katsenovich et al., 2016), at HCO_3 > 25 mM stable soluble uranyl carbonate species, such as $UO_2(CO_3)_3^{-4}$, become predominant at alkaline conditions. This might explain the relatively lower removal efficiency of U compared to "low" bicarbonate concentrations where uranium is present in the uranyl hydroxide form. The highest removal efficiency of U up to 99% was achieved in the compositions containing "low" bicarbonate concentration for all Ca and Si concentrations tested (Figure 9).

Speciation modeling was conducted via the Geochemist Workbench (GWB) version 10.0.04 to predict aqueous speciation and solid phases likely to be saturated for samples amended with calcium prepared at "low" and "high" bicarbonate concentrations (Figure 10, Figure 11). Modeling results were compared to uranium removal data obtained at silica concentration of 15mM, calcium concentration of 10mM and "low" and "high" concentrations of bicarbonate in the solution composition (Figure 9).

Speciation modeling suggested that in the range of silica, 7.5mM-25mM, and calcium, 5mM-10mM, concentrations tested there is no effect on the uranium speciation and saturation indices of formed minerals (Figure 10 and Figure 11). However, there was a noticeable effect of bicarbonate concentration on the formation of solid phases and aqueous species. At "low" bicarbonate concentrations, speciation modeling identified the highest saturation indices for uranyl silicate, Na-boltwoodite [$(Na)(UO_2)(HSiO_4)\cdot 0.5H_2O$], and calcium carbonate phases, such as aragonite and calcite (Figure 10). Apparently, strong complexation of uranium and silica resulting in the formation of Na-boltwoodite contributed to the higher efficiency of uranium removal on the level of 98-99% from the solution mixture. At "high" bicarbonate concentration, the system was saturated with calcium carbonate minerals such as aragonite and calcite. Na-boltwoodite was found close to the saturation only at pH 11. This suggests that uranium removal is mostly controlled by the co-precipitation with calcite and aragonite at pH conditions from 8 to 10.5; however, as pH increased to 11, Na-boltwoodite at saturation became an additional solid phase causative to the removal of uranium from the solution mixture. Aqueous speciation at "low" bicarbonate concentrations suggested the decrease in uranyl carbonate species concentrations starting from pH 8.1. At the same pH, concentration of negatively charged uranyl hydroxide $UO_2(OH)_4^-$ began to increase reaching a maximum value at pH 11. For samples containing "high" bicarbonate concentrations of 50mM in the composition, uranyl carbonate species retained almost the same across all pH values (Figure 11).

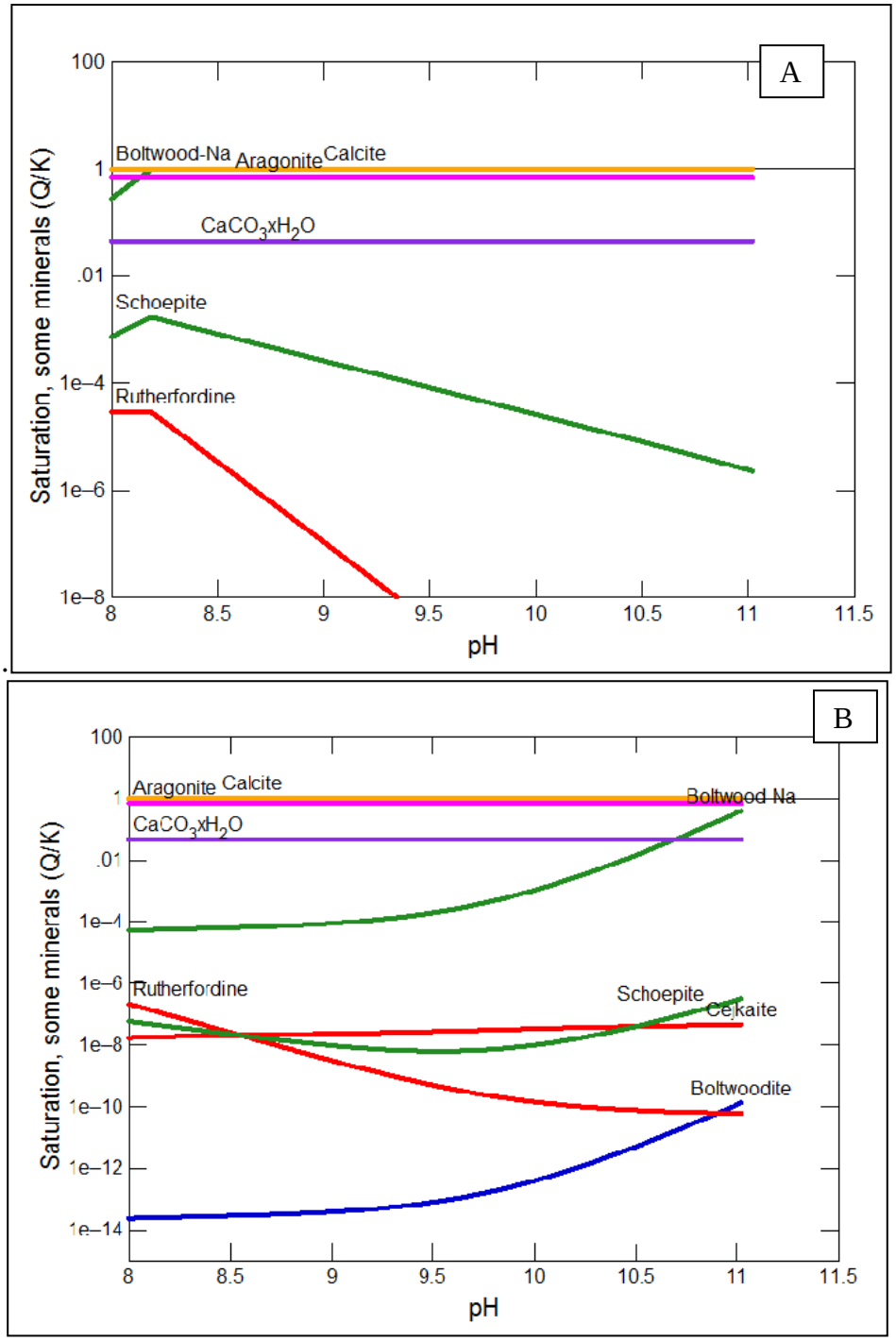

Figure 10. Diagrams of saturation indices of some of uranium-bearing mineral phases plotted as a function of pH. Sample composition includes 15 mM of Si, 10mM Ca and varied HCO3- concentrations. A) 3mM of $HCO3^-$, B) 50mM of $HCO3^-$.

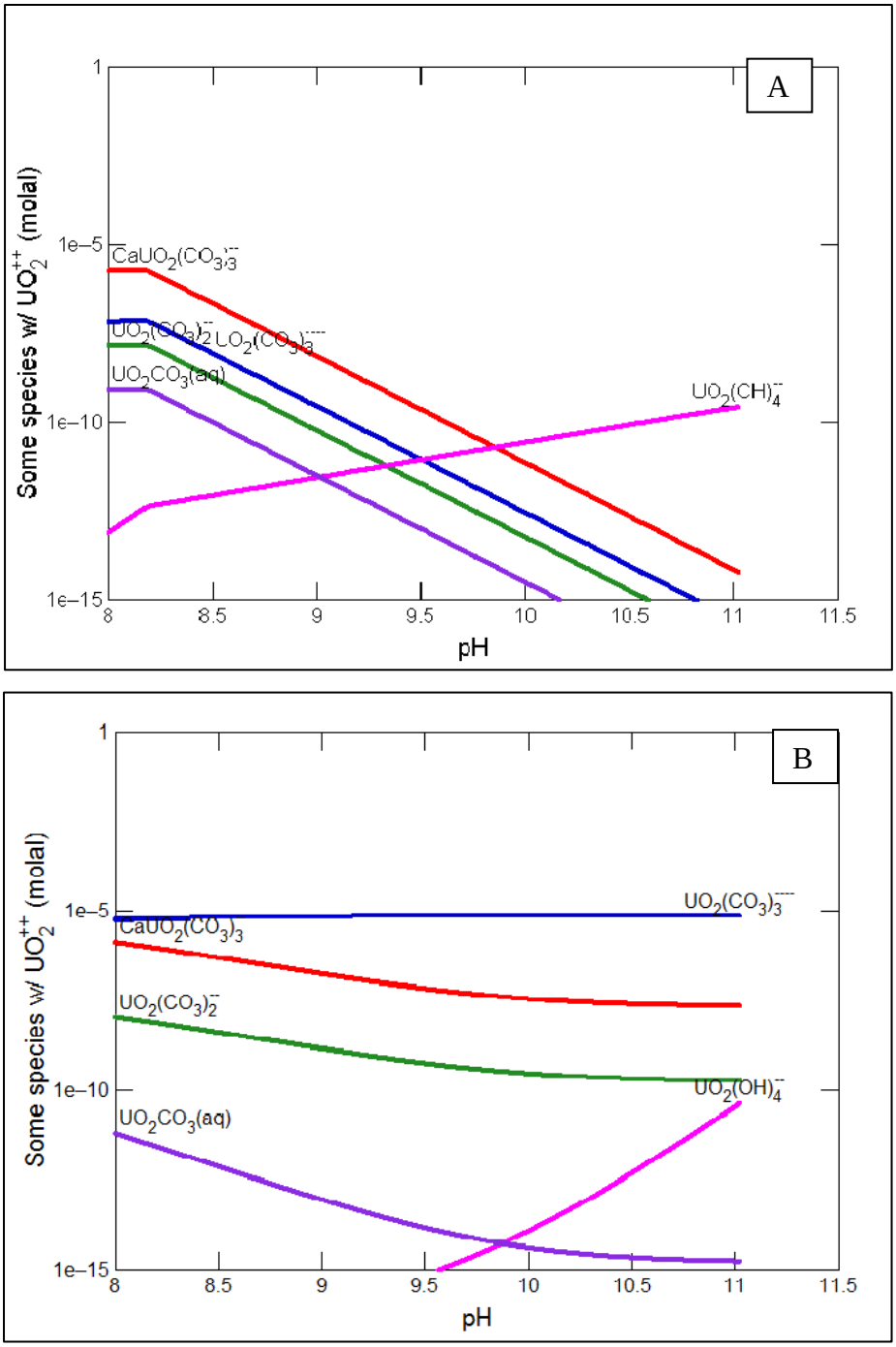

Figure 11. Diagrams showing uranium aqueous species concentrations plotted as a function of pH for samples amended with bicarbonate. Sample composition includes 15 mM of Si, 10mM Ca and varied HCO_3^- concentrations. A) 3mM of HCO_3^-, B) 50mM of HCO_3^-.

Samples containing Mg, which is one of the major constituents in the pore water composition, showed similar trends in removal efficiency of U (VI) as previously observed for samples containing Ca. Firstly, at "low" bicarbonate concentrations, Si concentrations of 15 and 25 mM and Mg concentrations of 5 and 10 mM, the removal efficiency of U (VI) was greater than 94%. In addition, the data also demonstrated that the higher bicarbonate concentration correlates with a

significant lower removal efficiency of U (VI) at Si concentrations of 15 and 25 mM and Mg concentrations of 5 and 10 mM (Figure 12A and 12B). Finally, it is visible that higher Si concentrations improve the general removal efficiency of U (VI) at "low" bicarbonate concentration and Mg concentrations of 5 mM.

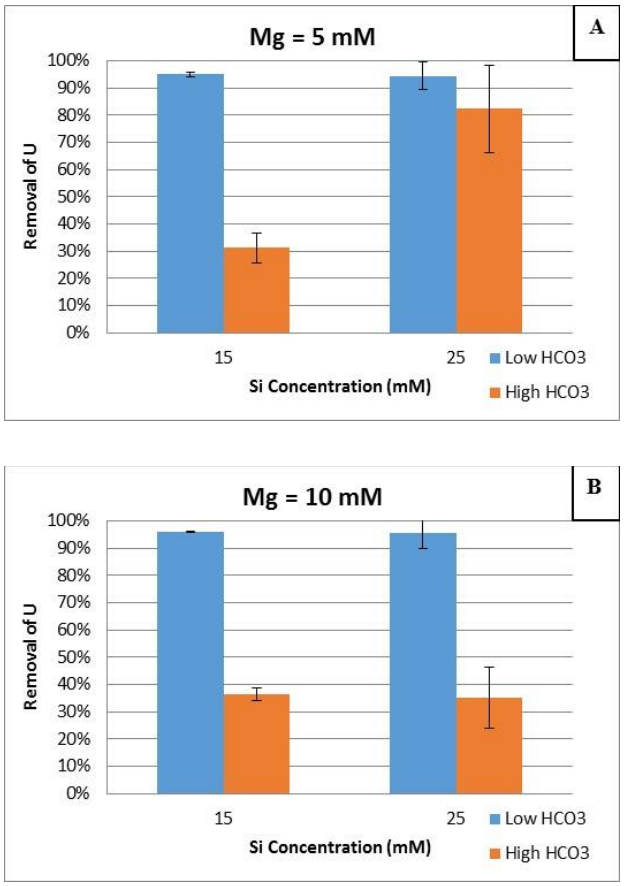

Figure 12. Percent removal of U (VI) tested at variable bicarbonate and silica concentrations in 5 mM Al amended solutions containing 2 mg/L U (VI) and (A) 5 mM; and (B) 10 mM of Mg.

The results of U removal in samples containing Fe, showed a relatively different trend to those containing Ca and Mg at Si concentrations of 7.5. Similar to the previous cases, under "low" concentrations of bicarbonate, U(VI) removal efficiencies are on the level of 80-87%, which can be attributed to the formation of stable solid uranyl silicates. However, this efficiency is lower compared to samples composed with Ca and Mg, where uranium reached 99% for Ca and 94-95% for Mg-amended samples (Figure 9, Figure 12). The results also showed that silica causes some interference with uranium removal as concentration of bicarbonate is increased to 50mM (Figure 13). At Si concentration of 7.5mM, the removal efficiency of uranium was found on the level of 81-84%, just slightly lower than samples composed of "low" bicarbonate concentrations. As the concentration of silica is increased to 15mM and 25mM, the removal efficiency was dropped to the 21-52% level (Figure 13). This tendency was found true for both ferric iron concentrations tested, 0.2mM and 5mM.

Speciation modeling suggested that the addition of iron into the solution composition resulted in the formation of iron phases, such as iron hydroxide and goethite. However, the increase in the concentration of ferric iron from 0.2mM to 5mM and silica concentration from 7.5mM to 25mM has not affected saturated indices of iron and uranium phases. As speciation diagrams showed

(Figure 14), the most significant factor affecting the formation of solid phases in the presence of iron was an increase in bicarbonate concentrations in the solution composition. At "low" bicarbonate concentrations of 3mM, solid phases were dominated by the uranyl silicate Na-boltwoodite phases; however, when bicarbonate concentration was increased, the formation of iron phases was predominant except at elevated 10.5-11 pH conditions when the formation of Na-boltwoodite phases prevailed (Figure 14).

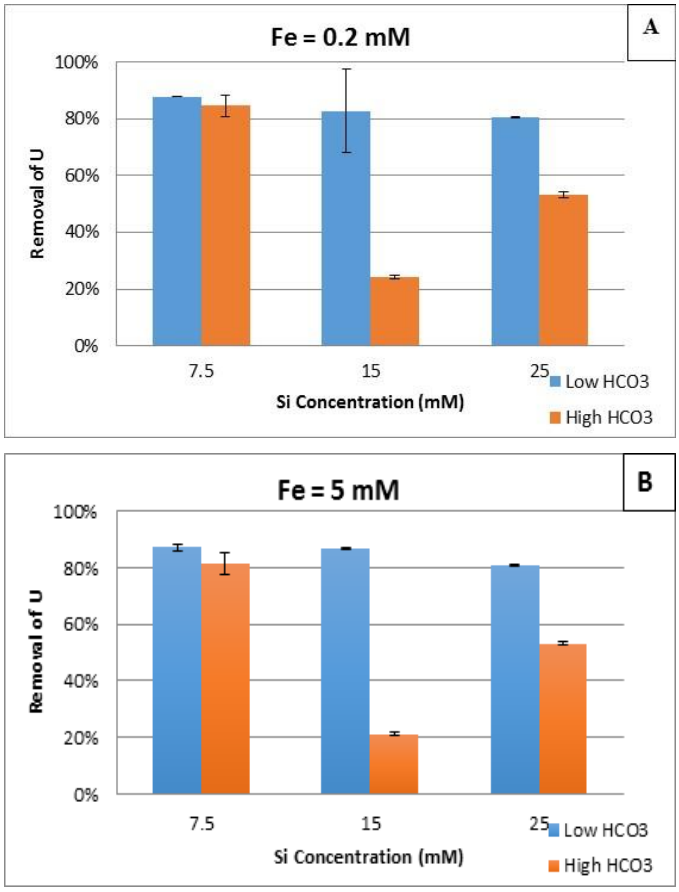

Figure 13. Percent removal of U (VI) tested at variable bicarbonate and silica concentrations in 5 mM Al amended solutions containing 2 mg/L U (VI) and (A) 0.2 mM of Fe^{3+}; and (B) 5 mM of Fe^{3+}.

Aqueous speciation at "low" bicarbonate concentrations suggested the decrease of two major uranyl carbonate species, $UO_2(CO_3)_3^-$ and $UO_2(CO_3)_2^-$, at approximately pH 9.5. In contrast, the concentration of negatively charged uranyl hydroxide $UO_2(OH)_4^-$ began to increase starting from pH 8, reaching a maximum value at pH 11. For samples containing "high" bicarbonate of 50mM, concentrations of highly soluble uranyl carbonate species remained almost the same across all pH values (Figure 15). This could be a reason for the decline of uranium removal efficiency at "high" bicarbonate concentrations. Another important observation from the experiments was that changes in ferric iron concentrations have not affected removal efficiencies of U at the range of silica concentrations tested.

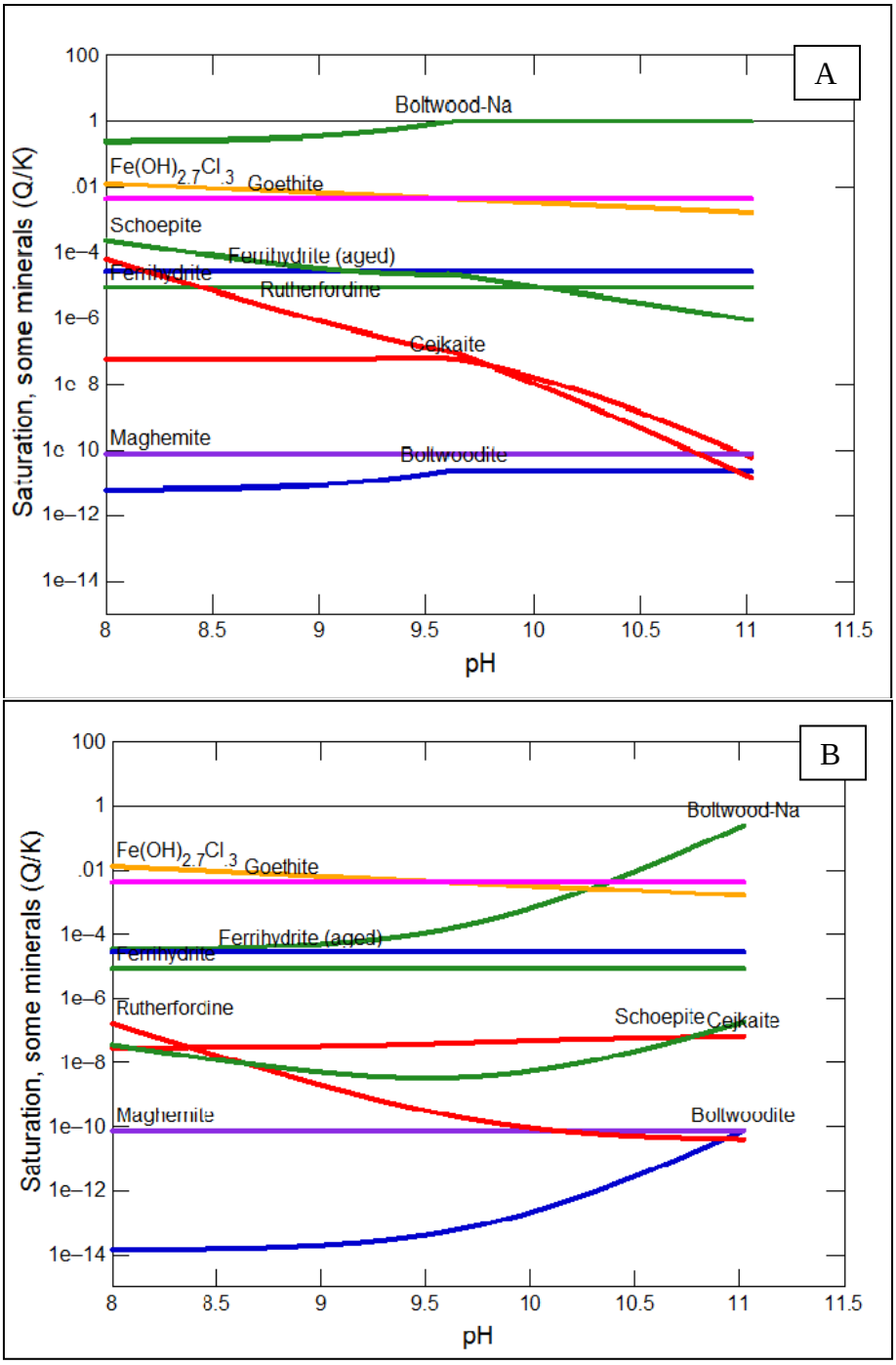

Figure 14. Diagrams of saturation indices of some of uranium-bearing mineral phases plotted as a function of pH. Sample composition includes 15 mM of Si and varied HCO3- concentrations. A) 3mM of HCO_3^-, 0.2mMFe or 5mMFe B) 50mM of HCO_3^-, 0.2mMFe or 5mMFe.

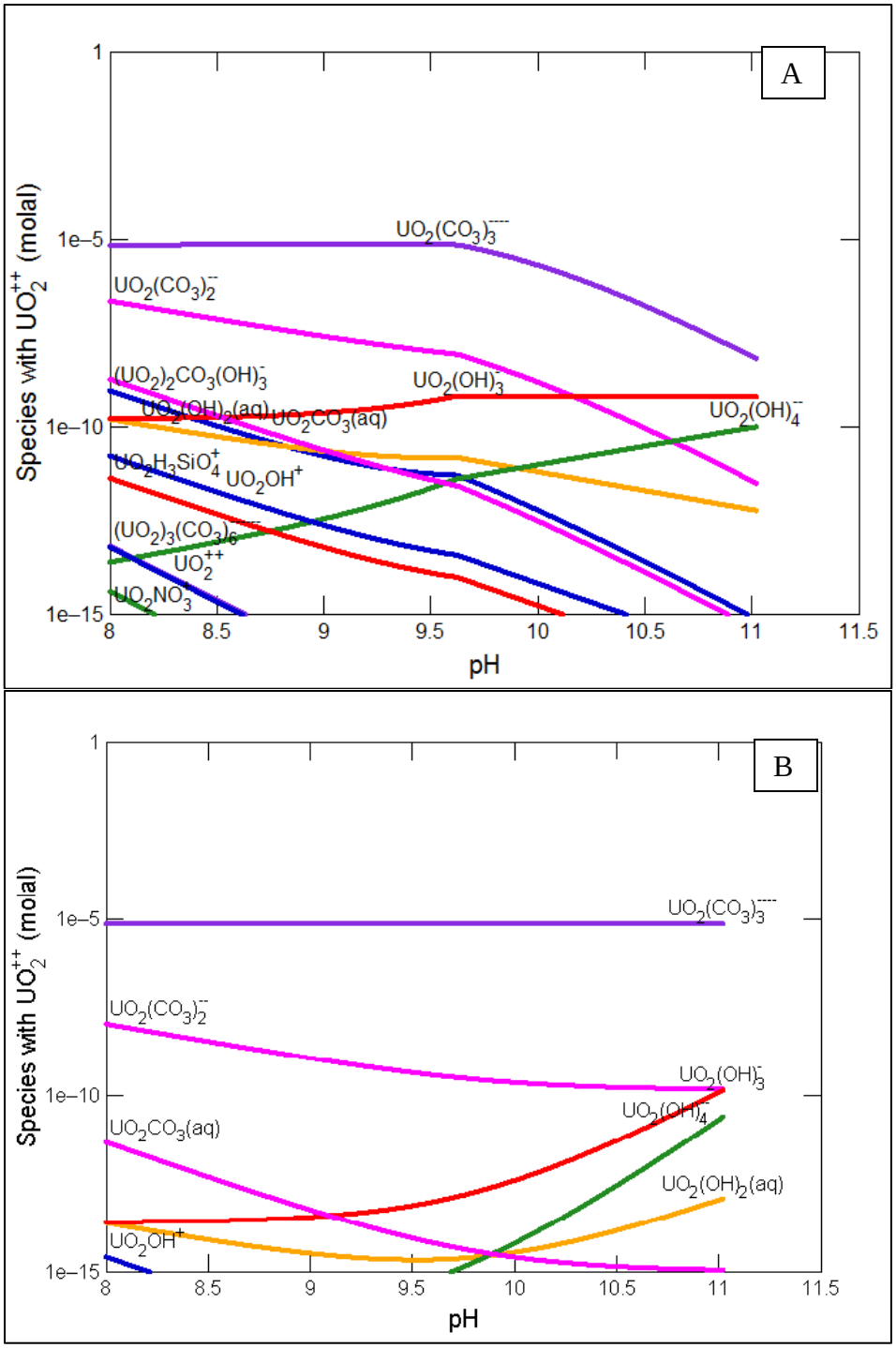

Figure 15. Diagrams showing uranium aqueous species concentrations plotted as a function of pH for samples amended with bicarbonate. Sample composition includes 15 mM of Si, 10mM Ca and varied HCO_3^- concentrations. A) 3mM of HCO_3^-, 0.2mMFe or 5mMFe B) 50mM of HCO_3^-, 0.2mMFe or 5mMFe.

4. Filtrate Solution Uranium Retention

Analytical results were evaluated to determine what component concentrations would maximize the fraction of U in the precipitate phase based on the concentrations of U left in their supernatants, or in other words, the U removal efficiency. This relied on the assumption that all

uranium introduced to the sample solutions was either retained in solution or precipitated/adsorbed onto the solid phase.

The results of the KPA analysis of the supernatant solutions were visualized using response surface diagrams (Figure 10). For this assessment all test concentrations for calcium-bearing samples were evaluated to display the relationship between the two variable concentrations, Ca and HCO_3, and the concentration of uranium in the supernatant phase. The initial concentration of uranium in all experiments was 2212±232 µg/L based on measurements of control samples prepared in triplicate.

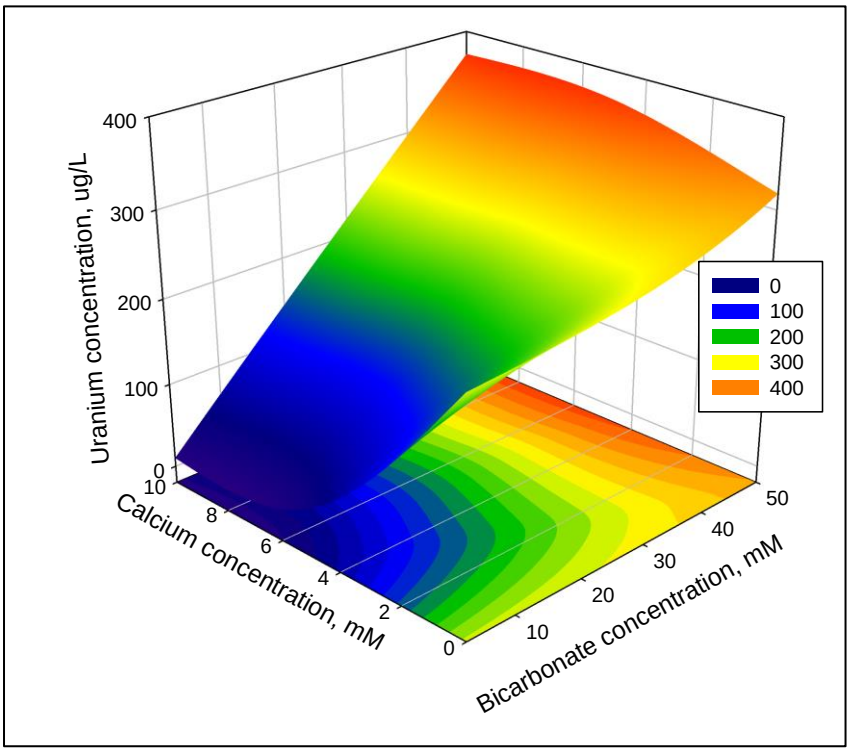

Figure 16. Response surface diagrams displaying filtrate solution uranium retention in samples.

The results of the sample sets show a clear and demonstrative positive correlation between the increasing concentration of bicarbonate in synthetic pore water solutions and the concentration of uranium in the post-treated supernatant solution. This finding suggests that with increasing sample bicarbonate concentration, the amount of uranium in the precipitate decreases. It is therefore safe to conclude that the "high" bicarbonate samples would be least likely to precipitate the uranium analyte.

This observed trend of uranium in the supernatant solutions increasing with added bicarbonate is likely indicative of the formation of highly soluble uranyl carbonates. In contrast, the trends in Figure 16 show that "low" bicarbonate samples have the least uranium remaining in the supernatant solutions and, therefore, have the most in the precipitate phase. This may be explained by the formation of uranyl silicates, which are relatively stables in the solid phases.

Additionally, there is correlation between the increasing calcium concentrations in sample solution and the concentration of uranium in the supernatant. The increasing calcium is associated with a decrease of uranium concentration in solution and an increase in the uranium precipitated. It is hypothesized that the increase in calcium could favor the removal of uranium

due to the co-precipitation with less soluble solids, such as calcium carbonates or calcium silicates, which could serve as nucleation sites provoking Si polymerization reactions and precipitation of silica (Iler 1979). Precipitated silica and calcium carbonate solid phases could lead to co-precipitation of uranium. In fact, considering the concentration of U injected as 2000 µg/L, the U precipitation/removal efficiencies from the aqueous phases ranged between 75-98%, the higher percentage being accounted for by samples containing 10mM of Ca and low in bicarbonate.

5. Continuous flow mini-column experiments

The following figures show the results of the U release from the continuous flow leaching experiment after approximately 51 collections. This corresponds to approximately two months for the two columns filled with uranium-containing precipitates prepared with "low" bicarbonate and "high" bicarbonate concentrations.

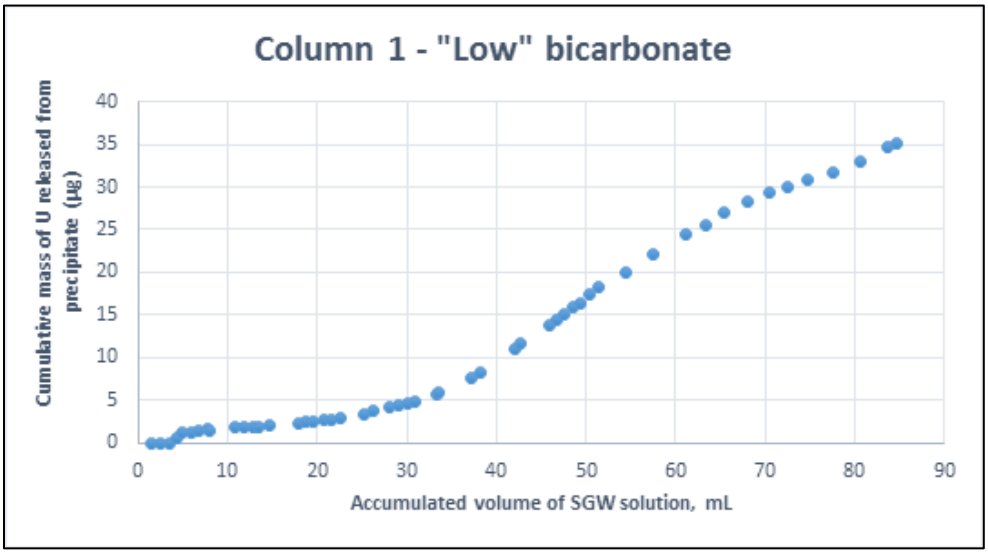

Figure 17. Cumulative mass of U in µg released from uranium-bearing precipitate in Column # 1 (Low bicarbonate).

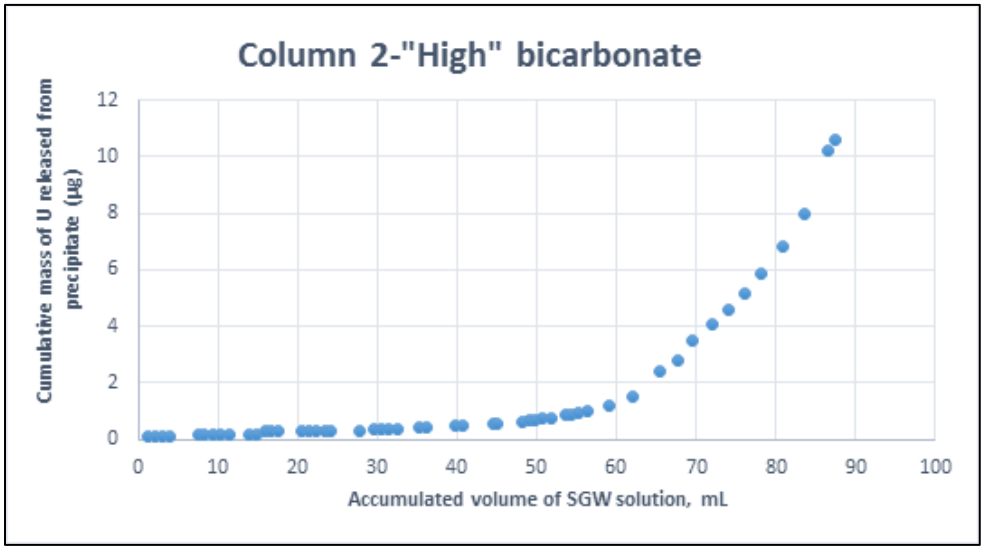

Figure 18. Cumulative mass of U in µg released from uranium-bearing precipitate in Column # 2 (High bicarbonate).

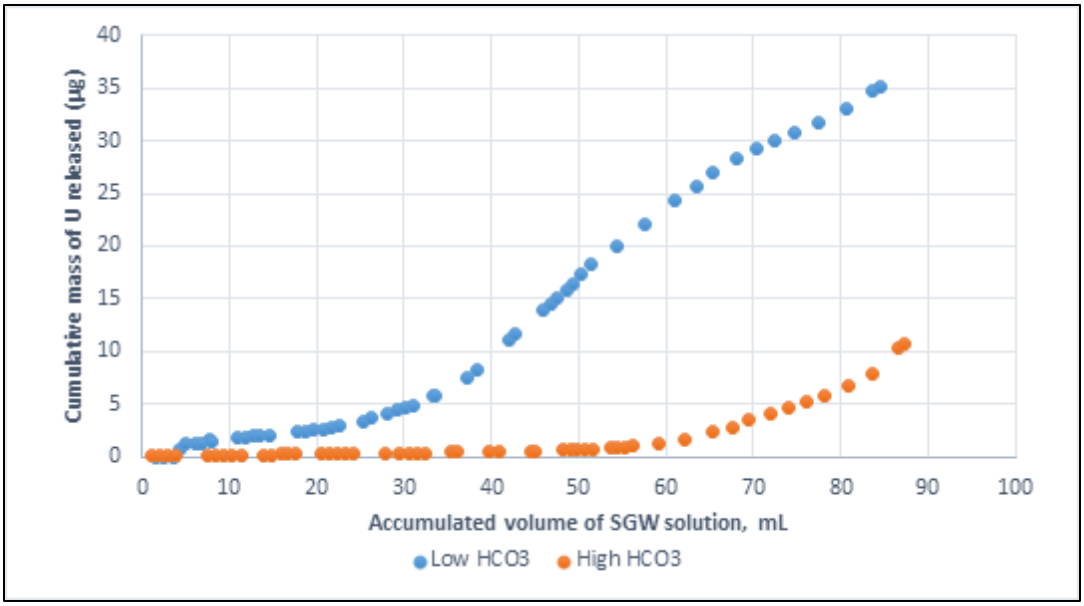

Figure 19. Cumulative mass of U in ug released from both columns for comparison.

It is important to note that an estimated 370 ug of U were contained in each column, which corresponds to the 100% of U present. Observing Figure 17 - Figure 19, it is evident that there is a significantly higher mass of U leached from precipitate prepared with "low" bicarbonate in samples, i.e. up to 35.2 ug after ~85mL of SGW solution amended with 3mM of HCO_3 was injected through the column. This volume of SGW is equivalent to approximately 220 pore volumes flowing through column 1 that resulted in 9.5% of U released from the solid precipitates. This is opposed to only approximately 2.6 µg leached (2.87% of U) in the presence of "high" bicarbonate concentrations. Therefore, there is evidence to state that in the presence of "low" bicarbonate concentrations, there is a higher potential risk of U release from the NH_3-treated sediments compared to "high" bicarbonate conditions using SGW solution amended with 3mM bicarbonate.

Electron Microprobe Sample Analysis

Materials and Methods

The sample preparation method for EPMA analysis closely followed a formerly used experimental procedure described in prior FIU ARC reports. An array of synthetic pore water solutions was prepared using stock solutions that were combined to achieve targeted final concentrations when diluted to volume (Table 13).

Table 13. Stock Solution & Synthetic Pore Water Concentrations for Sample Preparation

Stock Solution	Concentration (mM)	Synthetic Pore Water Concentrations (mM)
$CaCl_2 \cdot 6H_2O$	500.00	0/5/10
$NaHCO_3$	400.00	5/25/50
$Na_2SiO_3 \cdot 9H_2O$	422.24	100
$Al(NO_3)_3 \cdot 9H_2O$	50.00	5
$UO_2(NO_3)_2 \cdot 6H_2O$	210.06	2.1 (500 ppm U)
5% NH_3 in N_2 (gas)	Bubbled into solution until pH ≈ 11	

The procedure began with preparation of concentrated solutions of $NaHCO_3$, Na_2SiO_3, and $Al(NO_3)_3$ combined in a 50-mL vial to form the base of the various synthetic pore water solutions. The base solution was then pH adjusted using nitric acid to reach a value of about 8, consistent with the pH of pore water in the Hanford Site vadose zone. Next, the synthetic pore water solutions were bubbled with ammonia gas until theyreached a treatment pH range of approximately 11. After following this step, the base solutions were broken up into 10-mL aliquots in 15-mL vials with caps perforated to allow some air exchange. The final components, $CaCl_2$ and $UO_2(NO_3)_2$, were added in small volumes of highly concentrated solutions in order to reach desired concentrations when diluted. The added concentration of uranium was 500 ppm in these samples. The synthetic pore water pH was monitored as the samples re-established the pre-treatment pH range through the partitioning and liberation of the dissolved NH_3 gas. The change in pH was very slow initially, dropping by less than 0.5 in the first week. After three weeks of slow change, the samples were transferred to an orbital shaker and agitated gently for a fourth week before reaching the desired post-treatment pH range of 8-9. The solid precipitate phase and supernatant were separated by vacuum filtration using disposable 0.22 µm nitrocellulose filters. The collected filtered precipitates were dried at 30°C over 3 days while the supernatant filtrates and rinse solutions were labeled and stored for further analysis.

In order to prepare for electron microprobe analysis (EPMA), sample precipitates were cold-mounted in epoxy. This involved preparing 1-inch cylindrical epoxy molds which had ¼" holes drilled into their centers (Figure 20a). Promising samples, selected based on the results of prior analysis (Table 14), were crushed and mixed with small amounts of epoxy before being poured into the hole of the cured molds (Figure 20b). Samples then spent 5 minutes in a vacuum chamber at 25 in. Hg to evacuate any air bubbles before curing over 24 hours.

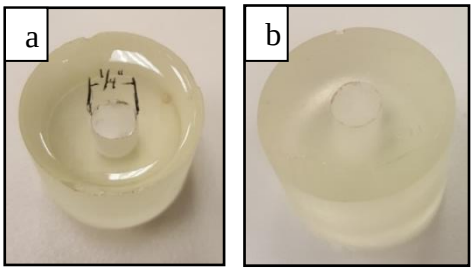

Figure 20. Epoxy mold (a) before and (b) after filling with resin + sample. mixture.

Table 14. Samples Elected for Epoxy Fixing and Analysis

Sample Labels		Key Variables
05-00A	05-00B	5 mM HCO_3^- and no Ca^{2+}
05-10A	05-10B	5 mM HCO_3^- and 10 mM Ca^{2+}
50-00A	50-00B	50 mM HCO_3^- and no Ca^{2+}
50-10A	50-10B	50 mM HCO_3^- and 10 mM Ca^{2+}

The eight cold-mounted in epoxy samples selected for electron microprobe analysis were shipped to collaborators at Pacific Northwest National Laboratory for cutting, grinding, and polishing steps which require specialized rad-sample-compatible equipment. The EPMA analysis and mapping of elements associated with uranium on the sample surface were initiated once cut and polished samples were received back at FIU.

The EPMA analysis and mapping of elements associated with uranium on the sample surface provided visual comparisons of the elemental associations present in the polished surfaces of uranium-bearing samples through high spatial resolution elemental analysis. A JEOL 8900R Superprobe equipped with 5 two-crystal WDS spectrometers and a single EDS-UTW detector was used to simultaneously detect multiple elements as the beam rastered across the sample surface. Prior to analysis, the polished samples were carbon coated and connected by copper tape to the aluminum sample holder to facilitate electrical conductivity during analysis. The instrument settings included a 20.0kV accelerating voltage, 5-10 micron spot size, and a 20 ms dwell time. For the majority of samples, an accumulation of 5 scans were used to create a comprehensive map for each targeted element (Figure 21).

In the micrograph, the elemental distribution maps present the abundance of silica across the entirety of the sample surface (Figure 21). The map for uranium, the analyte of particular interest in this study, shows that it is present at a quantity and distribution that aligns well with that of silica. The relationship between these distribution maps could signify the presence of a uranyl-silicate form, which is consistent with interpretations of sequential extraction analysis and predictive speciation modeling results. The role of aluminum is unclear in this comparative analysis. Though its distribution is similar to that of the more significant contributors, the peak areas of aluminum concentrations do not appear to align with distinctive peaks or valleys in the other targeted elements. Unlike other elements, sodium has a meager presence throughout the bulk of the analyzed area with some pockets of high concentration.

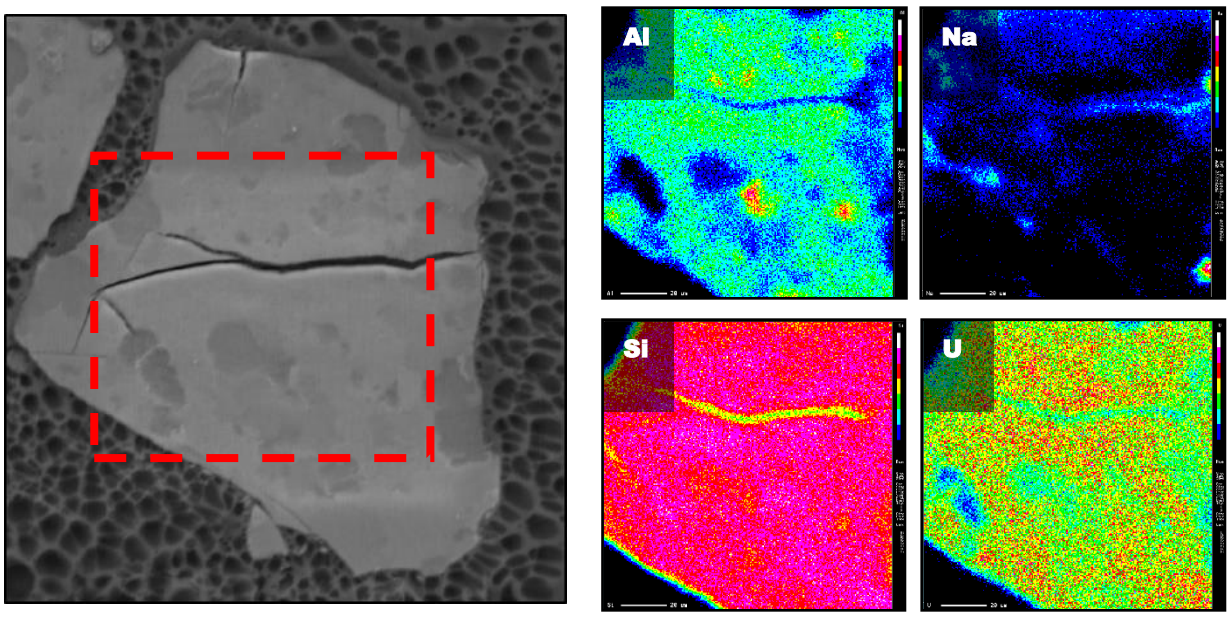

Figure 21. Sample micrograph and corresponding elemental maps. Ca-free sample prepared with 500 ppm U(VI), 100 mM Si, 5 mM Al, and 5 mM HCO_3

In the exhibited sample (Figure 22) prepared with 500 ppm U(VI), 100 mM Si, 5 mM Al, 5 mM HCO_3 and 10mM Ca, the elemental distribution maps of Si, Ca, Na, Al, and U were similar to the distribution presented on Figure 21, showing the abundance of silica across the entirety of the sample surface. The map for uranium shows that it is present at a quantity and distribution that aligns well with that of silica. The relationship between these distribution maps could signify the presence of a uranyl-silicate form. Sodium is aligned well with areas of Si and U presence with some pockets of high concentration. This is consistent with the interpretation of sequential extraction analyses results which suggest the presence of uranyl-silicate in the sample compositions, as well as predictive speciation modeling results for sodium boltwoodite solid phases. Aluminum is aligned well with areas higher in Si content, which could validate the formation of aluminosilicate minerals that is consistent with speciation modeling predictions.

In the sample prepared with 50mM HCO_3 and 10mM Ca, the elemental distribution maps present the abundance of silica across the entire sample surface (Figure 23, Figure 24 and Figure 25). The uranium map aligns well with silica. The formation of calcium carbonate solids is shown on the Ca map and its distribution is consistent with maps of other elements. Magnification of calcium carbonate particle locations on the U maps showed presence of uranium (blue dots) incorporated in calcium carbonate particles; however, the concentration of U in calcium carbonate is much lower compared to the rest of the sample. The Si map also showed that calcium carbonate granules have some coating, and the distribution of Si coincides with uranium allocations but at much lower concentrations for both elements compared to the rest of the sample. This might confirm the formation of calcium uranium silicate phases around the surface of the calcium carbonate granules. Similar to previous samples, aluminum is aligned well with areas higher in Si content suggesting the formation of aluminosilicates.

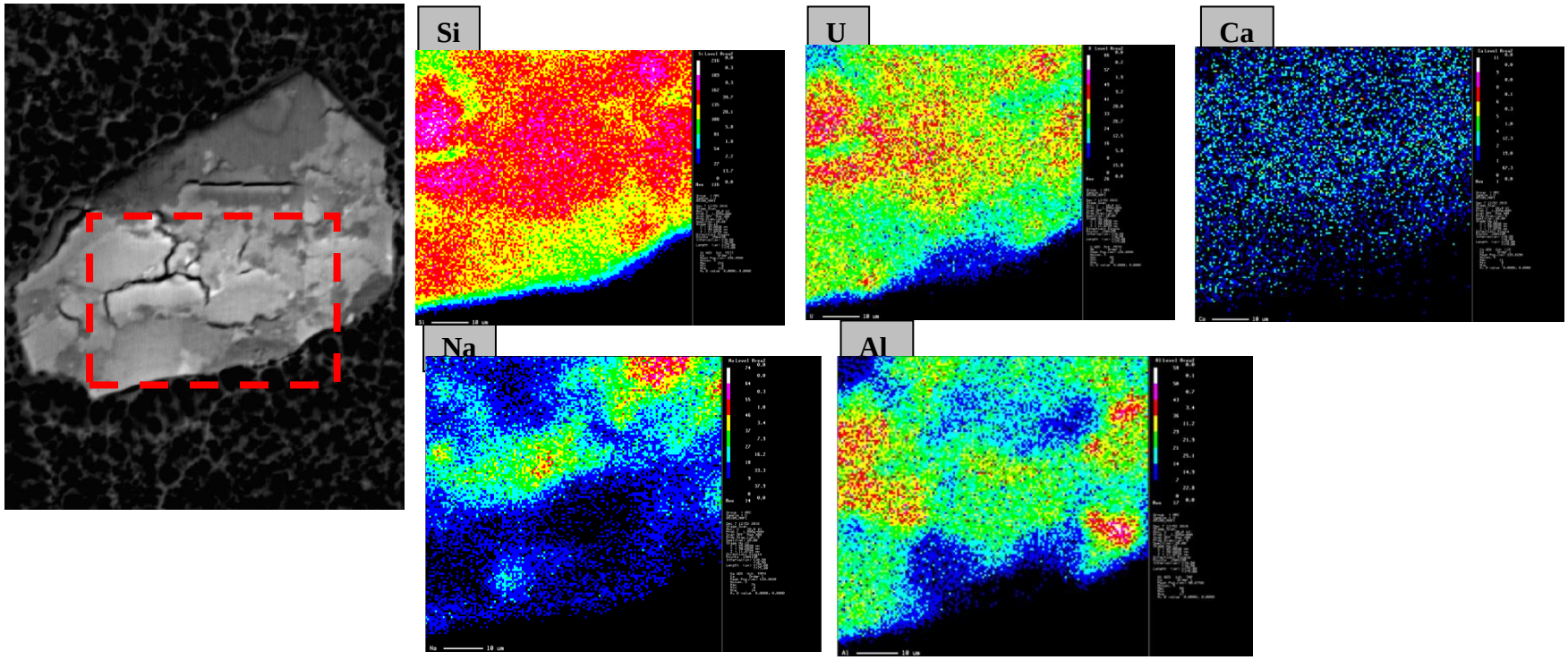

Figure 22. EPMA micrograph and corresponding elemental maps. Sample included 500 ppm U(VI), 100 mM Si, 5 mM Al, 5 mM HCO_3 and 10mM Ca.

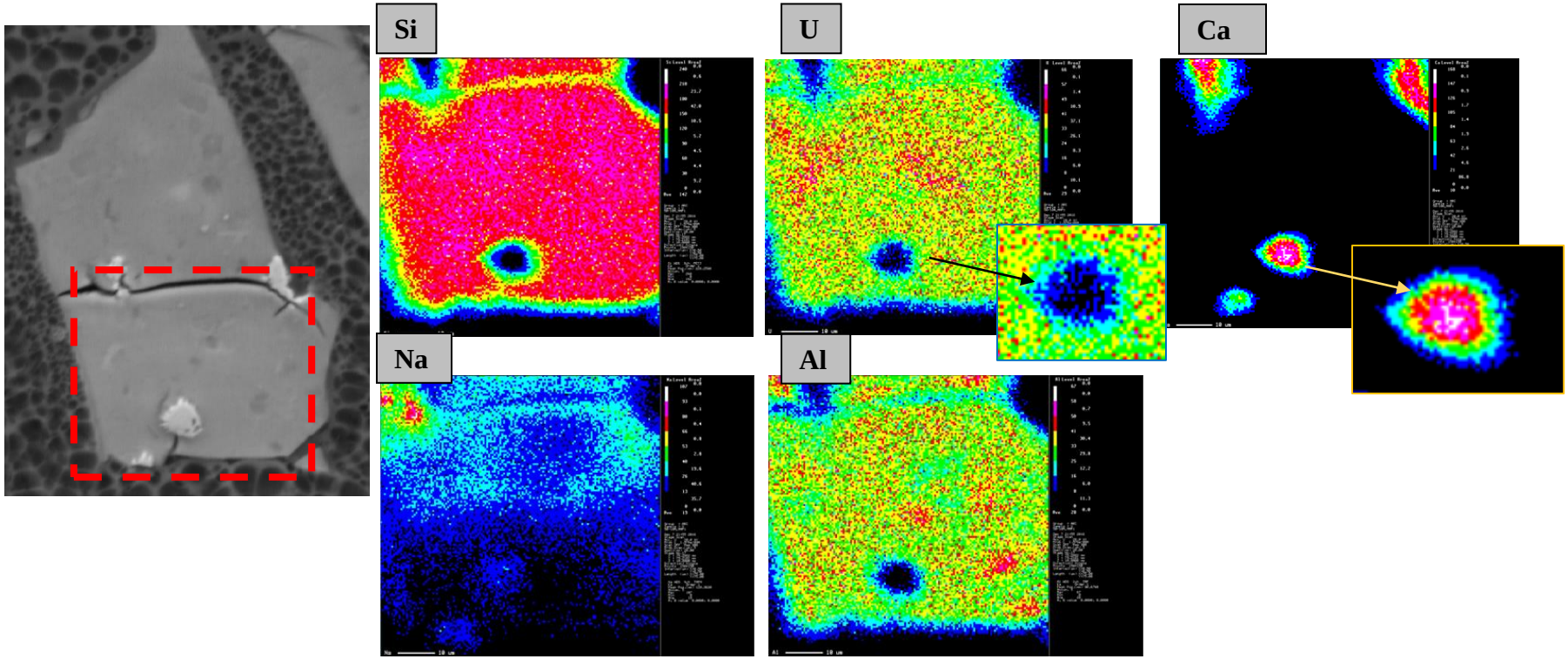

Figure 23. EPMA micrograph and corresponding elemental maps. This sample included 500 ppm U(VI), 100 mM Si, 5 mM Al, 50 mM HCO_3 and 10mM Ca.

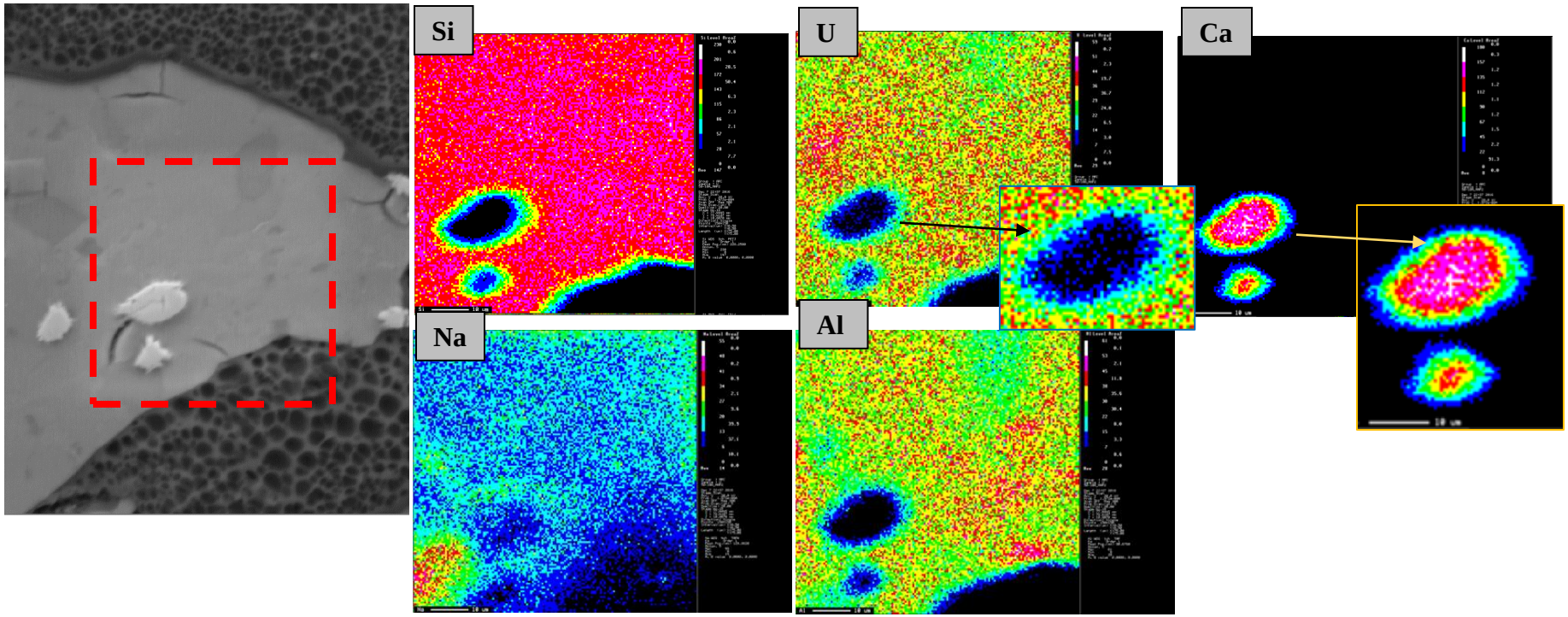

Figure 24. EPMA micrograph and corresponding elemental maps. This sample was prepared with 500 ppm U(VI), 100 mM Si, 5 mM Al, 50 mM HCO_3 and 10mM Ca in the composition.

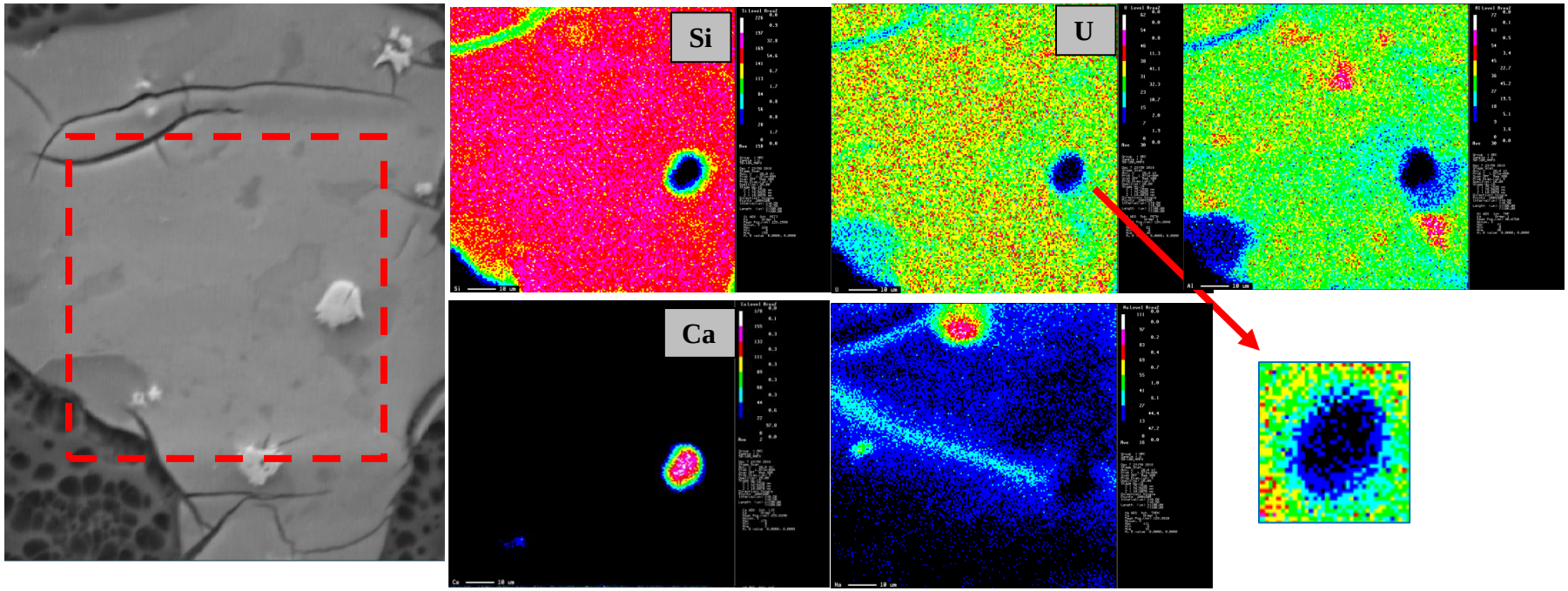

Figure 25. EPMA micrograph and corresponding elemental maps. This sample was prepared with 500 ppm U(VI), 100 mM Si, 5 mM Al, 50 mM HCO_3 and 10mM Ca in the composition.

Subtask 1.1: Future Work

The aim of this task is to understand the processes controlling U as the system returns to a neutral pH following NH_3 gas treatment. U will likely be adsorbed to mineral phases, co-precipitated with calcite, or complexed in the aqueous phase at high pH at low concentrations. At high concentrations of U, boltwoodites have formed prior to remediation following releases in Hanford sediments (Szecsody et al., 2010), but these will not be the major focus of this work as they are relatively insoluble compared to other phases of U present in the subsurface. However, the complex co-precipitation and coating processes immobilizing aqueous, adsorbed, and calcite-associated U which occur as the system returns to neutral pH must be understood. Year 8 will focus on understanding the dominant co-precipitation and coating processes occurring during and after base treatment via solid phase characterization and mineral dissolution experiments. This task will conduct laboratory experiments and modeling to identify the processes leading to formation of insoluble precipitates in the presence and absence of calcite-forming conditions. Through this work, we will better understand the formation and stability of precipitates formed under controlled conditions following ammonia gas injection including (1) coating of adsorbed U, (2) coating and/or dissolution of calcite-associated U, and (3) co-precipitation of aqueous U with dissolved cations from phyllosilicate minerals as the system returns to neutral pH. The focus for FIU Year 8 will be solid phase characterization including but not limited to TEM, SEM-EDS, EMPA, BET, XRD, and FTIR.

Subtask 1.1: Acknowledgements

Funding for this research was provided by U.S. DOE Cooperative Agreement DE-EM0000598. We truly appreciate Drs. Jim Szecsody and Nik Qafoku for their invaluable feedback in the interpretation of the data collected.

Subtask 1.1: References

Iler, R. K. (1979) The chemistry of silica: solubility, polymerization, colloid and surface properties, and biochemistry. *Canada: John Wiley &Sons Inc*.

Katsenovich, Y. P., C. Cardona, R. Lapierre, J. Szecsody & L. E. Lagos (2016) The effect of Si and Al concentrations on the removal of U (VI) in the alkaline conditions created by NH 3 gas. *Applied Geochemistry,* 73**,** 109-117.

Qafoku, N. P., C. C. Ainsworth, J. E. Szecsody & O. S. Qafoku (2004) Transport-controlled kinetics of dissolution and precipitation in the sediments under alkaline and saline conditions. *Geochimica et Cosmochimica Acta,* 68**,** 2981-2995.

Smith, S. C. & J. E. Szecsody (2011) Influence of contact time on the extraction of 233uranyl spike and contaminant uranium from Hanford Site sediment. *Radiochimica Acta International journal for chemical aspects of nuclear science and technology,* 99**,** 693-704.

Szecsody, J. E., M. J. Truex, M. J. Zhong, T. C. Johnson, N. P. Qafoku, M. D. Williams, W. J. Greenwood, E. L. Wallin, J. D. Bargar & D. K. Faurie (2012) Geochemical and Geophysical Changes during Ammonia Gas Treatment of Vadose Zone Sediments for Uranium Remediation. *Vadose Zone Journal***,** 1-13.

Subtask 1.2: Investigation on Microbial Meta-Autunite Interactions - Effect of Bicarbonate

Subtask 1.2: Introduction

Uranium contamination is a great environmental concern at many U.S. Department of Energy sites, including the Hanford Site 300 Area. Uranium mobility in the subsurface is affected by various factors such as the chemical composition of porewater and groundwater, soil mineralogy, and microorganisms that thrive under these conditions. Uranium exists in four oxidation states; the most important oxidation states are uranium (IV) and uranium (VI). Under oxidizing conditions, the highly soluble and stable uranyl ion, $UO2^{2+}$ dominates. However, in neutral or basic pH conditions, uranium undergoes hydrolysis in aqueous solutions and readily complexes with a wide variety of ligands such as carbonate, nitrate and phosphate. Carbonate anions are an important complexing agent for U(VI), forming stable and soluble negatively charged $UO_2(CO_3)_2^{2-}$ and $UO_2(CO_3)_3^{4-}$, as well as neutral uranyl-carbonate complexes such as UO_2CO_3 (Grenthe et al. 2004). The presence of carbonates clearly affects the dissolution of actinides and facilitates uranium desorption reactions from soil and sediments, thus increasing uranium mobility in natural waters (Langmuir 1997). These complexes have been identified in contaminated pore water at the Hanford Site and have been shown to inhibit the microbial reduction of U(VI) (Bernhard et al. 2001, Brooks and Murray 1981).

The addition of polyphosphate solutions is part of the selected remedy to decrease the concentration of soluble uranium in contaminated plumes. The polyphosphate solutions were prepared without calcium because there is sufficient available calcium in the sediments to react in-situ with the phosphate. The selection of this remedy was based on detailed investigations that demonstrated the effectiveness of the technology to sequester uranium in the subsurface (Wellman et al. 2008, Szecsody et al. 2012). The introduction of sodium polyphosphate into uranium-bearing saturated porous media results in the formation of uranyl phosphate solid phases (autunite) of general formula $X_{1\text{-}2}[(UO_2)(PO_4)]_{2\text{-}1}{\cdot}nH_2O$, where X is a monovalent or divalent cation. This remediation strategy resulted in a significant decline in uranium concentration compared to untreated sediments (Mehta et al. 2016, Szecsody et al. 2012, Mehta 2017).

The stability of the uranyl phosphate solids in the subsurface is a critical factor that allows for determining the long-term effectiveness of the sodium polyphosphate remediation strategy. The presence of soil bacteria can affect uranium mobility significantly. Bacteria, in an effort to obtain phosphorous, a vital nutrient for their metabolism, may dissolve uranyl-phosphate minerals, thus liberating uranium in the aqueous phase. In addition to the biological activity, the presence of bicarbonate ions seems to enhance the release of U(VI) into the aqueous phase (Gudavalli et al. 2013).

Water table fluctuations and multiple rise-and-fall cycles in the Colombia River created an oxic-anoxic interface in this region. Previous assessments of Hanford sediment samples collected from this area noted a decline in cultivable aerobic bacteria and suggested the presence of facultative anaerobic bacteria (Lin et al., 2012; Marshall et al., 2008). Therefore, understanding the role of facultative and anaerobic bacteria (e.g., *Shewanella*) as one of the factors affecting the stability of autunite solids is very important for designing a successful environmental remediation strategy.

Objectives

The objective of this research is to investigate the dissolution of synthetic and natural autunite mineral under reducing conditions by focusing on the bacterial strains of *Shewanella oneidensis* MR1 sp and microbial consortia enriched at PNNL from Hanford site sediments. This research will provide outlook better understanding of how different types of soil bacteria interact with meta-autunite in comparison with *Shewanella oneidensis* MR1 sp. Considering polyphosphate sequestration efforts that occurred in the 300 Area for the vadose zone (Szecsody et al. 2012) and some previous investigations on groundwater remediation for uranium (Wellman et al. 2008), this additional research is important to determine the long-term stability of the precipitated uranium phases.

Subtask 1.2: Methodology

1. Synthesis of sodium meta-autunite.

Synthetic sodium meta-autunite, Na $[UO_2\ PO_4]\ 3H_2O$, was synthesized by the direct precipitation method using uranyl nitrate, $UO_2(NO_3)_2\ 6H_2O$, obtained from International Bio-analytical Industries Inc. The experimental procedures followed the direct precipitation method described by Wellman et al. (2005) and modified from Vochten and Deliens (1980). The precipitation of Na-autunite was accomplished by mixing a uranyl nitrate solution and sodium phosphate dibasic solution, $Na_2HPO_4\ 7H_2O$, in a volumetric ratio of 1:7.5 while stirring at 70°C. The overall reaction is as follows:

$$Na_2HPO_4\,7H_2O + UO_2(NO_3)_2\,6H_2O \longrightarrow Na[UO_2PO_4]\,nH_2O + NaNO_3 + HNO_3$$

Heating was terminated after a yellowish green precipitate was formed, and stirring was continued until the solution returned to room temperature. The solids were cured for 24 hours without stirring followed by recovery from the solution using a disposable 0.45 µm filter. The crystals were washed with DI water heated to 70° C, followed by rinsing with isopropyl alcohol. The crystals were dried at room temperature until a constant weight was achieved. The synthesized autunite solids obtained by following the direct precipitation method were previously characterized by JSM-5900-LV low vacuum scanning electron microscope (SEM) at 15kV. The composition of the particles was analyzed using a Noran System Six Model 200SEM energy dispersive X-ray spectroscopy (EDS). The compositional analysis using EDS were used to calculate molar quantities of the elements. These calculations suggested that the chemical formula of the synthesized crystals is Na $[UO_2\ PO_4]$. The dried particles were then used for the dissolution experiments.

2. Bicarbonate media solution preparation

The media solution was prepared in 1 L of DIW buffered with 5.2 g of 0.02 M sodium-free HEPES buffer with pH adjusted to 7.3 with 1.0M NaOH. About 4.48 mL/L of sodium lactate ($C_3H_5NaO_3$, 60% w/w) was added to the solution to create a concentration of 24 mmol/L. The solution was divided into three 500-mL bottles and sterilized by autoclaving at 121°C, 15 psi for 15 min and cooled at room temperature. As the experiment is based on the investigation of bacteria interactions in the presence of different bicarbonate concentrations, potassium bicarbonate salt was added to two of the three autoclaved bottles to obtain 3 mM and 10 mM bicarbonate; the remaining bottle was kept bicarbonate-free. This accounts for a total of three concentrations of bicarbonate for the experiment tested. Next, the solutions were filter-sterilized

and the sterile bottles were purged with nitrogen gas and stored in the anaerobic chamber until the beginning of the experiment. Table 15 shows the composition of the media solutions.

Table 15. Composition of the sterile media solutions

0 mM HCO_3	**3 mM HCO_3**	**10 mM HCO_3**
5.2 g HEPES buffer (0.02 M)	5.2 g HEPES buffer (0.02 M)	5.2 g HEPES buffer (0.02 M)
4.48 mL sodium lactate (24 mmol/L)	4.48 mL sodium lactate (24 mmol/L)	4.48 mL sodium lactate (24 mmol/L)
	0.09912 g KCO_3	0.3304-g KCO_3

*pH was adjusted to 7.3 using sodium hydroxide

3. Shewanella oneidensis MR-1 growth conditions

Shewanella oneidensis MR1 strains were obtained from the Pacific Northwest National Laboratory (PNNL) and stored at −80°C in 25% glycerol prior to use. A starter culture was grown on sterile hard and liquid Luria-Bertani (LB) media prepared with 10.0 g of tryptone, 5.0 g of yeast extract, and 10.0 g of sodium chloride, with a pH of 7.0. Hard media required an addition of 15.0 g of agar. A fresh culture was grown in 15-mL tubes placed in the incubator at 30°C while being shaken at 100 rpm (C24KC refrigerated incubator shaker; New Brunswick Scientific). The total number of cells were counted by placing 10-uL into a glass hemocytometer (Fisher Scientific, Pittsburg, PA) or INCYTO C-Chip disposable hemocytometer (SKC America) and placing it under a microscope. Once the average cell count was obtained, it was multiplied by the dilution factor and the volume factor (10^4) in order to calculate the final concentration of cells per mL. The number of cells/mL in the stock suspension was used to estimate a desired volume (mL) of a bacterial suspension needed for the inoculation of each bottle. To account for viable bacteria, 10-uL from each test vial was uniformly spread on the sterile Petri dishes containing LB growth media mixed with 15 g/L of agar. Inoculated plates were kept inverted in an incubator at 30^{o}C. Viable microorganisms were calculated from the number of colony-forming units (CFU) found on a specific dilution.

4. Microbial consortia growth conditions

Twenty vials were prepared for each concentration of $KHCO_3$, totaling 60 biotic vials. Three vials from each set were left abiotic, which were sampled in parallel with the biotic samples by extracting 0.5-0.6 mL for each sampling event. After equilibration with the leaching solutions, the vials were inoculated with the bacteria consortia obtained from PNNL. The consortia culture enriched at PNNL was kept frozen at -80^{o}C in 50% glycerol and then grown on sterile, hard and liquid media prepared with 250 mg/L of tryptone, 500 mg/L of yeast extract, 0.024M of sodium lactate, 0.6 g/L $MgSO_4 \cdot 7H_2O$, and 0.07 g/L $CaCl_2 \cdot 2H_2O$ (TYL). Hard media required an addition of 15.0 g/L of agar. The concentration of sodium lactate in the growth media was the same as was included in the sterile media amended by bicarbonate to conduct the biodissolution experiments. The experimental vials and bottles with the media solutions amended with bicarbonate were kept in an anaerobic chamber filled with nitrogen gas for the entire duration of the experiment.

5. Autunite biodissolution experiments

The Na-autunite biodissolution experiments were performed by using 20-mL sacrificial glass scintillation vials. This approach was chosen to avoid possible microbial cross-contamination during sampling events. Each vial was filled with 19 mg of sodium autunite powder to provide a final U(VI) concentration of 4.4 mmol/L. For the biodissolution experiments using natural Ca-autunite mineral, the amount of autunite powder in each sample was 18 mg, providing a U(VI) concentration of 4.4 mmol/L. This concentration of uranium was chosen for comparison of the results with previous experiments. All prepared glass vials with autunite were covered with plastic caps and autoclaved for 15 min at 121ºC to ensure sterile conditions. Twenty vials were amended with 10 mL of sterile media solution at each bicarbonate concentrationconcentration (0, 3, and 10 mM $KHCO_3$) for a total of 60 vials. Two random samples of 10-uL were taken from the sacrificial vials and spread on agar plates to ensure no contamination was present. No growth was observed on these plates; so, the planned sampling schedule continued. Three control samples were taken before the solutions were amended with the experimental bacteria, *Shewanella* MRI. After autunite equilibration, the samples were inoculated to obtain an initial cell density of 10^6 cells/mL. The inoculum volume of 49-µL was determined based on the cell density in the culture-growing media, calculated by means of hemocytometer under a light microscope. Prior to inoculation growth, the media was washed with oxygen-free DIW and centrifuged to remove organic media components. In addition, abiotic control vials were kept for each bicarbonate concentration and sampled in parallel with the experimental vials. After inoculation, the samples were allowed to sit for a week before measurements began. Samples in the anaerobic glove box were shaken frequently. The samples were sacrificed at specific time intervals according to the sampling schedule. The interval of time between sampling events after the media equilibrated with the autunite and bacteria inoculation was about 3-4 days. The total number of sacrificial experimental vials for the duration of the experiment was calculated as 60. Experimental and control vials with the media solutions amended with bicarbonate were kept in an anaerobic glove box filled with nitrogen gas for the entire duration of the experiment.

6. Sampling and elemental analysis

Sampling was done in the anaerobic glove box by using a 1-mL syringe to extract 0.5-mL aliquots of solution and filtered with a 0.2-µm filter to remove any autunite particles that could interfere with uranium measurements. The solutions were filtered into a 1.5-mL brown glass sampler vial and acidified before storing at 4°C in the laboratory refrigerator for future chemical analysis. This was done for each control and experimental sample amended with bicarbonate. Since the presence of organic content in the solutions can interfere with uranium analysis, the samples collected during the experiments were pre-processed by wet and dry ashing procedures. About 0.150 mL was taken from each aliquot and placed into a clean 20 mL sacrificial vial. Wet digestion was performed by the addition of 500 µL of concentrated nitric acid (HNO_3) and 500 µL of concentrated hydrogen peroxide (H_2O_2) to each vial; the vials were placed on a heating plate until full evaporation was achieved and a white solid residue was acquired. Occasionally, some samples turned yellow while ashing; 0.5 mL of peroxide was added to these samples and the process was continued until a white precipitate was obtained. The dry samples were placed in a furnace preheated to 450°C for 15 min and then allowed to cool at room temperature. Finally, the precipitates obtained in the drying step were dissolved in 1 mL of 2 mol/L nitric acid and analyzed by means of the KPA instrument to determine uranium concentrations released into the aqueous phase as a function of time. In addition, calcium, sodium and phosphorous were

determined by means of inductively coupled plasma - optical emission spectroscopy (ICP-OES 7300 Optima, Perkin Elmer) using calcium and phosphorous standards (Spex CertiPrep).

Cell counting of the culture before being used for inoculation was conducted by means of a glass hemocytometer using a light microscope. The concentration of cells in the inoculum was constant on the level of log 6 cells/mL for both experiments with Na-autunite and Ca-autunite. The samples were inoculated after the uranium concentration reached equilibrium. Inoculated samples were sacrificed to collect aliquots for various analysis twice a week according to the sampling schedule. Aliquots were also isolated for the determination of cell viability on agar plates. The plates were incubated at 30°C to count viable colonies. Sampling also included the collection of cell suspensions which are currently being stored at -20°C for future protein content analysis by means of a bicinchoninic acid assay. The oxidative-reduction potential and the pH were recorded inside the glove box for each sample at the beginning of a sampling event.

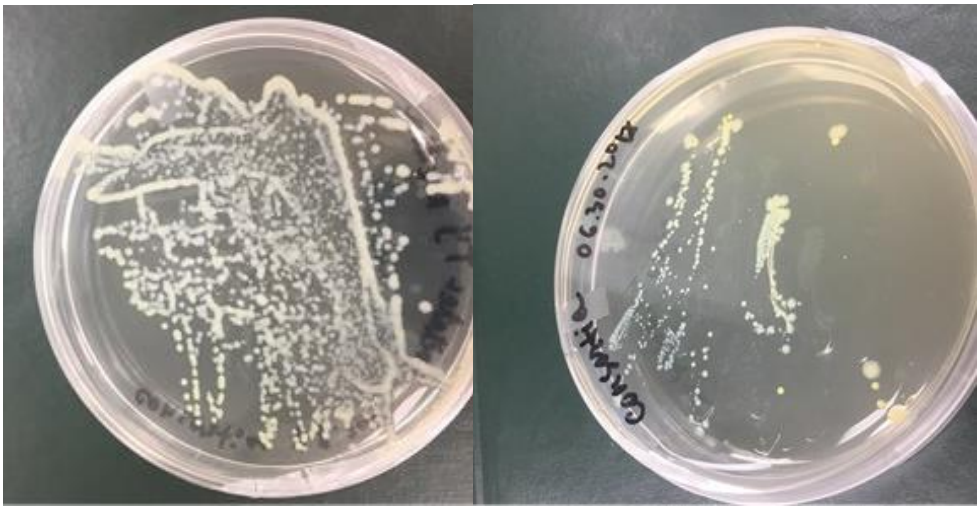

Figure 26. Consortia-based culture enriched at PNNL growing at TYL media (left) and LB media (right). Both cultures look very uniform with yellowish-white color colonies; however, culture grown on LB media has in addition several yellowish colonies.

Some autunite samples were prepared for SEM-EDS analysis. The samples were filtered and then treated with 4 ml of 2% glutaraldehyde in 0.1 M HEPES at 4^{o}C for 2h. The samples were then centrifuged, the supernatant was decanted and the material was washed with 4 ml of 0.05 M HEPES for 10 min. After discarding the supernatant, the material was "dehydrated" in 4 consecutive steps: treatment with 35%, 70%, 90% and 100% of ethanol for 10 min at room temperature under a biosafety cabinet.

Subtask 1.2: Results and Discussion

1. Elemental analysis for the dissolution of synthetic Na-autunite using Shewanella oneidensis MR1 cells

Figure 27 presents the concentrations of uranium measured by means of KPA in bicarbonate-free samples and in samples amended with 3 mM and 10 mM of bicarbonate. In the case of bicarbonate-free samples eas well as the samples amended with 3 mM of bicarbonate, the amount of uranium released in the aqueous phase did not significantly change, indicating that *Shewanella oneidensis* does not contribute to the release of uranium into the aqueous phase. For these two concentrations, there was an initial drop in uranium concentration within the first 10

days and then it stabilized for the remainder of the sampling period. The 10 mM bicarbonate samples showed an initial increase in uranium concentration before decreasing and stabilizing for the rest of the sampling period. All initial drops and increases in uranium occurred before inoculation took place. After inoculation, all samples at all concentrations showed stabilization.

Figure 28 and Figure 29 show the change in Na and P content amongst all sets of bicarbonate concentrations. After inoculation, there were increases in both calcium and phosphorus concentrations. About 40 after beginning the experiments, the uranium concentrations in the samples began to stabilize with only small fluctuations from their initial concentrations. The initial increase in phosphorus and calcium was not instantaneous and happened over a period of about 15 days.

Concentrations of sodium and phosphorus increased after microbial inoculation of the sacrificial samples and then gradually decreased. There was no significant difference in sodium concentrations between the 0 mM, 3 mM and 10 mM bicarbonate concentrations tested. The same is true for phosphorus concentrations. However, uranium concentrations for the 0 mM and 3 mM bicarbonate samples stayed relatively similar from the first day of inoculation whilethe 10 mM bicarbonate samples slightly increased after about 10 days but then stabilized close to the original concentration. The concentrations determined during sample analysis do not correspond to an ideal empirical formula of $Na[UO_2PO_4]$ as 1:1:1 for Na, P and U. Data results suggest that the liberation of U(VI) from sodium autunite influences incongruent reactions to release Na and P from the mineral structure.

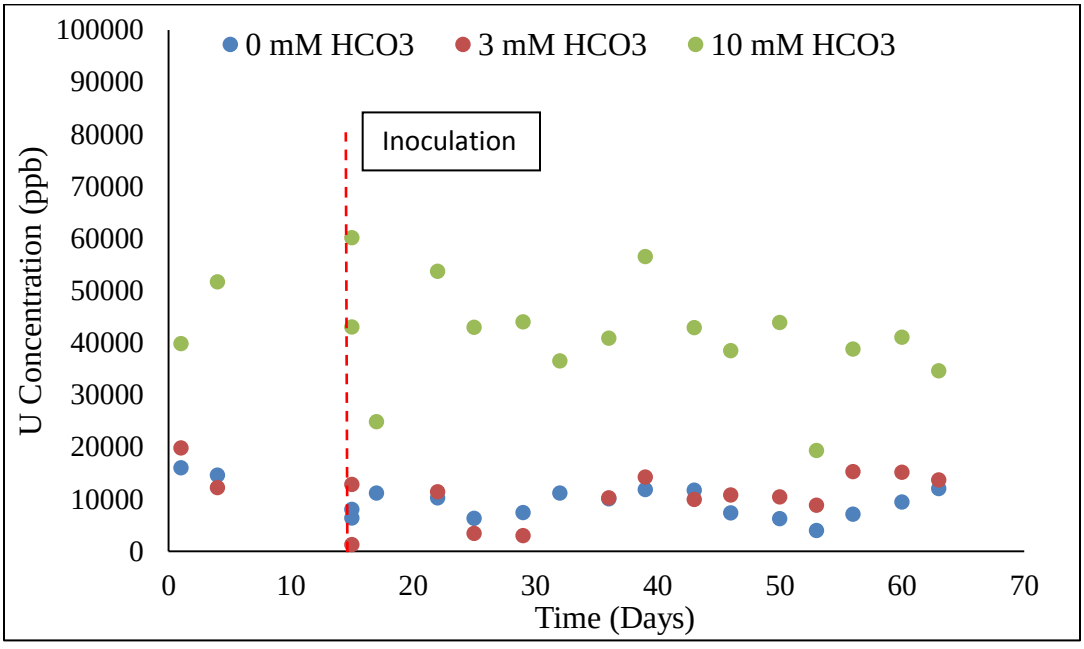

Figure 27. Uranium concentration as a function of time.

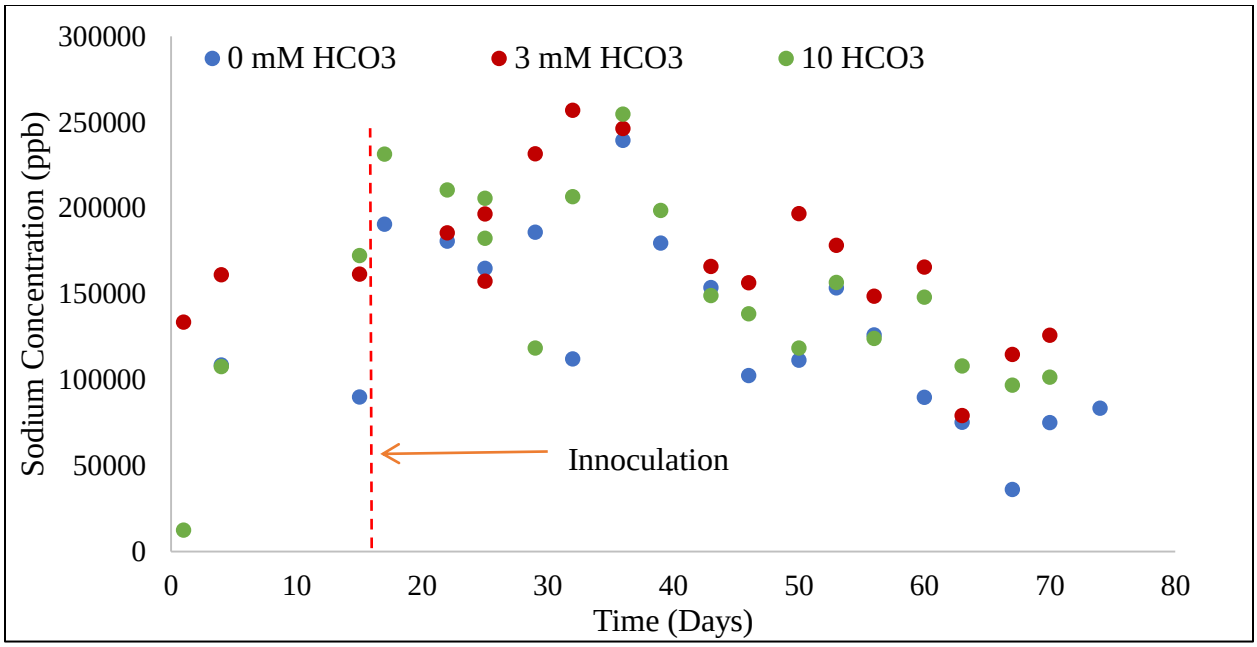

Figure 28. Concentrations of sodium released into the aqueous phase as a function of time under different HCO_3 concentrations.

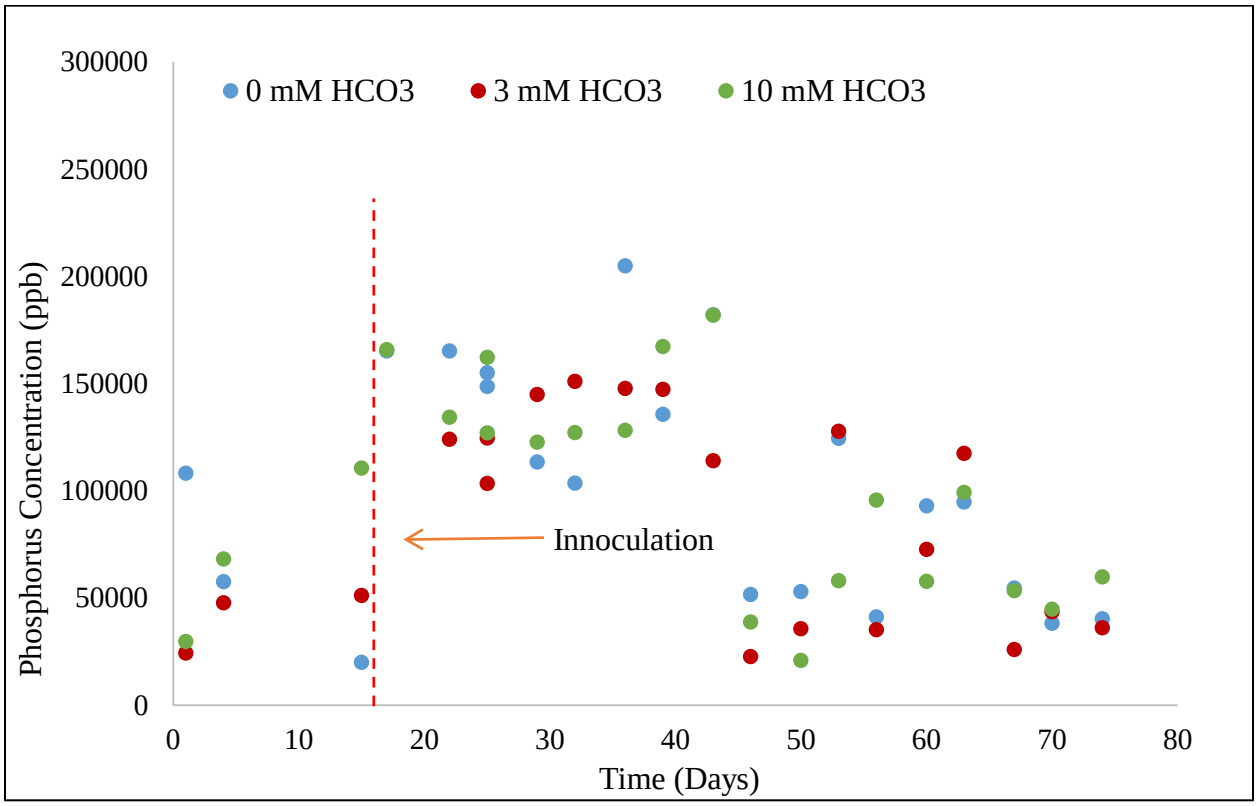

Figure 29. Concentrations of phosphorus released into the aqueous phase as a function of time under different HCO_3 concentrations.

2. Cell density and cell viability per plates

Direct visual cell counting using a hemocytometer under a light microscope, combined with a cell viability analysis using the spread plate method, was conducted for each sampling event. The initial inoculation cell density was 10^6 cells/mL (log 6 cells/mL) for all biotic samples. Cell viability, determined via counts of colony forming units (CFU/mL), was compared to the cell density obtained via direct cell counting. Figure 30 shows the log total of viable cells obtained from counting the number of CFU on plated samples. The total number of viable cells stayed relatively constant throughout the entire sampling period. Figure 31 shows the log total cells determined from counting about 10 uL samples under a microscope. The number of total cells is almost twice as high as the total number of viable cells, indicating that half of the microbe population present in the samples is not viable. The highest cell viability was observed in the presence of 10 mM of HCO_3. The log cell density variations for each bicarbonate concentration can be seen below in Figure 32 - Figure 34.

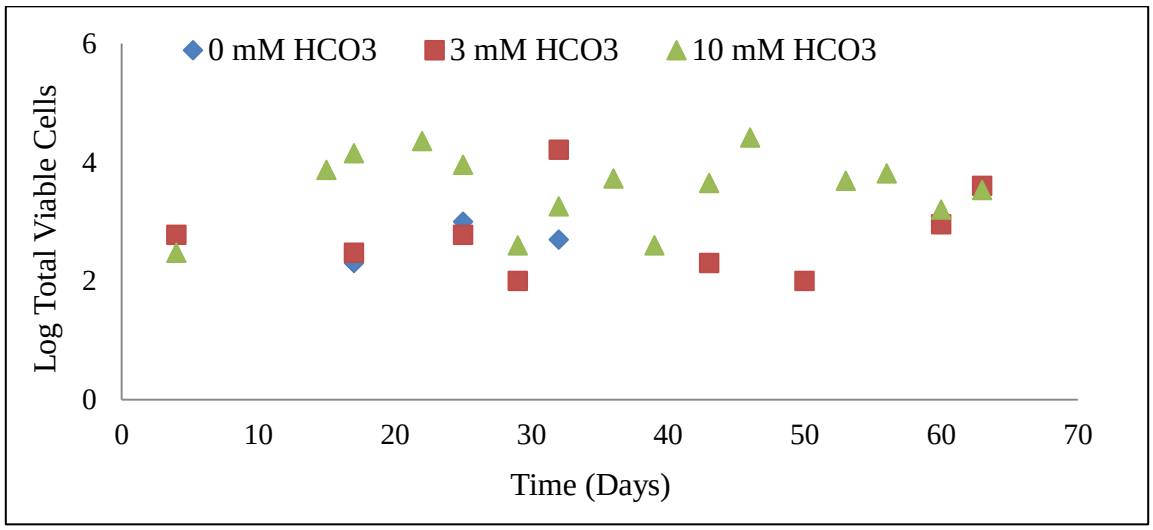

Figure 30. Total viable cells counted from plates

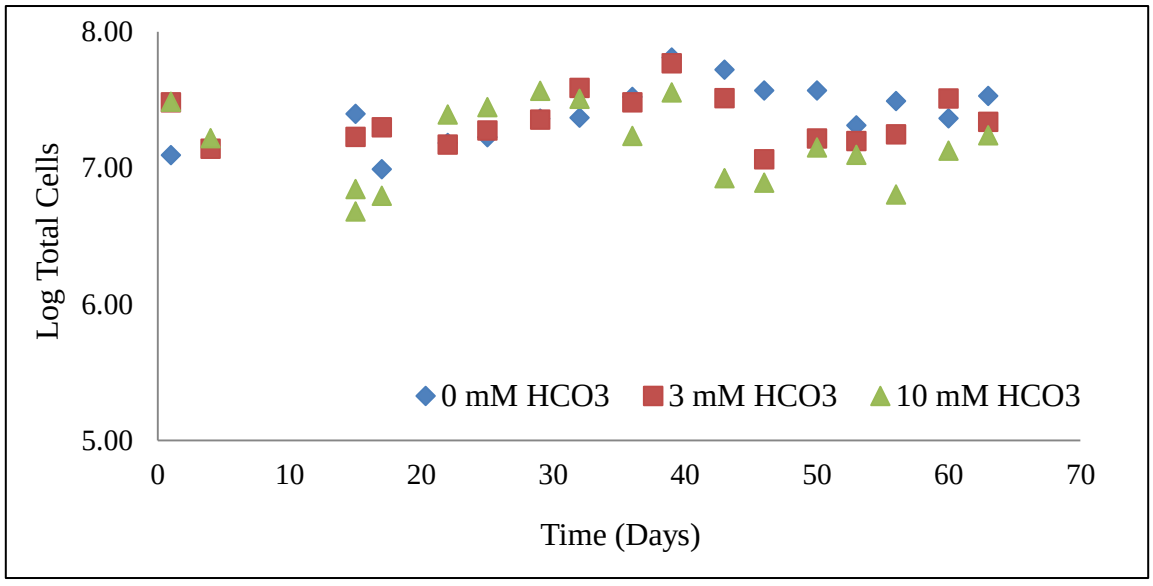

Figure 31. Total cells measured from microscope

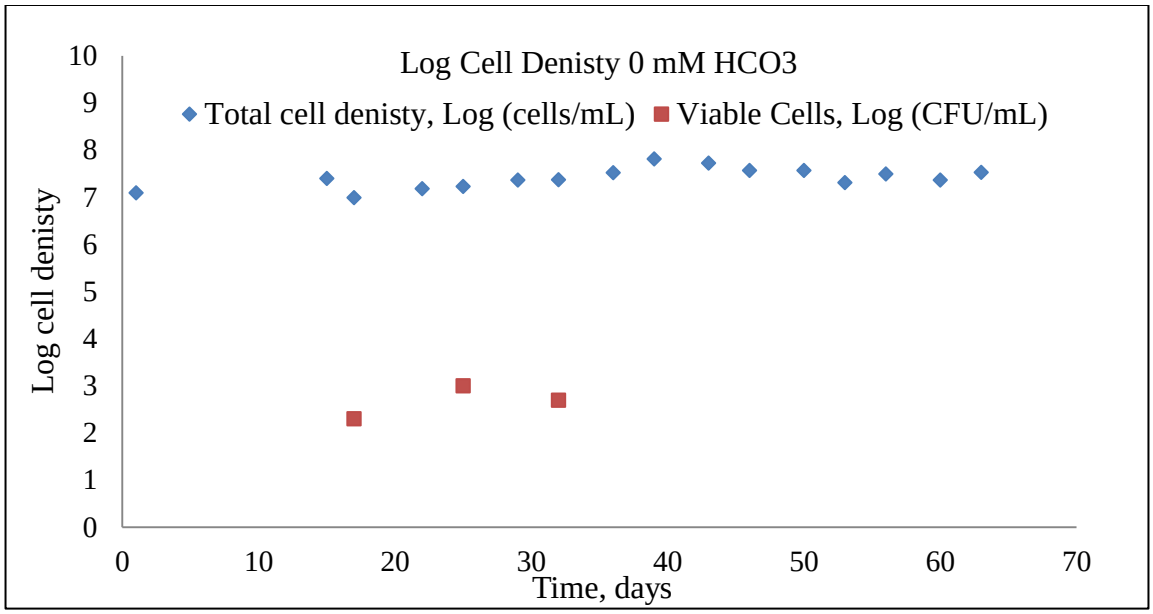

Figure 32. Log cell density of 0 mM HCO_3 samples

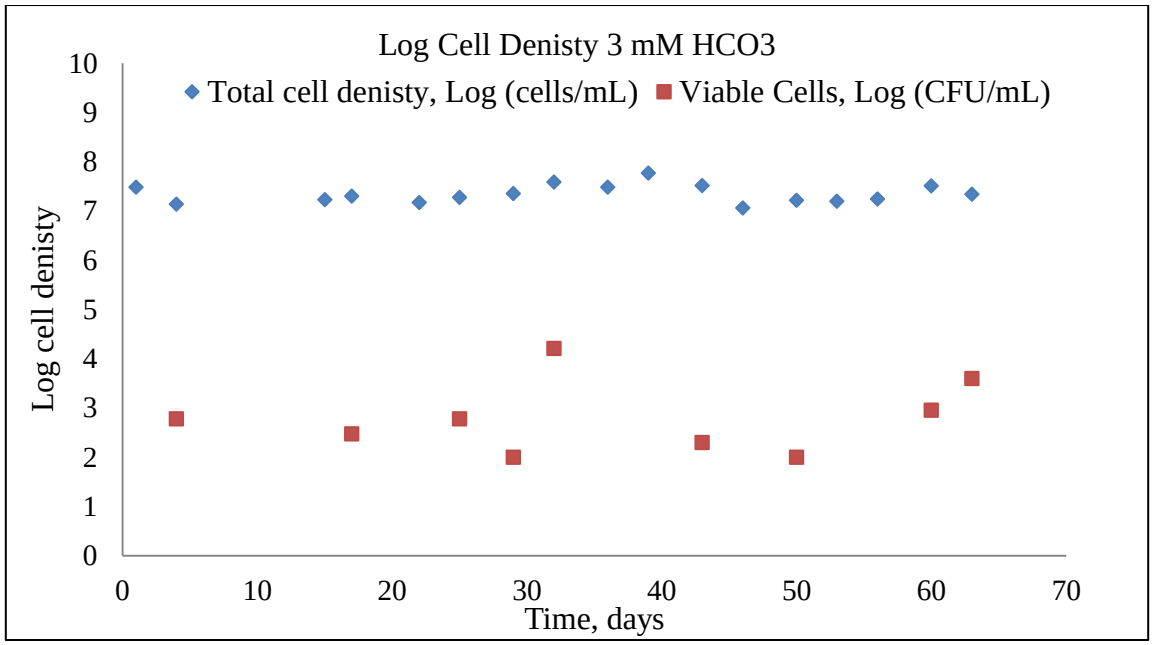

Figure 33. Log cell density of 3 mM HCO_3 samples

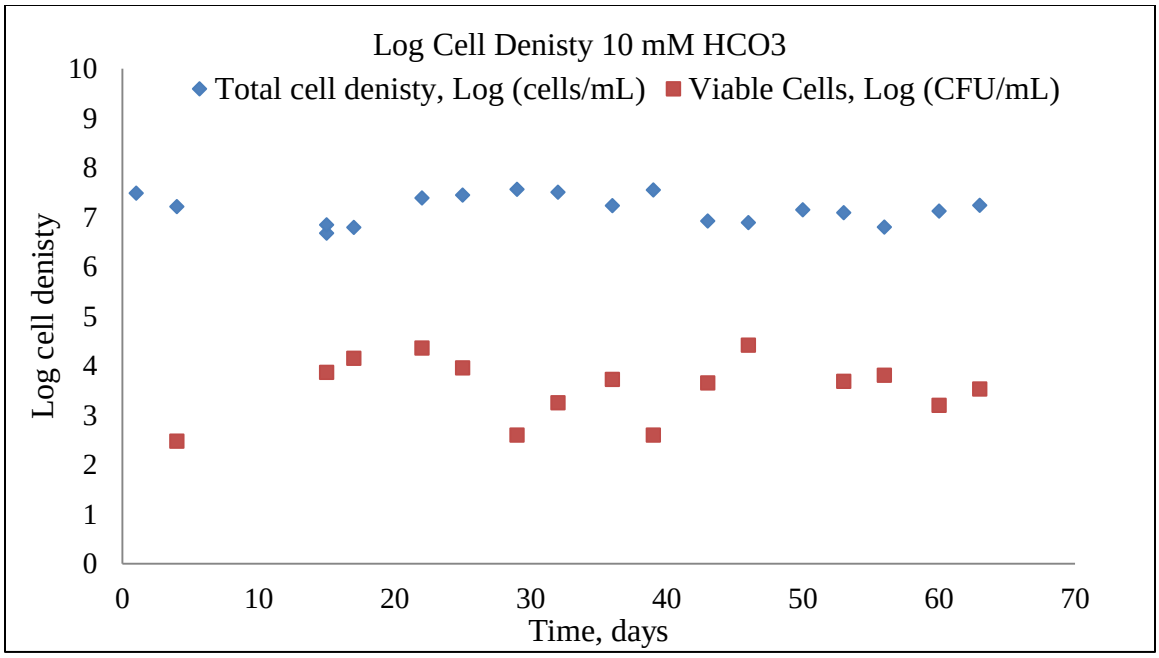

Figure 34. Log cell density of 10 mM HCO_3 Sasples

FIU is currently working on SEM/EDS analysis of post-treated synthetic autunite particles and these results will be included in the final technical report for this research.

3. SEM/EDS analysis

The main goal of the microscopy analysis was to evaluate changes in the autunite solids surface morphology in bicarbonate media inoculated with *Shewanella* cells. SEM images demonstrated bacterial attachment to the surface of the radioactive synthetic autunite mineral and suggested that Na-autunite mineral surface colonization by bacteria cells tended to increase with bicarbonate concentration (Figure 35). Bacteria colonization also led to the cells adhesion on the solid surface via special cell surface structures, fibrils, forming links between the cell and the solid surface. Images also showed greater destruction of autunite as bicarbonate concentration increased in the solution.

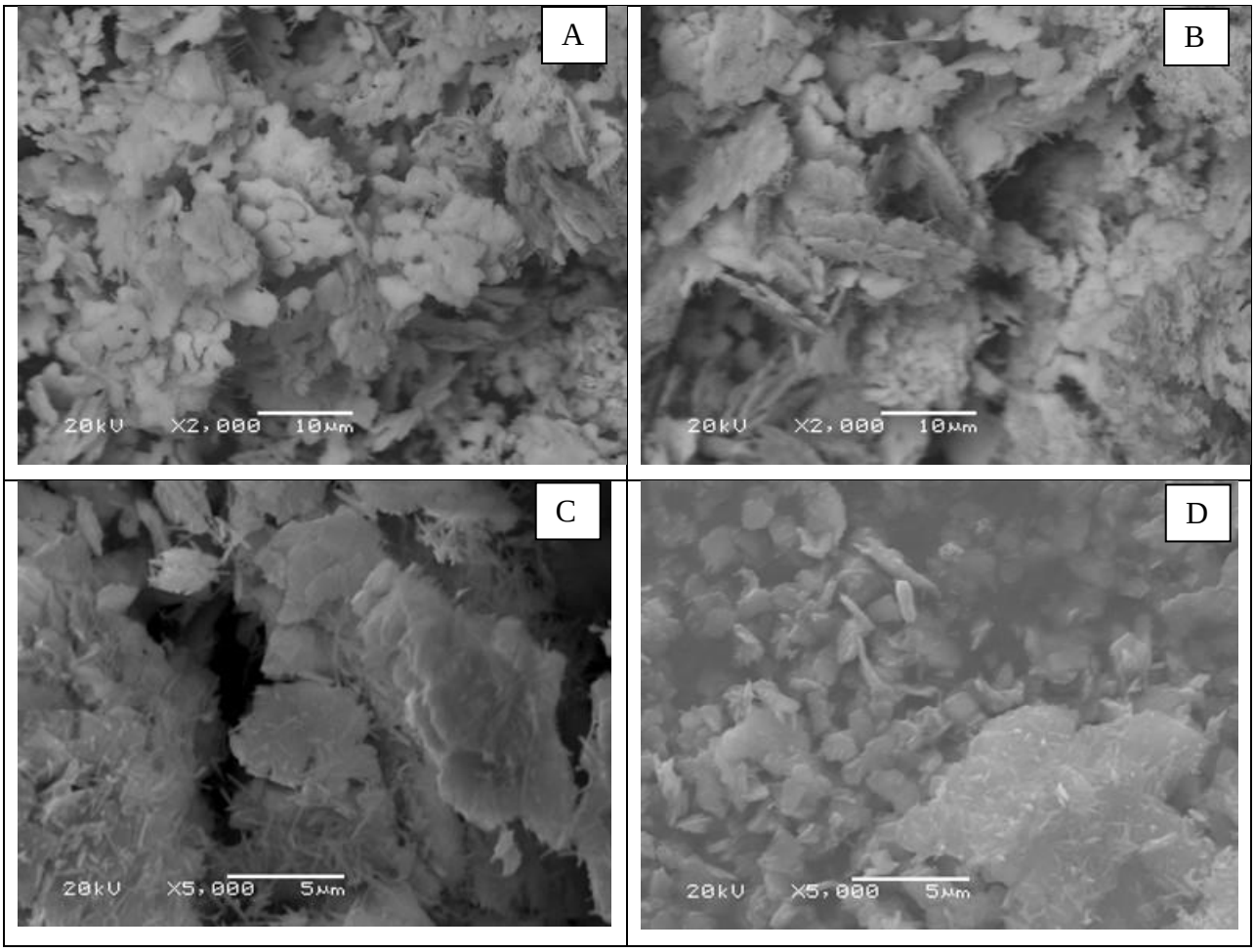

Figure 35. Scanning microscope images for post-treated synthetic autunite samples in the presence of *Shewanella* cells. Post-treated Na- autunite samples in the presence of 0 mM bicarbonate concentrations (A and B); Post-treated Na- autunite samples in the presence of 3 mM bicarbonate (C); Post-treated Na-autunite samples in the presence of 10 mM bicarbonate (D)

4. Elemental analysis for the dissolution of Natural Ca-autunite using microbial consortia

FIU currently finished sampling of sacrificial vials and prepared samples via dry and wet ashing

FIU completed sampling of the sacrificial vials and prepared samples via dry and wet ashing procedures for uranium analysis via the KPA instrument as well as for P and Ca analysis via ICP-OES. In addition, the samples were prepared for SEM/EDS and protein analysis via bicinchoninic acid assay. These results will be available in the final technical report for this research.

The results showed that the viability of the microbial consortia was in the range of 7.1-7.8 log CFU cell/mL (Figure 38), which is much higher than the experiment with *Shewanella* cells, which showed values in the range of 2-4.4 log CFU cell/mL (Figure 38).

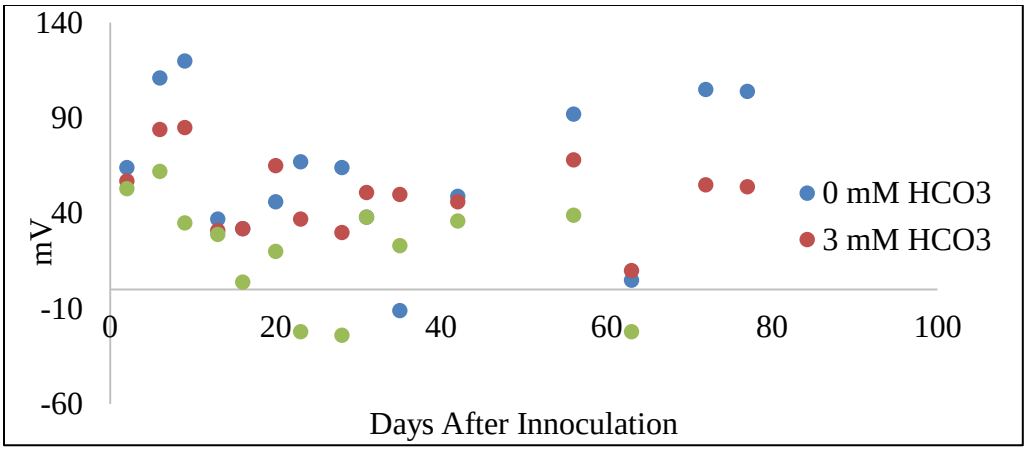

Figure 36. Oxidative-Reduction Potential (ORP) of samples

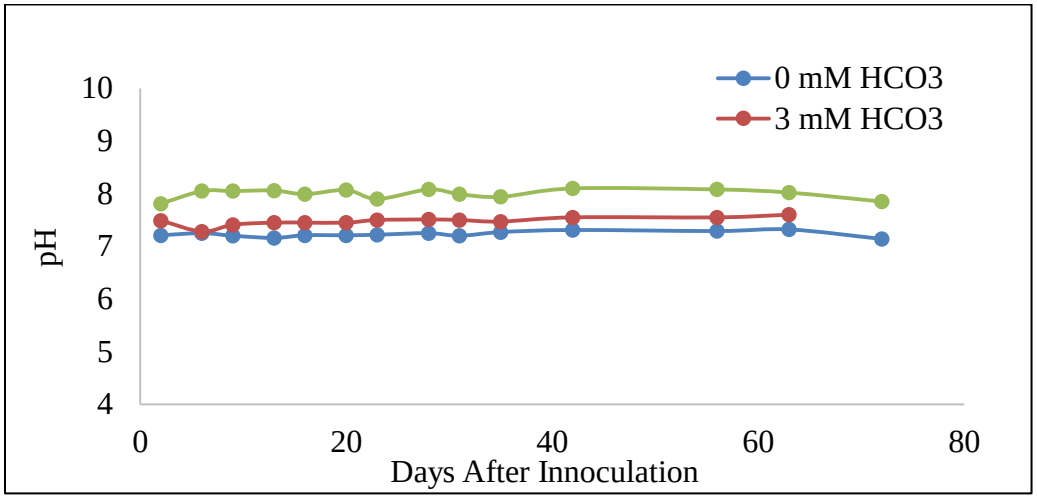

Figure 37. pH measurements

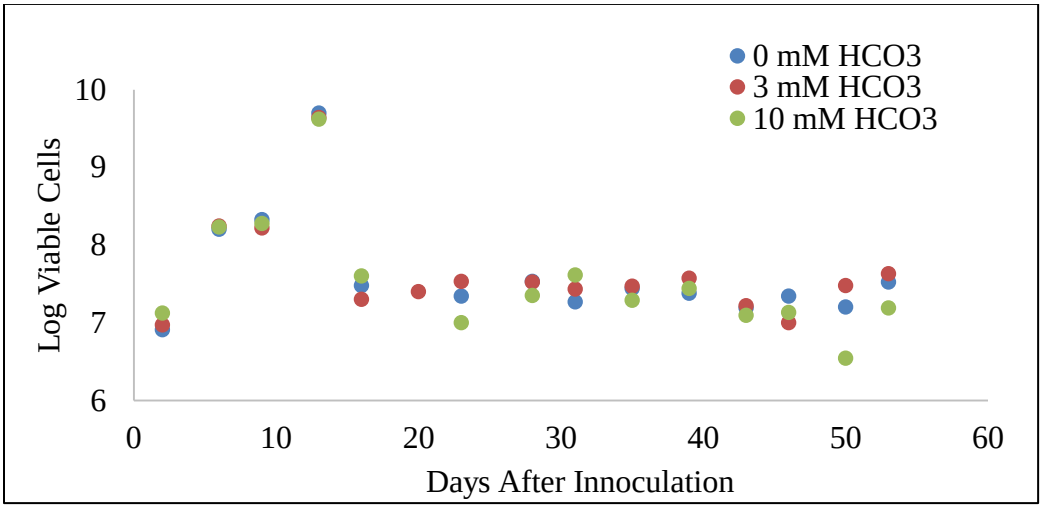

Figure 38. Total viable cells measured from plates

Subtask 1.2: Acknowledgments

Funding for this research was provided by U.S. DOE Cooperative Agreement DE-EM0000598. We appreciate Dr. Brady Lee for his support of this research and providing us with the *Shewanella* culture and microbial consortia enriched at PNNL.

Subtask 1.2: References

Bernhard, G., G. Geipel, T. Reich, V. Brendler, S. Amayri & H. Nitsche (2001) Uranyl (VI) carbonate complex formation: Validation of the Ca2UO2 (CO3) 3 (aq.) species. *Radiochimica Acta International journal for chemical aspects of nuclear science and technology,* 89**,** 511.

Brooks, B. & R. Murray (1981) Nomenclature for "Micrococcus radiodurans" and other radiation-resistant cocci: Deinococcaceae fam. nov. and Deinococcus gen. nov., including five species. *International Journal of Systematic and Evolutionary Microbiology,* 31**,** 353-360.

Grenthe, I., J. Fuger, R. J. Konings, R. J. Lemire, A. B. Muller, C. Nguyen-Trung & H. Wanner. 2004. *Chemical thermodynamics of uranium*. North-Holland Amsterdam.

Gudavalli, R. K., Y. P. Katsenovich, D. M. Wellman, M. Idarraga, L. E. Lagos & B. Tansel (2013) Comparison of the kinetic rate law parameters for the dissolution of natural and synthetic autunite in the presence of aqueous bicarbonate ions. *Chemical Geology,* 351**,** 299-309.

Langmuir, D. 1997. *Aqueous Environmental Geochemistry*. Upper Saddle River, New Jersey: Prentice Hall.

Mehta, S. (2017) Geochemical evaluation of uranium sequestration from field-scale infiltration and injection of polyphosphate solutions in contaminated Hanford sediments. *Applied Geochemistry,* 84**,** 133-153.

Mehta, V. S., F. Maillot, Z. Wang, J. G. Catalano & D. E. Giammar (2016) Effect of reaction pathway on the extent and mechanism of uranium (VI) immobilization with calcium and phosphate. *Environmental science & technology,* 50**,** 3128-3136.

Szecsody, J. E., L. Zhong, M. Oostrom, V. R. Vermeul, J. S. Fruchter & M. D. Williams. 2012. Use of Polyphosphate to Decrease Uranium Leaching in Hanford 300 Area Smear Zone Sediments. Pacific Northwest National Laboratory (PNNL), Richland, WA (US), Environmental Molecular Sciences Laboratory (EMSL).

Vochten, R. & M. Deliens (1980) Transformation of curite into metaautunite paragenesis and electrokinetic properties. *Physics and Chemistry of Minerals,* 6**,** 129-143.

Wellman, D. M., J. G. Catalano, J. P. Icenhower & A. P. Gamerdinger (2005) Synthesis and characterization of sodium meta-autunite, Na $[UO_2PO_4]\cdot 3H_2O$. *Radiochimica Acta,* 93**,** 393-399.

Wellman, D. M., E. M. Pierce, D. H. Bacon, M. Oostrom, K. M. Gunderson, S. M. Webb, C. C. Bovaird, E. A. Cordova, E. T. Clayton & K. E. Parker. 2008. 300 Area treatability test: Laboratory development of polyphosphate remediation technology for in situ treatment of uranium contamination in the vadose zone and capillary fringe. Pacific Northwest National Laboratory (PNNL), Richland, WA (US).

Subtask 1.3: Investigation of Electrical Geophysical Response to Microbial Activity in the Saturated and Unsaturated Environments

Subtask 1.3: Introduction

Column experiments were conducted during FIU Performance Year 7 relating to the spectral induced polarization (SIP) response of biofilm formation within vadose zone sediment. These experiments help to advance the understanding of geophysical and geochemical processes that occur in the subsurface. Significant uranium contamination at the U.S. Department of Energy's Hanford Site exists within the vadose zone (up to 76 m thick). The mobility of uranium in the oxidizing, carbonate-rich Hanford subsurface at pH ~8.0 is relatively high, which is explained by the formation of highly soluble and stable uranyl-carbonato complexes ($UO_2CO_3^0$, $UO_2(CO_3)_2^{2-}$ and $UO_2(CO_3)_3^{4-}$) dominating in groundwater and pore water compositions. This research is focused on the ability of geophysical electrical methods, particularly SIP to detect subsurface microbial activity in a porous medium. Remote geophysical sensing of the subsurface allows scientists to forego the drilling of expensive boreholes and rely instead on easily and cheaply deployed surface arrays in order to study processes occurring deep in the subsurface. Geophysical methods also allow the continuous collection of data autonomously, which can be remotely accessed and analyzed. The second goal of this work is to measure and record changes in pore water characteristics after microbe injection in columns.

The column experiments at FIU consisted of 1-D columns, which ran continuously for a year and were monitored using SIP and porewater chemical analyses. A continuation of this work is planned for FIU Performance Year 8 and will feature a more basic column approach for better detection of biofilms and microbial activities.

Background

The production of weapons grade plutonium during the second World War and the cold war has led to significant uranium contamination within the Hanford vadose zone. The Hanford 200 Area (divided into east and west) lies within the interior of the Hanford Plateau and contains 177 single- and double-shelled tanks used to store waste. The waste stored in these tanks is highly radioactive with exceedingly high levels of uranium as well as associated byproducts of the process of extracting Pu from the uranium oxide. Out of the 149 single-shelled tanks, 68 have leaked into the vadose zone. A study of borehole sediment from the BX tank farm shows that uranium exists in both mobile and immobile phases and is concentrated especially in the finer grained sediment as well as micro fractures within feldspars (Um et al., 2010).

One possible solution to uranium sequestration in the saturated zone is *in situ* injection of a soluble sodium polyphosphate amendment. A column-based laboratory study conducted for the 300 Area seems to show that a polyphosphate amendment would be effective at capturing uranium in an immobile form. This amendment would cause aqueous U(VI) to precipitate as autunite, a sodium uranyl phosphate mineral. Subsequent injection of a polyphosphate amendment could also lead to the formation of apatite, calcium phosphate, which can immobilize uranium. Autunite incorporates uranium as U(VI), which is the natural state of U in the saturated zone, rather than requiring the prior reduction of the element. Research has shown that a three part injection would be most effective: (i) a polyphosphate injection, (ii) followed by a calcium chloride injection, which is a calcium source for apatite formation, (iii) followed by a second polyphosphate injection (Wellman et al., 2008).

Limited field testing conducted in the 300 Area based on these conclusions found that although polyphosphate amendment caused a decline in U concentrations in the groundwater, these decreases were temporary and the U levels rose after a two month period. This study suggested that the technique would be suitable for vadose zone remediation and that apatite formation may not be suitable for the remediation of U in saturated conditions (Vermeul et al., 2009). In 2012, column experiments using smear zone sediment were conducted to further the study on the viability of polyphosphate injections. These columns were run for 4500 h and included both continuous-flow and stop-flow events. The study found that the efficiency of the method was high at the start and decreased over time. In total, the phosphate treated sediments leached 54% less U than untreated sediments. This study also concluded that maximizing no-flow reaction time between U and the phosphate amendment was necessary for effective remediation and also advocated the inclusion of xanthan, a glucose polymer and a common thickening agent (Szecsody et al., 2012).

Recently, a field test was conducted at the 300 Area in order to test the effectiveness of polyphosphate injection for vadose zone remediation. This test involved the injection of 90% orthophosphate and 10% pyrophosphate over 13 days. Mehta (2017) states that the primary mechanism for immobilization of U bearing phases is coating by $CaPO_4$ and that this coating will overtime form the highly insoluble mineral hydroxyapatite. Mehta also stated that, prior to treatment, the uranium in the 300 Area was associated with Fe oxides and clays. Initially, there was an increase in U concentrations measured at nearby monitoring wells due to desorption or dissolution of U bearing phases; however, U concentrations dropped in response to injections of the amendment. It was concluded that the amendment was successful at sequestering uranium in the low-flow smear zone sediments in the 300 Area.

Szecsody et al. (2012) suggests that xanthan could be used by microbes as a carbon source. This, combined with high levels of P from polyphosphate injections, could lead to the increase in microbial growth within low-flow zones. The increase in microbial activities has the potential to affect the chemical properties of the sediment and groundwater quality, affecting the mobility of uranium in the subsurface.

The increase in microbial population could also lead to the formation of biofilms on mineral surfaces in the subsurface. The formation of these microbial structures may be possible to remotely track using a geophysical technique known as spectral induced polarization (SIP).

Electrical geophysical methods allow geophysicists to understand subsurface properties by measuring the voltage response to an electric current. Similar to standard DC resistivity methods, most induced polarization (IP) methods employ four electrodes in galvanic contact with the sediment. Two of the electrodes are current electrodes which act as source and sink for an electric current; the other two electrodes are potential electrodes which measure a voltage response. Traditional IP techniques use time domain measurements in which a decay voltage is measured after a direct current is turned off (Reynolds, 1997). SIP is a type of IP method that measures a phase shifted voltage at various injection frequencies. An impedance, in terms of magnitude and phase angle, is then obtained and used as a measure of charge transport and storage (Binley and Kemna, 2005). SIP is sensitive to porewater conductivity, changes in pore geometry, mineral dissolution, and the presence of clays (Revil, 2012).

While SIP has seen use in the exploration for metallic ore bodies for several decades (Hao et al., 2015), several recent studies have explored other avenues for the technique, especially in the

detection of organic microbial biofilm. These experiments have included studies using artificial alginate biofilms (Ntarlagiannis and Ferguson, 2008) as well as live bacteria cells (Atekwana and Slater, 2009).

Bacteria in the subsurface usually form immobile colonies known as biofilms, which attach to surrounding mineral grains through the use of extracellular polymers. The formation of biofilm can lead to various physical changes in the microscopic structure of the sediment such as the constriction and clogging of pores and the dissolution and alteration of minerals. Since most bacterial cell surfaces have a negative electrical charge, living organisms can form an electrical double layer (EDL) on their surface when in contact with an electrolyte solution (Atekwana and Slater, 2009). This EDL can lead to polarization which may be detectable using SIP. The effects of iron and zinc sulfide biomineralization was studied by (Ntarlagiannis et al., 2005) in anaerobic columns; in this case, they detected an anomaly in the phase, which the authors attributed to polarization at the surface of biominerals. By studying changes in the complex conductivity due to bacterial growth, it may be possible to remotely detect biofilm formation using SIP.

Subtask 1.3: Methodology

1. Continuous Flow Column Set Up

Six clear PVC columns filled with Hanford sediment were set up at FIU (Figure 39, Figure 40). The body of each column was composed of clear PVC. Filters were installed within the ends of the columns to stop sediment from entering the inlet tubing. A 3D printed plastic disk with holes (~5 mm) were also placed at the column ends to support the filters.

These columns were equipped with coiled Ag-AgCl current electrodes at either end to supply current. On the side of the columns are four potential electrodes that were constructed by encasing a silver wire in agar gel prepared with a synthetic groundwater solution (Figure 41). This allowed for three distinct measurement points along the length of the column. There are also three porewater sampling ports along the side of the columns, which correspond with the silver electrode locations. The columns operated under saturated conditions and solutions flowed from the bottom with a flow rate of 50 mL/day. The flow was powered by an Ismatek peristaltic pump through a mix of flexible silicone and stiff Teflon tubing. In order to ensure an oxygen restricted environment inside the column, all solutions pumped through the columns were sparged with nitrogen gas for 10 minutes in order to remove dissolved gases and then connected to a nitrogen bag while being pumped. This was done in an effort to prevent gas bubble formation within the columns, which could interfere with both geophysical measurements and pore water sampling.

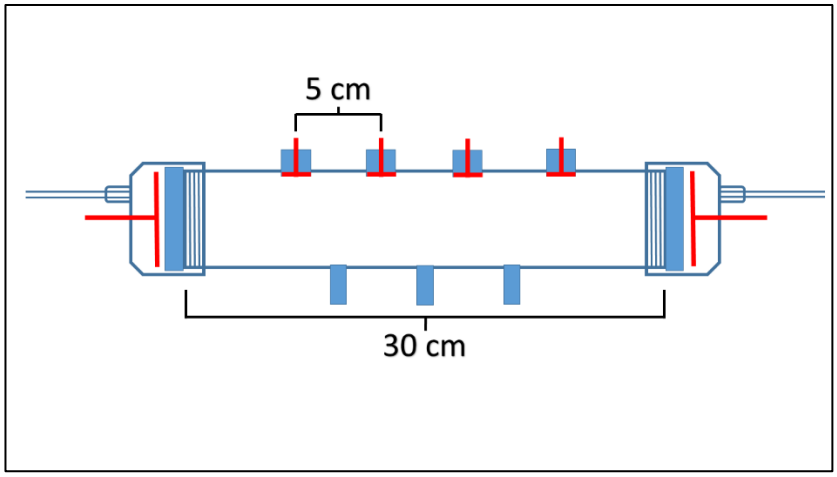

Figure 39. Scheme of the experimental soil column set-up

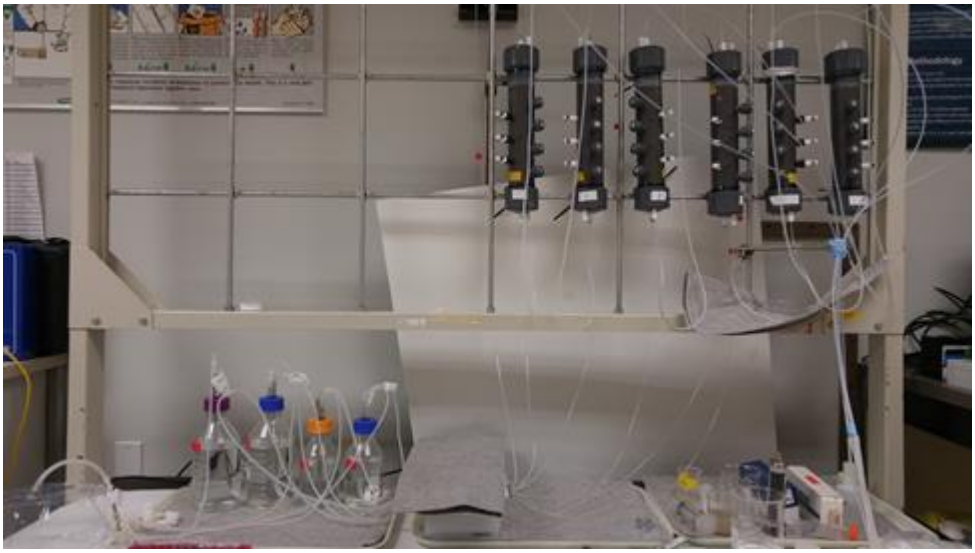

Figure 40. Current experimental setup at FIU.

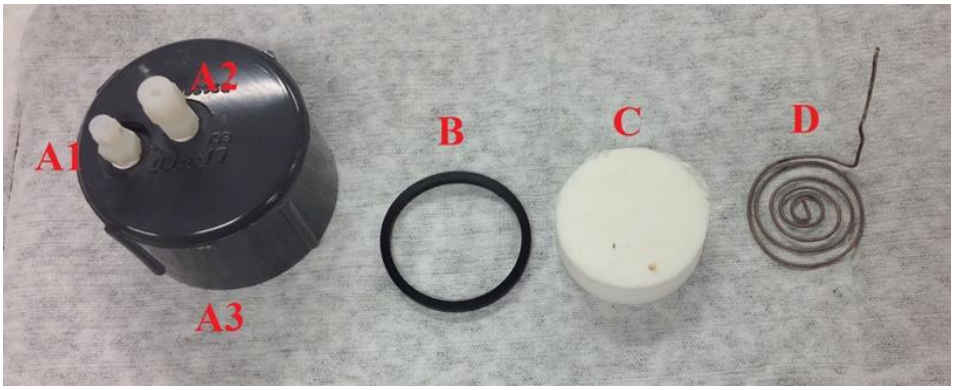

Figure 41. Various parts of end cap. A1 = current electrode port, A2 = influent/effluent port, A3 = end cap main body, B = rubber ring, C = porous plastic stopper (B and C were replaced by a 3D printed plastic stopper with mm scale holes in FIU's experimental column set-up), D = Coiled Ag-AgCl electrode.

2. Spectral Induced Polarization

SIP measurements were taken using a National Instruments Data Acquisition Card (DAQ) which is a PCI based device installed in a standard desktop computer. This card measures the potential and phase of the column as well as a reference resistor. This reference resistor is set to a value that is close to the bulk resistance of the columns in order to produce a more accurate measurement. Generally, the reference resistor was set to 1800 Ohms. The measurements were output by the proprietary software Signal Express (by National Instruments) into a series of text files, which were then analyzed using Python-based code written by DOE Fellow Alejandro Garcia. The code compiled all of the text files into Numpy zipped files (.npz) for easier analysis and then produced various plots of bulk resistivity and phase. During each measurement, the current was injected at 21 different frequencies ranging from 0.1 Hz to 10,000 Hz (although the card may be limited to 100 Hz) spaced logarithmically and, for each frequency, a phase and amplitude were measured. A background phase was also measured, which is the phase inherent to the circuit and DAQ card. This was subtracted from the phase measured from the columns.

3. Experiments conducted in Fall 2016

Initially, six columns were run during the fall of 2016 for a period of 5 months. SIP measurements and porewater samples were taken once a week. Four different solutions were pumped through the columns (Table 16). These included: synthetic groundwater (column 1), synthetic groundwater + 3 mM HCO_3 (column 2), synthetic groundwater + 1 g/L glucose (columns 3 and 5), and synthetic groundwater + 3 mM HCO_3 + 1 g/L glucose (columns 4 and 6). The synthetic groundwater base solution is made using only stock solutions A + B since the current setup only has HCO_3 in three of the six columns. The base solution was autoclaved in order to prevent contamination of the columns by foreign bacteria. Each container had enough solution to last for ten days at which point new solution was made.

Table 16. Contents of Each Column Fall 2016

Column 1	3
Column 2	3 mM HCO_3
Column 3	0 mM HCO_3 + 1g/L glucose
Column 4	3 mM HCO_3 + 1g/L glucose
Column 5	0 mM HCO_3 + 1g/L glucose+ inoculum
Column 6	3 mM HCO_3 + 1g/L glucose+ inoculum

The medium in which the microorganisms have been cultured is synthetic groundwater (SGW1). Table 17 shows the stock solutions (labeled A, B, and C) used to make SGW and the process used to make SGW follows.

Table 17. Stock Solutions for Artificial SGW

		Concentration (g/L)
A	$NaHCO_3$	12.1
	$KHCO_3$	1.6
B	$MgSO_4$	3.06
	$CaSO_4$	0.82
C	$Ca(NO_3)_2 \times 4H_2O$	5.43
	$CaCl_2 \times 2H_2O$	9.56

To create 1 L SGW: 10 mL each of solutions A and C and 20 mL of solution B were pipetted into 900 mL deionized water, then diluted to 1 L using deionized water. The SGW solution used also contained a concentration of yeast extract equal to 500 mg/L. The modified solution used did not contain bicarbonate and so was formed by pipetting 10 mL C and 20 mL B into 970 mL of deionized water. Pumping of the solution amended with glucose to columns 3, 4, 5 and 6 began on day 33 of the experiment.

The microbial consortia were cultured at PNNL in 50 mL SGW mixed with approximately 500 mg of Hanford sediment, 10 mg of autunite, and 50 mg of glucose. On a weekly basis, a 1-mL sample of each culture was taken and transferred to a fresh container. Microorganisms were originated from the sediment taken from a borehole and are naturally occurring in Hanford Site's vadose zone. Currently, the species of microbial consortia are unknown until molecular biology analyses can be conducted. These microorganisms were sent to FIU frozen and then kept in a 25% glycerol solution at -80ºC. Microorganisms were cultivated in the glucose with the tiny addition of Luria-Bertani (LB) media until the bacterial cell density (cells/mL) could be counted with the help of an INCYTO C-Chip disposable hemocytometer under a light microscope. Grown microbial consortia was washed in DIW water to remove the media solution and were injected via port 1 of columns 5 and 6 in the amount of log 8.92 cell/mL on November 15, 2016, which was day 115 from the beginning of the experiment. The total number of cells injected to each column was log 9.62 cells.

Pore water samples were collected once a week. These were taken by inserting a metal needle attached to a syringe into the sample ports and withdrawing water. Initially, about 2 mL of sample was taken; however, in order to facilitate more chemical analyses, this was increased to about 3 mL. Initial measurements included pH and conductivity (in mS/cm). Later, ORP was measured immediately after samples were collected and an extra 1.5 mL was taken for Fe^{2+} and total iron analyses using Ferrozine.

Conductivity measurements utilized a conductivity microprobe obtained from Microelecrtode, Inc.

4. Experiments conducted in Spring 2017

A second experiment was conducted during spring 2017 and ran for 1 month. It converted the original two control columns into microbial-bearing columns and SIP measurements were taken 5 times a week while porewater samples were collected 3 times a week (Table 18). All other operating parameters were identical to the fall 2016 work. The purpose of this second experiment was to obtain a higher temporal resolution of changes occurring in the column at the start of microbe growth.

Table 18. Contents of Each Column Spring 2017

Column Contents Spring 2017	
Column 1	0 mM HCO_3 + 1g/L glucose+ Inoculum
Column 2	3 mM HCO_3 + 1g/L glucose+ Inoculum

5. Chemical Analysis

a. Detection of iron via Ferrozine method

The concentrations of Fe^{2+} and Fe^{2+}+Fe^{3+} (total Fe) were measured using spectrophotometric methods via the ferrozine assay (Stookey, 1970) and the 1,10-phenanthroline method (Fadrus

and Malý, 1975). Ferrozine reagent is a dye which turns various shades of purple in reaction to Fe^{2+} in solution and the intensity of the dye is measured using an ultraviolet visible spectroscopy (UV-Vis) instrument.

In a 1.5 mL cuvette (clear plastic designed for the UV-Vis measurements), 200 µL of sample was added. If the sample concentration was believed to be greater than 30 mg/L, then the sample was first diluted by an appropriate amount. Afterwards, 0.3 mL of 0.15 M HCl and 1.5 mL of ferrozine solution was added to the cuvette. This was gently mixed and then set to rest for 10 minutes. After 10 minutes, the samples were placed in the UV-Vis and absorbance was measured at 562 nm.

For Fe^{2+}+Fe^{3+}, 0.5 mL of hydroxylamine HCl solution was added to the cuvette. This solution is a strong oxidizer and oxidizes all Fe^{3+} into Fe^{2+}. After ten minutes, this solution was placed in the UV-Vis and measured at 562 nm.

b. Analysis via ICP-OES instrument

Analysis for total Fe, P, Ca, and Mg was performed using inductively coupled plasma – atomic emission spectroscopy (ICP-OES). An ICP-OES (Figure 42) instrument uses an inert argon gas in order to excite atoms into emitting electromagnetic radiation of a specific wavelength. The wavelength emitted is unique for each element and the intensity of the light emitted is used to measure the concentration. The intensity is calibrated to the concentration using a calibration curve of known standards.

Preparation of samples for ICP-OES analysis was as follows: a 60 µL aliquot of sample was diluted into 5940 µL of 1% nitric acid resulting in a 100x dilution factor that effectively allowed samples to be re-run if any errors were encountered since each run used only approximately ~2 mL of solution A 1% nitric acid background sample was also prepared to account for elements dissolved in the 1% nitric acid.

c. Analysis via KPA instrument

In order to test for uranium concentration, a Chemchek™ kinetic phosphorescence analyzer (KPA-11) (Figure 5) was used. This instrument uses a laser in order to induce phosphorescence in an aqueous sample. The intensity of the phosphorescence is correlated to concentration through a calibration curve using known standards.

The presence of glucose and organic matter can interfere with KPA readings. As such, before being processed in the KPA, samples were both wet ashed and dry ashed, techniques designed to burn away organic matter. The process used for wet ashing is as follows: a 200 µL aliquot of sample was mixed with 500 µL 70% nitric acid and 200 – 300 µL of 35% hydrogen peroxide. This solution was then placed on a hot plate until all of the liquid had evaporated, leaving a white residue. If the residue was not white but rather yellow, then 35% hydrogen peroxide was added one drop at a time until it whitened. After wet ashing, the residue was dry ashed by being placed in a 450°C electric furnace for 15-20 minutes.

Once ashing was completed, the residue was re-dissolved in 1M nitric acid and then diluted to a greater volume using 1% nitric acid. Dilutions used included 10x, 100x, and 200x dilutions in order to get concentrations within calibration limits.

Figure 42 ICP-OES (Left) and KPA (Right)

Subtask 1.3: Results and Discussion

1. Chemical analysis for fall 2016 samples

Control columns 1 and 2 showed a similar trend for conductivity values, which didn't vary significantly, ranging between 400-600 µS/cm for samples collected from three different ports (). The addition of glucose in the inlet solution sharply increased conductivity values from the initial 400 µS/cm up to 1600 µS/cm in bicarbonate-free column 3. However, in column 4, where the inlet solution was amended with bicarbonate, conductivity values increased gradually from the initial 400 µS/cm and stabilized at the level of 1650 µS/cm after 130 days. The difference between port 1 and port 3 conductivity values were about 10%, with higher values recorded in port 3. The columns inoculated with microbial consortia on day 40 showed a sharp increase in conductivity from the initial value of 400 µS/cm to 1600 µS/cm by day 100 and then exhibited a slight decline on day 150 to 1250-1440 µS/cm for bicarbonate-free column 5 and 1060-1340 µS/cm for bicarbonate-amended column 6. So, the decline in conductivity values for column 6 was 10-15% higher compared to bicarbonate –free column 5 (Figure 43).

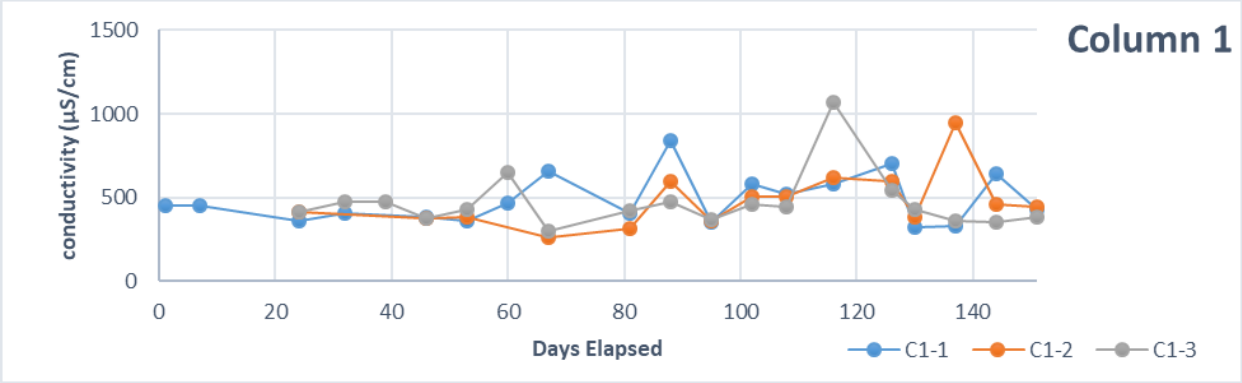

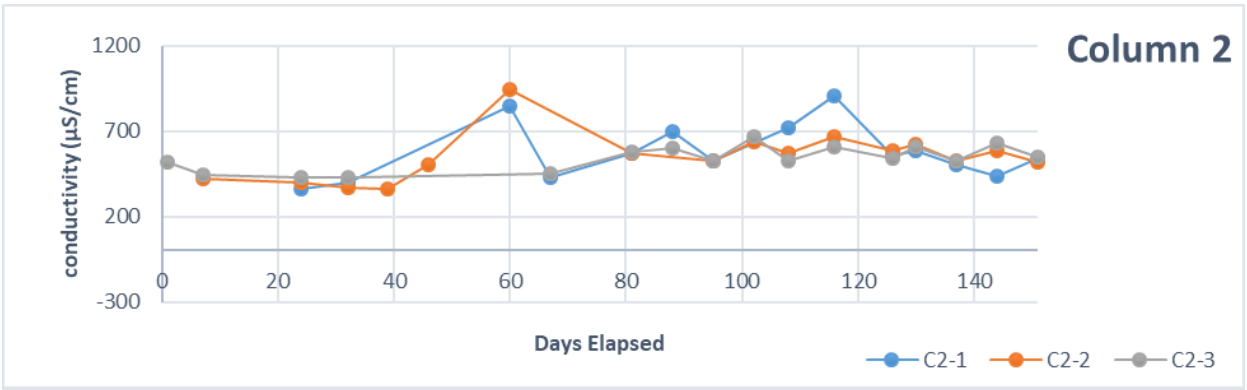
Column 2
conductivity (µS/cm)
1200
700
200
-300
0
20
40
60
80
100
120
140
Days Elapsed
C2-1
C2-2
C2-3

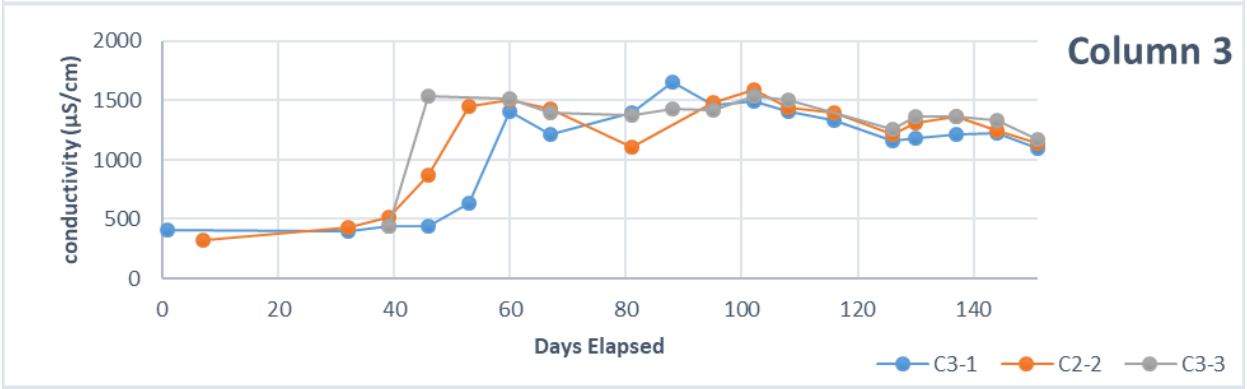
Column 3
conductivity (µS/cm)
2000
1500
1000
500
0
0
20
40
60
80
100
120
140
Days Elapsed
C3-1
C2-2
C3-3

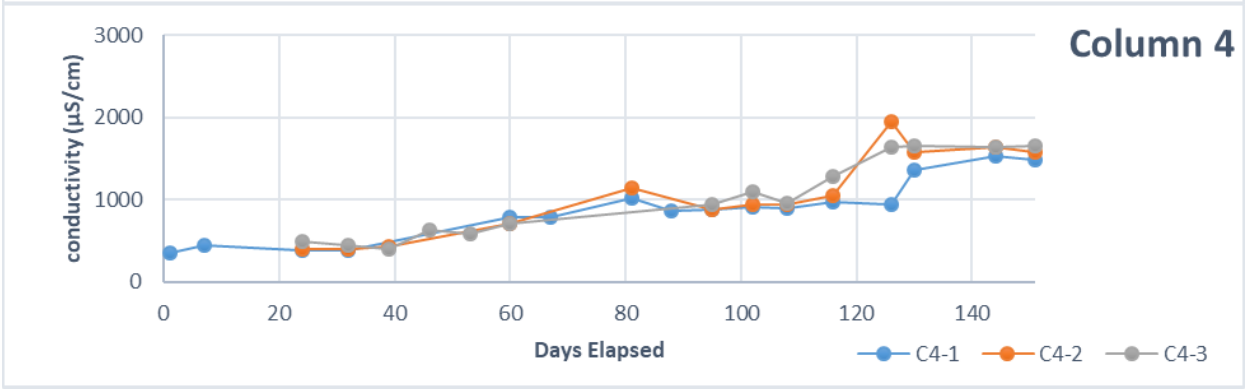
Column 4
conductivity (µS/cm)
3000
2000
1000
0
0
20
40
60
80
100
120
140
Days Elapsed
C4-1
C4-2
C4-3

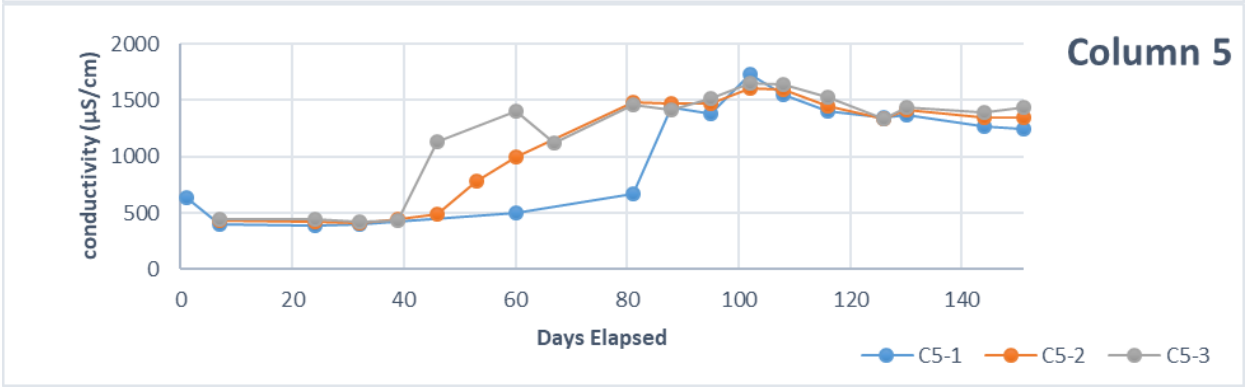
Column 5
conductivity (µS/cm)
2000
1500
1000
500
0
0
20
40
60
80
100
120
140
Days Elapsed
C5-1
C5-2
C5-3

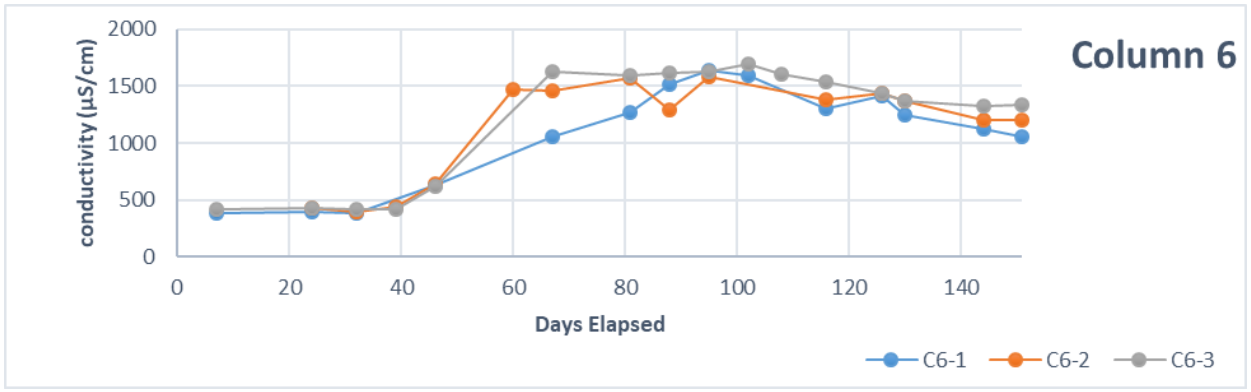

Figure 43. Results on conductivity measurements for each column.

The pH values measured in each port of the control columns 1 and 2 ranged between 7.5 and 8, which are typical values for Hanford pore and groundwater. The addition of glucose in column 3 resulted in a decrease of 1 pH unit from day 67 to 150. For the same period of time, pH values in column 4 amended with bicarbonate-bearing solution, decreased from 8 to 7.5. In inoculated columns 5 and 6, the pH decreased, showing a similar trend as columns 3 and 4; however, the decline in pH values on day 150 for column 6 was deeper and observed as 6.8 for port 1 and 7.2 for port 3 (Figure 44).

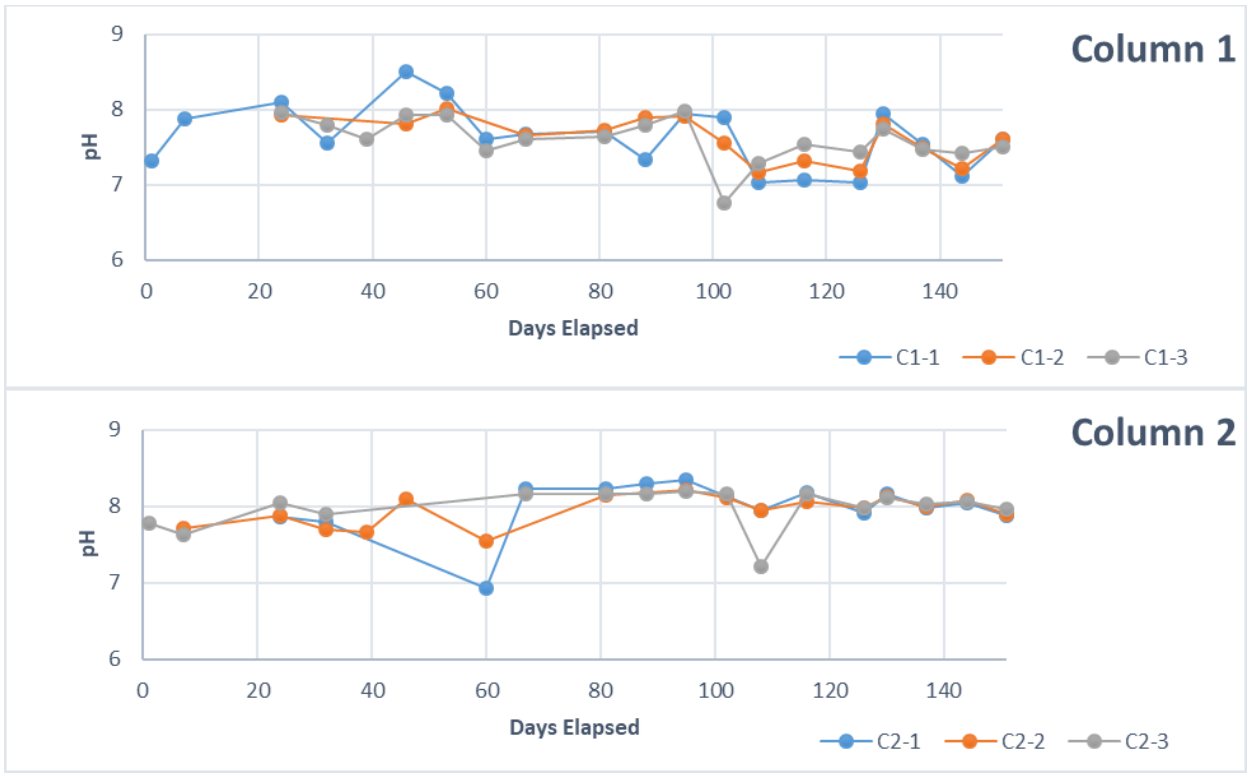

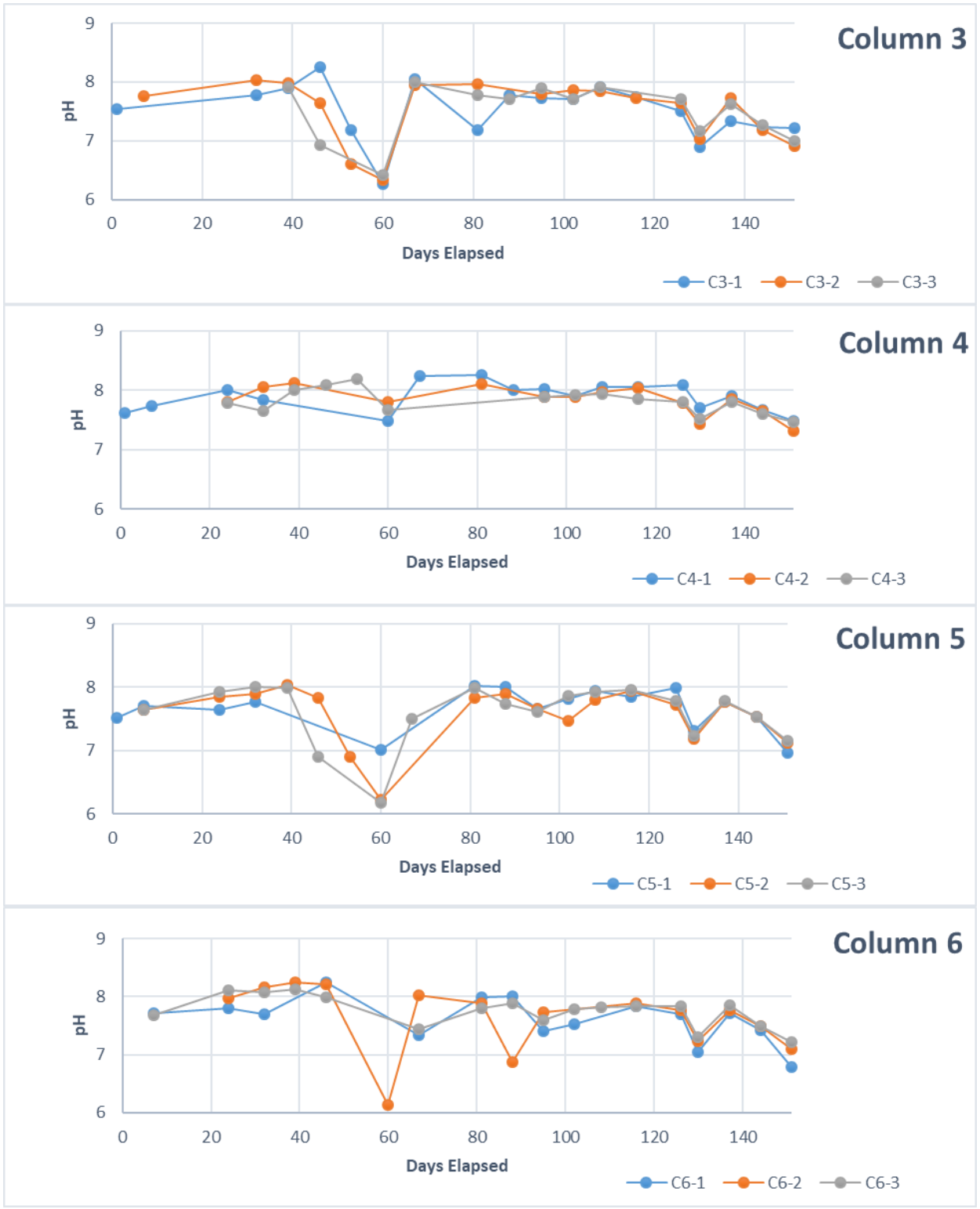

Figure 44. Results on pH measurements for each column.

The concentrations of total iron in aqueous samples collected from each port of control columns 1 and 2 were measured as 10 mg/L, on average. The addition of glucose as a carbon source in the inlet solution flowing into columns 3 and 4 caused a gradual increase in total Fe values up to

1000 mg/L in column 3. A smaller increase of total iron up to 200 mg/L for the same time period was recorded for column 4. The composition of Hanford soil includes a magnetite mineral, which is comprised of both divalent and trivalent iron. The addition of glucose stimulates the microorganisms naturally present in the sediment. This triggers a microbial alteration of the local oxidation reduction conditions and a pH that promotes biotransformation of Fe(III), which is generally present as a solid-phase, to Fe(II) (Zachara et al., 2001). In column 4, amended with bicarbonate, the concentration of ferrous iron released into solution was observed to be lower. Perhaps this is due to the formation of siderite solid phases under the range of studied pH conditions (Figure 45).

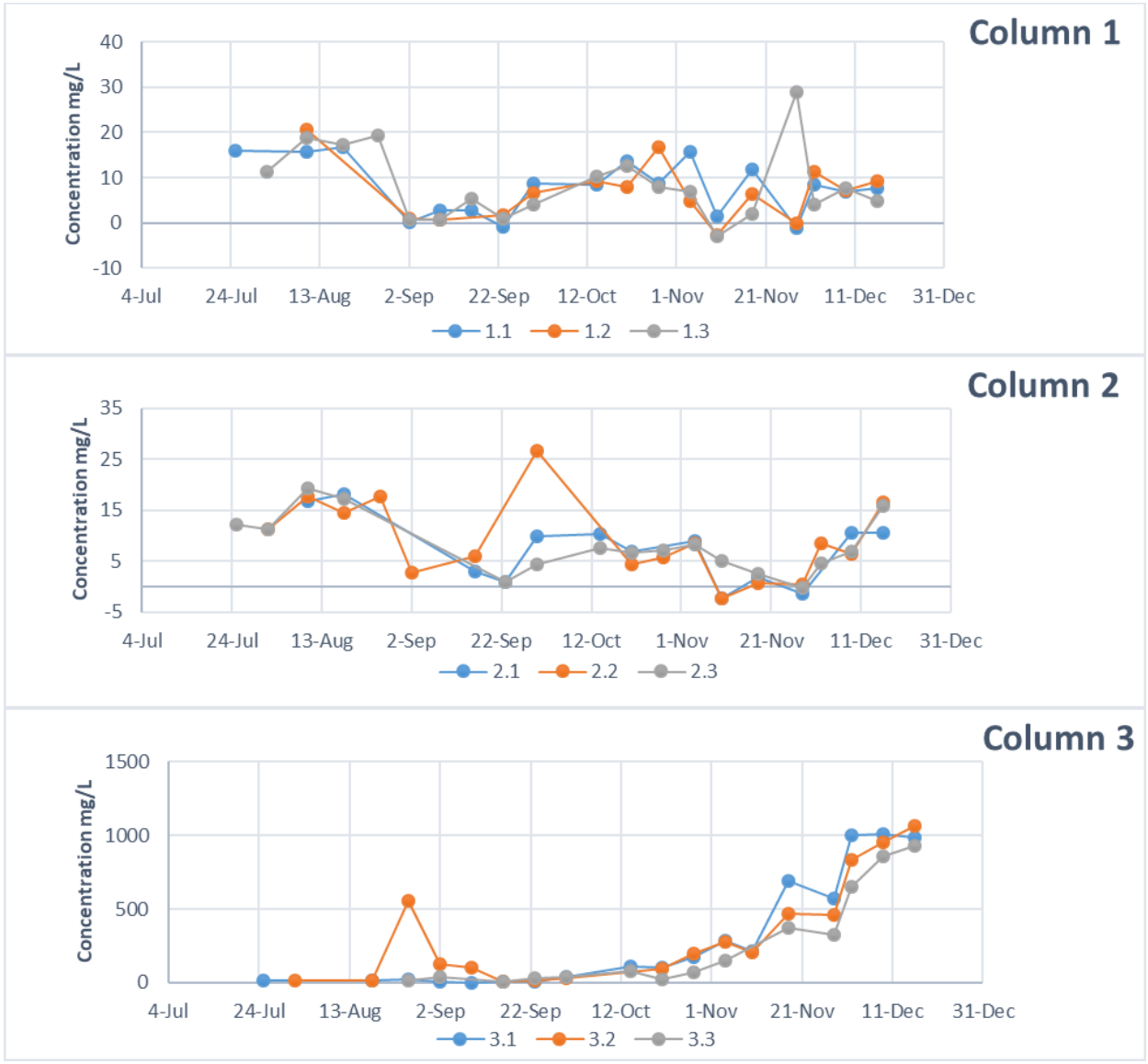

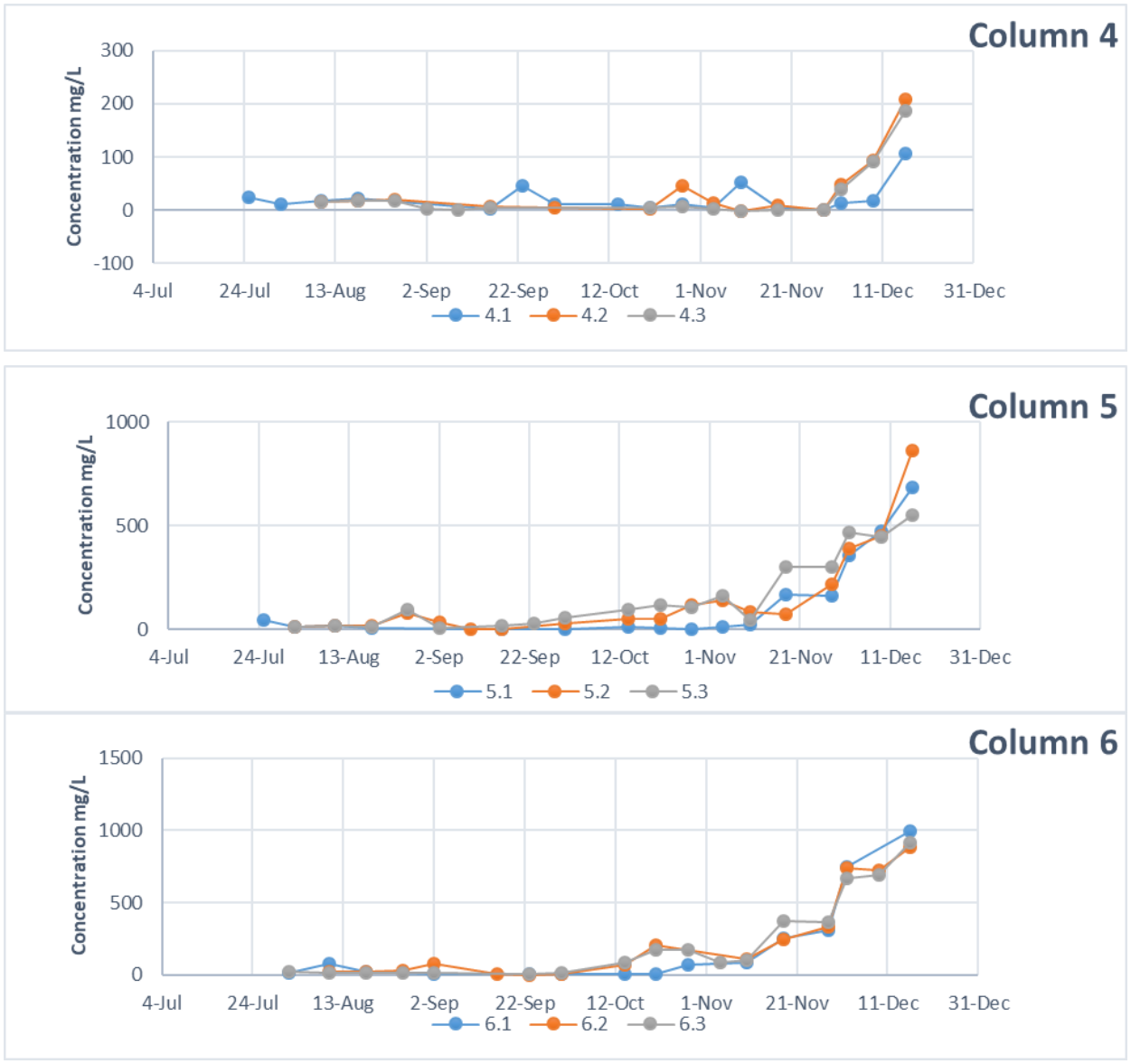

Figure 45. Measurements for total iron via ICP-OES for each column.

The experimentally observed changes in conductivity values were similar to fluctuations in Ca concentrations for all columns. In the control column 1, the Ca concentrations varied between 400-500 mg/L. In column 2 and in the presence of bicarbonate, the Ca concentrations in porewater samples stabilized at the level of 300 mg/L. The addition of glucose to columns 3 and 4 caused the concentration of Ca to increase. The calcium concentration increased sharply after the addition of glucose in column 3 and increased gradually in column 4, which was amended by bicarbonate. This gradual increase in calcium concentration might be due to precipitation of calcium carbonate or calcium phosphate solids. The columns inoculated with the microbial consortia showed a sharp increase in calcium concentration, from 500 mg/L to 2700 mg/L; however, after the addition of glucose and inoculum, Ca values fluctuated between 1000-2000 mg/L (Figure 46).

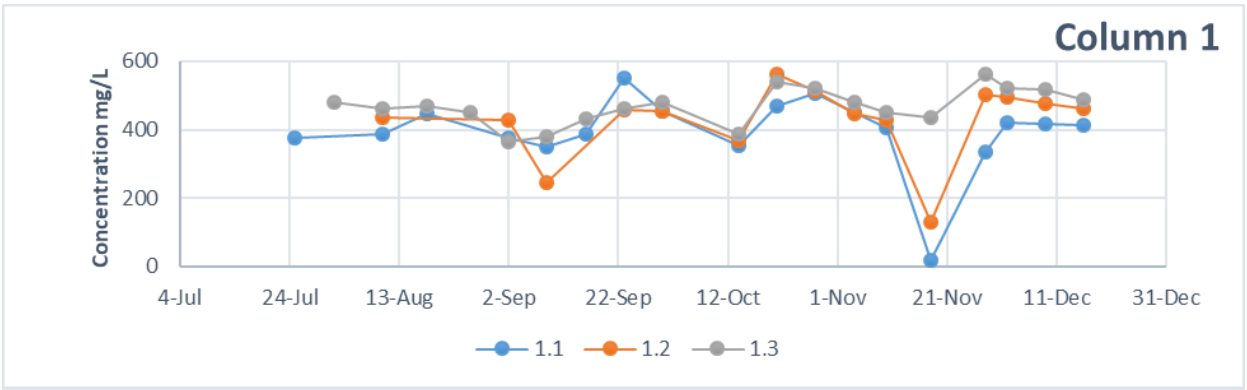
Column 1
Concentration mg/L
600
400
200
0
4-Jul
24-Jul
13-Aug
2-Sep
22-Sep
12-Oct
1-Nov
21-Nov
11-Dec
31-Dec
1.1
1.2
1.3

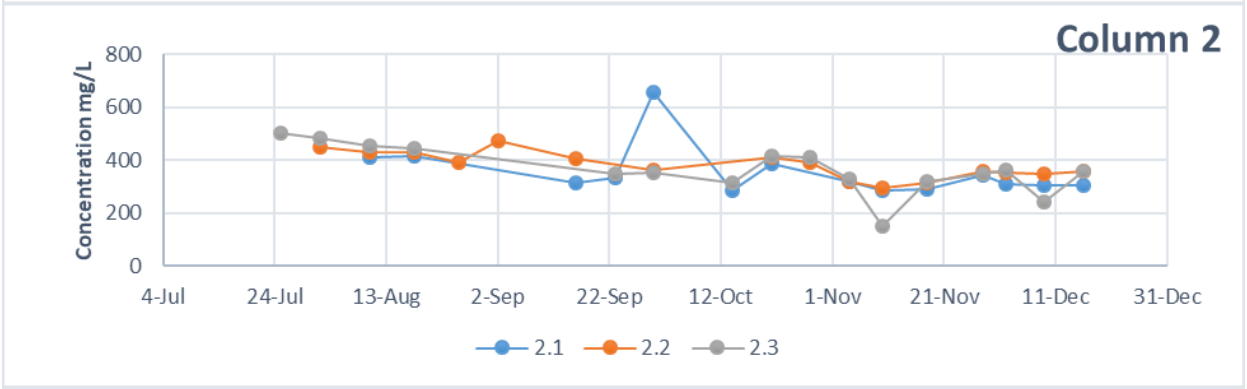
Column 2
Concentration mg/L
800
600
400
200
0
4-Jul
24-Jul
13-Aug
2-Sep
22-Sep
12-Oct
1-Nov
21-Nov
11-Dec
31-Dec
2.1
2.2
2.3

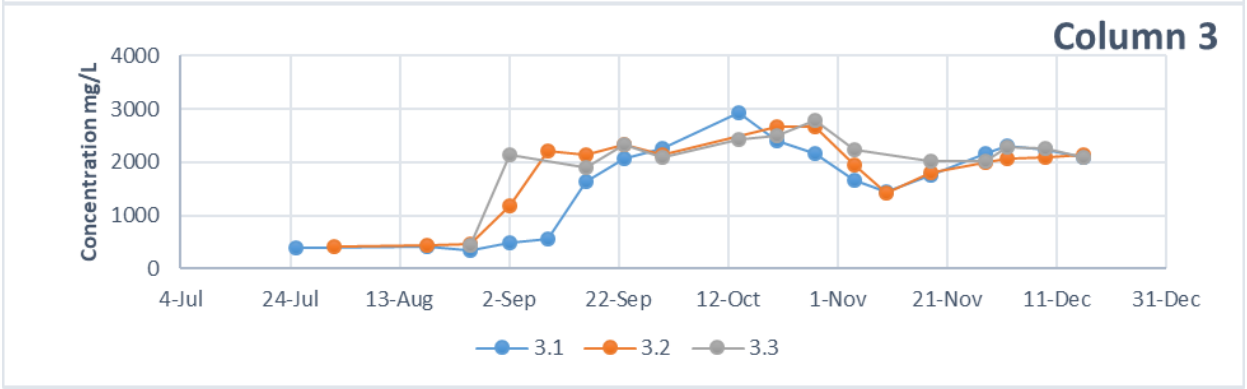
Column 3
Concentration mg/L
4000
3000
2000
1000
0
4-Jul
24-Jul
13-Aug
2-Sep
22-Sep
12-Oct
1-Nov
21-Nov
11-Dec
31-Dec
3.1
3.2
3.3

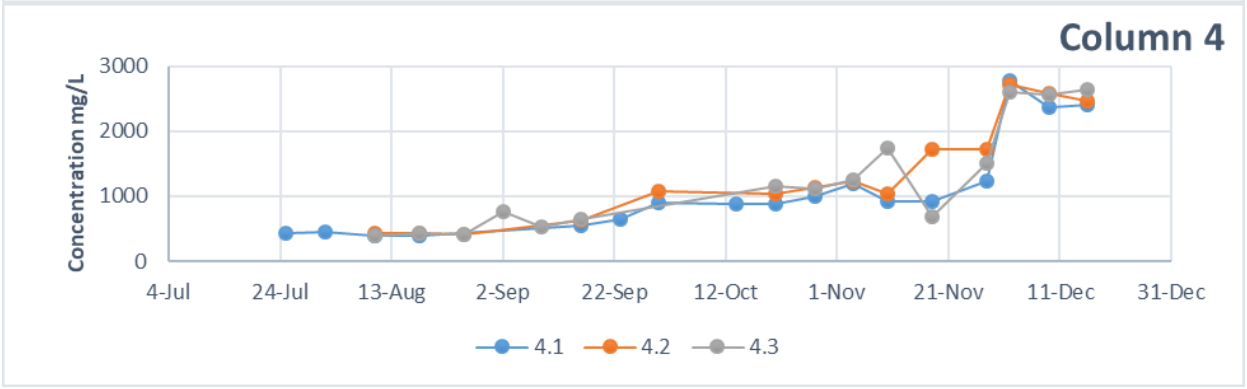
Column 4
Concentration mg/L
3000
2000
1000
0
4-Jul
24-Jul
13-Aug
2-Sep
22-Sep
12-Oct
1-Nov
21-Nov
11-Dec
31-Dec
4.1
4.2
4.3

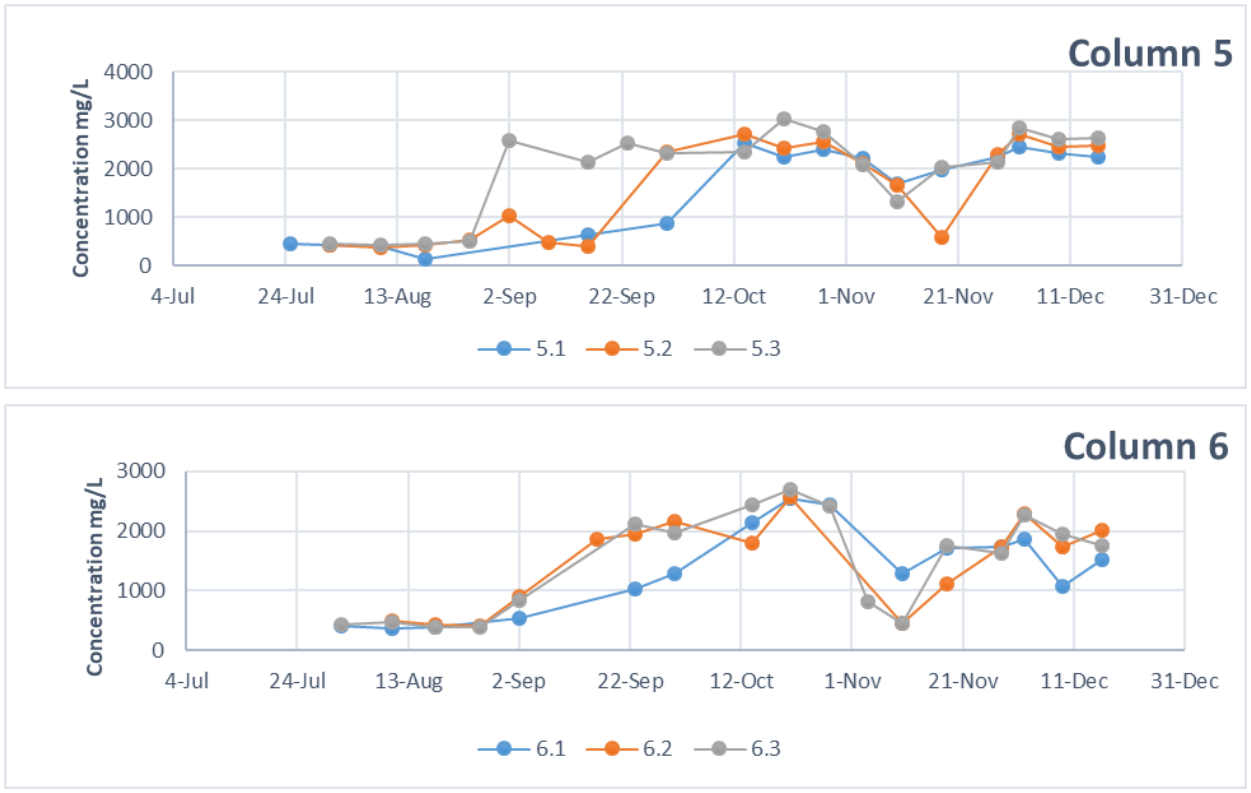

Figure 46. Calcium measurements for each column.

Autunite dissolution in the presence of aqueous bicarbonate and sediment microorganisms results in the release of uranium from the solution matrix. The liberation of U(VI) influences incongruent reactions to release Ca and P from the mineral structure (Wellman et al., 2006). Phosphorus concentrations were noted to decrease from the initial 6-10 mg/L to non-detectable values (Figure 47). This might be due to precipitation with calcium or formation of uranyl phosphate solids in the Hanford sediments. In addition, the presence of ferrous iron in the porewater solution could contribute to the removal of phosphorus from the aqueous solution due to formation of ferrous iron phosphorus phases (Li et al., 2012; Zhang et al., 2015).

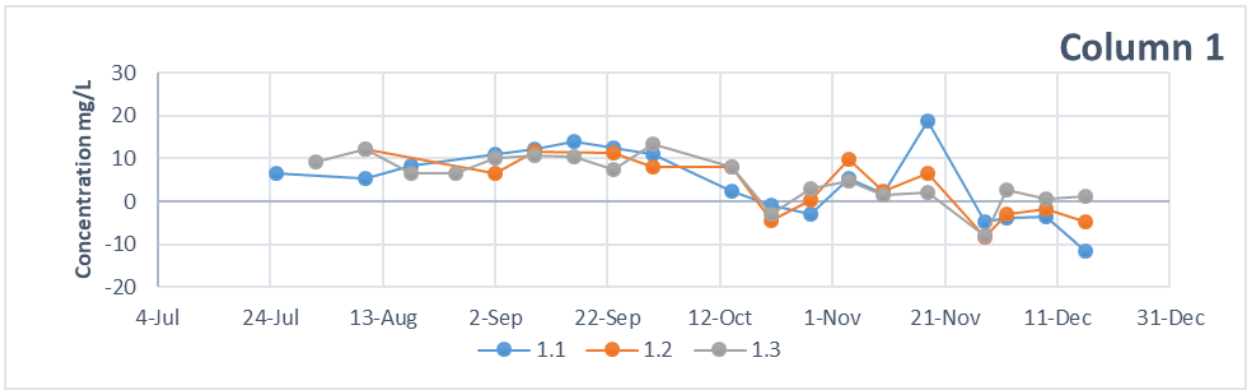

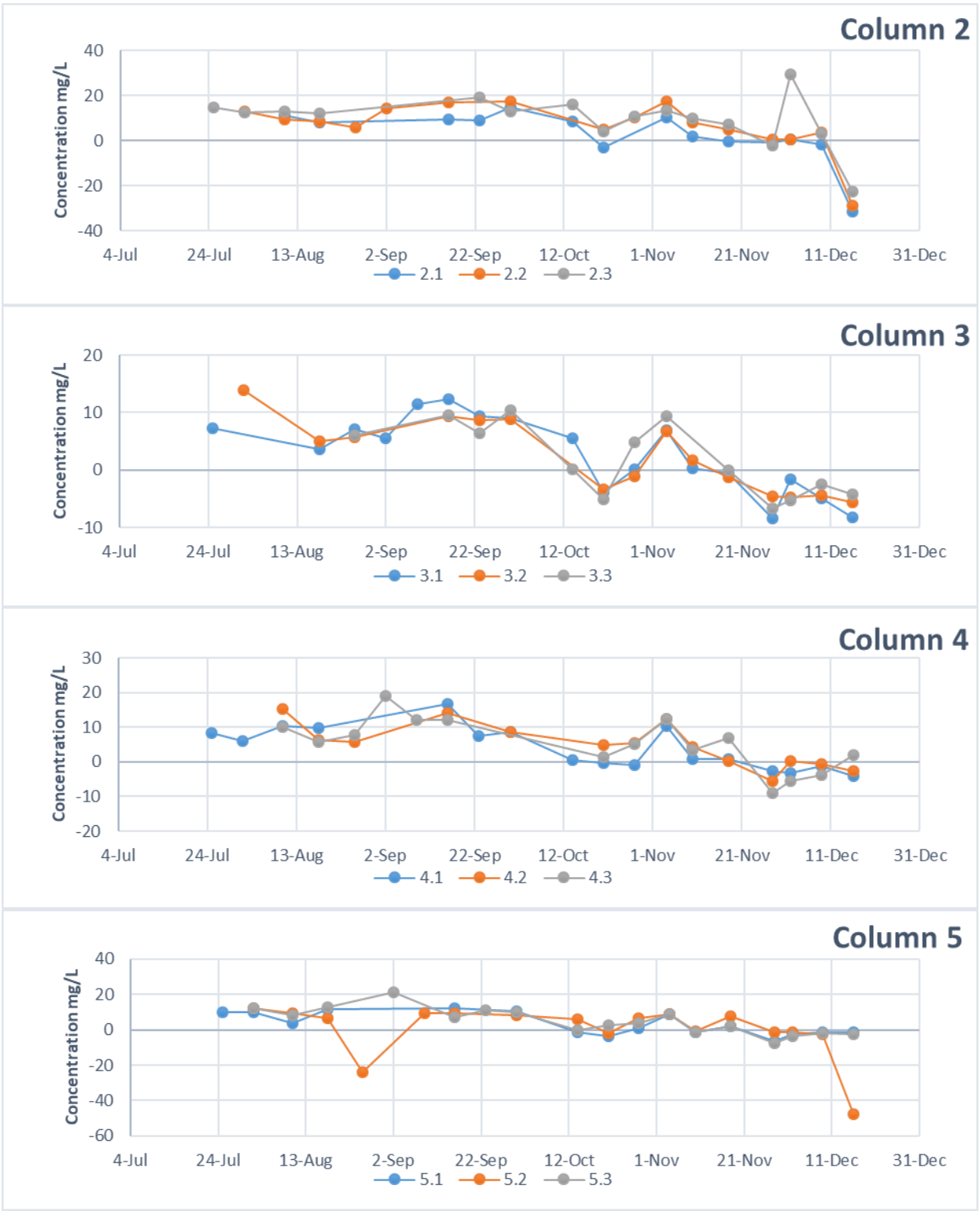
Column 2
Concentration mg/L
40
20
0
-20
-40
4-Jul
24-Jul
13-Aug
2-Sep
22-Sep
12-Oct
1-Nov
21-Nov
11-Dec
31-Dec
2.1
2.2
2.3
Column 3
Concentration mg/L
20
10
0
-10
3.1
3.2
3.3
Column 4
Concentration mg/L
30
20
10
0
-10
-20
4.1
4.2
4.3
Column 5
Concentration mg/L
40
20
0
-20
-40
-60
5.1
5.2
5.3

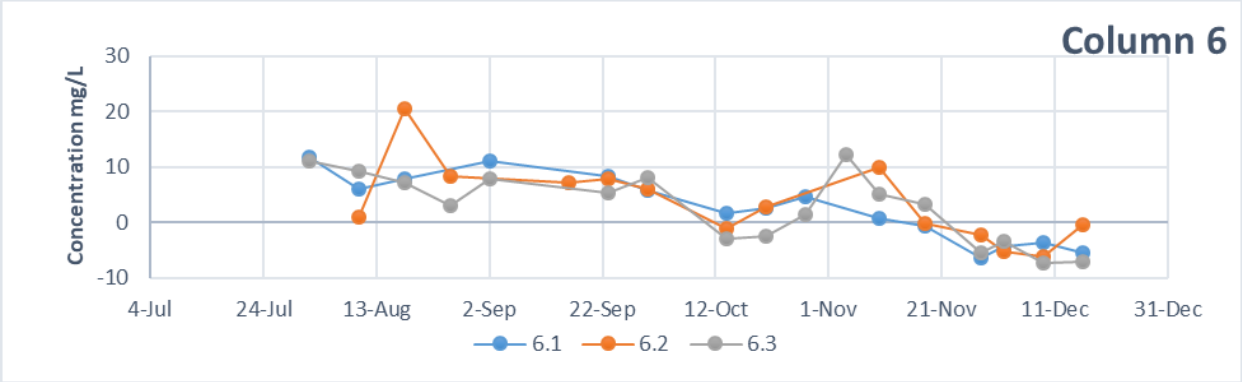

Figure 47. Phosphorus concentrations for each column.

Bulk resistivity remained relatively constant in column 1 but had a slight upward trend in column 2 until reaching equilibrium around 2 months after the experiments began (Figure 48-Figure 51). Columns with suspected microbial activity all saw resistivity values drop to approximately 100 Ωm over different spans of time. For columns 3, 5, and 6 this was a rapid change; however, column 4 seemed to show two distinct drops in resistivity, one in September and another in November with values not showing significant change throughout October. This change in resistivity generally corresponds to changes in the concentration of calcium measured through ICP-OES, which may indicate that this was the principle ion controlling the porewater conductivity.

Phase changes correlate to changes in the bulk resistivity. The phase spectra of column 1 remained constant over time. Column 2 saw a shift towards more negative phase values which remained constant after about 40 days of runtime; a white precipitate noted in the transparent tubing leading into column 2 may indicate the precipitation of calcite ($CaCO_3$), which may lead to pore clogging. The columns with glucose all saw the phase spectra shift from values of -0.020 mrad to 0 mrad. These changes are likely in some part related to the release of ions into solution such as Ca, Mg, and Fe.

SIP measurements during fall 2016

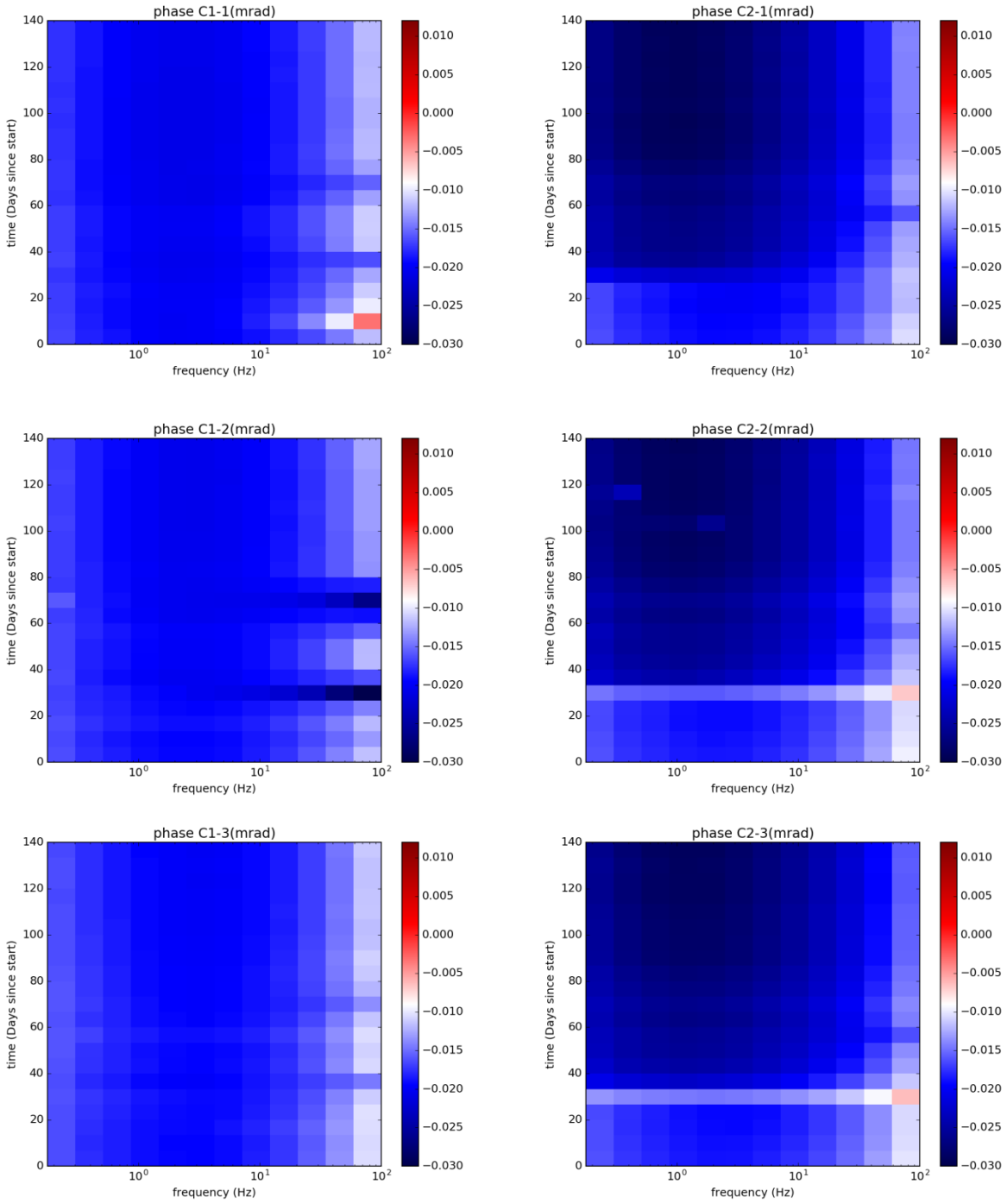

Figure 48. Phase spectra for Columns 1 and 2.

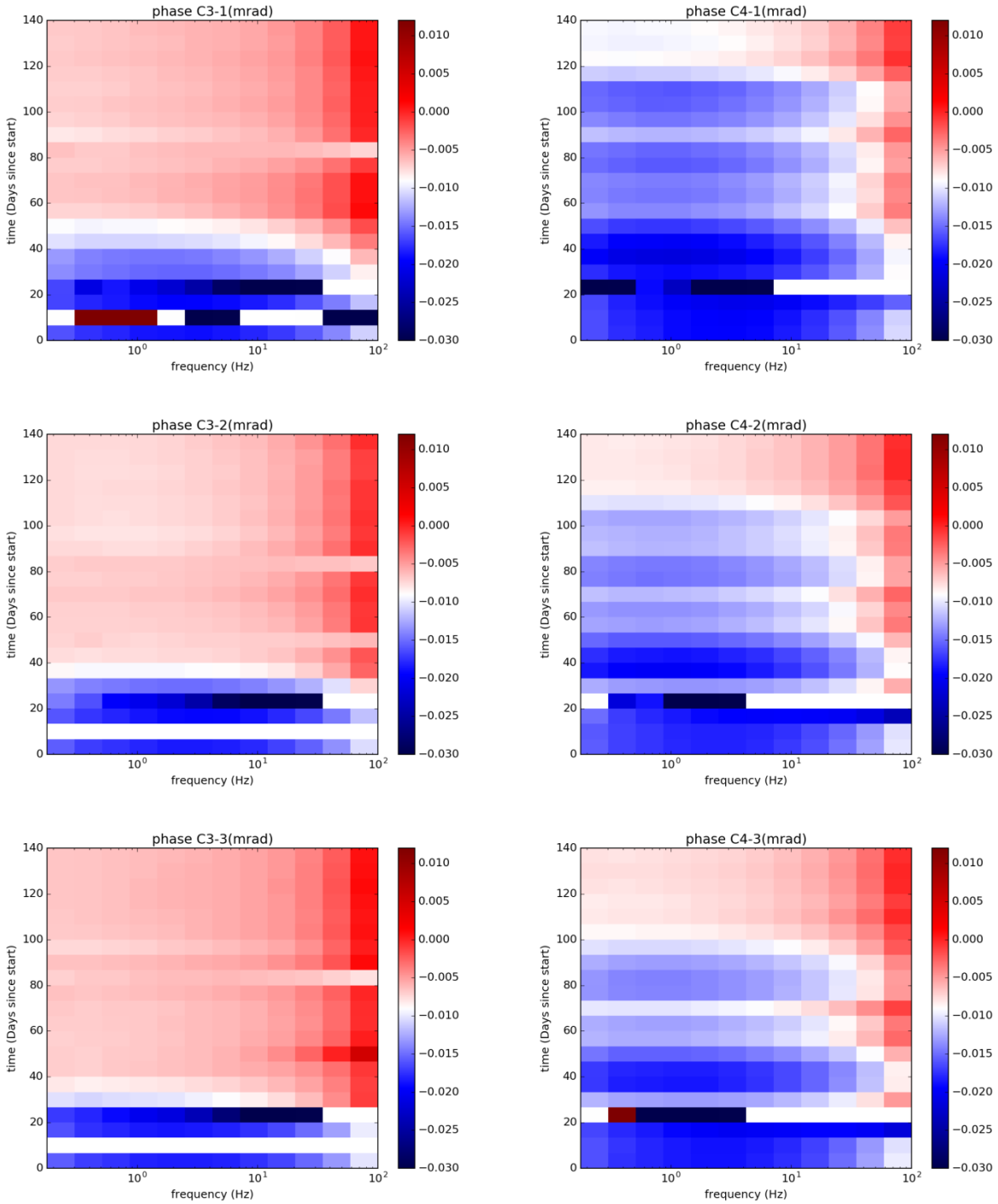

Figure 49. Phase spectra for Column 3 and 4.

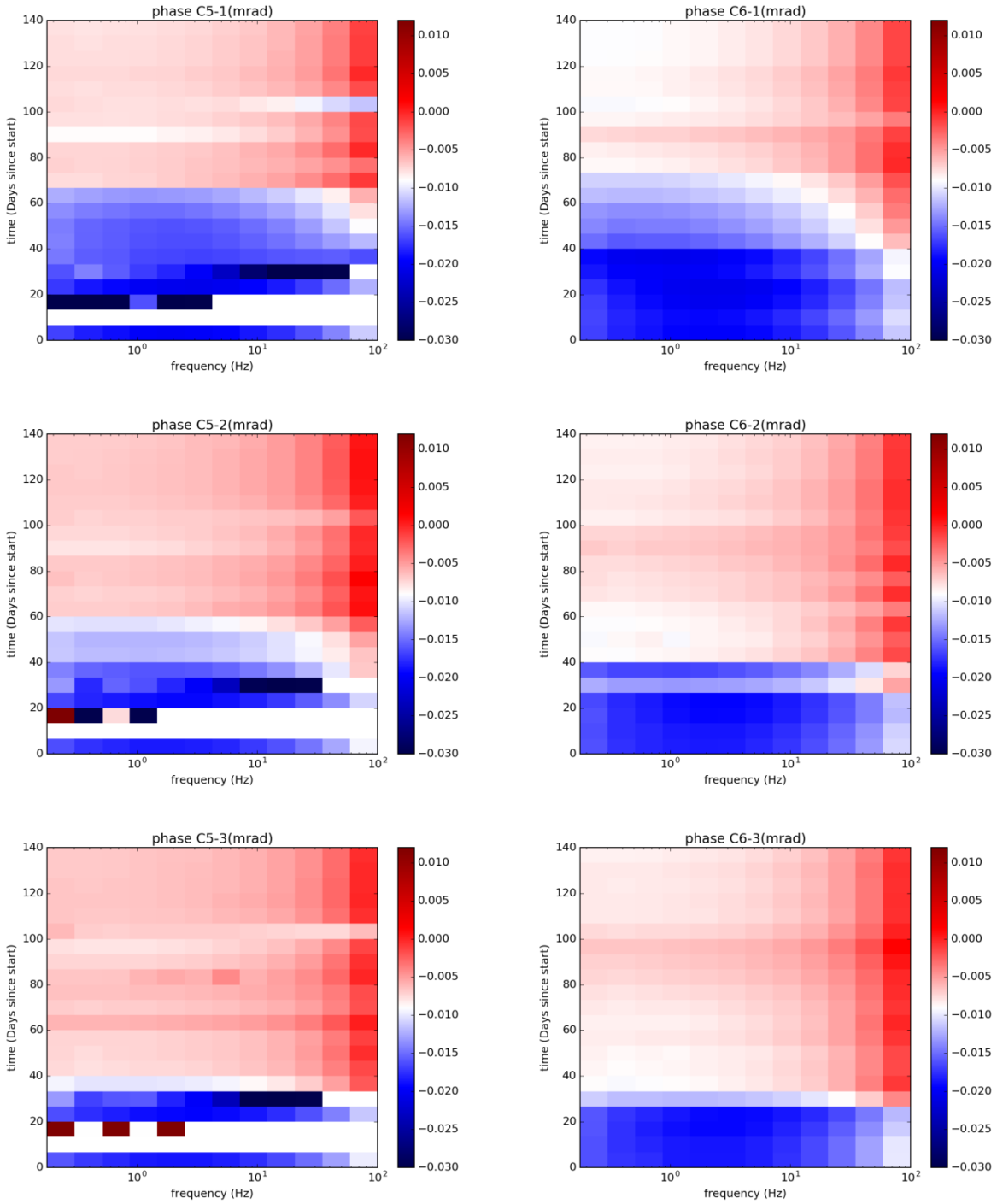

Figure 50. Phase spectra for Columns 5 and 6.

Figure 51. Bulk Resistivity for all Columns.

2. Chemical Analysis during spring 2017

Columns 1 and 2 had reached equilibrium at the end of the fall 2016 experiments. Shortly after inoculation with microbes, the resistivity of both columns was reduced to around 100 Ωm; this is similar to what occurred in the fall 2016 columns augmented with glucose. While changes in column 1 occurred at the same time independent of height, column 2 changes began at the top and migrated downward over time. Once again, the conductivity changes are likely in response to the release of ions such as Ca and Fe into solution (Figure 52 - Figure 60).

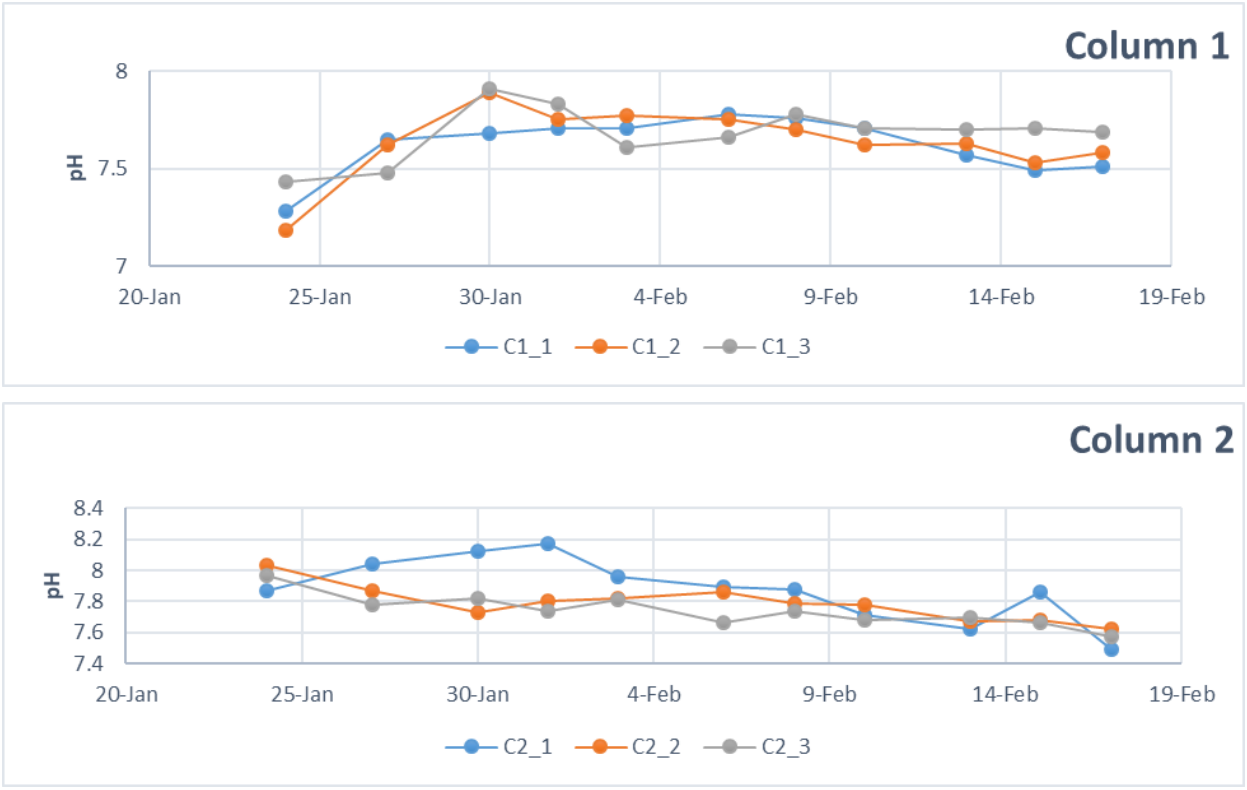

Figure 52. Results on pH measurements.

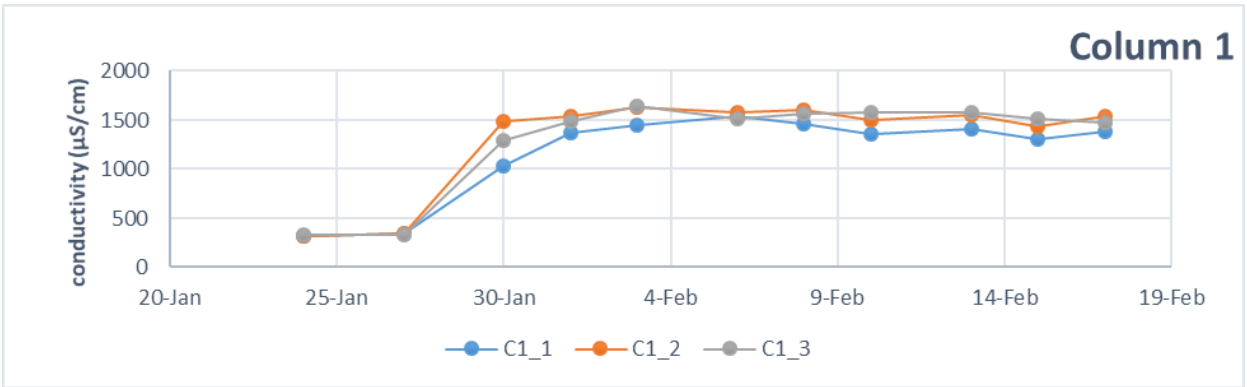

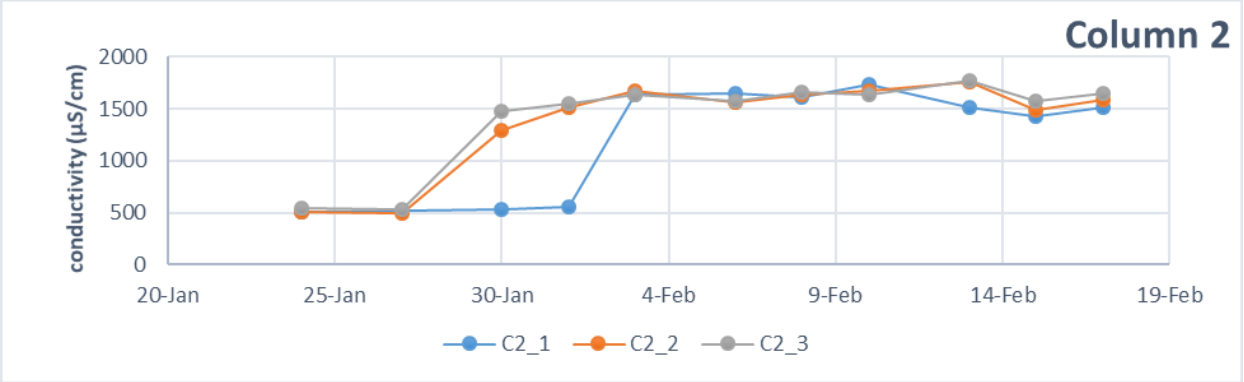

Figure 53. Results on conductivity measurements.

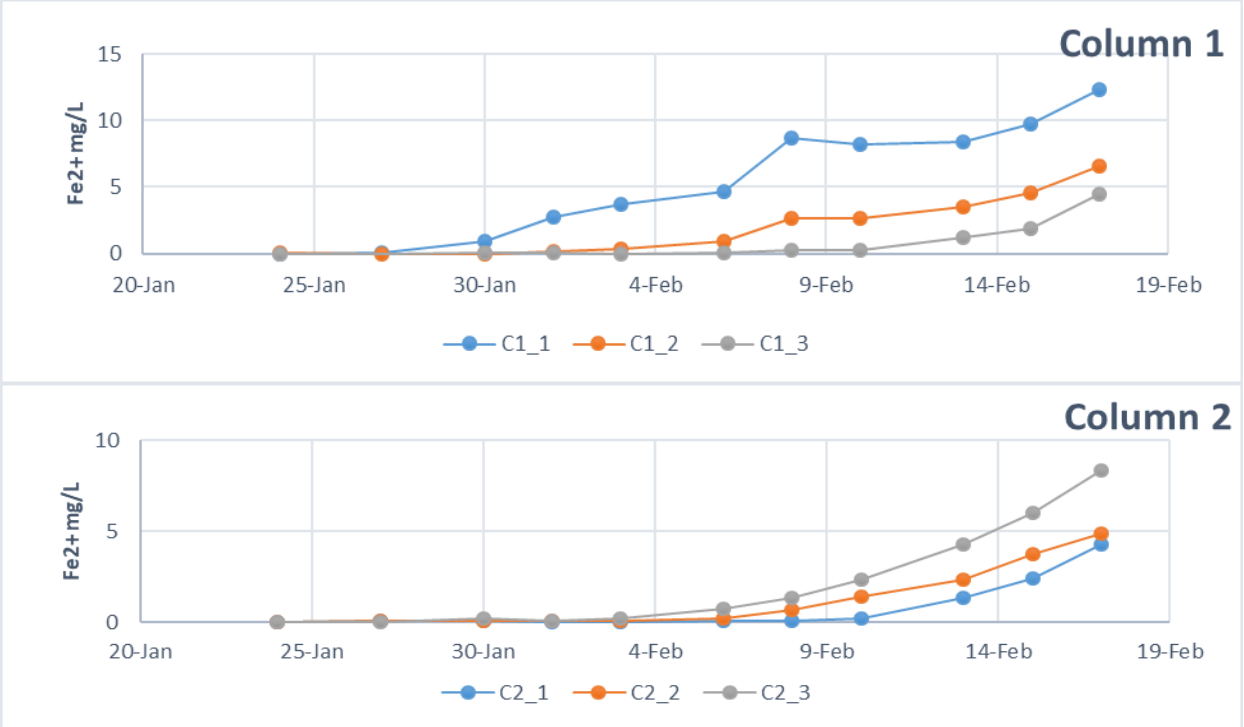

Figure 54. Results on ferrous iron measurements via ferrozine method.

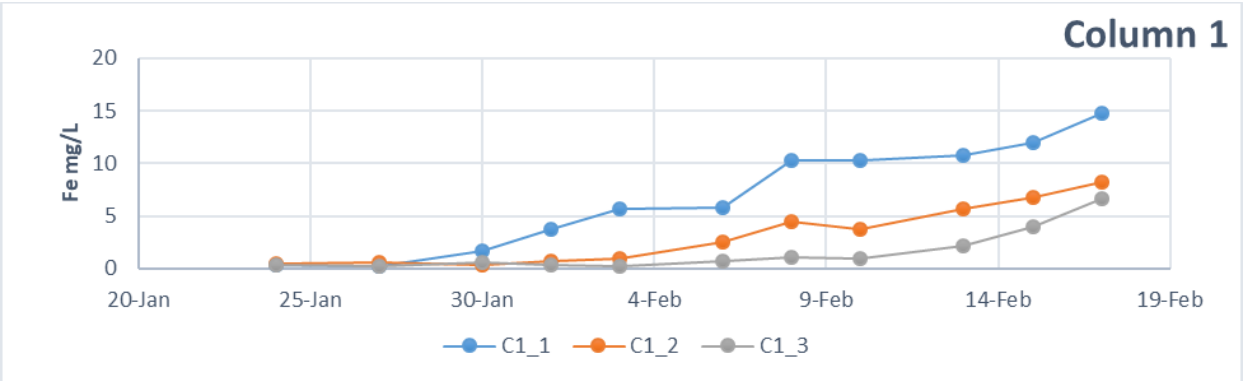

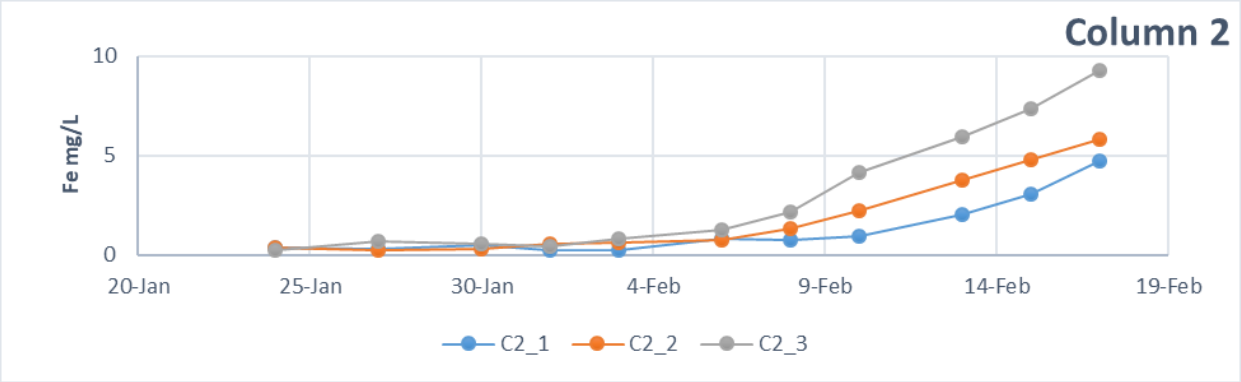

Figure 55. Results on total iron measurements via ferrozine and 1,10-phenanthroline methods.

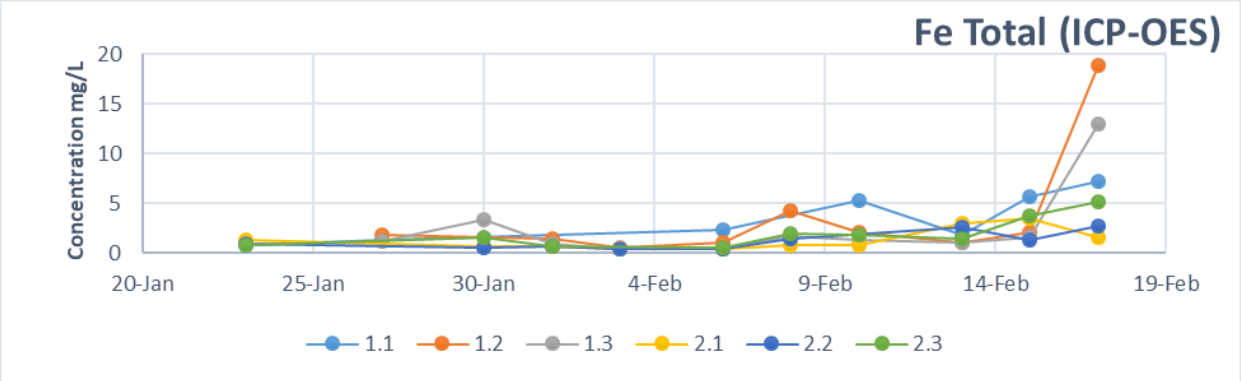

Figure 56. Results on total iron measurements via ICP-OES

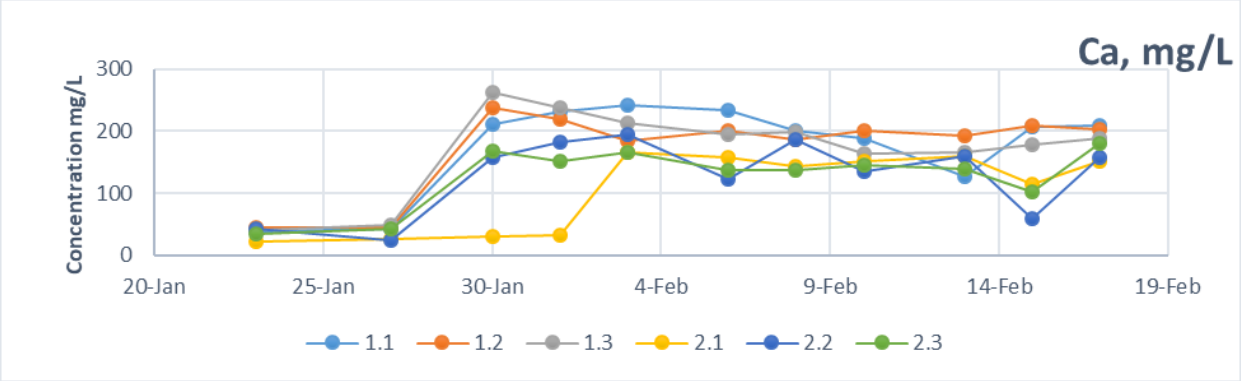

Figure 57. Results on calcium measurements

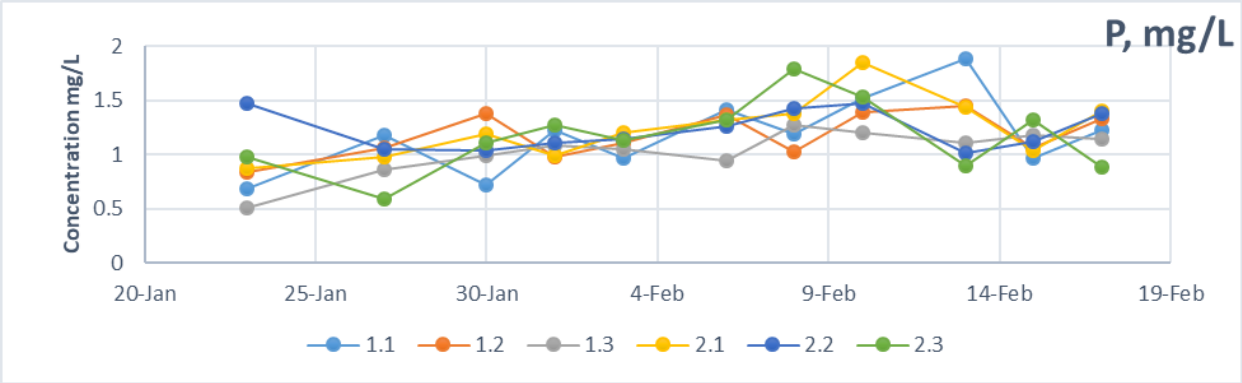

Figure 58. Results on phosphorus measurements

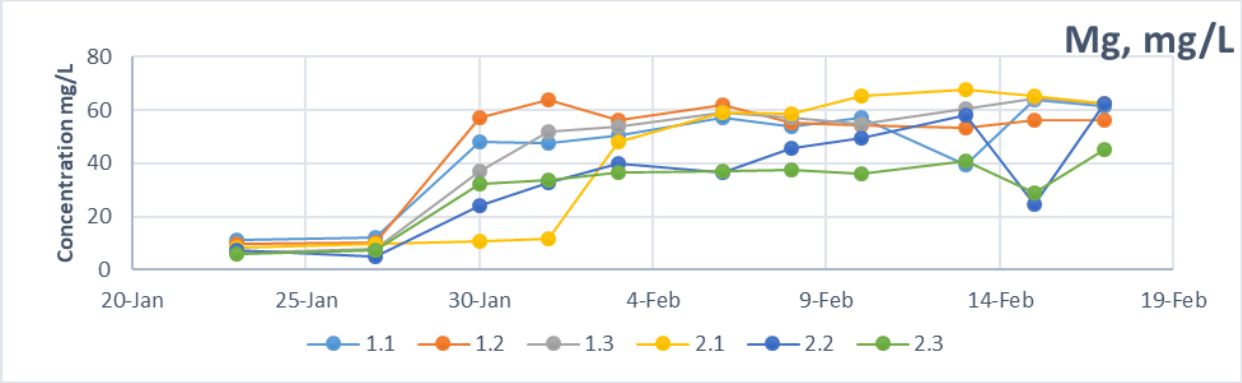

Figure 59. Results on magnesium measurements

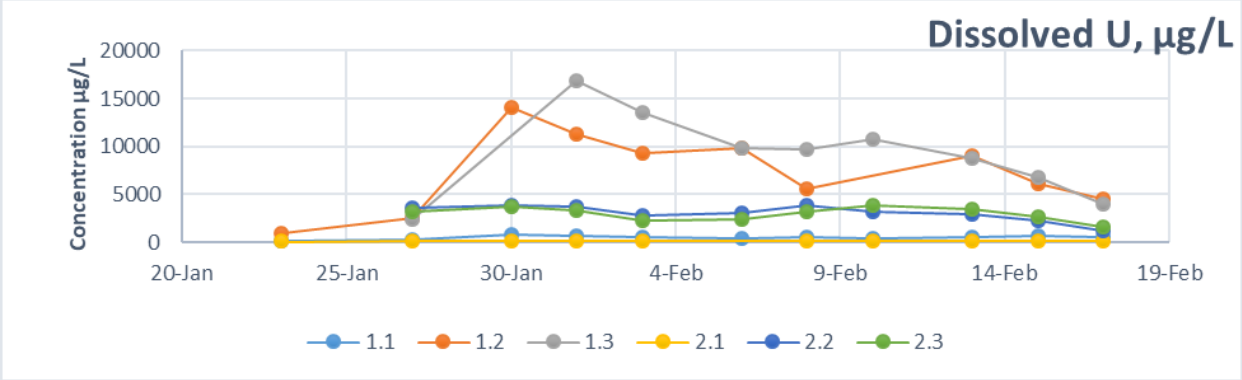

Figure 60. Results on uranium measurements via KPA

3. SIP measurements spring 2017

The phase spectra in both columns began shifting towards 0 mrad at the same time that resistivity began to decrease. Similar to previous experiments, these changes are in part related to ionic concentrations in solution as well as other changes occurring in the chemistry of the columns (Figure 61- Figure 62).

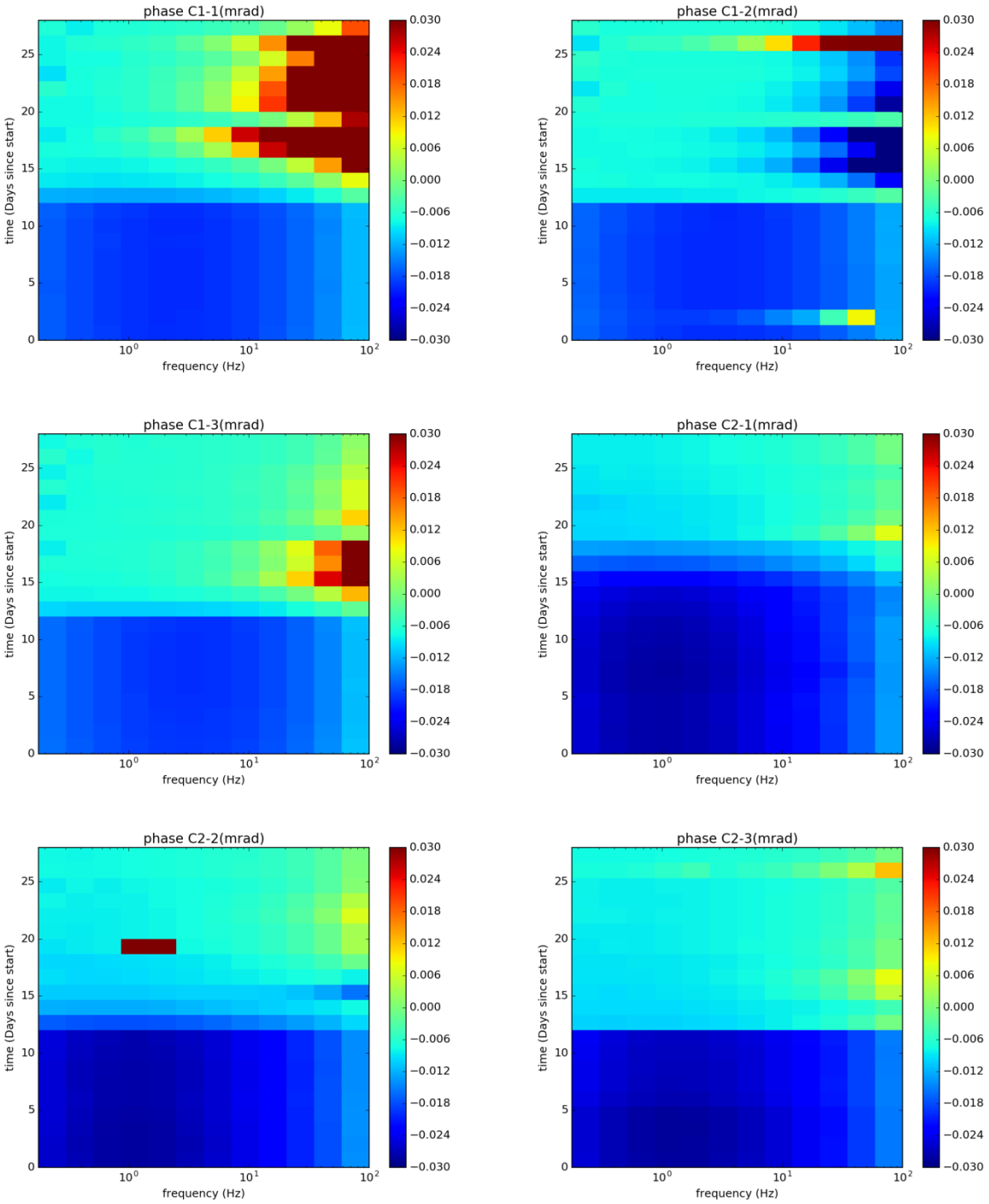

Figure 61. Phase spectra for Columns 1 and 2.

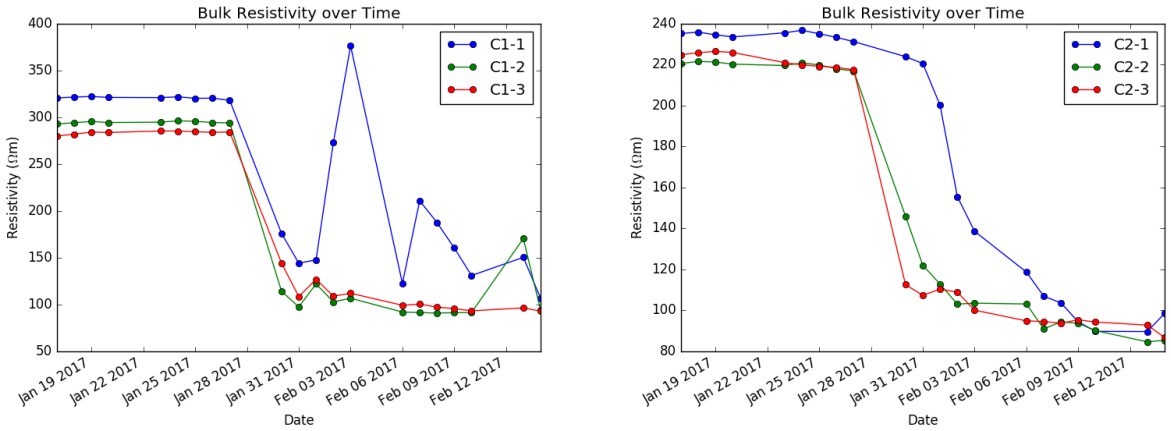

Figure 62. Bulk Resistivity for Columns 1 and 2.

Subtask 1.3: Conclusion

The microbial activities within the experimental columns have significant effects on the chemistry of the porewater and had effects which were detectable with SIP both as changes in the bulk resistivity and as changes in the frequency domain phase. These effects are due to a combination of factors including increased concentration of ions, possible clogging of pores, and the growth of biofilm. It is currently not understood how to distinguish between these effects and more basic research using simplified columns is necessary.

Columns with perceived microbe growth (all columns with glucose) showed a significant increase in dissolved Fe over time in part due to a shift from an oxidizing environment to a reducing environment. Uranium concentrations in the spring 2017 samples without bicarbonate showed a sharp increase which correlates to the sudden changes in pore water conductivity and SIP phase; over time, the concentrations trended down but remained higher than the samples with bicarbonate. The spring 2017 samples with bicarbonate seemed to maintain constant concentrations over time and were not affected significantly by changes occurring in the column.

Subtask 1.3: Future Work

FIU will work with PNNL to investigate the influence and corresponding electrical geophysical response of microbial activity in a set of basic experiments to test the SIP signal stability and reliability before proceeding to the next more complicated level. The experiments will address the following to validate the functionality of the SIP technique:

- Experiment 1: Set up soil-free SIP columns and operate with only autoclaved SGW.
- Experiment 2: Add autoclaved Hanford soil to the column and saturate with SGW.

  The SGW solution will be purged with oxygen to simulate aerobic conditions in the column or nitrogen to ensure anaerobic conditions within column. Conditions within the column will be kept aseptic; the SGW will be periodically changed to 10% bleach to flush the column between exchanges with SGW. To keep the conditions sterile, the experiments will not be run for an extended period of time.
- Experiment 3: Add heat deactivated microbial cells of known titer.

- Experiment 4: Add active microbial cells of known titer. This experiment will determine whether live cells produce different and distinct SIP signals. The results will be also compared to data obtained via the experiment utilizing only dead cells.
- The SIP signal measurements will be evaluated for each experiment to determine whether the signals are distinct for each of these contributing biogeochemical experimental conditions.

The general test methods for the columns will follow the same approach as was used during FIU Performance Year 7. The set up will include one-dimensional PVC columns. Potential electrodes will use the same design as used previously, a short silver wire encased in agar gel, to better facilitate contact with the soil. Current electrodes will be coiled Ag-AgCl and placed at either end. All sediments and solutions to be introduced to the columns will be autoclaved. A microbial culture (note: this is under discussion and could potentially be *Shewanella oneidensis* or a microbial consortia enriched at PNNL) will be used as inoculum for sediments to investigate if the geophysical techniques have the potential to improve detection of microbial activities in the subsurface. Measurements will be taken using a National Instruments data acquisition card connected to a standard Windows PC. Phase and conductivity will be measured at frequencies from 0.1 Hz to 100 Hz with measurements repeated five days a week. At the end of the experiment, sediment will be extracted to prepare samples for SEM/EDS analysis and to perform chemical analysis after sediment centrifugation. The sediment samples will undergo microscopy to count the bacteria.

Subtask 1.3: References

Atekwana, E. A., and Slater, L. D., 2009, Biogeophysics: A new frontier in Earth science research: Reviews of Geophysics, v. 47, no. 4.

Binley, A., and Kemna, A., 2005, DC Resistivity and Induced Polarization Methods, *in* Rubin, Y., and Hubbard, S., eds., Hydrogeophysics, Volume 50, Springer Netherlands, p. 129-156.

Fadrus, H., and Malý, J., 1975, Suppression of iron (III) interference in the determination of iron (II) in water by the 1, 10-phenanthroline method: Analyst, v. 100, no. 1193, p. 549-554.

Hao, N., Moysey, S. M., Powell, B. A., and Ntarlagiannis, D., 2015, Evaluation of Surface Sorption Processes Using Spectral Induced Polarization and a (22)Na Tracer: Environ Sci Technol, v. 49, no. 16, p. 9866-9873.

Li, Q., Wang, X., Bartlett, R., Pinay, G., Kan, D., Zhang, W., and Sun, J., 2012, Ferrous iron phosphorus in sediments: Development of a quantification method through 2, 2′-bipyridine extraction: Water environment research, v. 84, no. 11, p. 2037-2044.

Mehta, S., 2017, Geochemical evaluation of uranium sequestration from field-scale infiltration and injection of polyphosphate solutions in contaminated Hanford sediments: Applied Geochemistry, v. 84, no. Supplement C, p. 133-153.

Ntarlagiannis, D., and Ferguson, A., 2008, SIP response of artificial biofilms: GEOPHYSICS, v. 74, no. 1, p. A1-A5.

Ntarlagiannis, D., Williams, K. H., Slater, L., and Hubbard, S., 2005, Low-frequency electrical response to microbial induced sulfide precipitation: Journal of Geophysical Research, v. 110, no. G2.

Revil, A., 2012, Spectral induced polarization of shaly sands: Influence of the electrical double layer: Water Resources Research, v. 48, no. 2, p. n/a-n/a.

Reynolds, J. M., 1997, An Introduction to Applied and Environmental Geophysics, Wiley.

Stookey, L. L., 1970, Ferrozine-a new spectrophotometric reagent for iron.

Szecsody, J. E., Zhong, L., Oostrom, M., Vermeul, V. R., Fruchter, J. S., and Williams, M. D., 2012, Use of Polyphosphate to Decrease Uranium Leaching in Hanford 300 Area Smear Zone Sediments: Pacific Northwest National Laboratory (PNNL), Richland, WA (US), Environmental Molecular Sciences Laboratory (EMSL).

Um, W., Icenhower, J. P., Brown, C. F., Serne, R. J., Wang, Z., Dodge, C. J., and Francis, A. J., 2010, Characterization of uranium-contaminated sediments from beneath a nuclear waste storage tank from Hanford, Washington: Implications for contaminant transport and fate: Geochimica et Cosmochimica Acta, v. 74, no. 4, p. 1363-1380.

Vermeul, V. R., Bjornstad, B. N., Fritz, B. G., Fruchter, J. S., Mackley, R. D., Newcomer, D. R., Mendoza, D. P., Rockhold, M. L., Wellman, D. M., and Williams, M. D., 2009, 300 Area Uranium Stabilization Through Polyphosphate Injection: Pacific Northwest National Laboratory (PNNL), Richland, WA (US).

Wellman, D. M., Icenhower, J. P., Gamerdinger, A. P., and Forrester, S. W., 2006, Effects of pH, temperature, and aqueous organic material on the dissolution kinetics of meta-autunite minerals,(Na, Ca) 2-1 [(UO2)(PO4)] 2· 3H2O: American Mineralogist, v. 91, no. 1, p. 143-158.

Wellman, D. M., Pierce, E. M., Richards, E. L., Fruchter, J. S., and Vermeul, V. R., 2008, Uranium Plume Treatability Demonstration at the Hanford Site 300 Area: Development of Polyphosphate Remediation Technology for In Situ Stabilization of Uranium-8070: Pacific Northwest National Laboratory (PNNL), Richland, WA (US), Environmental Molecular Sciences Laboratory (EMSL).

Zachara, J. M., Fredrickson, J. K., Smith, S. C., and Gassman, P. L., 2001, Solubilization of Fe (III) oxide-bound trace metals by a dissimilatory Fe (III) reducing bacterium: Geochimica et Cosmochimica Acta, v. 65, no. 1, p. 75-93.

Zhang, Z., Wang, Y., Leslie, G. L., and Waite, T. D., 2015, Effect of ferric and ferrous iron addition on phosphorus removal and fouling in submerged membrane bioreactors: Water research, v. 69, p. 210-222.

Subtask 1.4: Contaminant Fate and Transport under Reducing Conditions

Subtask 1.4: Introduction

The Hanford Site in Washington State is the most contaminated nuclear site in the United States. Activities related to the chemical separations for plutonium extraction resulted in the production of hazardous liquid and radioactive solid wastes stored in underground storage tanks. Past practices for waste management activities and disposal operations resulted in leaks of mixed contaminant streams from some of these tanks, ponds, cribs and trenches, causing widespread subsurface contamination. Common co-mingled contaminants in the vadose zone and groundwater include U, ^{99}Tc, ^{3}H, ^{129}I, NO_3^- and CCl_4, all present in concentrations exceeding the drinking water standards. More specifically, approximately 69 TBq of ^{99}Tc has been introduced

into the vadose zone, either accidentally from leaks from the buried high-level waste tanks or intentionally via direct discharges (Szecsody et al., 2015).

Technetium-99 (Tc-99) is one of the major contaminants of concern at the Hanford Site. Technetium under oxidizing conditions is found as pertechnetate (TcO_4^-) whereas under reducing conditions it is found in the +4 valence state. Pertechnetate is highly soluble and sorbs very poorly onto sediments (Kaplan, Parker and Kutnyakov 1998). On the other hand, Tc(IV) is expected to either sorb onto the sediments or precipitate as insoluble $TcO_2 \cdot nH_2O$ (Icenhower et al. 2008). Technetium migration is affected by the porewater and groundwater chemical composition and soil mineralogy. Specifically, the presence of bicarbonates in Hanford porewater and iron minerals in Hanford soil may affect technetium's fate in the environment. Recent studies have identified the existence of stable, aqueous Tc(IV) carbonate-hydroxo complexes at circumneutral conditions, such as $Tc(CO_3)(OH)_3^-$ and $Tc(CO_3)(OH)_2$ (Eriksen Trygve et al. 1992, Paquette and Lawrence 1985, Alliot et al. 2009), indicating that despite Tc being reduced, it remains in the aqueous phase. Nevertheless, there is very limited data on the fate of those complexes and their interaction with soil components under reducing conditions.

Objectives

The objective of this research is to investigate the fate of Tc-99 in conditions related to the Hanford Site and explore the effect of bicarbonates on redox transformations of Tc-99. Specifically, the reduction of pertechnetate by Hanford soil and pure minerals relevant to the site, such as magnetite, was studied in the absence and presence of bicarbonates. Magnetite is an Fe (II,III) oxide found at the Hanford Site (Xie et al. 2003) and due to its high ferrous iron content, it could potentially provide the necessary electrons for the reduction of pertechnetate (+7 oxidation state) to TcO_2 (+4 oxidation state). Nevertheless, the existence of soluble Tc(IV)-carbonate complexes under circumneutral conditions has been recorded (Alliot et al. 2009) and therefore, the fate of Tc-99 in soil containing ferrous iron minerals and bicarbonates is not well understood. Ferrous iron minerals may provide the necessary electrons for the reduction of pertechnetate to amorphous TcO_2, but on the other hand, the presence of bicarbonates may act antagonistically and retain Tc-99 in the aqueous phase in its reduced form. Furthermore, the presence of bicarbonates may significantly affect Tc-99 mobility by facilitating the dissolution of prior-immobilized Tc(IV) in the form of TcO_2. There is limited data on Tc interaction with iron minerals under reducing conditions in the presence of bicarbonates, as well as on the re-solubilization of Tc(IV)-oxide due to the presence of carbonates. The present studies will provide new information on Tc(IV)-carbonate complexes as a potential mechanism for technetium migration in reducing geochemical environments by examining Tc-99 fate under conditions relevant to the Hanford Site.

Subtask 1.4: Methodology

1. Pertechnetate stock and working solutions

Pertechnetate stock solution was provided by Pacific Northwest National Laboratory (PNNL) as an 18-ml solution of NH_4TcO_4 with an initial concentration of 1000 mg L^{-1} of Tc-99 (10.2 mM). The stock solution was stored at 4^oC and was diluted to the desired final concentration for each experiment using deionized water which had been degassed with high purity N_2 and continuously stirred for 2h. In all experiments, the initial concentration of pertechnetate was 25μM unless stated otherwise.

2. Hanford sediment, characterization and pure minerals

Hanford sediment was provided by PNNL and was sieved in FIU's Soil and Groundwater Lab. Pure magnetite was purchased by Alfa Aesar in the form of ~325 mesh powder (hereafter referred to as micro-magnetite) and in the form of nanopowder (hereafter called nano-magnetite). Both commercial products had been nitrogen flushed and, upon arrival at FIU, were stored in the anaerobic glovebox under 98%:2% N_2:H_2 atmosphere. The specific surface area and the pore volume of Hanford sediment fractions were determined by nitrogen adsorption (BET method) available at FIU's Department of Mechanical Engineering, whereas the mineralogical analysis by means of X-ray diffraction (XRD) was performed at FIU's Advanced Materials Engineering Research Institute (AMERI). XRD data analysis was performed using MATCH! Software. Samples were prepared by crushing about 3 g of Hanford sediment to create a fine powder-like solid for the XRD analysis. The samples were crushed using a mortar and pestle in order to increase homogeneity. Figure 63 depicts an example of the morphology of the bulk soil fraction before and after grain size reduction. It is imperative for the morphology be as homogenous as possible, since the X-rays, in the case of a coarse sediment, may diffract several times on valleys and peaks formed by the sample's grains and this can lead to an increase in noise and weaker signals.

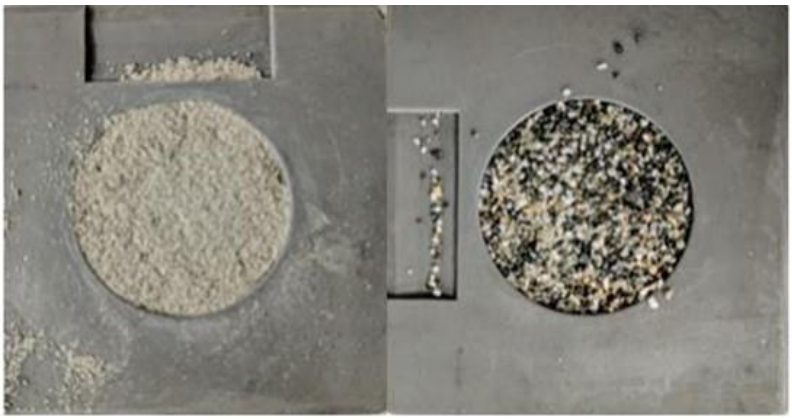

Figure 63. Example of Hanford sediment crushed (left) as opposed to not crushed (right) for XRD analysis

3. Batch experiments

a. Pertechnetate reduction in the presence of reducing agents

Preliminary experiments involved suspensions of 1g of Hanford sediment (average particle diameter d<300μm) and 50 mL of solution of TcO_4^- with an initial concentration equal to 50 μM. All suspensions contained 10^{-3}M Na-HEPES and pH was adjusted to 7.5 using 0.001M HCl, and contained 10 mM HCO_3^-. Samples were introduced to the anaerobic chamber in 98% N_2:2% H_2 atmosphere (Figure 64). Samples were spiked with small amounts of different reducing agents, namely $NaBH_4$, HCOOH, hydroquinone and $SnCl_2$, and the final concentration of each agent was equal to 1 mM. The stock solutions of the reducing agents were created by dissolving the appropriate amount of the solid with deionized water which had been purged with N_2 (2h of N_2 purging under continuous stirring). Eh and pH were monitored periodically by using a Hannah Instruments redox electrode (reference Ag/AgCl) and an Orion 9110D pH electrode, respectively. Periodically, aliquots were isolated for the determination of residual Tc-99 in the aqueous phase. Na-HEPES has been identified in literature as an appropriate buffer when studying Tc redox chemistry (Shi et al., 2011; Yalçintaş et al., 2015).

Figure 64. Anaerobic glovebox at FIU EC1227 where pertechnetate reduction experiments are currently taking place under 98% N_2 : 2% H_2 atmosphere.

b. Pertechnetate reduction by Hanford sediment and magnetite

300 mg of micro- and nano- magnetite were suspended in 30 mL of Tc-99 solution of 25 μM initial concentration. pH was adjusted to 6 and 8 using 0.001 M HCl. Samples were introduced to the anaerobic chamber in 98% N_2:2% H_2 atmosphere (Figure 64). Hanford sediment suspensions were created by bringing into contact 2.5g of Hanford sediment (average particle diameter d<300μm) with 30 mL of Tc-99 solution of 25 μM initial concentration, pH 8. The 2.5g of Hanford sediment contained 300 mg of magnetite, as determined by preliminary XRD analysis. Eh and pH were monitored periodically by using a Hannah Instruments redox electrode and an Orion 9110D pH electrode, respectively. Periodically, aliquots were isolated for the determination of residual Tc-99 in the aqueous phase. All experiments were performed in duplicate and each sample reading is reported within a 95% confidence level (2s) by the liquid scintillation counter.

c. Dissolution experiments

Upon achieving 100% reduction of pertechnetate by nano-magnetite, the samples were centrifuged at 4,500 rpm for 10 min and re-introduced to the anaerobic glovebox. Magnetite was further detained at the bottom of the vial with the aid of a magnet and the pertechnetate-free supernatant was removed with a 1-ml syringe. Consequently, 40 mL of 5 mM HCO_3^- were added to the vial and the vial was equilibrated inside the anaerobic glovebox. Periodically, aliquots were isolated for the determination of Tc-99 in the aqueous phase due to TcO_2 dissolution in the presence of bicarbonates, as a function of time.

4. Tc-99 analysis

The Tc-99 analysis in the aqueous phase was performed by using a Perkin Elmer Tricarb 2910 liquid scintillation counter (Figure 65). The speciation of Tc(IV) and Tc(VII) in the aqueous phase was performed by solvent extraction, using chloroform and tetraphenylphosphonium chloride (TPPC). After extracting an appropriate amount from the aqueous phase, the sample was filtered through a 0.2 μm filter and the appropriate amount of 4 mM TPPC was added to create a final TPPC:TcO_4- molar ratio higher than 40:1. Chloroform was added to a final volume

of 1 mL and the sample was vortexed lightly. Once TPPC is in contact with water, it dissociates to form $(C_6H_5)_4P^+$ and Cl^- which complex with Tc(VII), giving very stable complexes. Hence, tetravalent technetium ends up in the aqueous phase and heptavalent technetium ends up in the organic phase (Kopunce et al., 1998; Yalçintaş 2015). The sample was centrifuged at 14,500 rpm for 5 min and an amount of each phase (aqueous and organic) was transferred to a plastic scintillation vial that contained 5 mL of fluorescent cocktail (Ultima Gold, Perkin Elmer). The samples were measured for 5 min in the liquid scintillation counter.

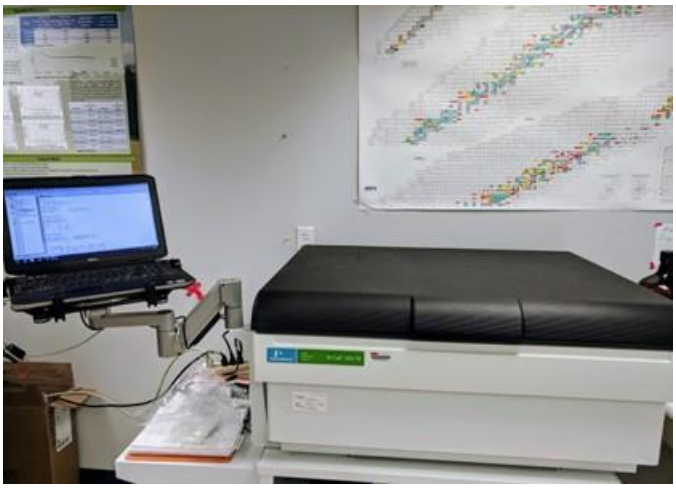

Figure 65. Perkin Elmer TriCarb 2910 TR Liquid Scintillation Counter used throughout the experiments

Subtask 1.4: Results and Discussion

1. Soil characterization

Sieving of Hanford soil (567g) was performed in the lab in an effort to identify major soil fractions (Figure 66) and to consequently perform specific surface area analysis (BET). The preliminary results assisted in identifying the appropriate fraction of soil to be used for the experiments. The largest soil fraction has a mean particle diameter of 500 µm<d< 2mm, making up approximately 35% of the soil, followed by the soil fraction 300 µm<d< 500 µm with approximately 33% of the soil. The remainder of the fractions was combined to make the remaining 32% of the soil with d< 300 µm.

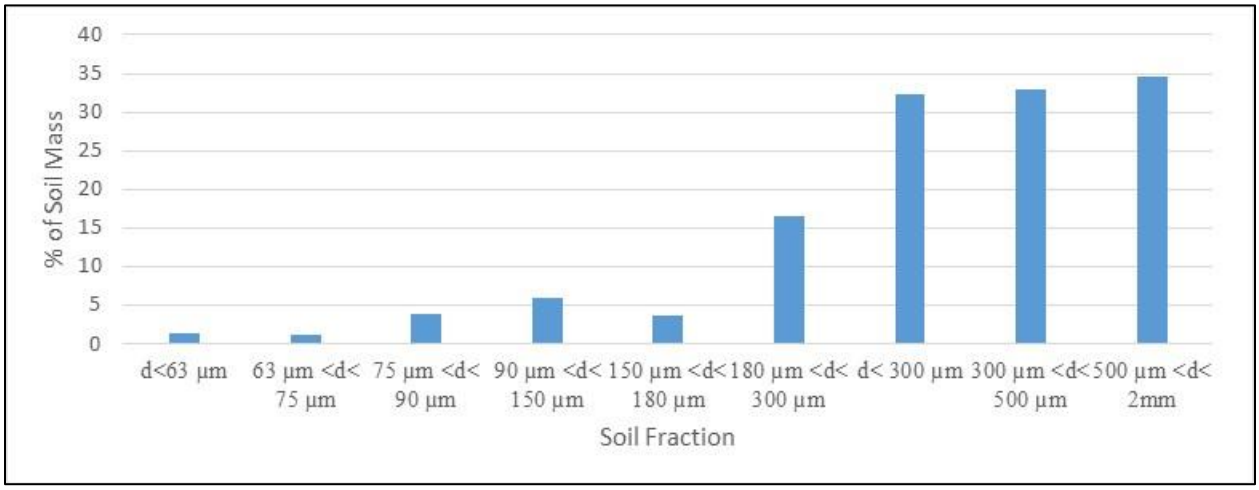

Figure 66. Percentage of soil mass as a function of fractions collected during Hanford sediment sieving

The specific surface area and the pore volume of the three Hanford sediment fractions collected are presented in Table 19. As expected, the fine fraction (d<300 µm) exhibits higher specific surface area and pore volume; specifically, the specific surface area and pore volume are double of the corresponding numbers of the other fractions. On the other hand, the intermediate and coarse fraction (300 µm<d<500 µm and 500 µm<d<2mm, respectively) have the same specific surface area and pore volume. Based on these results, the two upper fractions have been merged to one due to sharing the same characteristics.

Table 19. Surface area (m^2/g) and pore volume (cm^2/g) for three different fractions of Hanford sediment

Soil Fraction	Surface Area (m^2/g)	Pore Volume (cm^2/g)
d<300 µm	10.67	0.0144
300 µm<d<500 µm	5.36	0.0075
500 µm<d<2 mm	5.73	0.0082

* Sample Density (2.65 g/cm^2)

The two different fractions were analyzed by X-Ray Diffraction and the preliminary qualitative results are presented in Figure 67 and Figure 68. The samples were run from 2 to 40 2-theta and results revealed the presence of quartz, microcline, calcite, and magnetite for the bulk fraction, whereas the presence of quartz and magnetite was identified for the fine fraction. It is important to note that the legends in Figures 5 and 6 give a percentage that is associated with peak matches, not the percentage of mineral in the soil. In both figures, quartz seems to have the highest peak match when compared to some of the other possible matches. Based on the preliminary results by XRD, the primary reflection peaks for quartz (26.6°), microcline (21.1°) and calcite (29.45°) were identified in accordance with previous PNNL publications (Serne et al., 2004).

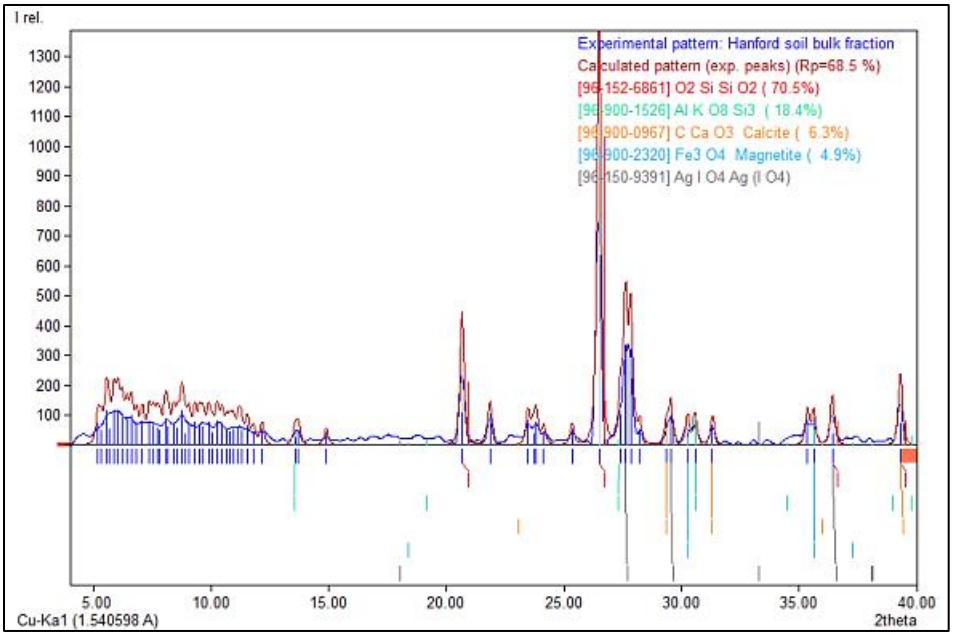

Figure 67. XRD analysis diagram of the bulk fraction for a range 2-40 2θ

To improve the reliability of the results, as well as increase the percent of peak matches for some of the other mineral candidates that may be present in the sediment in smaller percentages, the samples were reanalyzed by means of XRD in a range of 3 to 80 2-theta, in order to increase the possibility of peak matches after 40 2-theta. The spectra are presented in Figure 69 and Figure 70 for the bulk and the fine fractions, respectively, and the quantitative analysis is presented in Table 20. The results from the 3 to 80 2-theta run were used for the quantitative analysis of the Hanford sediment mineralogy throughout this report.

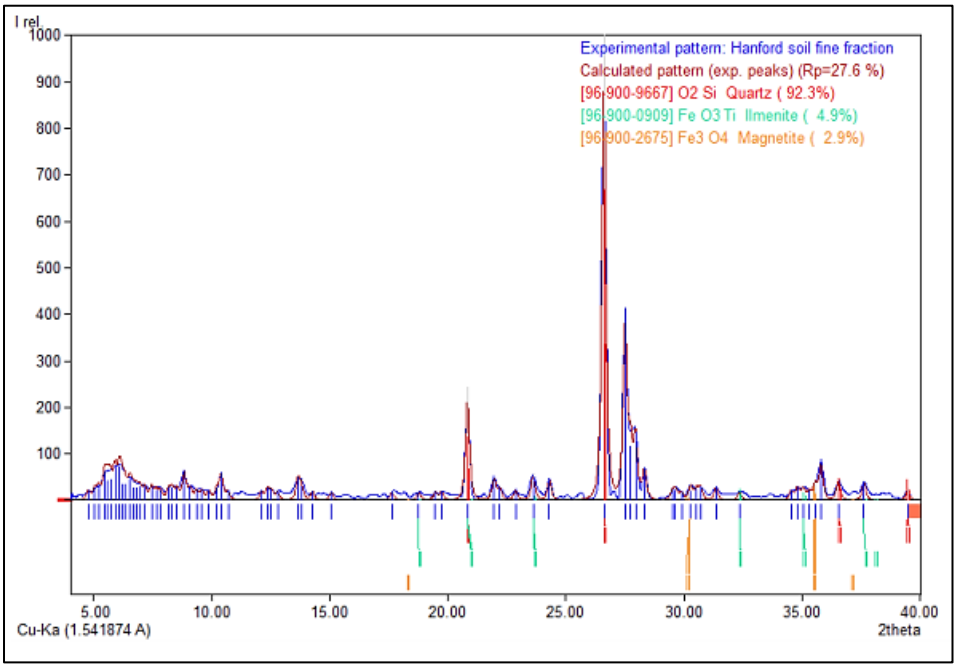

Figure 68. XRD analysis diagram of the fine fraction for a range 2-40 2θ

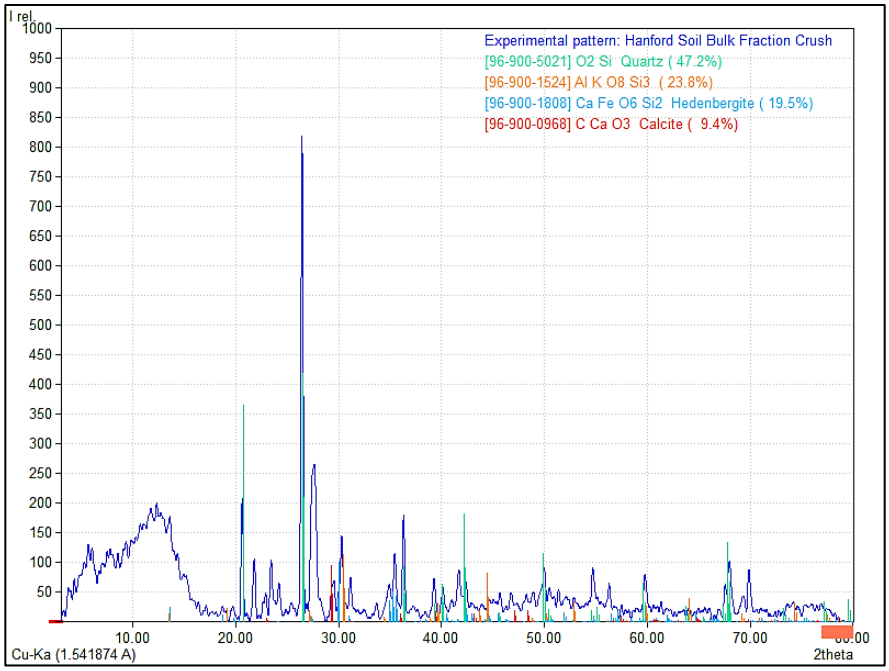

Figure 69. XRD analysis diagram of the bulk fraction for a range 2-80 2θ

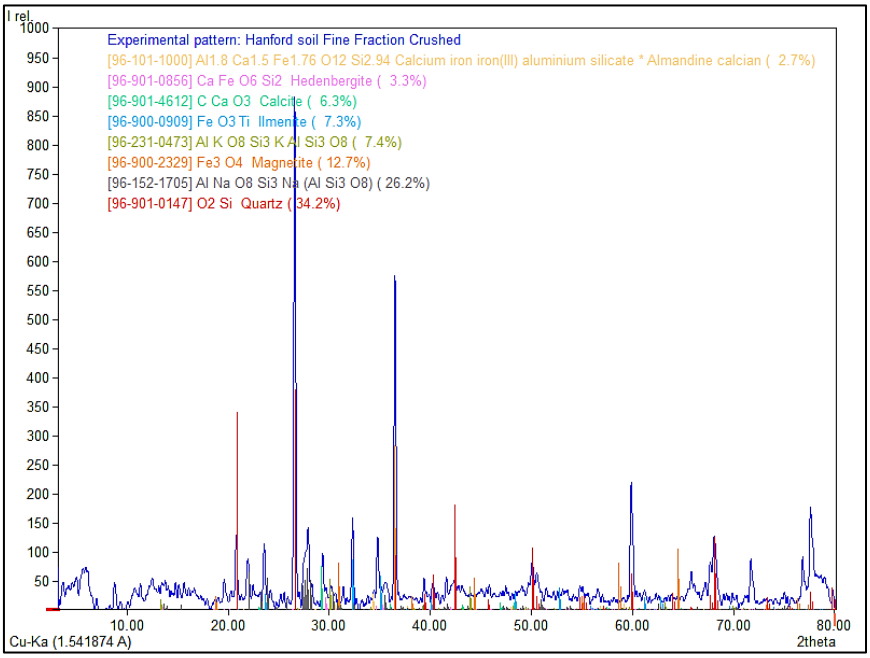

Figure 70. XRD analysis diagram of the fine fraction for a range 2-80 2θ

Table 20. XRD mineralogical analysis for two fractions of Hanford sediment

Bulk Fraction (300 µm<d< 2mm)							
	Quartz	Microcline[1]	Pyroxenes[2]	Calcite			
Amount (%)	47.2	23.8	19.5	9.4			
Fine Fraction (d< 300 µm)							
	Quartz	Microcline[1]	Magnetite	Plagioclase[3]	Ilmenite	Calcite	Pyroxenes[2]
Amount (%)	34.2	26.2	12.7	7.4	7.3	6.3	3.3

[1] In the form of $KAlSi_3O_8$
[2] In the form of $(Ca,Fe)Si_2O_6$
[3] In the form of $NaAlSi_3O_8$

In both figures, quartz is present with the highest percentage, but that percentage is smaller in the fine fraction. The presence of ferrous iron minerals, such as magnetite (a Fe(II,III) oxide) and ilmenite, were identified in the fine fraction compared to the bulk fraction. Ferrous iron may play a significant role in the reduction of Tc-99 and act as an electron donor, affecting its mobility in the environment. Similar results have been reported in literature for sediment and soil samples from different Hanford areas. Xie et al. (2003) researched the geochemical composition and mineralogy of the 200 Area (HF Area, samples from 25-100 ft depth) and from Ringold (depth 200-500 ft). A total of 55 samples were analyzed by means of electron microprobe (EM) and the major minerals identified were quartz at approximately 38% by weight (wt), plagioclase ~22% wt, microcline ~15% wt, amphiboles ~5.5% wt, pyroxenes ~5% wt, and magnetite ~4.5% wt. Szecsody et al. (2013) collected sediments from Hanford, Ringold, and Cool Creek and the mineralogical analysis was performed by means of XRD. The study concluded that quartz and plagioclase are the major minerals present in all sediment samples.

2. Pertechnetate reduction in the presence of reducing agents

Preliminary experiments were performed in order to assess the capacity of different inorganic and organic reducing agents to maintain the reducing conditions in the samples located in the anaerobic glovebox. Samples contained Na-HEPES (0.001 M) in order to maintain pH values within the desired range (7.5±0.5), 10 mM HCO_3^- and each reducing agent at a concentration of 0.001 M. In Figure 71, the fluctuation of Eh as a function of time is presented.

The experimental results revealed that all reducing agents maintained reducing conditions in the samples. Nevertheless, sodium dithionite was not deemed appropriate for future use due to the high fluctuation of Eh values during measurement, which is likely related to the degradation of $Na_2S_2O_4$ in circumneutral conditions (Lem and Wayman, 1970; Yalcintas, 2015). Sodium thiosulfate was also excluded from future use due to the possible formation of technetium sulfides (Rard et al., 1999). The organic acids' ability to maintain stable Eh readings was found to be highly dependent on the hydrogen content of the anaerobic glovebox, as opposed to the rest of the reducing agents, where stable Eh readings were recorded despite H_2 content fluctuation (±0.5%) in the glovebox. Furthermore, stannous chloride and ferrous chloride were not chosen for future use due to the formation of a solid phase in circumneutral conditions. Quantitative reduction of Tc(VII) to Tc(IV) has been reported in the presence of Sn(OH)Cl solids (Yalcintas et al., 2015) under circumneutral conditions. Nevertheless, the introduction of foreign solid

phases to the system is not desirable. These preliminary experiments provided significant insight into the system's equilibration time and Eh stability due to the presence of reducing agents (and the absence of iron and titanium-bearing minerals present in Hanford soil).

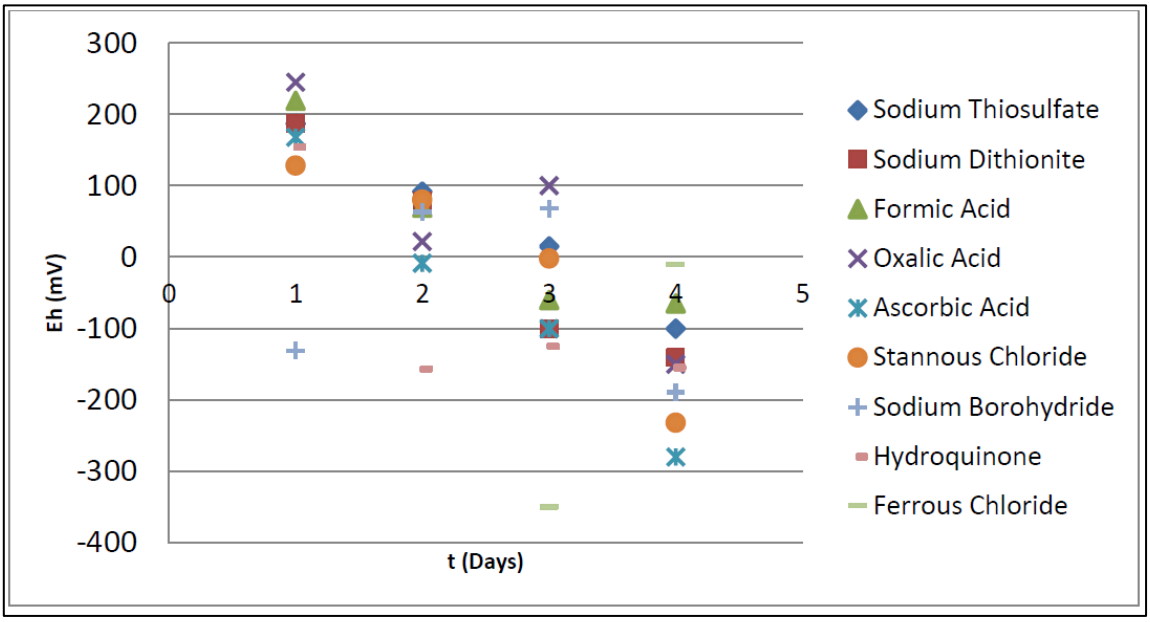

Figure 71. Eh (mV) values as a function of time for samples containing different reducing agents in the absence of Hanofrd sediment

The experiment was then repeated under identical conditions in the presence of 1g of Hanford sediment (average particle diameter d<300µm) and 0.001 and 0.002 M of $NaBH_4$, formic acid and hydroquinone for 3 weeks. Eh fluctuation as a function of time throughout the experimental process is presented in Figure 72.

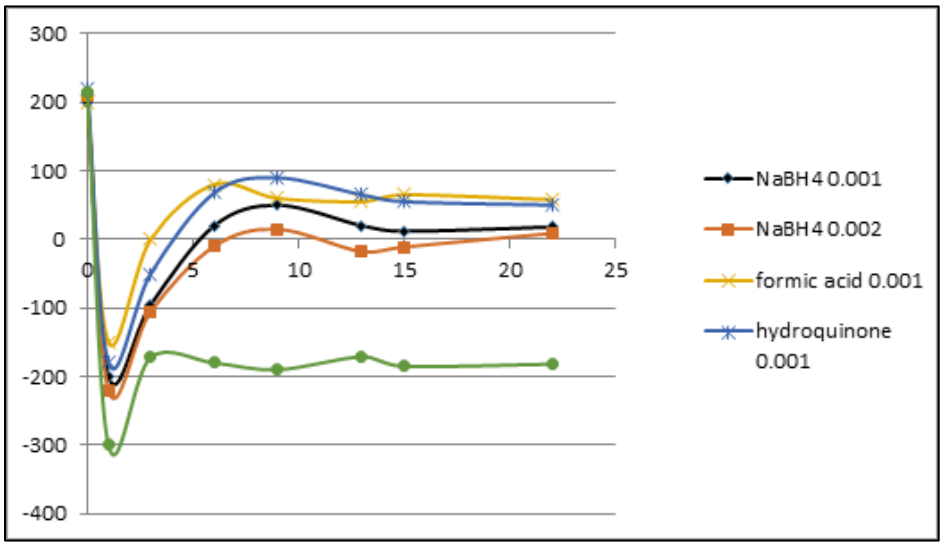

Figure 72. Eh (mV) values as a function of time for samples containing different reducing agents in the presence of 1g Hanofrd sediment (d<300µm)

As can be seen in Figure 10, the introduction of a reducing agent in the aqueous phase incites an immediate plunge of the Eh values and then equilibration takes place and Eh values stabilize in a

time period of 5-7 days. $SnCl_2$ is one of the strongest reducing agents and managed to keep the Eh values very low, slightly above the border of water reduction (Yalçintaş 2015). All reducing agents induce conditions that favor the reduction of Tc(VII) to Tc(IV), which in circumneutal conditions, usually will take place for Eh values below 100 mV (Icenhower et al., 2008).

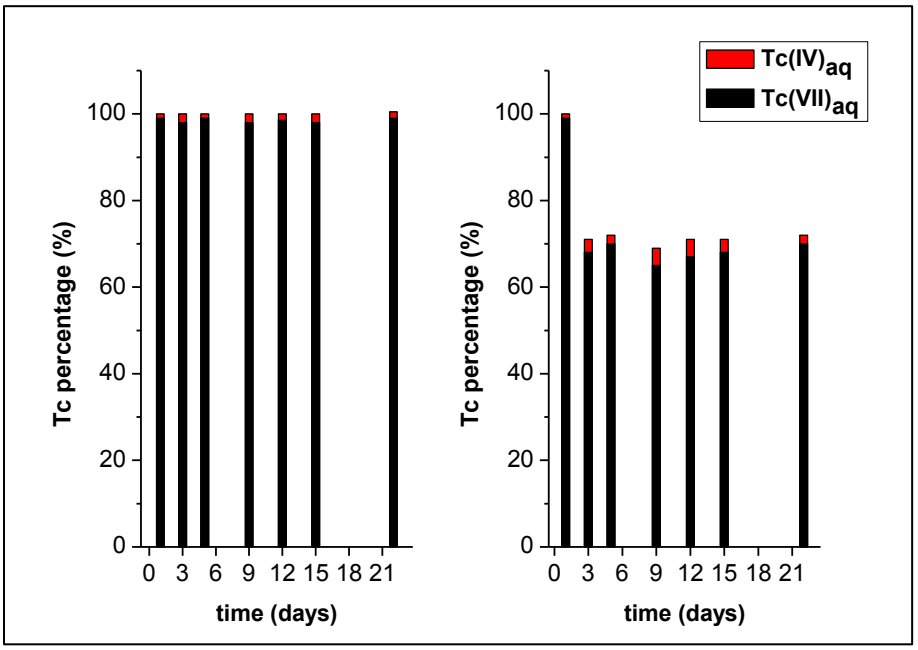

Figure 73. Tc percentage in the aqueous phase as a function of time for Hanford soil suspensions in the presence of hydroquinone, formic acid and in plain N_2-H_2 atmosphere (left) and in the presence of $NaBH_4$ (right).

As can be seen in Figure 73, despite the recorded reducing conditions, the presence of reducing agents such as formic acid and hydroquinone, as well as in the absence of a reducing agent in the aqueous phase (plain N_2-H_2 atmosphere), Tc-99 is found in the +7 oxidation state. Despite this seeming paradox, Tc can be encountered as pertechnetate even under reducing conditions, since the steric distribution of electron donors is more important for the redox reaction Tc(7+) to Tc(4+) rather than the overall Eh values (Icenhower et al., 2008). Similar results have been recorded in plain Tc solution in the presence of hydroquinone (in the absence of a mineral or a solid phase) by Yalçintaş (2015) and Kobayashi et al. (2013) in the presence of hydroquinone in diluted NaCl systems. Overall, it was concluded that the oxidized form of hydroquinone was incapable of providing the 3 e^- needed for the reduction of pertechnetate to Tc(4+). In the case of $SnCl_2$, a fast and complete reduction was observed within 3 days, where the full quantity of technetium was removed from the aqueous phase. Similar results have been reported in literature (Yalçintaş et al., 2015), where complete reduction was observed within 7 days. $SnCl_2$ was used for comparison reasons, since the undesirable formation of an insoluble salt under circumneutral conditions based on the reaction $SnCl_2$ (aq) + H_2O (l) ⇌ Sn(OH)Cl (s) + HCl (aq), would render its use very limited. In the case of $NaBH_4$, after 3 days, the concentration of Tc_{aq} decreased by 35%; nevertheless, the remaining technetium in the aqueous phase was encountered in the +7 oxidation state. This is an additional indication of the importance of electron donation for the reduction of pertechnetate to Tc(IV), since the reaction decreased the concentration of Tc_{aq} by 35% after 3 days and then remained in a steady state. The concentration of $NaBH_4$ did not seem to affect the outcome of the reaction under the conditions studied. Finally, it should be noted that

all samples contained a ratio of Tc:HCO_3^- equal to 200:1, much higher than the 30:1 cited in literature (Eriksen et al., 1992), which would likely favor the formation of Tc(IV)-carbonate complexes under circumneutral conditions and prevent the precipitation of TcO_2.

3. Pertechnetate reduction by Hanford sediment and magnetite

Hanford sediment and magnetite (micro- and nano- magnetite) were introduced to the anaerobic glovebox in a 98% N_2:2% H_2 environment. pH levels stabilized after 4 days, whereas Eh values stabilized after 2 days. It is noteworthy that after 24h inside the anaerobic chamber in an oxygen-depleted atmosphere, Eh values were still at oxidizing levels. The level of equilibration in the literature may vary depending on the substrate; nevertheless, the samples in each case were equilibrated for several days: 3 days for magnetite suspensions in 3% H_2 atmosphere (Cui and Eriksen, 1996), 4 days for Fe(II) minerals sorbed on goethite (Peretyazhko et al., 2009) and 7 days for magnetite and mackinawite suspensions (Yalcintas et al., 2016).

As can be seen in Figure 74, nano-size magnetite at pH 6 reduces pertechnetate 100% within 40 days. On the other hand, the preliminary results with nano-size magnetite at pH 8 indicate a much slower rate of reduction. A possible explanation for this could be the fact that pertechnetate reduction is favored in acidic conditions, based on the reaction:

$$TcO_4^- + 4H^+ + 3e^- \leftrightarrow TcO_2(s) + 2H_2O$$

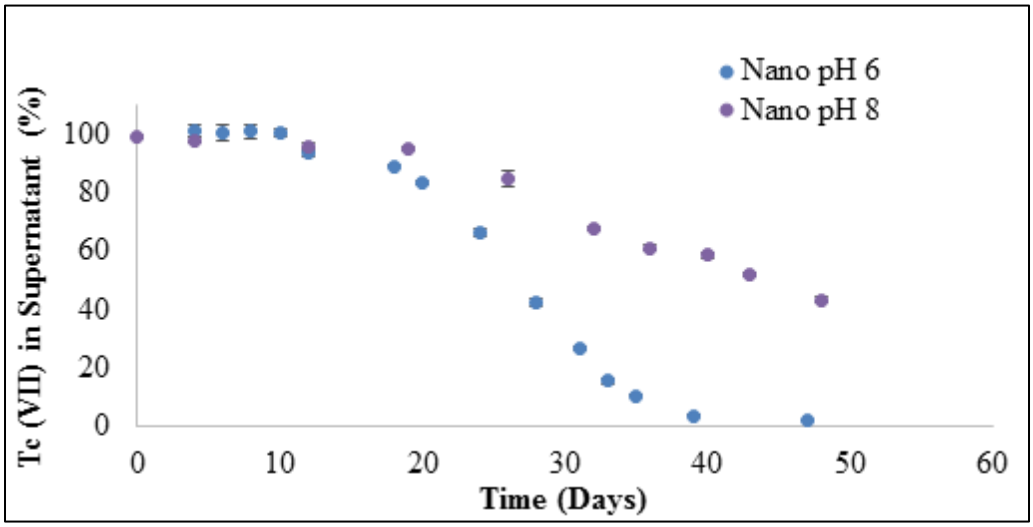

Figure 74. Pertechnetate reduction as a function of time by nano-magnetite at pH 6 and 8

Another factor that may play role in the faster reduction of pertechnetate in acidic conditions is the presence of ferrous iron in the aqueous phase. In the case of nano-size magnetite at pH 6, the levels of ferrous iron were measured periodically throughout the experiment using the ferrozine method (Verschoor and Molot, 2013) and were equal to 5 mg/L, whereas in the case of both micro- and nano-magnetite at pH 8, ferrous iron levels were below detection levels (<50 μg/L). The ferrous iron results for pH 8 imply that since pertechnetate reduction is taking place and practically no ferrous iron is detected in the aqueous phase, the reaction is due to the electron donation of the mineral (heterogeneous reaction). Interestingly, at pH 6, the levels of ferrous iron are significant and the role of $Fe(II)_{aq}$ is ambiguous: it is not clear if the faster reduction rate is facilitated by the presence of $Fe(II)_{aq}$, despite the fact that the $Fe(II)_{aq}$ concentration did not fluctuate as a function of time. To this end, FIU prepared additional control samples under

identical conditions in the absence of solid mineral ($[TcO_4^-]_{init}$ = 25μM, $Fe(II)_{aq,init}$ 5 ppm, pH 6 under anaerobic conditions) in order to monitor more closely the $Fe(II)_{aq}$:$Fe(III)_{aq}$ ratio and identify the effect of aqueous ferrous iron in the pertechnetate reduction. The reduction of pertechnetate by Fe(II) in the aqueous phase, although thermodynamically feasible, has been reported to be kinetically hindered (Cui and Eriksen, 1996; Peretyazhko et al., 2009). Zachara (2007) also confirmed that $Fe(II)_{aq}$ may contribute, if present, to pertechnetate reduction at neutral and alkaline conditions (pH>7), but not in acidic conditions. Peretyazhko (2009) suggested the following scheme to describe the affinity of Tc(VII) heterogeneous reduction by Fe(II):

$Fe(II)_{aq}$ ~ Fe(II) sorbed in phyllosilicates << structural Fe(II) << Fe(II) sorbed on Fe(III) oxides

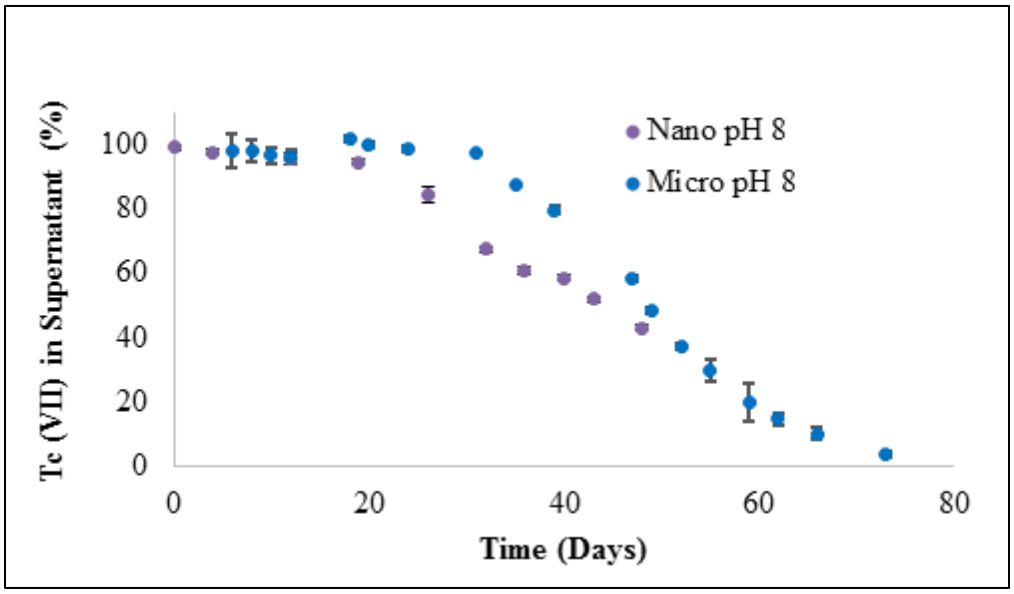

Figure 75. Pertechnetate reduction as a function of time by nano- and micro-magnetite at pH 8

On the other hand, at pH 8, nano-magnetite seems to reduce pertechnetate much faster, at least in the early stages of the reaction. The mass of magnetite is the same in both sets (micro- and nano-magnetite); hence the difference in reduction rate may be due to the difference in specific surface area (nano-magnetite exhibits larger surface area than micro-magnetite, as per commercial specifics), since the specific surface area plays an important role in heterogeneous reactions (McBeth et al., 2011). An additional explanation for the different behavior of the same mineral could potentially be the different Fe(II):Fe(III) ratio between micro-magnetite and nano-magnetite (currently under investigation).

Preliminary experiments with Hanford sediment at pH 8 revealed a pattern of Hanford sediment similar to that of micro-magnetite (Figure 76). After 30 days of contact, no pertechnetate reduction was observed, whereas ~40% TcO_4^- was reduced by nano-magnetite at the same time. The Hanford sediment and the magnetite samples contained the same amount of magnetite, but the Hanford sediment contained higher levels of Fe(II) iron due to the presence of ilmenite and pyroxenes (Table 20) and perhaps a faster reduction of peretechnetate may have been expected.

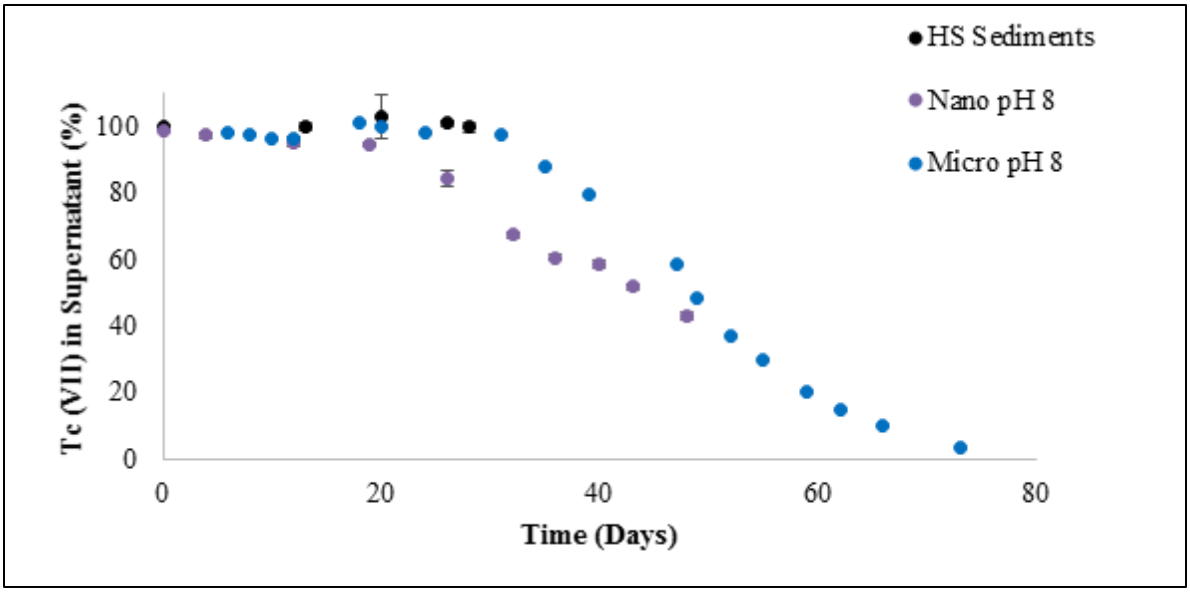

Figure 76. Pertechnetate reduction as a function of time by nano- and micro-magnetite and Hanford sediment at pH 8

4. Dissolution experiments

The immobilized TcO_2 on nano-magnetite was re-suspended in 40 mL of 5 mM HCO_3^-, pH 8 (priorly purged with N_2 and equilibrated under anaerobic conditions for 5 days). Eh values were constant throughout the experiment and equal to -150mV. The dissolution results are presented in Figure 77.

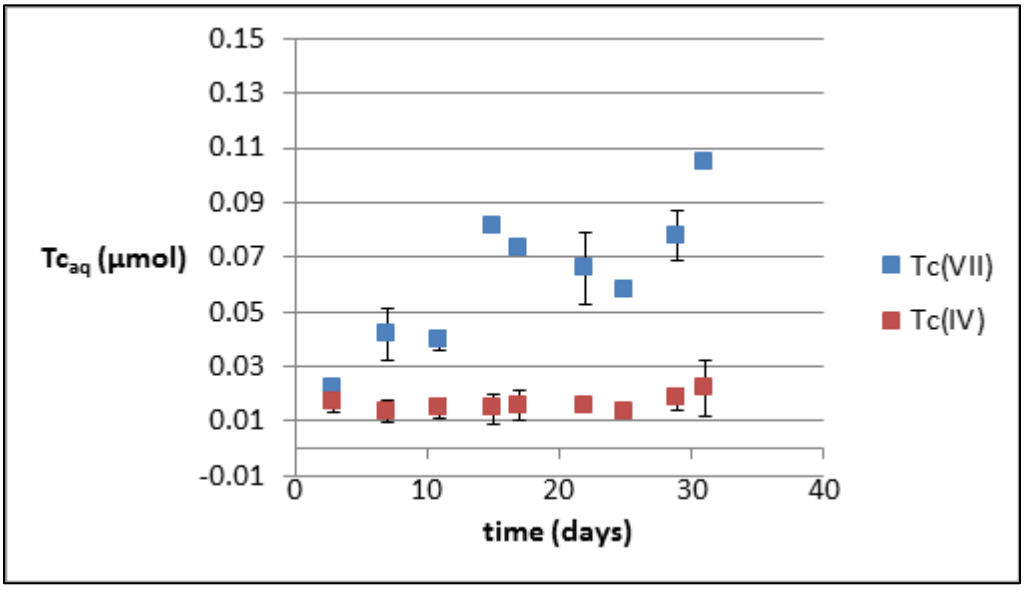

Figure 77. Tc-99 µmol in the aqueous phase as a function of time, at pH 8, for TcO2 immobilized on nano-magnetite. Tc(VII) and Tc(IV) soluble species were determined with CH3Cl/TPPC extraction

The solubility of TcO_2 for pH values above 2 can be written as:

$$TcO_2{\cdot}nH_2O(s) \rightarrow TcO(OH)_2 + (n\text{-}1)H_2O \quad \text{(Icenhower et al., 2008)}$$

and depends on the presence of oxygen and the crystallinity of TcO_2. In FIU's experiments, oxygen levels were constant and lower than 1 ppm. Poorly crystalline TcO_2 (amorphous) dissolves 10 times more rapidly than crystalline TcO_2 (Rard et al., 1999; Lieser et al., 1987). Another factor that needs to be taken into account is the potential radiolysis of the water near the surface of $TcO_2 \cdot nH_2O$ which can cause oxidation and dissolution of the solid to yield TcO_4^- (Meyer et al., 1991). Thus, if any appreciable amount of Tc(VII) is present in the aqueous phase, this may lead to overestimated solubility measurements. In FIU's case, the concentration of Tc(IV) in the aqueous phase had already reached a steady state as early as day 3, whereas the existence and erratic pattern of TcO_4^- may be due to radiolutic phenomena in the solid-water interface. The average solublity of TcO_2 sequestered by nano-magnetite in the presence of 5 mM HCO_3^- was found to be $4.0 \cdot 10^{-7} \pm 0.4 \cdot 10^{-7}$ M based on the concentration of Tc(IV) in the aqueous phase, which is within the reported range of amorphous TcO_2 in anoxic waters of pH 7-8 (10^{-7}-10^{-6} M) (Icenhower et al., 2008) and corresponds to 2.1±0.3% dissolution of the sequestered solid TcO_2. The solubility of crystalline TcO_2 is signficantly lower: 10^{-8}-$10^{-8.4}$ (Eriksen et al., 1992; Rard et al., 1999). Assuming that TcO_2 sequestered by nano-magnetiteis of amorphous or poorly crystalline nature, the solubility does not seem to be enhanced due to the presence of HCO_3^-. Further experimentation of dissolution studies in the presence of higher HCO_3^- concentrations and in the absence of bicarbonate will strengthen this conclusion further. The levels of ferrous iron throughout the experiment was below detection limit (<50 μg/L).

Despite the fact that TcO_4^- concentrations are not taken into consideration for the calculation of solubility in the presence of bicarbonates, in a given geological environment, the presence of Tc(VII) must be considered. Even under sufficiently reducing codnitions, the possible formation of pertechnetate from oxidizinbg agents formed by radiolysis may become important.

Subtask 1.4: Future Work

FIU will attempt to characterize the ferrous:ferric iron ratio of micro- and nano- magnetite by mineral dissolution and determination of Fe(II) by the ferrozine method. Future experiments include pertechnetate reduction in the presence of HCO_3^- at pH 8 with the aim to compare the reduction rate by Hanford sediment and magnetite in the presence of bicarbonates, as well as to investigate the formation of soluble Tc(IV)-carbonate complexes. As far as dissolution experiments are concerned, the experiments will be concluded with dissolution experiments at higher bicarbonate concentration (e.g. 50mM) and in the absence of bicarbonates.

Subtask 1.4: Acknowledgements

Funding for this research was provided by U.S. DOE Cooperative Agreement DE-EM0000598. We truly appreciate Dr. Nik Qafoku from PNNL for support of this research.

Subtask 1.4: References

Alliot, I., C. Alliot, P. Vitorge & M. Fattahi (2009) Speciation of technetium(IV) in bicarbonate media. *Environmental Science and Technology*, 43**,** 9174-82

Cui D, Eriksen T.T., 1996. Reduction of pertechnetate in solution by heterogeneous electron transfer from Fe(II)-containing Geological Material. *Environmental Science and Tehcnology*, 30, 2263-2269

Eriksen Trygve, E., P. Ndalamba, J. Bruno & M. Caceci. 1992. The Solubility of $TcO_2 \cdot nH_2O$ in Neutral to Alkaline Solutions under Constant pCO_2. *Radiochimica Acta,* 67.

Icenhower, J., W. Martin, N. Qafoku & J. Zachara. 2008. The Geochemistry of Technetium: A Summary of the Behavior of an Artificial Element in the Natural Environment Pacific Northwest National Laboratory.

Kaplan, D. I., K. E. Parker & I. V. Kutnyakov. 1998. Radionuclide distribution coefficients for sediments collected from borehole 299-E17-21: Final report for subtask 1a. Richland: Pacific Northwest National Laboratory

Kobayashi T., Scheinost A., Fellhauer D., Gaona X., Altmaier M., 2013. Redox behavior of

Tc(VII)/Tc(IV) under various reducing conditions in 0.1M NaCl solutions. *Radiochimica Acta*

101, 323-332

Kopunec R., Abudeab F.N, Skraskova S. 1998. Extraction of pertechnetate with tetraphenylphosphonium in the presence of various acids, salts and hydroxides. *Journal of Radioanalytical and Nuclear Chemistry* 230 (1-2), 51-60

Lem WJ and Wayman MD 1970. Decomposition of aqueous dithionite. 1. Kinetics of decomposition of aqueous sodium dithionite. *Canadian Journal of Chemistry* 48, 782-790

Lieser KH, Bauscher CH, Nakashima T., 1987. Dissolution of TcO_2 in aqueous solutions under various conditions. *Radiochimica Acta*, 42, 191-200

McBeth JM, Lloyd JR, Law GT, Livens FR, Burke IT, Morris K, 2011. Redox interactions of technetium with iron bearing minerals. *Mineralogical Magazine* 75(4), 2419-2430

Meyer RE, Arnold WD, Case FI, O' Kelley GD, 1991. Solubilities of Tc(IV) oxides. *Radiochimica Acta*, 55, 11-18

Paquette, J. & W. E. Lawrence (1985) A spectroelectrochemical study of the technetium(IV)/technetium(III) couple in bicarbonate solutions. *Canadian Journal of Chemistry*, 63**,** 2369-2373

Peretyazhko T., Zachara JM, Heald SM, Jeon BH, Kukkadapu RK, Liu C., Moore D., Resch CT., 2009. Heterogeneous reduction of Tc(VII) by Fe(II) at the solid-water interface. *Geochimica et Cosmochimica Acta*, 72, 1521-1529

Rard, J., Rand, M., Anderegg, M., Wanner, H., 1999. Chemical Thermodynamics of Technetium, OECD Nuclear Energy Agency.

Serne, RJ, BN Bjornstad, DG Horton, DC Lanigan, CW Lindenmeier, MJ Lindberg, RE Clayton, VL LeGore, RD Orr, IV Kutnyakov, SR Baum, KN Geiszler, MM Valenta, TS Vickerman and H. T. Schaef. 2004. Characterization of Vadose Zone Sediments Below the T Tank Farm: Boreholes C4104, C4105, 299-W10-196 and RCRA Borehole 299- W11-39. PNNL-14849, Pacific Northwest National Laboratory, Richland, Washington.

Shi L, Belchik SM, Plymale AE, Heald S, Dohnalkova AC, Sybirna K, Bottin H, Squier TC, Zachara JM, Fredrickson JK. 2011.Purification and Characterization of the [NiFe]-Hydrogenase of Shewanella oneidensis MR-1. *Applied and Environmental Microbiology* 77(16), 5584-5590.

Szecsody, J. E., Truex, M. J., Qafoku, N. P., Wellman, D. M., Resch, T., & Zhong, L. 2013. Influence of acidic and alkaline waste solution properties on uranium migration in subsurface sediments. *Journal of Contaminant Hydrology*, 151, 155-175.

Szecsody JE, MJ Truex, L Zhong, JP McKinley, NP Qafoku, BD Lee, and SD Saurey. 2015. Remediation of Technetium in Vadose Zone Sediments Using Ammonia and Hydrogen Sulfide Gases . *Vadose Zone Journal* 14(7)

Verschoor M.J. Molot A.L. (2013). A comparison of three colorimetric methods of ferrous and total reactive iron measurement in freshwaters. *Limnology and Oceanography: Methods,* 11. 113-125

Xie, Y., Murray, C., Last, G., R. Mackley. 2003. Mineralogical and bulk-rock geochemical signatures of Ringold and Hanford formation sediments, PNNL-14202, Pacific Northwest National Laboratory, Richland, Washington.

Yalçintaş E. 2015. Redox, solubility and sorption chemistry of technetium in dilute to concentrated saline systems. KIT Publishing

Yalçintaş E, Gaona X, Scheinost AC, Kobayashi T, Altmaier M, Geckeis H. 2015 Redox chemistry of Tc(VII)/tc(IV) in dilute to concentrated NaCl and MgCl2 solutions. *Radiochimica Acta* 103(1), 57-72

Yalçintaş E., Scheinost AC, Gaona X., Altmaier M. 2016. Systematic XAS study on the reduction and uptake of Tc by magnetite and mackinawite. *Dalton Transactions*, 45, 17874-17885

Zachara J.M., Heald S.M., Jeon B.H., Kukkadapu R.K., Liu C., McKinley J.P., Dohnalkova A.C., Moore D.A. (2007). Reduction of pertechnetate [Tc(VII)] by aqueous Fe(II) and the nature of solid phase redox products. *Geochimica et Cosmochimica Acta* 71, 2137-2157

TASK 2: REMEDIATION RESEARCH AND TECHNICAL SUPPORT FOR SAVANNAH RIVER SITE

TASK 2: EXECUTIVE SUMMARY

Flow-through column and batch experiments were conducted at the Florida International University (FIU) Applied Research Center (ARC) to estimate the sorption and desorption properties of humic substances onto Savannah River Site (SRS) sediment and to study the mobility of uranium through humate sorbed sediment. The use of humic acid could be applied to various DOE sites for contaminant stabilization; however, information is needed to optimize this technology and prepare it for actual field deployment and regulatory acceptance. Experiments were designed to study the behavior of humate, specifically Huma-K and modified humic acid, at different pH levels to help develop a model to predict the sorption/desorption. Also experiments were performed to identify the morphological and physico-chemical characteristics of sediments that are affected by chronic acid leaching (compared to clean background soil) and correlate the selected properties with the sorptive characteristics of the sediments for SRS contaminants of concern. The identification of the physico-chemical characteristics that are affected due to exposure to acid and their role in radionuclide sorption by the soil will help to achieve a better understanding of the mobility of the contaminants of concern. For example, properties such as porosity and surface area may increase as a result of acid leaching and affect radionuclide retention.

Subtask 2.1: Investigation on the Properties of Acid-Contaminated Sediment and its Effect on Contaminant Mobility

Subtask 2.1: Introduction

The Savannah River Site (SRS) was established as one of the major sites for the production of materials related to the U.S. nuclear program during the early 1950s. An estimated 36 metric tons of plutonium were produced during the period 1953-1988. Since then, it has become a hazardous waste management facility responsible for nuclear storage and remediation of contaminated soil and groundwater from radionuclides. The groundwater at the F/H Area Seepage Basins Groundwater Operable Units at SRS was impacted by operations of the Hazardous Waste Management Facilities (HWMFs). Approximately 1.8 billion gallons (7.1 billion liters) and 1.6 billion gallons (6.0 billion liters) of low-level waste solutions have been received in the F and H areas, respectively, originating from the processing of uranium slugs and irradiated fuel at the separation facilities. The effluents were acidic (wastewater contaminated with nitric acid) and low-activity waste solutions containing a wide variety of radionuclides and dissolved metals. Waste solutions were transported approximately 3,000 feet from each processing area through underground vitrified clay pipes to the basins. After entering the basin, the wastewater was allowed to evaporate and to seep into the underlying soil. The purpose of the basins was to take advantage of the interaction with the basin soils to minimize the migration of contaminants to exposure points. Though the seepage basins essentially functioned as designed, the acidic nature of the basin influent caused mobilization of metals and radionuclides resulting in groundwater contaminant plumes.

Currently, more than 235 monitoring wells at the site are sampled for a variety of chemical and radioactive parameters. Groundwater monitoring results have indicated the presence of elevated

levels of metals, radionuclides and nitrates. Significant chemical differences exist between the groundwater from the two areas. The F Area groundwater contains higher concentrations of dissolved metals than that in the H Area. The constituents of concern (COCs) associated with the F Area HWMF groundwater plume are tritium, uranium-238, iodine-129, strontium-90, curium-244, americium-241, technetium-99, cadmium, and aluminum. The COCs in H Area are tritium, strontium-90, and mercury (Wan et al. 2012, Dong et al. 2012).

Objectives

The objective of subtask 2.1 is to identify the morphological and physico-chemical characteristics of sediments that are affected by chronic acid leaching (compared to clean background soil) and correlate the selected properties with the sorptive characteristics of the sediments for SRS contaminants of concern. The identification of the physico-chemical characteristics that are affected due to exposure to acid and their role in radionuclide sorption by the soil will help to achieve a better understanding of the mobility of the contaminants of concern. For example, properties such as pore volume and surface area may change as a result of acid leaching and affect radionuclide retention.

Subtask 2.1: Methodology

1. Creation of acid treated soil profiles

Two SRS background soil (mean particle diameter 0.18<d<2mm) suspensions in HNO_3, pH 2.5, were created, each in triplicate (Table 21). The first was equilibrated undisturbed, allowing for saturation in the aqueous phase and secondary mineral precipitation. In the second, the aqueous phase was replenished every 7 days in order to avoid saturation and secondary mineral precipitation. An aliquot was isolated from the supernatant on a daily basis for the determination of Si, Al and Fe in the aqueous phase due to kaolinite and goethite dissolution.

Table 21. Soil Mass and Volume in the Triplicate SRS Soil Suspensions (mean particle diameter of the soil is 0.18<d<2mm)

Soil mass (g)	HNO_3, pH 2.5, volume (ml)
4.2264	130
4.2395	130
4.2439	130

Soil from the SRS F/H Area acidic plume (called hereafter FAW-5) was received from Savannah River National Laboratory, courtesy of Dr. Miles Denham.

2. Elemental analysis and speciation studies

Al, Fe and Si concentrations in the aqueous phase were determined by ICP-OES. Speciation studies for the identification of aqueous species as well as saturated solids under the conditions studied was performed with Visual Minteq. Uranium was determined by Kinetic Phosphorescence Analysis (KPA).

3. Soil characterization studies

Specific surface area and pore volume of each acidified soil profile were determined through nitrogen adsorption (BET) available at FIU's Department of Mechanical Engineering. SEM-EDS studies and elemental analysis of the solid substrates were performed at Florida Center of Analytical Electron Microscopy (FCAEM) located at FIU's Modesto Maidique Campus.

4. Batch uranium sorption experiments

Batch sorption experiments were performed by bringing in contact acidified soil with 10 ml of U(VI) solution, C_{init} = 500 μg/L. In equilibrium studies, the soil mass was equal to 200 mg. In solid:liquid ratio experiments, the soil mass ranged from 50-400 mg. The pH of sorption experiments ranged from 4.5-8.

Subtask 2.1: Results and Discussion

1. Acidified soil profiles and speciation studies

In the case of the triplicate samples where secondary precipitation was allowed to take place (called "Sat" hereafter), the monitoring results for Al, Fe and Si in the aqueous phase are presented in Figure 78 and Figure 79. The experimental points are derived from the triplicate batch experiments and the error bars represent the standard deviation. Figure 78 reveals an identical pattern for Al and Si release in the supernatant as a function of time: a gradual increase of the concentration is observed from the first day up to the eighth day and then a sharp decrease in the concentration takes place and a plateau is observed beyond day 16. For the time period of 1-8 days, the concentrations of Al and Si are practically the same, taking into consideration the two elements are very close in atomic mass.

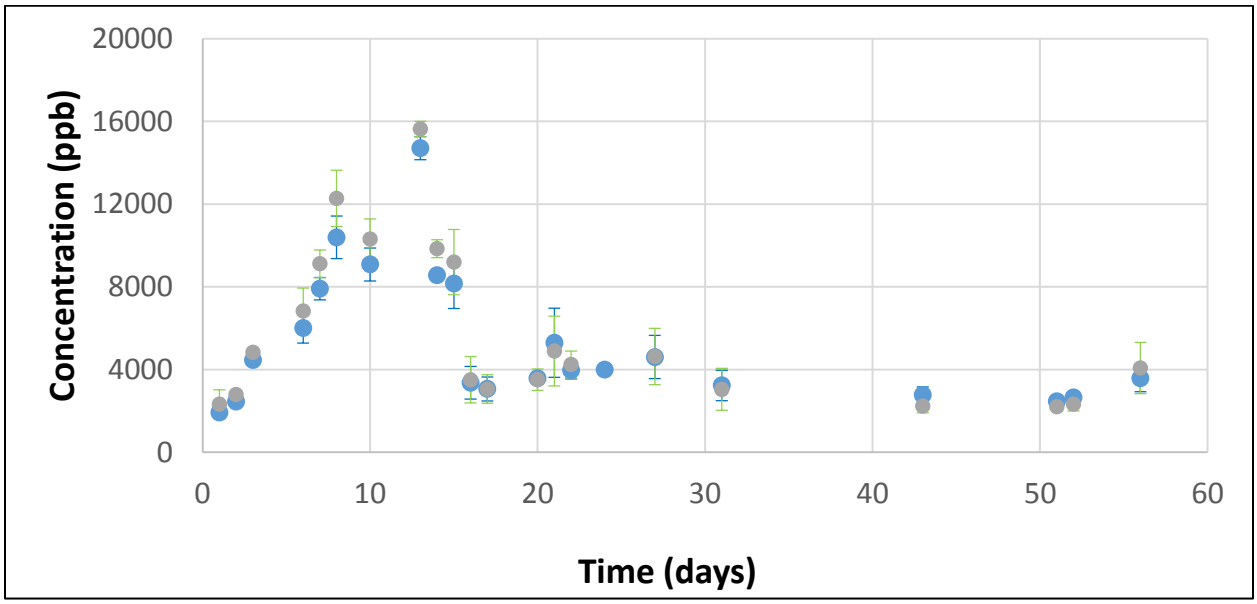

Figure 78. Concentrations of Al (blue dots) and Si (green dots) as a function of time in the soil leachates, as a result of soil-HNO_3 contact for the "Sat" acidified soil profile

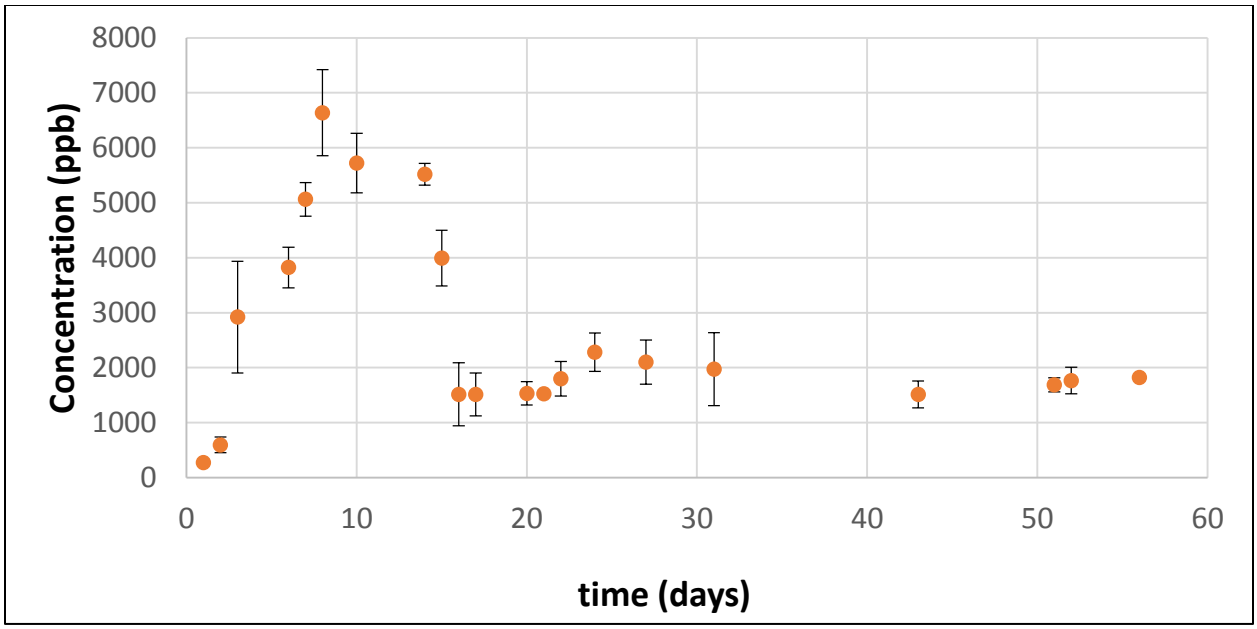

Figure 79. Concentrations of Fe as a function of time in the soil leachates, as a result of soil-HNO_3 contact for the "Sat" acidified soil profile

Furthermore, the average rate of release was calculated for the two elements for this time period and was found to be $3.5 \cdot 10^{-11} \pm 0.9 \cdot 10^{-11}$ mol/ml·min and $3.8 \cdot 10^{-11} \pm 1 \cdot 10^{-11}$ mol/ml·min for Al and Si, respectively. All experiments were performed at room temperature (20° C). The quartz dissolution rate at pH 2.5 and 70° C is reported to be $6.4 \cdot 10^{-14.3}$ mol/ml·min (Knauss and Wolery, 1987) and is expected to be magnitudes of order lower at room temperature. Hence, the preliminary results indicate that Al and Si release is taking place due to kaolinite dissolution; quartz dissolution had very little effect, if any. Furthermore, there seems to be no preferential leaching of one element over the other; on the contrary, there seems to be a stoichiometric release of Al and Si in the supernatant, since these two elements are found in equimolar composition in kaolinite's structure, $Al_2Si_2O_5(OH)_4$. In literature, it has been reported that kaolinite dissolves congruently at 25° C for pH values lower than 4 and higher than 11, but incongruently in the in-between range (Carroll and Walther, 1990; Huerats et al., 1999). The result for Day 13 is believed to be an outlier.

Iron follows a very similar pattern of release in the aqueous phase (Figure 79); nevertheless, the maximum amount of iron released (Day 8) is significantly lower than that of Al and Si: 6.6 ppm of Fe, as opposed to 12.2 ppm of Si and 10.4 ppm of Al. The average rate of Fe release was calculated as $7.2 \cdot 10^{-12} \pm 2 \cdot 10^{-12}$ mol/ml·min, significantly lower than the corresponding rates of Al and Si release. This result may have been expected, since the concentration of Fe in the SRS soil in the form of goethite is smaller than that of Al and Si, in the form of kaolinite (Anagnostopoulos et al., 2016).

The gradual decrease in the concentrations of the elements under study and the creation of a plateau can be explained by speciation calculations. With the aid of Visual Minteq, a list of aqueous species and saturated solids was created under the conditions studied and is presented in Table 22. Concentrations of Al, Fe and Si in the calculations were derived from the Day 8 experimental point ("peak") and the atmospheric CO_2 was included, as well.

Table 22. Major aqueous and saturated species at pH 2.5 for the experimental conditions studied as predicted by Visual Minteq software

Aqueous species	Saturated solids
Al^{3+}	Goethite - FeO(OH)
H_4SiO_4	Hematite – Fe_2O_3
Fe^{3+}	Lepidocrocite – γ-FeO(OH)
$Fe(OH)^{2+}$	Quartz – SiO_2

The software predicts the formation of several Fe and Si bearing solids that are in equilibrium with the Fe and Si aqueous species (plateau). Nevertheless, under the conditions studied, there were no aluminosilicates or other Al-bearing solids predicted, a fact that would explain the decrease in Al concentration. An explanation for this phenomenon could be the co-precipitation of Al during the formation of iron- and silicon-bearing solids.

The experiment was repeated but with the supernatant being replenished every 7 days. The monitoring results for Al, Fe and Si in the aqueous phase are presented in Figure 80 and Figure 81.

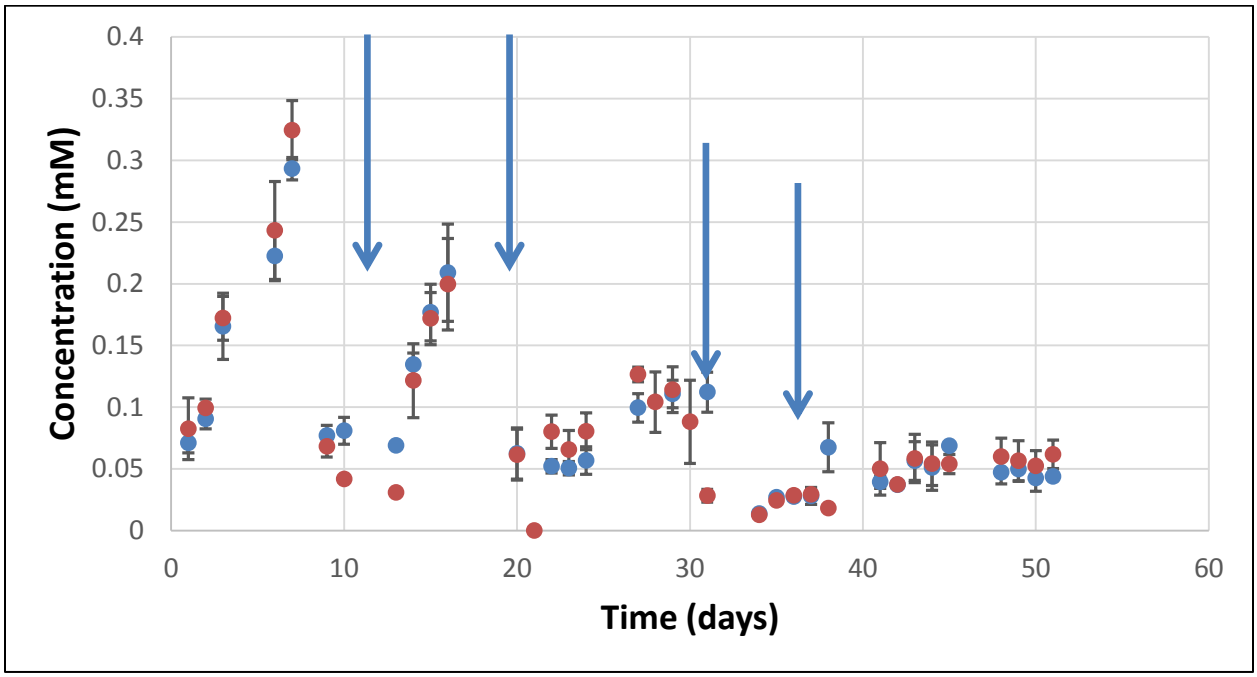

Figure 80. Al (blue dots) and Si (red dots) concentrations (mM) in the aqueous phase due to kaolinite and goethite dissolution, as a function of time. Error bars represent relative standard deviations from triplicate samples. Arrows show when the aqueous phase was replenished.

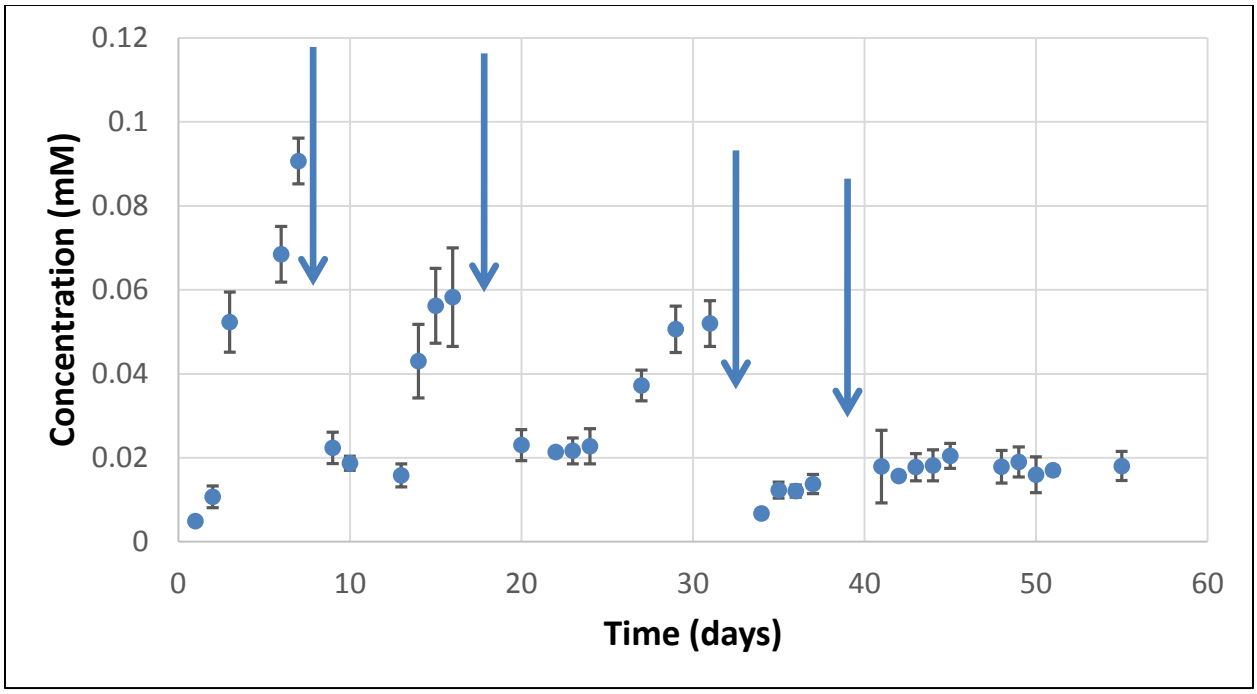

Figure 81. Fe concentrations in the aqueous phase due to goethite dissolution, as a function of time. Error bars represent relative standard deviations from triplicate samples. Arrows show when the aqueous phase was replenished.

The elemental concentration gradually increased for all elements during the first 7 days and, once the supernatant was replenished, the concentration dropped to the initial levels. A lag period was observed for all three elements after each replenishment; the concentration of the elements remained stable for the first 3-4 days and then gradually increased. Furthermore, the maximum amount of each element released into the supernatant was significantly smaller than the corresponding amount during the first cycle. For example, the maximum concentration of Al during the first cycle was found to be 8 ppm, while for the second cycle it was 5.6 ppm; for Fe, it was 5 ppm during the first cycle versus 3.5 ppm during the second; and for Si, it was 9 ppm during the first cycle versus 5.6 ppm during the second. This pattern may be explained by the assumption that acid first "washes out" all fine particles present in the soil, which are more readily available due to their higher specific surface, and during the second and third cycle, the remaining larger particles are more slowly dissolved. Finally, there seems to be no preferential dissolution of Al and Fe so far, since the concentrations are similar.

In Table 23, the rates of Al, Fe and Si released in the aqueous phase for the different experimental cycles are presented. The rates of Al and Si released in both cycles were practically the same whereas the release rate of Fe was lower in all cycles. In all cases, the release rate in the second cycle was lower than the one from the first cycle for the same element.

Table 23. Average rates of release of Al, Fe and Si in the aqueous phase for two experimental cycles: days 1-7 and days 13-16, followed by the relative standard deviation

	Rate of release (mol ml^{-1} min^{-1})		
	Al	**Fe**	**Si**
Cycle 1 (Days 1-7)	$3.5 \cdot 10^{-11} \pm 0.8 \cdot 10^{-11}$	$7.2 \cdot 10^{-12} \pm 2 \cdot 10^{-12}$	$3.8 \cdot 10^{-11} \pm 1 \cdot 10^{-11}$
Cycle 2(Days 13-16)	$6.9 \cdot 10^{-12} \pm 2 \cdot 10^{-12}$	$2.0 \cdot 10^{-12} \pm 0.7 \cdot 10^{-12}$	$6.0 \cdot 10^{-12} \pm 2 \cdot 10^{-12}$

The triplicate samples were removed from the platform shaker after 1, 3 and 5 cycles; the aqueous phase was discarded and the samples were dried in the oven at 150^{o}C for 48h. In Figure 82, the different acidified soil profiles are presented: the loss of the characteristic red color due to the presence of iron can be witnessed even with the bare eye.

Figure 82. "Sat" acidified profile (upper left), soil after 1 cycle (7 days) contact with HNO_3 (upper right), after 3 cycles (30 days) contact with HNO_3 (lower left) and after 5 cycles (50 days) contact with HNO_3 (lower right)

2. Soil specific surface area and SEM-EDS studies

The specific surface area and pore volume properties of each acidified soil were determined by nitrogen adsorption (BET method) and are presented in Table 24.

Table 24. Specific surface areas and pore distribution for each acidified soil profile, followed by the relative standard deviation.

Acidified soil profile	Specific Surface Area (m^2/g)	Pore volume (mm^3 / g)
1 cycle acidification	0.14 ± 0.02	0.89 ± 0.1
3 cycles acidification	0.07 ± 0.01^{a}	0.35 ± 0.2^{b}
5 cycles acidification	0.07 ± 0.03^{a}	0.50 ± 0.1^{b}
Sat	0.23 ± 0.02	2.1 ± 0.4^{c}
Background (untreated)	0.41 ± 0.02	2.1 ± 0.3^{c}

Note: Same superscripts (a, b and c) denote statistically the same values (t-test, P>0.05 for 95% confidence level)

The experimental findings indicate a clear decreasing trend in the specific surface area and pore volume of the acid exposed soil, when compared to background (untreated soil). The specific surface area and the pore volume values of the acidified soil that contains secondary precipitates fall between those of the background soil and category A, indicating both competing mechanisms: a balance between acidification (mineral loss) and secondary mineral contribution/precipitation.

Elemental analysis of each soil profile was performed by SEM-EDS. The results of elemental analysis are presented in Table 25. The concentration of Al and Fe decreased in soil profiles as the time of exposure to acid increased, which is in agreement with the preliminary leaching kinetic experiments.

Table 25. Concentrations of Al, Fe and Si in each soil profile determined by SEM-EDS

Acidified soil profile	Elemental concentration (mg g^{-1} soil)		
	Al	Si	Fe
1 cycle	88 ± 30	380 ± 50	57 ± 20
3 cycles	29 ± 20	470 ± 30	18 ± 8
5 cycles	10 ± 7	520 ± 10	4 ± 2
Sat	43 ± 20	420 ± 5	56 ± 6
Plume soil (FAW-5)	131 ± 28	745 ± 66	87 ± 9

On the other hand, the concentration of Si increased for soil profiles from 1 cycle to 5 cycles of contact with HNO_3, showing that the longer the exposure of the soil to acid, the higher the removal of Al and Fe due to dissolution. In Figure 83 , the EDS spectra for soil profiles of 1 cycle and 5 cycles of acidification are presented.

As it can be seen in, the peak of Al diminishes and the already small peak for Fe is almost absent; soil profile C consists mostly of quartz. For the soil profile where secondary precipitation was allowed (i.e., the "Sat" soil profile), the percentage of Si and Fe remained at the same levels as compared to soil profile A. This may be due to the precipitation of hematite and amorphous silica, as predicted by speciation studies conducted earlier this year using Visual Minteq software. On the other hand, no secondary aluminum precipitates were predicted by the software. The concentrations of Al, Fe and Si in the plume soil were significantly higher than the acidified soil profiles. The levels of Fe in the plume soil were similar to the background soil from the SRS F/H Area (89±2 and 70±7 for mean particle diameter $d<63\mu m$ and $63<d<180\mu m$, respectively), whereas the concentrations of Al and Fe were almost double (Anagnostopoulos et al., 2017).

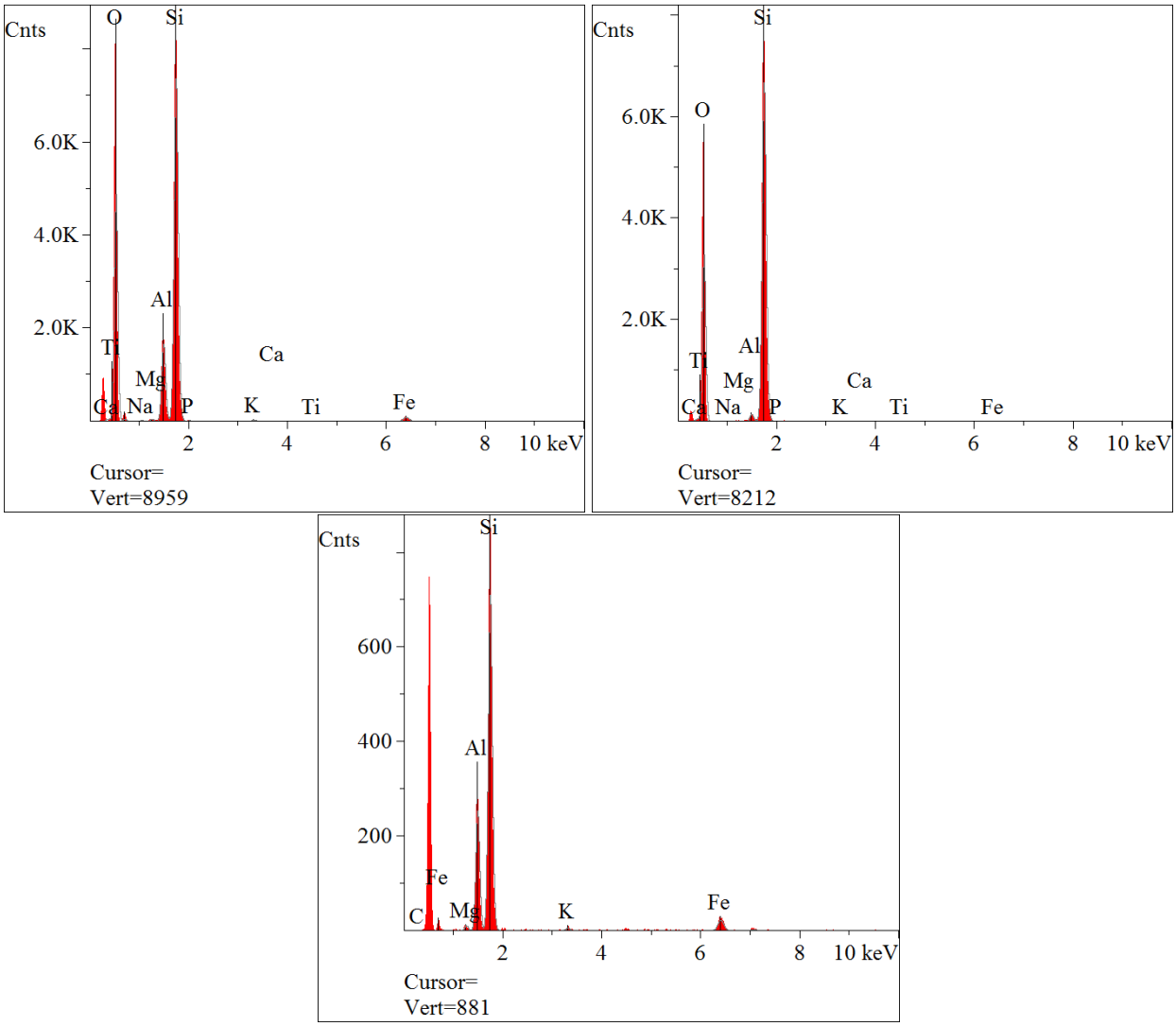

Figure 83. EDS spectra for soil after 1 cycle of contact with HNO_3 (upper left) and after 5 cycles of contact with HNO_3 (upper right), as well as plume soil, FAW-5 (down)

3. Batch uranium sorption experiments

Batch uranium sorption experiments were performed by bringing 200 mg of each soil profile in contact with 10 mL of solution containing an initial uranium concentration equal to 500 µg L^{-1} at pH values of 3, 4.5, 7 and 8 on a rotary shaker at 110 rpm for 24h. The sorption results are presented in Table 26.

The normalized sorption results of the different acidified soil profiles and the plume core soil (FAW-5) as µg of U(VI) sorbed per soil mass (g), as well as per surface (mg of U(VI) / m^2 of each substrate) are presented in Table 27.

Table 26. U(VI) uptake by the different profiles of acidified soil, expressed in terms of uranium percent removal, at pH values 3, 4.5, 7 and 8

Acidified soil profile	% U(VI) Removal			
	pH 3	pH 4.5	pH 7	pH 8
FAW-5	0	15 ± 2	72 ± 6	70 ± 12
A (7 days)	0	11 ± 3	38 ± 1	29 ± 5
B (30 days)	0	5 ± 1	39 ± 2	24 ± 3
C (50 days)	0	0	20 ± 4	18 ± 4
Sat	0	11 ± 2	44 ± 9	24 ± 2
Background	0	18 ±2	61 ± 6	

Table 27. Sorption capacity of different acidified profile soil substrates expressed as uptake per mass and uptake per surface for pH values 4.5, 7 and 8 with relative standard deviation

Acidified profile	U(VI) sorption					
	pH 4.5		pH 7		pH 8	
	µg /g	mg/m^2	µg /g	mg/m^2	µg /g	mg/m^2
1 cycle	275 ± 52	2.61 ± 0.66	950 ± 57	9.02 ± 1.5	725 ± 58	6.88 ± 1.2
3 cycles	125 ± 50	1.87 ± 0.86	975 ± 20	14.6 ± 3.3	600 ± 55	8.96 ± 1.0
5 cycles	0	0	500 ± 20	6.44 ± 2.5	450 ± 20	5.79 ± 1.3
Sat	275 ± 51	1.19 ± 0.25	1100 ± 75	4.76 ± 0.48	600 ± 18	1.15 ± 0.04
Background	450 ± 53	1.10 ± 0.13	1525 ± 30	3.72 ± 0.12		

The results for FAW-5 (plume core soil) normalized per mass and surface will be provided in a future report, since the experimental data of the specific surface area and pore distribution will be provided by SRNL.

Interestingly all soil profiles showed zero to very low sorptive capacity at pH 3 and 4.5, respectively. At pH 7, the plume soil removed a similar amount of U(VI) from the aqueous phase as the background soil, a fact that may be attributed to their similar iron content. At pH 8, the plume soil exhibited by far higher retention of uranium compared to the acidified soil, which was rather expected due to iron content (Table 25). It is evident from Table 27 that when the sorption results are normalized as mg of U(VI) sorbed per area, the acidified soil that has been through 1 cycle of acidfication exhibited the highest uptake at circumneutral conditions, whereas the "Sat" samples (samples that secondary precipitates were allowed to form) exhibited the lowest uptake. On the other hand, a comparison of the uptake per mass reveals that acidified soil and plume soil exhibited very similar uptake per mass. Sorption expressed in terms of radionuclide mass per substrate mass (µg U(VI)/g) may provide misleading results, since all of the samples may contain the same amount of substrate; nevertheless, the specific surface area and the Fe content were not the same.

Sorption was also found to be less at pH 8 compared to pH 7 across the board. This experimental finding could be explained by the different U(VI) aqueous speciation at pH 7 and pH 8. With the aid of speciation software Visual Minteq, Table 28 was compiled and contains the major uranyl species at different pH values.

Table 28. Major uranyl species at pH 7 and 8 using Visual Minteq.

Species	% at pH 7	% at pH 8
$UO_2CO_3(OH)_3^-$	73	63
$UO_2(OH)_2$	3	-
UO_2CO_3 (aq)	10	2
UO_2OH^+	7	-
$(UO_2)_3(OH)_5^+$	5	-
$UO_2(OH)_2$	2	-
$UO_2(CO_3)_2^{2-}$	-	22
$UO2(CO_3)_3^{4-}$	-	12

As can be seen in Table 28, 73% of uranyl species were negatively charged at pH 7, whereas 98% of the uranyl species are negatively charged at pH 8.

Similar studies have assumed that the most reactive component of the soil towards uranium is Fe (in goethite) according to the complexation reaction:

$2 > FeOH^{-0.5} + UO_2^{2+} = (FeOH)_2\ UO_2^+$ at pH>4.0 (Anagnostopoulos et al., 2017; Dong et al., 2012).

Given the fact that the background soil consists of ~95% quartz and quartz exhibits p*k* values ~4.5 (Leung et al., 2009; Liu et al., 2014), it is safe to assume that the net charge of the surface at both pH 7 and 8 is overall negative. Despite the fact that surface complexation is not dependent on electrostatic interactions, the existence of opposite charges between the surface and the aqueous species still "facilitates" the approach between active centers and radionuclides, which may end up binding by complexation. Hence, at pH 8, where all the aqueous uranium species are negatively charged, interaction between substrate sites and uranium may not be "facilitated".

The concentrations of Fe, Al and Si in the aqueous phase, as a result of soil-aqueous phase contact for a 24h equilibration, were determined by means of ICP-OES and are presented in Table 29.

The experimental findings shown in Table 29 indicate that the amount of Al, Fe and Si released in the supernatant when sorption was performed at pH 3 and 4.5 are independent of the pH values. The results of the ICP analysis revealed several interesting trends. The concentration of Al, Fe and Si at pH 6.8 and 8 was at least 5 times higher than the concentrations detected when sorption experiments took place at pH 3 and 4.5. Furthermore, a decrease in each element's concentration was observed for both pH values going from soil profile 1 cycle towards 3 cycles, which was rather expected since the amount of kaolinite and goethite decreased as well. Finally, the concentrations detected for the soil profile where secondary mineral precipitation was allowed during leaching experiments were at similar levels as the soil profile for 1 cycle.

Congruent kaolinite dissolution has been cited in literature for pH<4 (as opposed to incongruent dissolution pH 5-10) (Huertas et al., 1999); nevertheless, the levels of Al and Fe in the supernatant in circumneutral and mildly alkaline conditions may be affected by precipitation of aluminum and iron secondary phases (Carroll and Walther, 1990; Huertas et al., 1999). Furthermore, the levels of Al, Fe and Si as presented in Table 29 were significantly higher than the levels of background soil equilibrated for 24h at pH 3 and 7 (Anagnostopoulos et al., 2017).

Table 29. Al, Fe and Si concentrations (ppb) detected in the aqueous phase for each acidified soil for pH values 3, 4.5, 7 and 8

Acidified soil profile	**pH 3**			**pH 4.5**		
	Al	**Si**	**Fe**	**Al**	**Si**	**Fe**
1 cycle	439 ± 12	188 ± 20	380 ± 80	485 ± 60	155 ± 20	412 ± 38
2 cycle	346 ± 50	204 ± 25	460 ± 100	330 ± 10	150 ± 37	400 ± 10
3 cycle	269 ± 40	123 ± 30	420 ± 40	275 ± 70	120 ± 14	410 ± 51
Sat	312 ± 25	119 ± 22	460 ± 109	277 ± 50	117 ± 18	570 ± 100
FAW-5 (plume soil)	2386 ± 238	1284 ± 79	843 ± 103	2671 ± 567	1400 ± 99	941 ± 255
Acidified soil profile	**pH 6.8**			**pH 8**		
	Al	**Si**	**Fe**	**Al**	**Si**	**Fe**
1 cycle	2330 ± 100	5400 ± 100	1497 ± 63	4481 ± 80	9870 ± 200	2314 ± 42
2 cycle	1620 ± 300	5000 ± 600	986 ± 200	1602 ± 295	6011 ± 650	2384 ± 51
3 cycle	552 ± 40	1230 ± 30	420 ± 40	1178 ± 70	4693 ± 200	2204 ± 101
Sat	3782 ± 54	6778 ± 150	2503 ± 30	3739 ± 259	8810 ± 421	2864 ± 221
FAW-5 (plume soil)	2330 ± 100	5400 ± 100	1497 ± 63	4481 ± 80	9870 ± 200	2314 ± 42

Batch sorption experiments testing the "Sat" and the FAW-5 samples in different solid:liquid ratios were performed by keeping the initial uranium concentration and the aqueous phase volume the same (C_{init}=500 μg/L and 10 ml, respectively) and altering the substrate mass (50, 100, 200 and 400 mg). The pH was adjusted to 7. The experimental results are presented in Figure 84 and Figure 85, for "Sat" and FAW-5, respectively.

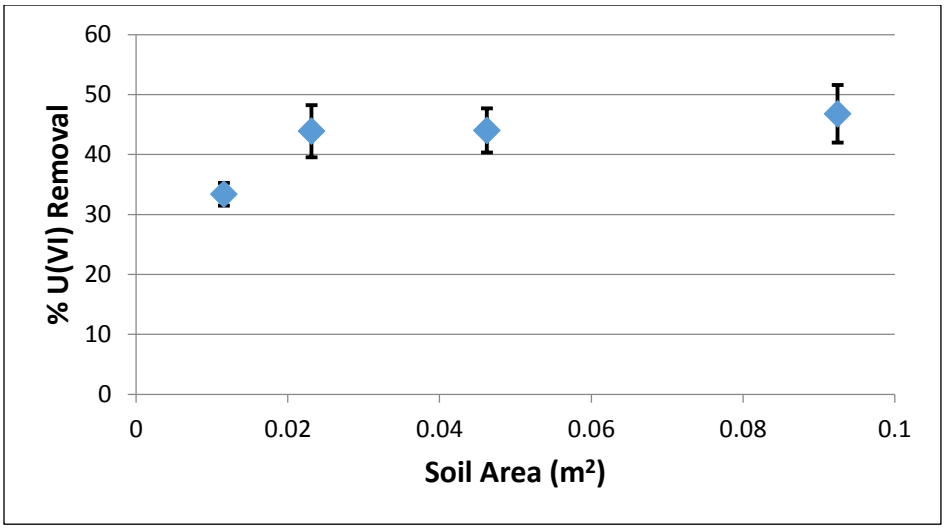

Figure 84. Perecentage of uranium removal from the aqueous phase as a function of soil area for soil samples "Sat", pH 7, 24h equlibration time.

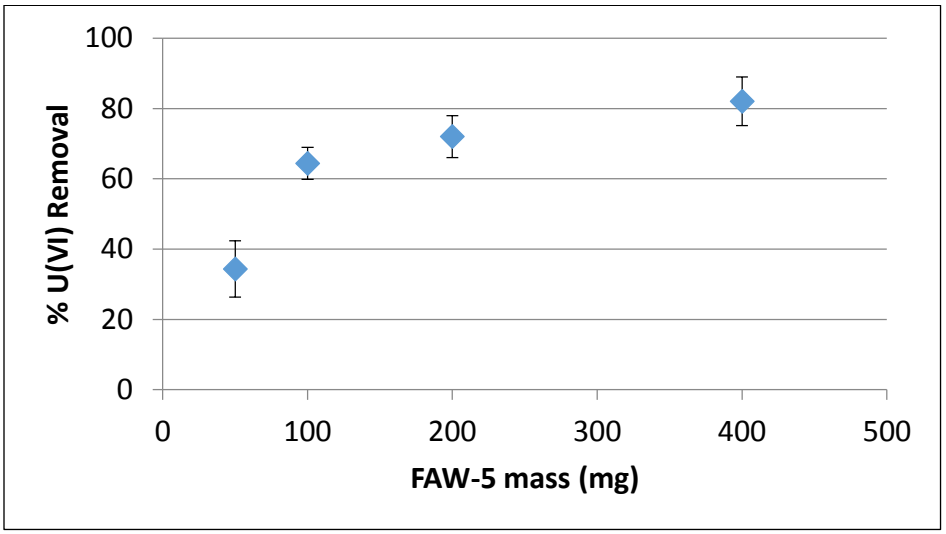

Figure 85. % U(VI) removal form the aqueous phase as a function of FAW-5 soil mass after 24 of contact.

Usually, when uptake is a surface phenomenon, there is a linear correlation between uptake and the substrate's mass (and consequently surface area); whereas, when there is little linear correlation, other mechanisms contribute (e.g. chemical sorption) to the phenomenon (Anagnostopoulos et al., 2012). As can be seen in Figure 84, an increase in the available area did not significantly affect the uranium removal, with the exception of the first experimental point. There does not seem to be a linear correlation between uranium removal and the substrate's surface area. Nevertheless, Figure 84 reveals a plateau; a possible explanation behind this behavior could be the fact that despite the increase in mass (and hence, soil surface) after a given point, substrate agglomerations did not fully expose the area (and consequently, the number of active sites) to the aqueous phase, leading to a plateau of removal. It should be noted that the removal at the plateau was not quantitative; the plateau was at ~45% U(VI) removal. Figure 85 reveals a slight increase in uranium removal with an increase in soil mass, but there seems to be no linear correlation between the soil's mass and the uranium removal. This observation implies

that sorption of uranium on FAW-5 soil is not a phenomenon dependent on the available surface of the substrate for reaction with uranium in the aqueous phase.

Subtask 2.1: Future Work

All uranium batch sorption experiments were equilibrated for 24h. Future kinetic experiments, especially for Sat and FAW-5 profiles, will be performed to identify the kinetic pattern of uranium uptake by these two different profiles at circumneutral conditions. FAW-5 and Sat differ significantly in Fe content, which has been shown to play a critical role in uranium uptake.

Subtask 2.1: References

Anagnostopoulos VA, Manariotis ID, Karapanagioti HK, Chrysikopoulos CV. 2012 .Removal of mercury from aqueous solutions by malt spent rootlets. *Chemical Engineering Journal* 213, 135-141

Anagnostopoulos VA, Katsenovich Y, Denham M. 2017. Sodium silicate treatment for the attenuation of U(VI) by iron-bearing sediments in acidic groundwater plumes. *Journal of Chemical Technology and Biotechnology* 92(8), 1919-1927

Carroll S.A., Walther J.V. (1990). Kaolinite dissolution at 25^{o}, 60^{o} and 80^{o} C. *American journal of Science* 290, 797-810

Dong, W., Tokunaga, T.K., Davis, J.A., Wan, J. 2012. Uranium(VI) adsorption and surface complexation modeling onto background sediments from the F-Area Savannah River Site. *Environmental Science and Technology,* 46(3), 1565-71.

Huertas J.H., Chou L., Wollast R. (1999) Mechanism of kaolinite dissolution at room temperature and pressure. Part II:kinetic study. *Cosmochimica et Geochimica Acta* 63, 3261-327

Knauss K.G., Wolery T.J. (1987). The dissolution kinetic of quartz as a function of pH and time at 70^{o}C. *Cosmochimica et Geochimica Acta* 52, 43-53

Liu X., cheng J., Lu X., Wang R., Surface acidity of quartz: understanding the crystallographic control. *Physical Chemistry chemical Physics.*, 2014, 16, 26909-26916

Leung K., Nielsen I. M. B., and Criscenti L. J., Elucidating the bimodal acid-base behavior of the water-silica interface from first principles, *Journal of American Chemical Society*, 2009, 131, 18358-18365.

S. Ong, X. Zhao, and K. B. Eisenthal, Polarization of water molecules at a charged interface: second harmonic studies of the silica/water interface, *Chemical Physics Letters*, 1992, 191, 327-335.

Wan, J., Tokunaga, T.K., Dong, W., Denham, M.E., Hubbard, S.S. 2012. Persistent Source Influences on the Trailing Edge of a Groundwater Plume, and Natural Attenuation Timeframes: The F-Area Savannah River Site. *Environmental Science & Technology,* 46(8), 4490-4497.

Subtask 2.2: The Synergistic Effect of Humic Acid and Colloidal Silica on the Removal of Uranium (VI)

Subtask 2.2: Introduction

Constructed during the 1950s, the Savannah River Site (SRS) became one of the major producers of plutonium for the United States during the Cold War. Beginning with the implementation of the environmental cleanup program in 1981, SRS has become a hazardous waste management facility responsible for the storage and remediation of contaminated soil and groundwater from radionuclides. Approximately 1.8 billion gallons of acidic waste containing radionuclides and dissolved heavy metals was disposed in F/H Area seepage basins. This led to the unintentional creation of highly contaminated groundwater plumes, consisting of radionuclides with an acidic pH of 3 to 5.5. The acidity of the plumes contributed to the mobility of several constituents of concern (COC) such as tritium, uranium-238, iodine-129, and strontium-90 for the F-Area plume and tritium, strontium-90 and mercury for the H-Area plume. This investigation will focus on uranium (VI), which is a key contaminant of concern in the groundwater plume of the F-Area.

Initially, removal of contaminants from the polluted groundwater was implemented with a pump-and-treat and re-inject system constructed in 1997. Downgrade groundwater within the system would be pumped to the water treatment facility and re-injected upgrade within the aquifer. The effectiveness and sustainability of this process diminished over time. Therefore, it was discontinued and replaced with a funnel-and-gate process in 2004. This new process injects sodium hydroxide directly into the gates of the F-Area groundwater to effectively raise pH levels. By raising the pH of the groundwater, a treatment zone is created by reversing the acidic nature of the contaminated sediments and producing a negative net charge on the surface of sediment particles. As a result, the adsorption of cationic contaminants is expected to be enhanced. So far, this process has resulted in a decrease of Sr and U concentrations, though the concentration of iodine has been unaffected by this treatment. The solution used for the injections contains a high carbonate alkalinity in order to overcome the surface acidic conditions and natural partitions in the groundwater system. To maintain the neutral pH in the treatment zone, systematic injections are required. The continuous use of high concentrations of a carbonate solution to raise pH could re-mobilize uranium previously adsorbed within the treatment zone, though this has not been observed in the monitoring data.

Humic substances (HS) are major components of soil organic matter. HS are polyfunctional organic macromolecules formed by the chemo-microbiological decomposition of biomass or dead organic matter. These substances are usually divided into three main fractions: humin (insoluble at all pH values), humic acid (soluble at pH greater than 3.5), and fulvic acid (soluble at all pH values) (Chopping, et al.1992).

Humic acid carries a large number of functional groups such as aromatic rings, carboxyl groups, phenols, aliphatic chains, etc (Tipping, 2002). Humic acid is an important ion exchange and metal complexing ligand with a high complexation capacity. The ability of humic acid to chemically bind to metals influences in their migration behavior and fate in natural systems (Davis, 1982; Plancque et al., 2001). Various studies have suggested that the retention of U(VI) via sorption in the presence of HA is a complex process. For instance, HA can form an organic coating on the surface of oxides and minerals that can enhance the sequestration of metals (Davis, 1984; Zachara et al., 1994; Labonne-Wall et al., 1997; Perminova et al., 2002). Ivanov et al. (2012) studied the sorption of U (VI) sorption onto bentonite in the presence and absence of

HA. The study found that uranium sorption in the presence of HA was enhanced at low pH (below 3.8) while at moderate pH (3.8 and 6.5) uranium sorption is reduced compared to the absence of HA. At high pH (7 and 9), uranium sorption is reduced for both the presence and absence of HA (Ivanov et al., 2012). Also, Krepelova et al. (2007) not only found that U(VI) sorption onto kaolinite is influenced by pH, U(VI) concentration, the presence of inorganic carbon species, and HA but also that U(VI) prefers to be adsorbed onto kaolinite as a uranyl-humate complex (Krepelova et al., 2007).

This investigation analyzed the synergistic interactions between U(VI) ions, HA and colloidal silica under varying pH conditions from 3 to 8 and the presence of sediment collected from SRS FAW1. Multi-component batch systems were constructed to effectively analyze the removal behavior of U(VI).

Subtask 2.2: Methodology

Removal behavior of U(VI) was studied through multi-component batch systems with a pH range from 3 to 8 in order to evaluate adsorption affected by the pH. FIU previously investigated the synergetic effect of colloidal silica and HA on uranium removal by preparing five batches with various combinations of Si and HA (Lagos, et al., 2014). Expanding on this research, FIU prepared samples with 30 ppm HA to study the sorption behavior of uranium at an intermediate HA concentration. Sediment samples used in the experiments were collected at SRS from FAW1 at a depth of 70-90 feet and shipped to FIU. SRS sediment was sieved, and the sediment fraction with diameter $\leq$ 2 mm was retained and used throughout the experiments. Control samples were prepared in triplicate, containing deionized water (DIW) and 30 ppm U(VI), to account for any sorption of uranium to the container.

- Batch 2: Si (3.5 mM) + U(VI) (30 ppm) + HA, (no sediments)
- Batch 3: U(VI) (30 ppm) + HA, (no Si or sediments)
- Batch 5: Sediments + Si (3.5 mM) +U (VI) (30 ppm) + HA
- Batch 6: Sediments + U(VI) (30 ppm) + HA, (no Si)
- Control: U(VI) (30 ppm), (no SI, HA, or sediments)

Fumed colloidal silica, silicon (IV) oxide 99%, and humic acid sodium salt (50-60% as humic acid) were obtained from Fisher Scientific. Stocks of HA and Si were prepared in DIW at 2000 ppm and 100 ppm, respectively. A commercial 1000 ppm uranyl nitrate stock solution in 2% nitric acid (Fisher Scientific) was used as a source of U(VI). The resulting sample mixtures were spiked with uranium to yield a concentration within a solution matrix of 30 ppm. Table 30 presents the amount of stock solutions needed to yield 30 ppm of HA, respectively, with 3.5 mM of Si and 30 ppm of U(VI). Triplicate samples for each batch were prepared; uranium was added to each sample prior to adjusting the pH. The pH of the mixture was then adjusted to the required value using 0.1 M HCl or 0.1 M NaOH (Figure 86). Control samples were prepared in DIW amended with U(VI) at a concentration of 30 ppm U(VI) to test for U(VI) losses from the solutions due to sorption to the tube walls and caps. All samples were prepared to initially have 20 mL of total volume in the sample tube. All control and experimental tubes were vortexed and then kept on the shaker at 100 rpm for 24 hours at room temperature.

After being shaken for 24 h at 100 rpm, the samples with 30 ppm HA were centrifuged at 2700 rpm at 22°C for 30 minutes (Figure 87). All samples, after being centrifuged, were filtered using a 0.45 μm syringe filter yielding a 3-mL aliquot. Aliquots for KPA [U(VI) analysis] and ICP-OES (Fe and Si analysis) were prepared by taking a 300-μL aliquot for KPA and a 500-μL

aliquot for ICP-OES from the filtered solutions and doing a 240x dilution with 1% HNO_3. Filtered and unfiltered samples were then prepared for analysis via KPA and ICP.

Table 30. Experimental Matrix with Components for 30 ppm Humic Acid Experiments

Batch #	Constituents					
	SiO_2 mL	Humic Acid mL	Uranium mL	Sediment mg	Water mL	Total Volume mL
Batch No. 2	2.1	6	0.05	0	11.4	20
Batch No. 3	0	6	0.05	0	13.5	20
Batch No. 5	2.1	6	0.05	400	11.4	20
Batch No. 6	0	6	0.05	400	13.5	20

Figure 86. Experimental setup.

Figure 87. Shaker and centrifuge experimental setup.

Subtask 2.2: Results and Discussion

Uranium removal was calculated using the uranium concentration from the control samples, Figure 88 and Figure 89 shows the average U(VI) percent removal from the triplicate samples. Unfiltered and filtered samples in Figure 88 and Figure 89 show a 22% increase in uranium removed for filtered samples compared to unfiltered samples. For the unfiltered samples and filtered samples, the highest removal was at pH 5 and pH 6, respectively. There is more removal in the filtered samples compared to the unfiltered samples due to removal of uranium binding to the colloidal particles in the solution via filtration. As shown in Figure 88 and Figure 89, colloidal silica influences the removal of uranium at the pH range greater than pH 5; this could be due to the binding capabilities of uranium to silica colloids.

The high uranium removal in unfiltered batch 3 at pH 3 and pH 8 was inconsistent with the final results; a possible error may have occurred with the sample at marked pH conditions. Maximum uranium removal was observed at pH 6 for all unfiltered samples among batches tested. Batch 5 containing HA, Si, uranium and sediment, showed the highest removal of all with 62% and 69% of uranium removed, respectively, for unfiltered and filtered samples. The overall percentage of uranium removed increased as pH increased from 3 to 5 and then started to decrease as pH further increased with a significant change in uranium removed occurring at pH 5. Non-sediment batches revealed lower U(VI) removal compared to sediment-containing batches; sediment-bearing samples showed a 18% increase in uranium removed with an increase in pH. Also, it is likely that in the presence of sediment, surface-induced precipitation for humic acid and colloidal silica might occur. This can enhance the removal of uranium compared to non-sediment samples, in which agglomeration has to occur before precipitation. The addition of silica in non-sediment batches significantly improved U(VI) removal between pH 6 through pH 8 in both unfiltered and filtered batches.

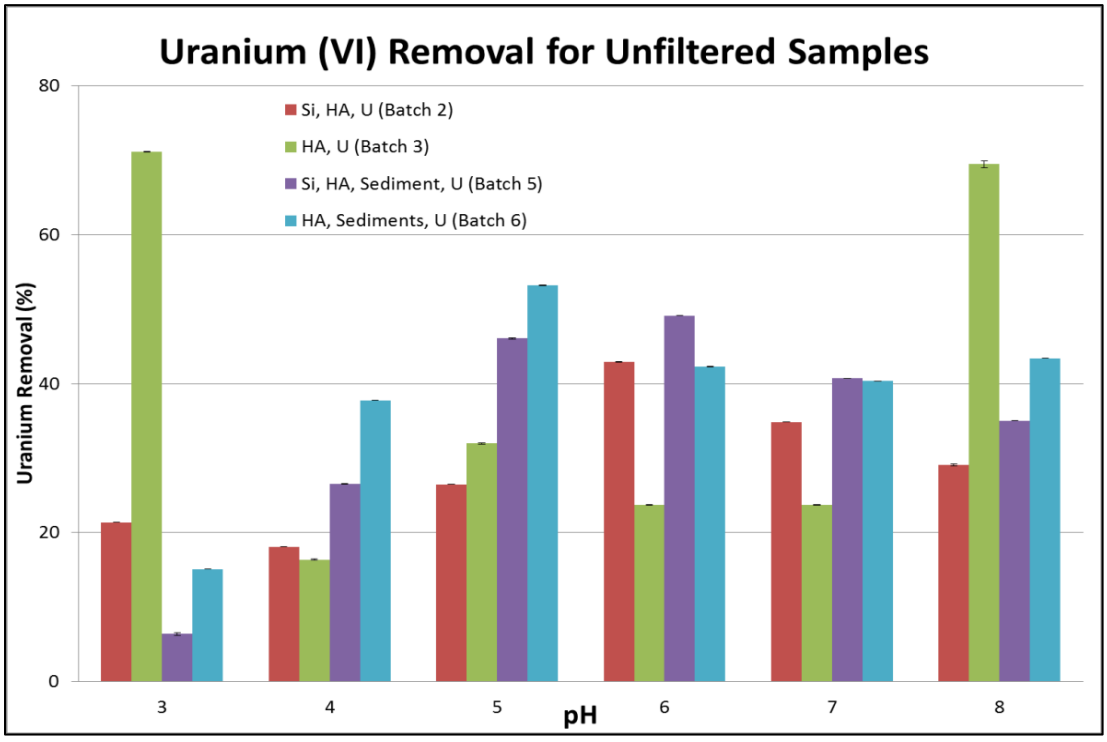

Figure 88. Uranium removal for unfiltered samples for batches 2, 3, 5 and 6.

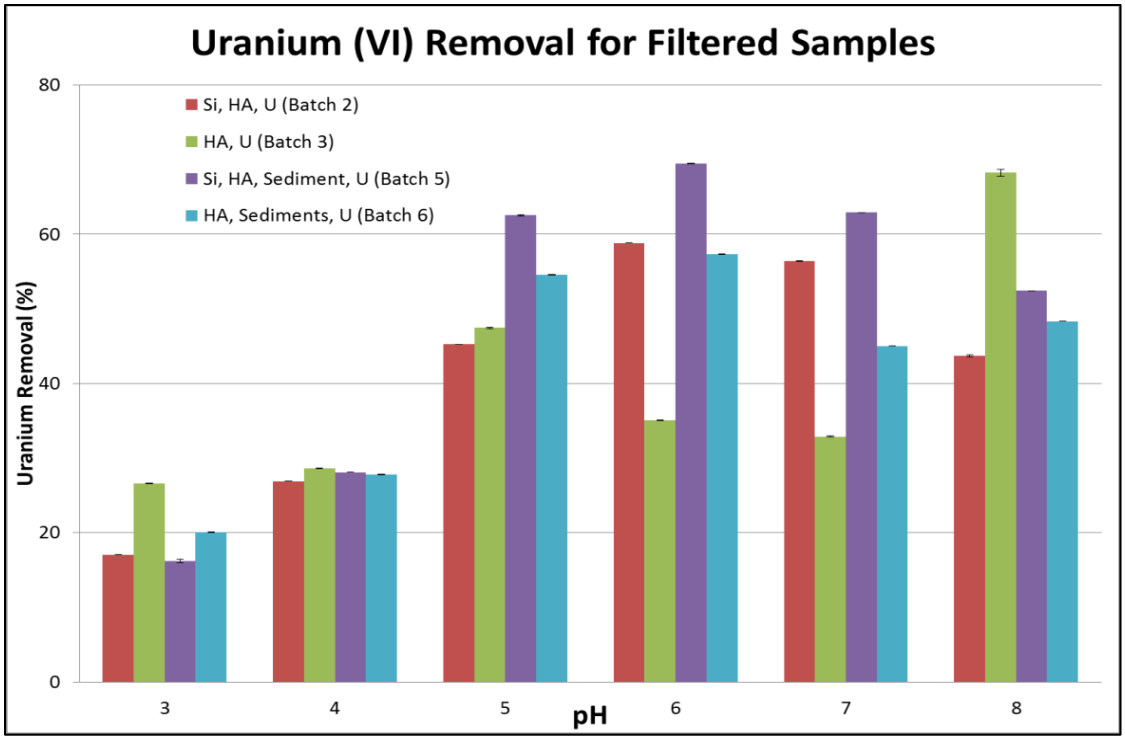

Figure 89. Uranium removal for filtered samples for batches 2, 3, 5 and 6.

1. pH 3 and pH 4

At acidic pH conditions, the percentages of uranium removed for non-sediment batches and sediment batches are between 16-29% and 6-37%, respectively (Table 31). The solubility of HA is low at low pH while U(VI) is present as highly soluble uranyl ions (Krepelova, 2007a). Krepelova et al. (2007b) reported that HA enhances sorption of the U(VI) onto sediment in acidic conditions. At acidic pH, less uranium removal was observed for all batches; this could be because most of the functional groups of humic acid are protonated, so there is going to be fewer binding sites available for complexation. Also, since most of the functional groups of humic acid are protonated, humic acid molecules may adopt a more collapsed structure, hindering the access of uranyl ions to those binding sites. It is likely that, at pH 3-4, sediments play a more important role in the removal of uranium. Sediments contain quartz minerals and quartz has a point of zero charge at pH 2-3. This means that at pH > 3, the surface of these minerals can provide a negative surface charge for the positively charged uranium species to be sorbed by electrostatic attraction (Dong and Wan, 2014). For the filtered samples not containing sediments, silica doesn't play an important role in the removal of uranium. The filtered samples have an 18% increase in U removal at pH 3 and 4 than the unfiltered samples.

Table 31. Uranium removal of unfiltered and filtered batch sample at pH 3 and 4.

	Unfiltered Samples		Filtered Samples	
pH 3	**U(VI) % removal**	**Std. Dev**	**U(VI) % removal**	**Std. Dev**
Batch 2	21.39	0.00	17.04	0.02
Batch 3	71.17	0.05	26.58	0.03
Batch 5	6.40	0.20	16.22	0.00
Batch 6	15.11	0.03	20.09	0.03
pH 4	**U(VI) % removal**	**Std. Dev**	**U(VI) % removal**	**Std. Dev**
Batch 2	18.12	0.03	26.92	0.04
Batch 3	16.39	0.05	28.59	0.00
Batch 5	26.56	0.02	28.11	0.01
Batch 6	37.78	0.01	27.81	0.02

2. pH 5 and pH 6

The average uranium removal for all batches at pH 5 and 6 is shown in Table 32. The percentage of uranium removed for batches 2, 3, 5 and 6 was found to be 35-69% for filtered samples and 26-53% for unfiltered samples. At pH 5 and 6, the overall percentage of uranium removed was the highest for all of the samples; the highest percentage removed was 69% at pH 6. Some studies have observed that uranium sorption reaches a maximum sorption edge close to pH 6 in the presence of quartz. The studies suggested that the formation of aqueous U (VI) hydroxyl complexes enhances the sorption onto quartz minerals (Prikryl et al., 2001; Du et al., 2017). Humic acid becomes more soluble with the increase of pH. Therefore, at pH 6, humic acid might reduce uranium sorption due to formation of aqueous humic-U(VI) complexes. Suspended colloidal silica in solution greatly influences the effectiveness of the removal of uranium for the filtered samples. With the increase of pH, silanol groups (SiOH) on the surface of colloidal silica become more deprotonated (SiO^-), and this enhances the complexation with the positive charge U (VI) species that dominate at pH 5-6. There is a considerable difference in percentage removed for the non-sediment-containing samples and the sediment-containing samples at pH 5 and 6. The batches containing sediment have a higher percentage of removal than the batches that don't contain sediment. This could be the result of additional binding sites for uranium ions on the sediment.

3. pH 7 and pH 8

The percentage of uranium removal in the unfiltered and filtered batches was found to be between 23-69% and 32-68%, respectively, and the percentage of uranium removal remained constant at pH 7 and 8 (Table 33). In the presence of CO_2, the percentage of uranium sorbed onto sediment increased as pH increased to neutral pH conditions (pH 7 and 8). At increasing pH conditions, the uranium species binds more effectively to the hydroxyl and carbonate ions present in the solution. A decline in uranium sorption was observed at pH 7-8 for batches containing colloidal silica, probably due to electrostatic repulsion between the negatively charged colloidal silica, humic acid, and the surface of the sediments with uranium species such as uranyl-carbonates that predominate at this pH range. In addition, the filtered samples indicated

that a fraction of uranium remains in the aqueous solution associated with colloidal silica. At high pH, the proton-binding sites of HA molecules are sufficiently dissociated to carry a significant charge, thus reducing any binding potential (Tipping, 2002). Alkaline pH conditions create electrostatic repulsion between uranium and humic acid, thus allowing less uranium removal. The samples containing sediment vs samples not containing sediment did not seem to have much effect on the uranium removal at pH 7 and 8.

Table 32.Uranium removal of unfiltered and filtered batch sample at pH 5 and 6.

	Unfiltered Samples		Filtered Samples	
pH 5	**U(VI) % removal**	**Std. Dev**	**U(VI) % removal**	**Std. Dev**
Batch 2	26.48	0.01	45.24	0.04
Batch 3	31.96	0.07	47.45	0.01
Batch 5	46.07	0.11	62.53	0.01
Batch 6	53.21	0.01	54.58	0.00
pH 6	**U(VI) % removal**	**Std. Dev**	**U(VI) % removal**	**Std. Dev**
Batch 2	42.93	0.01	58.83	0.01
Batch 3	23.75	0.03	35.05	0.06
Batch 5	49.15	0.01	69.47	0.02
Batch 6	42.26	0.05	57.29	0.04

Table 33. Uranium removal of unfiltered and filtered batch sample at pH 7 and 8.

	Unfiltered Samples		Filtered Samples	
pH 7	**U(VI) % removal**	**Std. Dev**	**U(VI) % removal**	**Std. Dev**
Batch 2	34.87	0.03	56.41	0.03
Batch 3	23.71	0.06	32.88	0.16
Batch 5	40.73	0.00	62.92	0.00
Batch 6	40.35	0.00	45.02	0.00
pH 8	**U(VI) % removal**	**Std. Dev**	**U(VI) % removal**	**Std. Dev**
Batch 2	29.08	0.12	43.71	0.09
Batch 3	69.47	0.43	68.24	0.40
Batch 5	35.05	0.02	52.42	0.02
Batch 6	43.42	0.01	48.35	0.04

Subtask 2.2: Future Work

The focus of this research was to study the effect of varying uranium concentrations in the presence of HA and colloidal silica at variable pH. The next focus will be to investigate the mechanisms of the synergetic interactions of humic acid and colloidal silica on the removal of uranium in the presence of the pure minerals commonly found in soils of the F/H Area. It is important to understand how the pure soil minerals affect uranium removal in the presence of HA and colloidal silica at variable pH conditions.

Subtask 2.2: Acknowledgements

Funding for this research was provided by U.S. DOE Cooperative Agreement number DE-EM0000598. We truly appreciate Dr. Miles Denham and Dr. Brian Looney from SRNL for their valuable input and support of this research. XRD analyses were conducted at FIU AMERI facilities.

Subtask 2.2: References

Chen, C., and X. Wang, 2007. Sorption of Th (IV) to silica as a function of pH, humic/fulvic acid, ionic strength, electrolyte type. *Applied Radiation and Isotopes* 65, 155-163.

Choppin, G.R., 1992. The role of natural organics in radionuclide migration in natural aquifer systems. *Radiochim. Acta* 58/59, 113.

Davis, J.A., 1982. Adsorption of natural dissolved organic matter at the oxide/water interface. *Geochim. Cosmochim. Acta* 46, 2381-2393.

Davis, J.A., 1984. Complexation of trace metals by adsorbed natural organic matter. *Geochim. Cosmochim. Acta* 48, 679-691.

Dong, W; Wang, J. 2014. Additive surface complexation modeling of uranium (VI) adsorption onto quartz-sand dominated sediments. Environ. Sci. Technol, 48, 6569-6577.

Du, L; Li, S; Li, X; Wang, P; Huang, Z; Tan, Z; Liu, C; liao, J; Liu, N. (2017). Effect of humic acid on uranium(VI) retention and transport through quartz columns with varying pH and anion type. Journal of Environmental Radioactivity, 177, 142-150.

Ivanov, P., Griffiths, T., Bryan, N.D., Bozhikov, G. and S. Dmitriev, 2012. The effect of humic acid on uranyl sorption onto bentonite at trace uranium levels. *J. Environ. Monit.,* 14, 2968 - 2975.

Kobayashi M., Juillerat F., Galletto P., Bowen P., and Borkovec M., 2005. Aggregation and Charging of Colloidal Silica Particles: Effect of Particle Size, Langmuir, 21 (13), 5761-5769 DOI: 10.1021/la046829z

Koopal, LK, Y. Yang, A.J. Minnaard, P.L.M. Theunissen, W.H. Van Riemsdijk, 1998. Chemical immobilisation of humic acid on silica. Colloids and Surfaces A: Physicochemical and Engineering Aspects 141, 385-395.

Krepelova, A., 2007. Influence of Humic Acid on the Sorption of Uranium(VI) and Americium(III) onto Kaolinite (Dissertation).

Krepelova, A., Brendler, V., Sachs, S., Baumann, N., Bernhard, G., 2007. U(VI)-Kaolinite Surface Complexation in Absence and Presence of Humic Acid Studied by TRLFS. Environ. Sci. Technol. 2007, 41, 6142-6147.

Krestou A., Panias D., 2004, Uranium (VI) speciation diagrams in the $UO_2^{2+}/CO_3^{2-}/H_2O$ system at 25^{o}C, The European Journal of Mineral Processing and Environmental Protection, Vol.4, No.2, 1303-0868, 2004, pp. 113-129.

Labonne-Wall, N., Moulin, V., Vilarem, J.P., 1997. Retention properties of humic substances onto amorphous silica: consequences for the sorption of cations. *Radiochim. Acta,* 79, 37-49.

Lagos, L., Katsenovich, P., Gudavalli, R., et al., 2014. Rapid Deployment of Engineered Solutions for Environmental Problems at Hanford. Yearend Technical Report, June 30, 2014, U.S. Department of Energy Office of Environmental Management Office of Science and Technology under Grant No. DE-EM0000598.

Perminova, I.V, Hatfield, K., Hertkorn, N., 2002. Use of humic substances to remediate polluted environments: from theory to practice. In the proceedings of the NATO Advance Research Workshop, Springer, P.O Box 17, 3300 AA Dordrech, The Netherland.

Plancque, G., Amekraz, B., Moulin, V., Toulhoat, P., Moulin, C., 2001. Molecular structure of fulvic acids by electrospray with quadrupole time-of-flight mass spectrometry. *Rapid Commun. Mass Spectrom*. 15, 827-835.

Prikryl, J; Jain, A; Turner, D; Pabalan, R. (2001). Uranium^{VI} sorption behavior on silicate mineral mixtures. Journal of Contaminant Hydrology, 47, 241-253.

Tipping, E., 2002. Cation Binding by Humic Substances. Vol. 12. Cambridge UP, p. 266.

Wang, X. K.; Dong, W. M.; Dai, X. X.; Wang, A. X.; Du, J. Z.; Tao, Z. Y. 2000, Sorption and desorption of Eu and Yb on alumina: mechanisms and effect of fulvic acid. Appl. Radiat. Isot. 52, 165-173.

Zachara, J.M., Resch, C.T., Smith, S.C., 1994. Influence of humic substances on Co^{2+} sorption by a subsurface mineral separate and its mineralogical components. *Geochim. Cosmochim. Acta* 58, 553-566.

Subtask 2.3: Humic Acid Batch Sorption and Column Experiments with SRS Soil

Subtask 2.3: Introduction

The Savannah River Site (SRS), located 13 miles south of Aiken in South Carolina, was a defense nuclear processing facility owned by the U.S. government. During the Cold War, from 1953 to 1988, SRS produced a large amount of radioactive and hazardous acidic waste from the production of plutonium and irradiated fuel (Dong et al., 2012). The acidic waste solutions containing low-level radioactivity from numerous isotopes were discharged into a series of unlined seepage basins in the F/H Area. At that time, it was believed that most of the radionuclides present in the waste solution would bind to the soil, precluding the migration of the radionuclides. However, sufficient quantities of uranium isotopes, ^{129}I, ^{99}Tc, and tritium migrated into the groundwater, creating an acidic plume (Denham and Vangelas, 2008). For many years, efforts have been made by the Department of Energy to clean up the site and remediate the groundwater. Groundwater contaminated by operation of the F-Area Seepage Basins remains acidic with a pH as low as 3.2 near the basins and increasing downgradient to 5, and has

concentrations of uranium and other radionuclides that exceed the Environmental Protection Agency (EPA) designated maximum contaminant levels (Wan et al, 2011). In an effort to remove the contaminants from the groundwater, pump-and-treat and re-inject systems were implemented in 1997. Downgradient contaminated groundwater was pumped up to a water treatment facility, treated to remove metals (through osmosis, precipitation/flocculation, and ion exchange), and then re-injected upgradient within the aquifer (Wan et al., 2012). The pump-and-treat water treatment unit eventually became less effective, generating large amounts of radioactive waste. The maintenance of the pump-and-treat water treatment unit was very expensive, and this prompted the research for new remedial alternatives. In 2004, the pump-and treat system was replaced by a funnel and gate system in order to create a treatment zone via injection of a solution mixture composed of two components, sodium hydroxide and carbonate. The injections were done directly into the gates of the F-Area groundwater to raise pH levels. The purpose of the treatment zone was to reverse the acidic nature of the contaminated sediments, thereby producing a more negative net charge on the surface of sediment particles and enhancing the adsorption of cationic contaminants. This system of remediation required a systematic re-injection of the base to raise the pH to near neutral values. However, the continuous use of high concentrations of a carbonate solution to raise the pH creates a concern of possible re-mobilization of uranium that was previously adsorbed within the treatment zone since U(VI) in the presence of bicarbonate ions forms soluble aqueous uranyl-carbonate complexes, though this has not been observed in monitoring data.

Savannah River National Laboratory (SRNL) has been testing an unrefined, low cost humic substance known as Huma-K as an amendment that can be injected into contaminant plumes to enhance sorption of uranium and Sr-90. The advantage of using an unrefined humic substance is that it is inexpensive, and can be used for full scale deployment of remediation technologies.

Humic substances (Figure 90) are ubiquitous in the environment, occurring in all soils, waters, and sediments of the ecosphere (Killops et al., 2004). Humic substances consist of complex organic compounds formed by the decomposition of plant and animal tissue. This decomposition process is known as humification, where the organic matter is transformed naturally into humic substances by microorganisms in the soil (Tipping, 2002). Humic substances are divided into three main fractions: humic acid (HA), fulvic acid (FA), and humin. Their size, molecular weight, elemental composition, structure, and the number and position of functional groups vary. These humic molecules have functional groups such as carboxylic acids, alcohols, and amides among others that can interact with metals forming humic-metal complexes. Therefore, it is possible that metals can interact with soil that has been amended with humic substances.

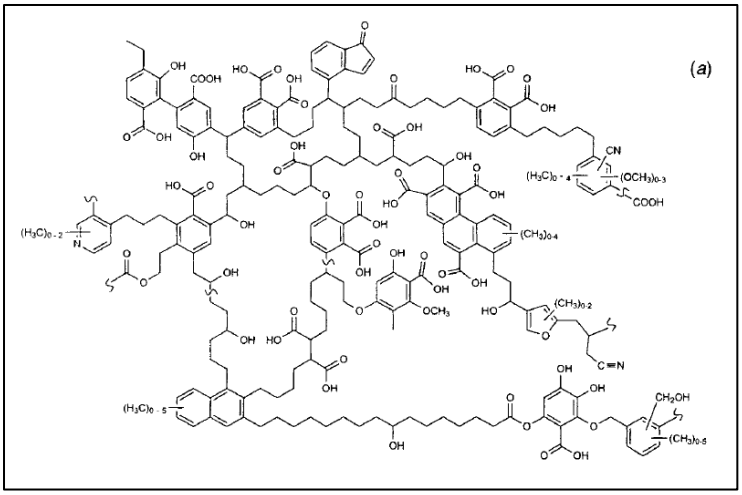

Figure 90. Soil humic acid structure proposed by Schulten and Schnitzer.

Some studies have shown that HA is as an important ion exchange and metal-complexing ligand, carrying a large number of functional groups with high complexing capacity that can greatly affect the mobility behavior of actinides in natural systems (Choppin, 1988). Concentration and pH are the main factors affecting the formation of complexes between humic molecules and metals. It is generally understood that the sorption of metal ions on the mineral surfaces in the presence of HA is enhanced at low pH and reduced at high pH (Ivanov et al., 2012). In addition, Keprelova et al. (2006) showed that U(VI) prefers to be adsorbed onto kaolinite as a uranyl-humate complex.

The objective of this study is to determine if the low cost unrefined humate solution known as Huma-K can be used to facilitate uranium adsorption to control the mobility of uranium in acidic groundwater. Huma-K is an organic fertilizer used by farmers to stimulate plant growth and facilitate nutrient uptake. It is a water soluble potassium salt of humic and fulvic acids that comes from the alkaline extraction of leonardite (a low-rank coal). Leonardite has a very high content of humic substances due to decomposition by microorganisms. Also, compared to other sources of humic substances, leonardite has a higher humic/fulvic acid content. The extraction of humic/fulvic acid from leonardite is performed in water with the addition of potassium hydroxide (KOH), and the resulting liquid is freeze-dried to produce the amorphous crystalline black powder/shiny flakes as seen in Figure 91.

Figure 91. Huma-K

Currently, Florida International University's (FIU) Applied Research Center (ARC) aids SRNL in research by conducting flow through column experiments to investigate sorption/desorption properties of humate, known as modified humic acid (mod-HA), along with the correlation it has on the mobility of uranium through humic acid sorbed sediment.

Subtask 2.3: Methodology

1. Sorption Experiment of Uranium onto SRS Sediment with and without Huma-K Amendment

a. Kinetic Sorption Experiment at pH 4

In this study, SRS sediments (from FAW-1 at 70-90 ft depth) collected from the F-Area were used. All the experiments were done at laboratory ambient temperature (between 20 and 23°C). A Huma-K stock solution of 1000 mg L^{-1} was prepared by dissolving 1000 mg of Huma-K in 1 L of deionized water.

For the kinetic experiments, an initial uranium concentration of 0.5 mg L^{-1} was brought in contact with 200 mg of SRS sediment at pH 4 and constant ionic strength (I = 0.01M $NaClO_4^-$) as shown in Figure 92. The samples were vortex mixed and placed on a platform shaker (Figure 93). At predetermined time intervals, the samples were withdrawn and centrifuged at 2700 RPM (Figure 94). The concentration of the supernatant was measured by kinetic phosphorescence analyzer (KPA) in order to quantify the removal of uranium at different time intervals (Figure 95). It is important to note that prior to the addition of uranium, the sediments were pre-equilibrated for 48 hours.

For the sediments amended with Huma-K, 20 mL of Huma-K solution with fixed concentrations (20 mg L^{-1} and 100 mg L^{-1}) at pH 4 was initially brought in contact with 200 mg of SRS sediment for five days to be equilibrated on the platform shaker. After five days, the samples were centrifuged, and the supernatant was replaced by deionized water (I = 0.01M $NaClO_4^-$) spiked with uranium (C_0 = 0.5 mg L^{-1}) at pH 4. The samples were vortex mixed and placed on a platform shaker. At predetermined time intervals, the samples were withdrawn and centrifuged at 2700 RPM. The supernatant was analyzed by KPA. The pH for all of the samples was monitored daily and adjusted with 0.1 M HCl or 0.1 M NaOH. The amount of uranium sorbed at time t was calculated using the formula:

$$q_t = (C_0 - C_t)V/w$$

where:

q_t = amount of uranium sorbed to the sediments at time t

C_0 = initial concentration of uranium

C_t = concentration of uranium at any time

V = total volume of solution used in the sample

w = weight of SRS sediment in the sample

Figure 92. Samples with SRS sediment

Figure 93. Shaker table with samples

Figure 94. Centrifugation

Figure 95. Kinetic phosphorescence analyzer

2. Flow Through Column Experiments

a. Sediment Characterization

Sediment previously obtained from SRS and characterized by FIU during 2014 was used in the experiments. The sediment was obtained from FAW-1 at a depth of 60'-70'. The sediment was disaggregated with minimal force to avoid creating new mineral surfaces due to fracturing and abrasion using a 2-mm sieve to collect sediment of particle size ≤2 mm.

b. Column Experiments

Glass columns (25 mm x 300 mm) obtained from Ace Glass Inc. were used to conduct the flow-through column experiment to study the sorption/desorption of humate onto SRS sediment and to study the mobility of uranium through humate sorbed sediment. The columns, fitted with Teflon® adapters containing 350 micron screen support and a layer of glass wool (Figure 96), was filled with a known mass of oven-dried sediment obtained from SRS (Figure 97).

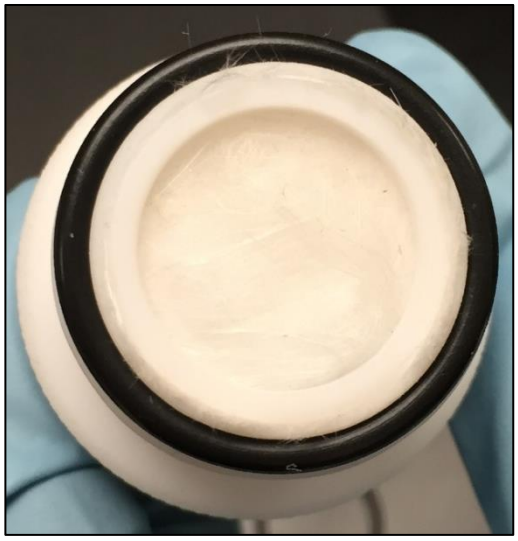

Figure 96. Teflon ® adapter with layer of glass wool.

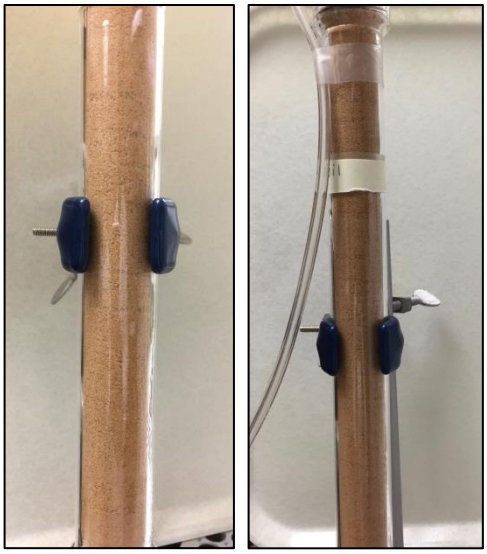

Figure 97. Column with SRS sediment before and after saturation with DIW.

c. Column Tracer Test

A rhenium tracer test was performed to obtain transport parameters. The columns were first saturated with deionized water (DIW) from the bottom of the column to the top in order to remove air bubbles. The flow of DIW was continued until an effluent flow rate of 2.0 ml/min was achieved. After flow was equilibrated, 2.93 ml of a 250 ppm rhenium solution was injected from the base of the column. Samples of the effluent were collected in pre-weighed containers at regular intervals. After each interval, the sample containers were re-weighed and the rhenium concentration was analyzed using ICP-OES. Samples were collected until all of the rhenium was recovered. The data collected was used to determine the mean residence time, the pore volume, and the peclet number. The residence distribution function, E(v), as a function of volume fractions (Levenspiel, 1972) was calculated using Eq. 1:

$$E(v) = \frac{C(v)}{\int_0^\infty C(v)\,dv} \qquad \text{Eq. (1)}$$

Where:
v - Volume of effluent
C(v) - Concentration of rhenium

The mean residence time (t_m), and pore volume (V_p) (Shook et al., 2005) were estimated using Eq. 2 and Eq. 3:

$$t_m = \frac{\int_0^\infty t\,E(t)\,dt}{\int_0^\infty E(t)\,dt} = \int_0^\infty t\,E(t)dt \qquad \text{Eq. (2)}$$

$$V_p = \frac{\int_0^\infty v\,E(v)\,dv}{\int_0^\infty E(v)\,dv} = \int_0^\infty v\,E(v)dv \qquad \text{Eq. (3)}$$

Where:

t - Time
E(t) - Residence distribution function in terms of time
v - Volume of effluent
E(v) - Residence distribution function in terms of volume

Variance and the dimensionless Peclet number (P_e), which represents the ratio of the rate of transport by convection to the rate of transport by diffusion or dispersion, were determined by solving the 1D dispersion/advection equation (Bischoff et al., 1963; Fogler et al., 1992; Mibus et al., 2007):

$$Variance\ (\sigma^2) = \int_0^\infty (v - v_p)^2\ E(v)\,dv \qquad \text{Eq. (4)}$$

$$\frac{\sigma^2}{t_m^2} = \frac{2}{P_e^2}\left(P_e - 1 + e^{-P_e}\right) \qquad \text{Eq. (5)}$$

Where:
v - Volume of effluent
v_p - Pore volume
E (v) - Residence distribution function in terms of volume

d. Sorption/Desorption of Humate

After the tracer test, the column was preconditioned using pH adjusted artificial groundwater (AGW). Artificial groundwater that mimics SRS groundwater characteristics was prepared according to Storm and Kabak (1992) by dissolving 5.4771 g $CaCl_2$, 1.0727 g Na_2SO_4, 3.0943 g $MgCl_2$, 0.3997 g KCl, and 2.6528 g NaCl in 1 L of deionized water (Barnstead NANOpure water purification system). A mass of 0.84995 g $NaNO_3$ was dissolved to obtain a 0.01M $NaNO_3$ solution. One (1) mL of the stock solution was then diluted into 1 L of deionized water acidified to the desired pH to create a working solution. AGW pH adjusted to 3.5 was pumped from the bottom of the column until the pH of the effluent solution reached equilibrium (at pH 3.55). Once the pH of the effluent reached equilibrium, approximately one pore volume (PV) of 10,000 ppm mod-HA solution, pH adjusted to 9 using 0.1 M HNO_3, was pumped at the same flow rate (1.97 ml/min) used during the tracer test. After injecting 1 PV of the mod-HA solution, the AGW solution (with pH 3.5) was pumped into the column until the effluent concentration reached approximately 2% of the initial concentration; effluent samples were collected to measure the change in pH and concentration of mod-HA. The concentration of mod-HA in the effluent was measured immediately after collecting the sample to ensure the desired end point of the desorption phase was achieved. The samples were analyzed using a Thermo Scientific Genesys 10S UV-Vis spectrophotometer; calibration of the UV-Vis was performed using standards in the range of 1 to 25 ppm and at a wavelength of 254 nm (Figure 98). Also, the E_4/E_6 ratio (ratio between the absorbance at 465 nm and 665 nm) and the E_{Et}/E_{Bz} ratio (ratio of absorbance at 253 nm and 220 nm) were measured using the UV-Vis spectrophotometer (Regginal E., Ray W., 1997).

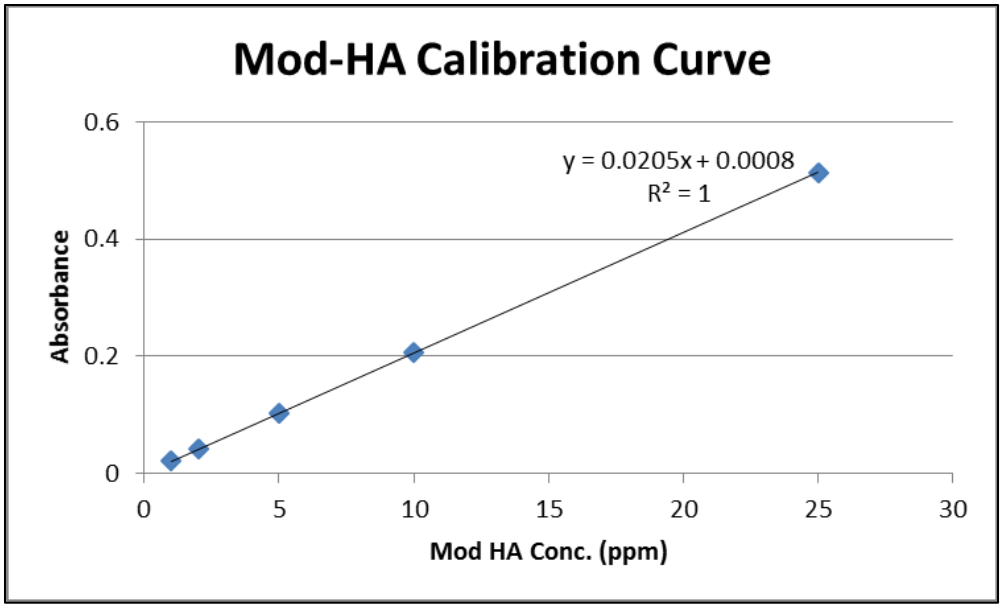

Figure 98. Modified humic acid calibration curve.

e. Sorption/Desorption of Uranium

After the humate sorption and desorption experiment, 2 PV of 100 ppb uranium prepared with AGW at pH 3.5 was injected through the column to study the mobility of uranium. The desorption of uranium was then studied by injecting 2 PV of 3.5, 4.5 and 5.5 pH adjusted AGW solutions, respectively. The samples collected were analyzed via KPA to measure the concentration of uranium.

Subtask 2.3: Results and Discussion

1. Kinetic Sorption Experiment

Kinetic experiments offer valuable information about the rate of the reaction and the reaction mechanism involved in the sorption process. The kinetic sorption experiment of uranium showed that equilibrium is reached at different time periods for each system (Figure 99a). In the absence of Huma-K, uranium sorption to SRS sediment is characterized by a fast uptake, reaching equilibrium within 8 hours. At a concentration of 1000 mg/kg of Huma-K, there was a significant decrease in the uranium sorption kinetic rate (7 days). However, at a concentration of 2000 mg/kg of Huma-K, the uranium sorption kinetic rate increased (3 days). Therefore, the uranium sorption kinetic rate depends on the relative concentrations of Huma-K present in the SRS sediment.

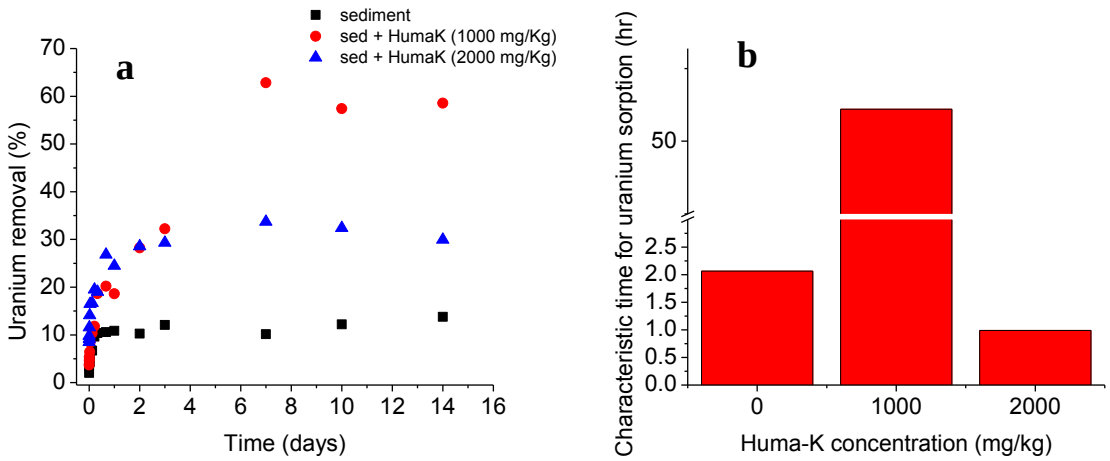

Figure 99. (a) The kinetics of uranium sorption on sediments with and without Huma-K (10 gr/L of sediment, pH 4, and I = 0.01 M NaClO4). (b) Characteristic times for the sorption of uranium on various Huma-K concentrations.

For the interpretation of experimental kinetic data, differences between sorption rates in systems with varying Huma-K concentrations was determined based on an objective mathematical parameter, namely the characteristic time for overall sorption reactions (Figure 99b). Characteristic time ($t_{1/2}$) is defined as the time needed to reach a specific fraction of the final equilibrium concentration. Generally, long characteristic times (large $t_{1/2}$ values) indicate slow sorption kinetics; short characteristic times (small $t_{1/2}$ values) represent fast kinetics. Systems with the same sorption kinetics show the same fraction of the equilibrium surface concentration sorbed at any given point in time, independent of the individual equilibrium values approached. Hence, comparable values of $t_{1/2}$ indicate similar sorption kinetics (Tinnacher et al., 2013).

Characteristic times were determined by calculating the fraction of uranium reached over time while assuming the last experimental time-points represent equilibrium surface concentrations. For example, for an equilibrium surface concentration of 6.22 mg/kg of uranium, 3.42 mg/kg represents 55% of the equilibrium surface concentration. In a similar way, the other fractions of uranium reached over time were calculated. By plotting these fractions as a function of time (Figure 100), the characteristic time is determined based on a linear regression. The characteristic time (open circle) represents the intercept between individual regression lines and the line showing 50% of the equilibrium surface concentration. For uranium sorption to SRS sediment, characteristic times calculations indicate a varying effect of Huma-K on uranium sorption kinetics (Figure 99b). At a concentration of 1000 mg/kg of Huma-K, the characteristic time for uranium sorption to SRS sediment (52.2 h) was significantly increased relative to the corresponding plain sediment system (2.06 h). This indicates that uranium sorption is slowed in the presence of a low Huma-K concentration. In contrast, at a concentration of 2000 mg/kg of Huma-K, a significant decrease in the characteristic time for uranium sorption (0.98 h) was observed, meaning that uranium sorption kinetics become significantly faster. This is probably due to a higher number of reactive sites. The sorption kinetics can be affected by different factors such as uranium diffusion and a limited number of effective surface site available for uranium sorption.

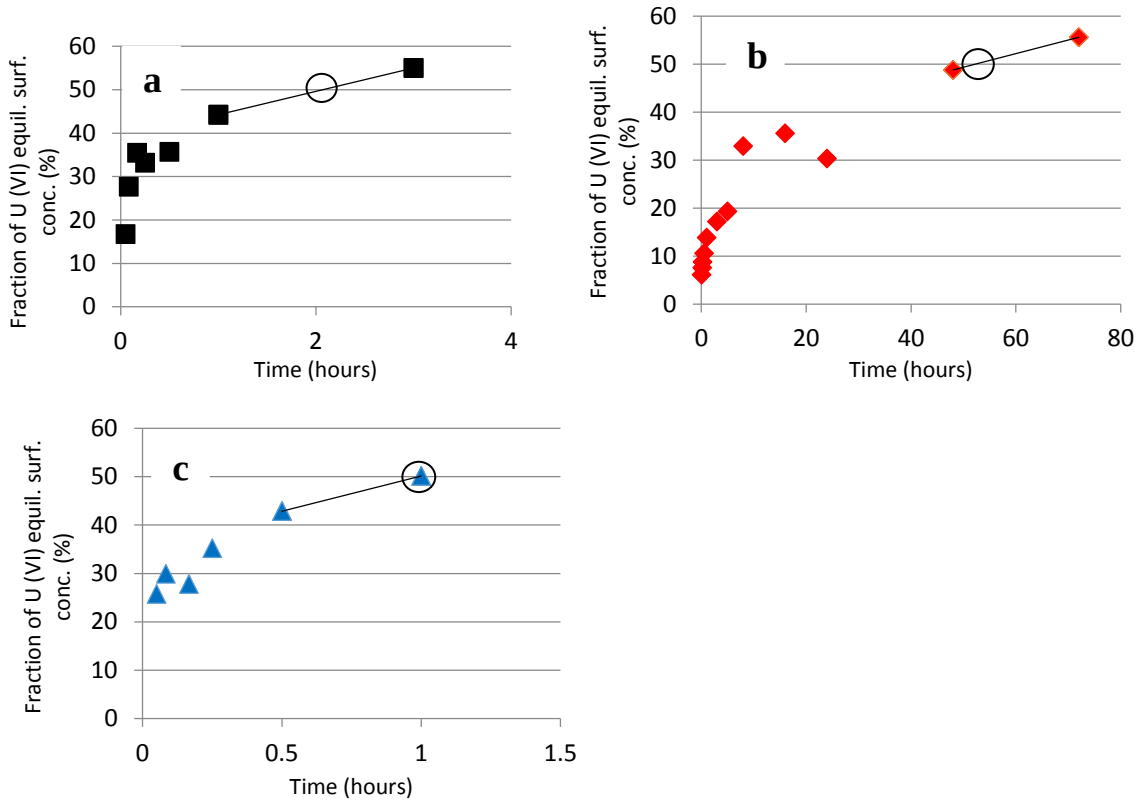

Figure 100. Fraction of uranium concentration sorbed over the course of kinetic experiment at pH 4: (a) sediment, (b) Sed + Huma-K (1000 mg/kg), and (c) Sed + Huma-K (2000 mg/kg).

Huma-K influenced the sorption of uranium as shown in Figure 99a. At a concentration of 1000 mg/kg of Huma-K, the removal of uranium was higher (60%) compared to plain sediment (10%) and sediment with 2000 mg/kg of Huma-K (30%). The decrease in uranium sorption at a concentration of 2000 mg/kg results from a higher amount of desorbed Huma-K from SRS sediment. Desorbed Huma-K can form aqueous complexes with uranium. As a result, there is competition between uranyl-humate complex formation in the aqueous phase and surface complexation. At a concentration of 1000 mg/kg of Huma-K, there is some Huma-K desorbed but not as much as in the case of higher Huma-K. This probably leads to a lower level of formation of aqueous uranyl-humate complexes; as a result, the removal is higher (Figure 99a). In the absence of Huma-K, the removal of uranium by SRS sediment is lower compared to the other two systems due to a low number of binding sites.

The kinetic sorption reaction was evaluated based on various kinetic models including first, second, pseudo-first, and pseudo-second order models. The model that best described the experimental data was pseudo-second order (R^2 is closer to unity) for the three systems as shown in Table 34. There was a very good agreement between the maximum uptake calculated value (q_e, calculated) by the pseudo-second order model and the equivalent experimental value (q_e, experimental). The pseudo-second order model assumes that the controlling step might be attributed to chemical sorption involving complexation, coordination and/or chelation (Kushwaha and Sudhakar, 2013).

Table 34. Kinetic Models

Kinetic Model	Parameter	Sediment	Sed + HumaK (1000 mg/kg)	Sed + HumaK (2000 mg/kg)
	q_e, experimental (mg/kg)	6.22	30.7	16.5
First Order	q_e, calculated (mg/kg)	3.04	5.17	7.90
	R^2	0.31	0.60	0.40
Second Order	q_e, calculated (mg/kg)	2.63	4.21	7.28
	R^2	0.20	0.32	0.30
Pseudo-first	q_e, calculated (mg/kg)	1.67	26.5	7.03
	R^2	0.07	0.95	0.66
Pseudo-second	q_e, calculated (mg/kg)	6.57	31.7	15.6
	R^2	0.98	0.96	0.99

Since sorption is a complex process where different mechanisms may be occurring at the same time, the Morris-Weber model (intra-particle diffusion) was used in an effort to determine the rate-limiting step of the sorption process. In the Morris-Weber model, the C value obtained from the intercept of the plot reflects the resistance of mass transfer in the boundary layer. If the intercept C = 0, intra-particle diffusion is the rate-limiting step. However, this is not always the case and the sorption kinetics may be controlled by film diffusion, intra-particle diffusion or other mechanisms simultaneously. Therefore, the plot would be multi-linear and the intercept would not equal to zero (Cheung et al, 2007; Qiu et al., 2009). The Morris-Weber plot for the three systems (Figure 101) showed multi-linearity, indicating that there are multiple steps that influence the sorption kinetics of uranium. The first step is attributed to either external mass transfer from the solution to the surface of the adsorbent or instantaneous sorption of the most readily available reactive sites. The second step can be ascribed to the interior boundary layer diffusion, and the third step is the final equilibrium step (Rengaraj et al., 2004).

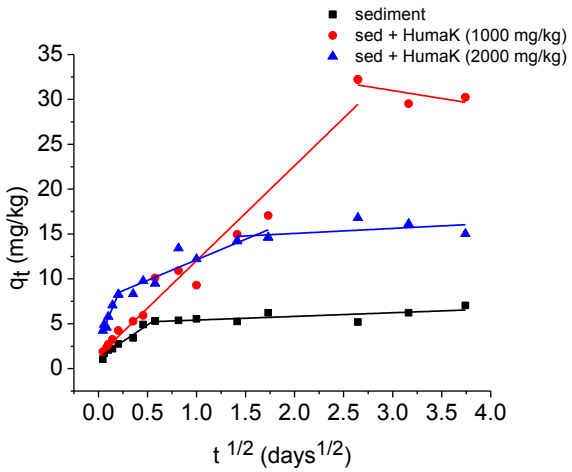

Figure 101. Weber-Morris plot of U (VI) sorption

2. Flow Through Column Experiments

a. Optimization of Tracer Test

The column tracer test was optimized by conducting a total of three rhenium tracer tests with rhenium solutions containing 1000 ppm, 500 ppm, and 250 ppm, respectively. Results from the 1000 ppm tracer test indicated that the initial injection of 2.475 mL of 1000 ppm rhenium solution (2.475 mg) was too high and the total sample collection time (thirty samples collected at 3 minute intervals) was too short; extended sampling is needed to fully recover the rhenium. A second rhenium tracer test at 500 ppm with an increased collection time was conducted. A volume of 1.9175 mL of 500 ppm rhenium solution (0.9587 mg) was injected, which resulted in 81.5% rhenium recovery by collecting forty samples over a total of 216 minutes at 5 and 7 minute intervals. Based on the 500 ppm rhenium tracer test data, a third tracer test was next performed by injecting 1.97 mL of 250 ppm rhenium solution (0.4925 mg). Forty samples were collected over a total of 214 minutes at 4 and 7 minute intervals. The 250 ppm tracer test data concluded that 0.4485 mg of rhenium was recovered from the column, representing a 91% recovery. After concluding the optimization of the rhenium tracer test, a new column experiment was conducted to study the effect of mod-HA on uranium mobility.

b. Rhenium Tracer Test

The column was filled with 266.42 g of oven-dried SRS sediment that was sieved through a 2-mm sieve. After the column was filled and saturated with DI water, a rhenium tracer test was performed by following the procedure detailed in the methodology section. The effluent flow rate was set to 2.0 ml/min and 2.93 ml of a 250 ppm rhenium solution (0.73 mg) was injected from the base of the column. Forty samples were collected in pre-weighed containers over a total of 214 minutes at 4 and 7 minute intervals. After each interval, the sample containers were re-weighed and the rhenium concentration was analyzed using ICP-OES. The data analysis concluded that 0.75 mg of rhenium was recovered from the column at 102% recovery with an effective flow rate of 1.97 mL/min. The data obtained from the tracer test is presented in Figure 102 and Table 35. Figure 102 shows the change in concentration of rhenium versus the volume of collected effluent fractions. The pore volume, variance and Peclet number were calculated using equations 1-5 as described in the methodology section and the data is presented in Table 35

and Table 36. The results show that the column has a pore volume of 104 ml and a low variance value that positively correlates with a smaller distribution spread.

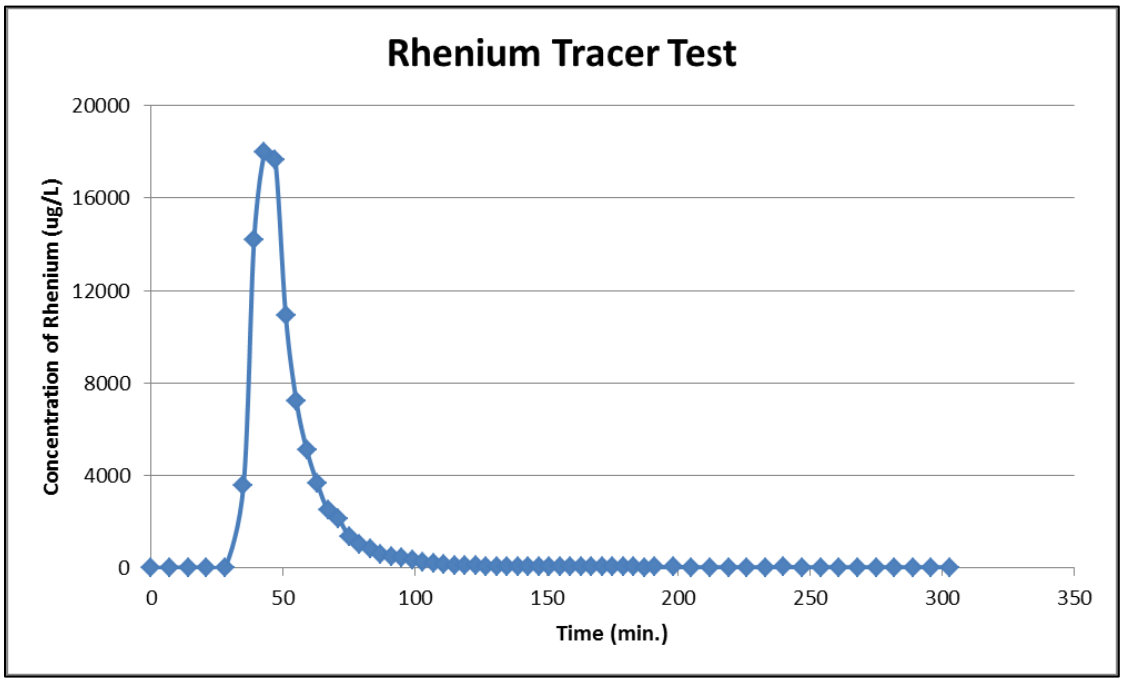

Figure 102. Concentration of measured rhenium.

Table 35. Tracer Test Results

Sediment weight (g)	Flow rate (ml/min)	Rhenium added (mg)	Rhenium recovered (mg)	Recovery (%)	Pore volume (ml)
266.42	1.97	0.7325	0.75	102	104

The dimensionless Peclet number (Pe) is defined as the ratio of the rate of transport by convection to the rate of transport by diffusion or dispersion (Eq. 6). Pe, found experimentally from the tracer test, was used to calculate effective dispersion (Table 36); the values of the Peclet number were used to correlate the effect of dispersion on the effluent tracer concentration.

$$Pe = \frac{rate\ of\ transport\ by\ convection}{rate\ of\ transport\ by\ diffusion\ or\ dispersion} = \frac{UL}{D_a} \qquad \text{Eq. (6)}$$

Where:
L - characteristic length term (m)
D_a - effective dispersion coefficient (m^2/s)
U - average interstitial velocity (m/s)

Table 36. Transport Parameters Determined by Rhenium Tracer Injection

U (m/s)	Variance, σ^2	Pe	Dispersion (m^2/s)	1/Pe=D/uL	Dispersion
6.69×10^{-5}	2.25×10^{-03}	8.32	2.41×10^{-7}	0.120	Low

c. Sorption and Desorption of Humate

After concluding the rhenium tracer test, AGW with pH adjusted to 3.5 was injected from the bottom of the column until the pH of the effluent solution reached equilibrium at pH 3.42. One (1) PV of 10,000 ppm of humate with pH adjusted to 9 was then injected at a flow rate of 1.97 mL/min. The mod-HA solution was stirred continuously while pumping to avoid settling. After injecting approximately 1 PV of the humic solution (mod-HA), AGW at pH 3.5 was injected into the column until the concentration of mod-HA reached approximately 2% of the initial concentration while collecting effluent samples at 4 minute intervals. The concentration of humic acid in the effluent samples were measured immediately after sample collection in order to ensure that the desired end point of the desorption phase was achieved. It was observed that approximately 2.2 PV of AGW with pH adjusted to 3.5 was required to reach 2% of the initial humic acid concentration. The effluent sample pH was also measured and recorded. Figure 103 shows the breakthrough curve of humic acid sorption and desorption in the column and the change in pH. It is evident from the curve that most of the humic acid injected into the column was retained and no humic acid was observed in the effluent solution until after 0.61 pore volumes. After 0.61 pore volumes, the concentration of humic acid increased and reached a peak value of approximately 7,163 ppm while the pH steadily increased. From previous batch experiments, it was concluded that there may be precipitation of humic acid at pH < 6.3; when HA at pH 9 was injected into the column at pH 3.5, precipitation and re-dissolution of HA might have occurred as the pH of the solution increased; this would explain the spread of the breakthrough curve compared to that of the non-reactive tracer breakthrough curve. Because of precipitation, the amount of HA sorbed is inconclusive and the term “retained” is used over “sorbed” in this report. Around 1.3 PV, the concentration of HA started to decrease and the concentration of humic acid in the effluent reached 20 ppm after injecting approximately 3.37 PV of AGW at pH 3.5. Table 37 shows the results obtained from sorption and desorption of mod-HA; the pH of the column changed from 3.42 to 6.92 while retaining approximately 228.47 mg of humic acid out of 862.22 mg of humic acid injected, resulting in a retention total of 857.56 mg of humic acid per kg of sediment.

Since the unrefined humic acid solution was composed of humic acid and fulvic acid of different sizes and molecular weights; the E_4/E_6 ratio was used to determine which humic fraction sorbed onto the sediments. The E_4/E_6 ratio was calculated by dividing the absorbance of the sample at 465 nm by 665 nm. Researchers have found that the E_4/E_6 ratio increases as the average molecular weight of humic substances decreases. The range of values of the E_4/E_6 ratio from a wide variety of literature sources for humic acids and fulvic acids are 3.8-5.8 and 7.6-11.5, respectively; however, the E_4/E_6 ratios obtained during the experiment were in the range of 5.0 - 8.0. Where the concentration of humic acid in the effluent was high, the experimental E_4/E_6 ratios were in the range of 4.0 - 6.0, meaning that the fraction of humate bound to the sediments consists of humic acid molecules.

The E_{ET}/E_{BZ} ratio was calculated in order to determine the degree and possible nature of substitution. The ratio was calculated by measuring the absorbance at 253 nm and 220 nm, corresponding to the electron-transfer band and the benzenoid band, respectively. The intensity of the absorbance, especially the electron-transfer band, has a significant increase when substitution increases. The benzene band is almost unaffected. A low E_{ET}/E_{BZ} ratio indicates scarce substitution in the aromatic rings or substitution with aliphatic functional groups, while a high E_{ET}/E_{BZ} ratio indicates the presence of O-containing functional groups (hydroxyl, carbonyl, carboxyl, and ester groups) on the aromatic ring. The ratios vary from 0.03 (benzene ring) to between 0.25-0.35 for phenolic compounds and above 0.40 for aromatic rings with carbonyl and carboxylic groups. The values of the E_{ET}/E_{BZ} ratios were observed to be around 0.4-0.8, indicating that the aromatic structures in these humic molecules probably have a higher degree of substitution with oxygen-containing functional groups.

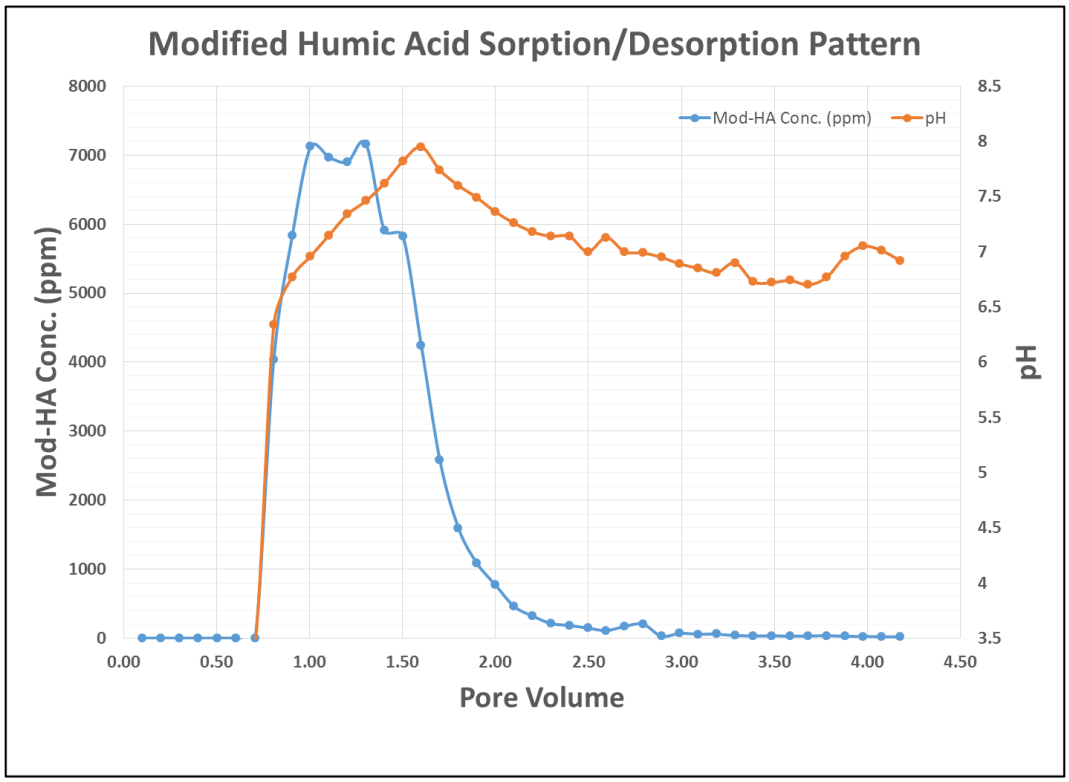

Figure 103. Concentration profile of HA in the effluent of the column

Table 37. Soprtion/Desorption of Modified Humic Acid

Sediment Weight (g)	pH		Humic acid			
	Initial	Final	Injected (ml)	Injected (mg)	Recovered (mg)	Retained (mg/kg)
266.42	3.42	6.92	82.43	862.22	633.75	857.56

d. Sorption and Desorption of Uranium

Sorption and desorption of uranium in the humate sorbed column was studied by injecting 2 PV of a 100 ppb uranium solution prepared with SRS AGW at pH 3.5 followed by injection of 2 PV

each of AGW at pH 3.5, 4.5 and 5.5. Figure 104 shows the change in the concentration of uranium and change in pH while injecting the uranium solution through the column. As 100 ppb of uranium at pH 3.5 was injected into the column, the pH of the column decreased from 6.92 to 6.76.

Figure 105 shows the change in humic acid concentration during injection of uranium and AGW solution at pH 3.5. Approximately 2.39 mg of humic acid was recovered from the effluent solution during the uranium injection; no humic acid was recovered during injection of AGW at pH 3.5, 4.5, or 5.5.

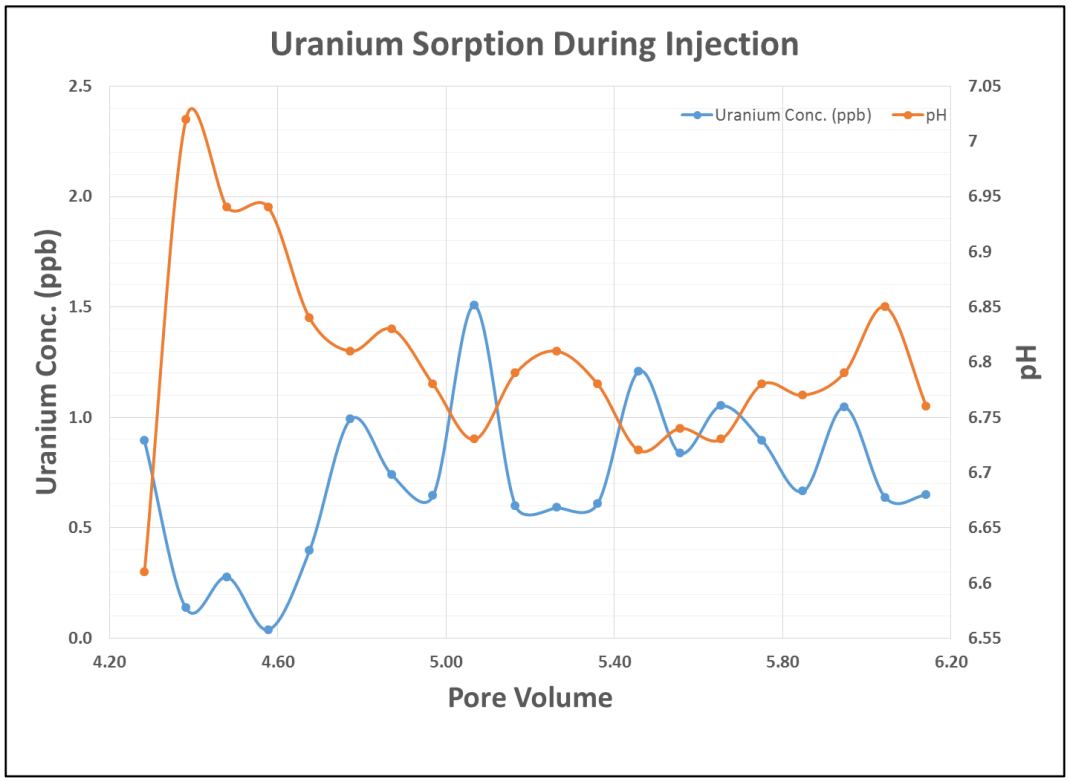

Figure 104. Change in uranium concetration and pH during uranium injection.

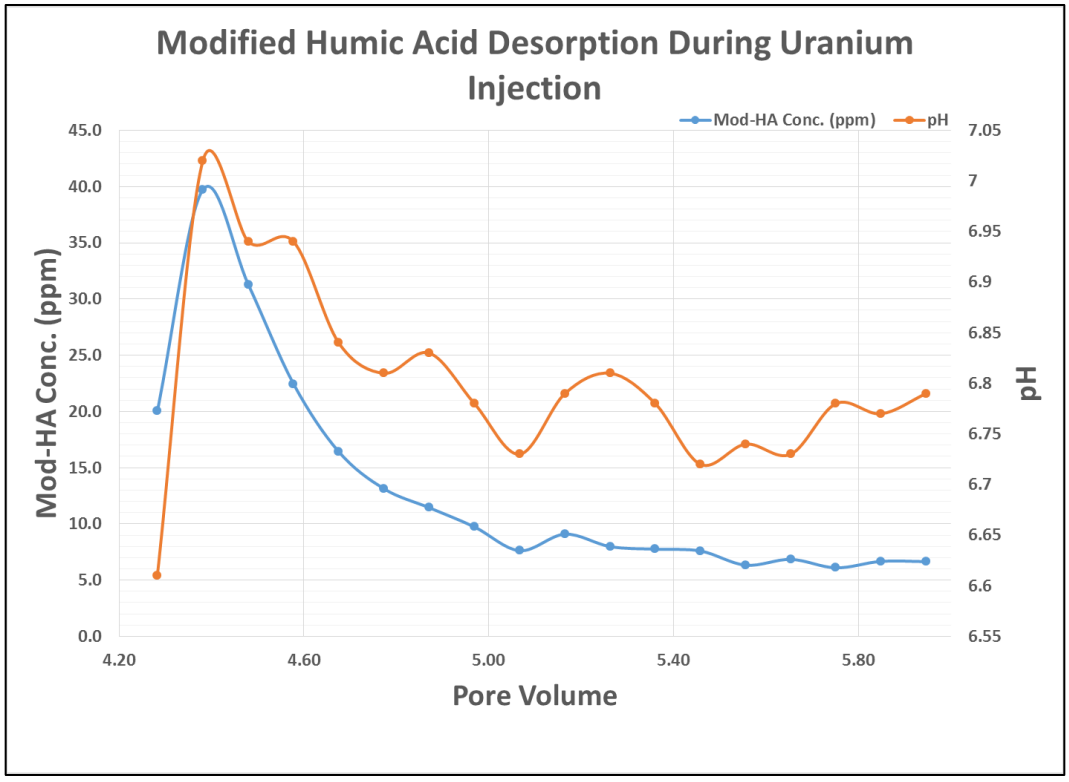

Figure 105. Change in Modified humic acid concentration during uranium injection.

Figure 106 shows the change in uranium concentration and pH in the effluent solution during injection of the uranium solution and AGW (pH adjusted to 3.5 - 5.5). Approximately 20.05 µg of uranium (200.48 ml of 100 ppb) was injected into the column; the total amount of uranium recovered was 0.59 µg. The concentration of uranium in the effluent solution was below the detection limit of KPA so the samples were spiked with a known amount of 100 ppb uranium solution and reprocessed to obtain the concentration of uranium in the samples. Table 38 shows the results obtained from sorption and desorption of uranium; overall, approximately 73.04 µg/kg of uranium was sorbed on to mod-HA treated sediment.

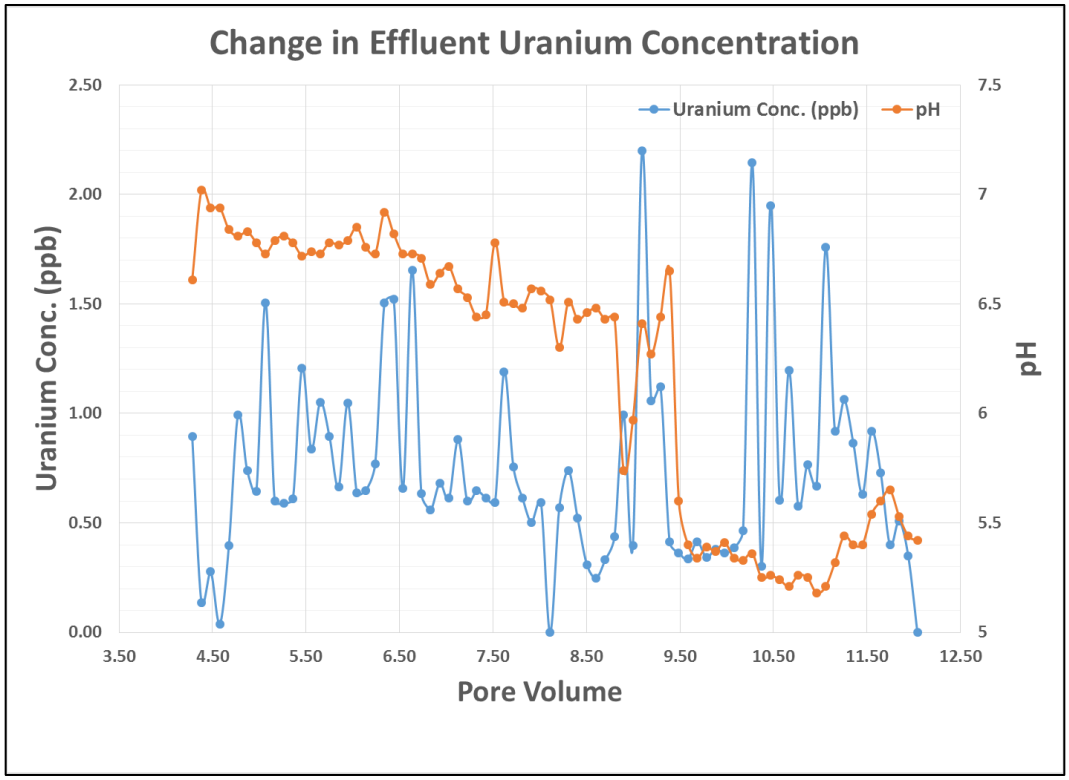

Figure 106. Change in uranium concentraion during sorption and desoprtion of uranium.

Table 38. Soprtion/Desorption of Uranium

Sediment weight (g)	pH		Injected (ml)	Injected (µg)	Recovered (µg)	Retained (%)	Retained (µg/kg)
	Initial	Final					
266.42	6.92	5.42	200.48	20.05	0.59	97.06	73.04

e. Comparison of Mod-HA to Huma-K

The column experiments conducted with Huma-K and modified humic acid had approximately same amount of sediments, humate and initial pH. As seen in Table 39, the amount of humate injected into the mod-HA column was was higher compared to the Huma-K column (Lagos et al. 2016). The amount of mod-HA retained (857.57 mg/kg) in the column was greater than that of the Huma-K retained (669.33 mg/kg). Also, the final pH of these two columns is different; Huma-K had a higher final pH compared to mod-HA, which might have resulted in the higher humate retention in the mod-HA column. Huma-K was shown to precipitate at pH < 6.3; additional experiments are needed to study the precipitation of mod-HA with pH to better explain the increased retention of humate in the mod-HA experiment. The amount of uranium retained was also greater in the case of the mod-HA column, resulting in 97% of uranium retention compared to only 81% uranium retention observed for Huma-K (Table 40).

Table 39. Sorption/Desorption of Humate

	Sediment weight (g)	pH		Injected (mL)	Injected (mg)	Recovered (mg)	Retained (mg/kg)
		Initial	Final				
Huma-K*	256.31	3.55	8.79	82.9	829	657.44	669.33
Mod-HA	266.42	3.42	6.92	82.43	862.22	633.75	857.57

Table 40. Sorption/ Desorption of Uranium

	Sediment weight (g)	pH		Injected (ml)	Injected (µg)	Recovered (µg)	Retained (µg/kg)
		Initial	Final				
Huma-K*	256.31	8.79	4.43	163.70	16.37	3.05	51.95
Mod-HA	266.42	6.92	5.42	200.48	20.05	0.59	73.04

* data from previous experiment, Lagos et al. 2016

Subtask 2.3: Future Work

Future work will focus on additional batch experiments, exploring the removal of uranium using Huma-K as a low-cost remediation method. This study will evaluate the effect of pH and initial uranium concentrations, as well as expand the investigation of U(VI) desorption via the following batch experimental design:

- Savannah River Site sediments + uranium
- Sediments coated with HS + uranium
- HS + uranium

This research will improve the understanding of the removal of uranium when Huma-K is used as a remediation method.

FIU will continue to investigate the sorption behavior of Huma-K and Mod-HA materials under varying pH conditions and the effect of sorbed HA on uranium mobility in porous media. Also investigate the effect of pH on mod-HA precipitation.

Subtask 2.3: Acknowledgements

Funding for this research was provided by U.S. DOE under contract DE-EM0000598. We truly appreciate Dr. Miles Denham and Dr. Brian Looney from SRNL for their valuable contributions and support of this research.

Subtask 2.3: References

Bear, Jacob, Hydraulics of Groundwater, McGraw-Hill Book Company, New York 1979.

Bischoff K., Levenspiel O., (1963) Adv. Chem. Eng. 4, p. 95.

Blake, G.R., and Hartge, K.H., (1986). Bulk Density. In: Klute, A. (Ed.), Methods of Soil Analysis. Part 1. Physical and Mineralogical Methods. American Society of Agronomy-Soil Science Society of America, 677 South Segoe Road, Madison, WI, 363-375.

Blake, G.R., and Hartge, K.H., (1986). Particle Density. In: Klute, A. (Ed.), Methods of Soil Analysis. Part 1. Physical and Mineralogical Methods. American Society of Agronomy-Soil Science Society of America, 677 South Segoe Road, Madison, WI, 377-382.

Cheung, W.H., Y.S. Szeto, and G. McKay, *Intraparticle diffusion processes during acid dye adsorption onto chitosan.* Bioresource Technology, 2007. 98(15): p. 2897-2904.

Choppin Gregory, R., *Humics and radionuclide migration*, in *Radiochimica Acta*. 1988. p. 23.

Danielson, R.E., and Sutherland, P.L., (1986). Porosity. In: Klute, A. (Ed.), Methods of Soil Analysis. Part 1. Physical and Mineralogical Methods. American Society of Agronomy-Soil Science Society of America, Madison, WI, 443-450.

Denham, M. and K.M. Vangelas, *Biogeochemical gradients as a framework for understanding waste-site evolution.* Remediation, 2008. 19(1): p. 5-17.

Dong, W., et al., *Uranium(VI) adsorption and surface complexation modeling onto background sediments from the F-Area Savannah River Site.* Environmental Science & Technology, 2012. 46(3): p. 1565-1571.

Dong, W., Tokuanga, T. K., Davis, J. A., Wan, J., (2012). Uranium(VI) Adsorption and Surface Complexation Modeling onto Background Sediments from the F-Area Savannah River Site. Environ. Sci. Technol. 46, 1565-1571.

Fogler, H., S., (1992). Elements of Chemical Reaction Engineering, PTR Prentice-Hall, Inc., 837p.

Ivanov, P., et al., *The effect of humic acid on uranyl sorption onto bentonite at trace uranium levels.* Journal of Environmental Monitoring, 2012. 14(11): p. 2968-2975.

Killops, S., et al., *Long-term fate of organic matter in the geosphere*, in *Introduction to Organic Geochemistry*. 2004, Blackwell Publishing Ltd. p. 117-165.

Křepelová, A., S. Sachs, and G. Berhard, *Uranium(VI) sorption onto kaolinite in the presence and absence of humic acid.* Radiochimica Acta, 2006. 94(12): p. 825-833.

Kushwaha, S. and P.P. Sudhakar, *Sorption of uranium from aqueous solutions using palm-shell-based adsorbents: a kinetic and equilibrium study.* Journal of Environmental Radioactivity, 2013. 126(Supplement C): p. 115-124.

Leonel Lagos, Yelena Katsenovich, Ravi Gudavalli, Angelique Lawrence, Reinaldo Garcia, Shimelis Setegn, David Roelant, Vasileios Anagnostopoulos, Hilary P. Emerson, Mehrnoosh Mahmoudi, 2016. Rapid Deployment of Engineered Solutions for Environmental. Florida International University, Applied Research Center.

Levenspiel, O., Chemical Reaction Engineering, 2nd Ed., (1972), John Wiley &Sons.

Mibus, J., Sachs, S., Pfingsten, W., Nebelung, C., Bernhard, G., (2007). Migration of Uranium (IV)/(VI) in the Presence of Humic Acids in Quartz Sand: a Laboratory Column Study, Journal of Contaminant Hydrology, Volume 89, Issues 3-4, Pages 199-217.

Milling, M. R., Amidon, M. B., Denham M. E., Looney B. B., (2013). Preliminary Data Report: Humate Injection as an Enhanced Attenuation Method at the F-Area Seepage Basins, Savannah River Site (U). (SRNL-STI-2013-00514).

Ptak, T., Piepenbrink, M., Martac E. (2004). Tracer Tests for the Investigation of Heterogeneous Porous Media and Stochastic Modelling of Flow and Transport - a Review of some Recent Developments, Journal of Hydrology, 122 - 163.

Qiu, H., et al., *Critical review in adsorption kinetic models.* Journal of Zhejiang University, Science, A, 2009. 10(5): p. 716-724.

Regginal R. Engebretson, Ray Von Wandruszka, The effect of molecular size on humic acid associations, In Organic Geochemistry, Volume 26, Issues 11-12, 1997, Pages 759-767, ISSN 0146-6380, https://doi.org/10.1016/S0146-6380(97)00057-0.

Rengaraj, S., et al., *Removal of copper from aqueous solution by aminated and protonated mesoporous aluminas: kinetics and equilibrium.* Journal of Colloid and Interface Science, 2004. 273(1): p. 14-21.

Shook, G. M., Forsmann, J. H., (2005). Tracer Interpretation Using Temporal Moments on a Spreadsheet (INL/EXT-05-00400).

Storm, R.N., Kaback, D.S. 1992. SRP Baseline Hydrogeologic Investigation: Aquifer Characterization, Groundwater Geochemistry of the Savannah River Site and Vicinity (U). Westinghouse Savannah River Company, Savannah River Laboratory.

Tinnacher, R.M., et al., *Effects of fulvic acid on uranium(VI) sorption kinetics.* Environmental Science & Technology, 2013. 47(12): p. 6214-6222.

Tipping, E., *Cation binding by humic substances*. 1st ed. 2002, New York, USA: Cambridge University Press.

Wan, J., Dong, Wenming, and Tokunaga T. K., (2011) Method to Attenuate U(VI) Mobility in Acidic Waste Plumes Using Humic Acids, Environ. Sci. Technol. 2011, 45, 2331–2337

Wan, J., et al., *Persistent source influences on the trailing edge of a groundwater plume, and natural attenuation timeframes: The F-Area Savannah River Site.* Environmental Science & Technology, 2012. 46(8): p. 4490-4497.

Wan, J., *Method to Attenuate U(VI) Mobility in Acidic Waste Plumes Using Humic Acids.* Environmental science & technology. 45(6): p. 2331-2337.

Wan, J., Tokuanga, T. K., Dong, W., Denham M. E., Hubbard, S. E., (2012). Persistent Source Influences on the Trailing Edge of a Groundwater Plume, and Natural Attenuation Timeframes: The F-Area Savannah River Site. Environ. Sci. Technol. 46, 4490-4497.

TASK 3: SURFACE WATER MODELING OF TIMS BRANCH

TASK 3: EXECUTIVE SUMMARY

This task involves the development of an integrated, fully distributed hydrology and transport model to be used as a tool for assessment, evaluation and monitoring of the fate and transport of sediment and contaminants in Tims Branch at SRS. Tims Branch is a small stream-scale ecosystem located in the A and M areas of SRS that has received direct discharges of wastewater from on-site process and laboratory facilities. At various times, this wastewater contained uranium, nickel, aluminum, mercury, other metals and radionuclides, and organic solvents. In the lower portion of Tims Branch, currently discharging groundwater contains trace levels of organic solvent. A number of innovative treatment methods were deployed to limit the contaminant flux to Tims Branch, including a wetland treatment system (northern tributary in 2000) and a mercury removal system that uses a tin (II) reagent and air stripping (outfall tributary in 2007). Together, these treatments effectively eliminated all local anthropogenic mercury inputs to this ecosystem. The tin-based treatment has resulted in concomitant discharge of low-levels of inorganic tin (as small micro particles and nanoparticles). The controlled discharge of tin to Tims Branch as a known step function with high quality records on the quantity and timing of the release makes this stream-scale ecosystem an ideal testbed to study complex systems science in a relatively well defined ecosystem that experienced controlled changes in boundary conditions, and provides a unique opportunity for the released tin to serve as a potential tracer for sedimentation and particle transport processes in the stream.

During FIU Performance Year 7, FIU's research has supported SRS and DOE EM's Office Subsurface Closure goals by conducting a targeted stream-scale study in the Tims Branch ecosystem to monitor the fate and transport of sediment and contaminants in Tims Branch and examine the response of the ecosystem to innovative EM-developed remediation treatment technologies that have eliminated anthropogenic mercury sources from this watershed. Work for this year has primarily involved development of overland and stream flow models to simulate the hydrology of Tims Branch and its response to extreme hydrological events. This report describes efforts over the past year, which were focused on refinement of the Tims Branch surface water model and preliminary model calibration. The report also briefly describes the preliminary stages of development of the MIKE 11 stream flow model of the A-014 outfall tributary and the field work conducted to collect data to assist in the model calibration process.

Subtask 3.1: Modeling of Surface Water and Sediment Transport in the Tims Branch Ecosystem

Subtask 3.1: Introduction

Tims Branch is a small braided, marshy, second-order stream that starts at the northern portion of SRS and passes through Beaver Ponds 1-5 and Steed Pond, and eventually discharges into Upper Three Runs (Figure 107). Its drainage area is nearly 16 km^2 (Batson et al., 1996). The average width of the stream varies between 2 to 3 m. Two major tributaries of Tims Branch originate from the A014 and A011 outfalls, which are approximately 230 m apart. They connect with the main stream of Tims Branch 1,400 m from the A014 outfall (Hayes, 1984). Flow in Tims Branch is strongly influenced by groundwater discharge (Mast and Turk, 1999). Because of the water

table elevation and Tims Branch bed elevation, it is considered to be a losing stream (surface water discharges into the groundwater) near the A/M outfalls and a gaining stream (groundwater discharges into the stream) further south toward the confluence with Upper Three Runs (Looney et al., 2010; Varlik, 2013).

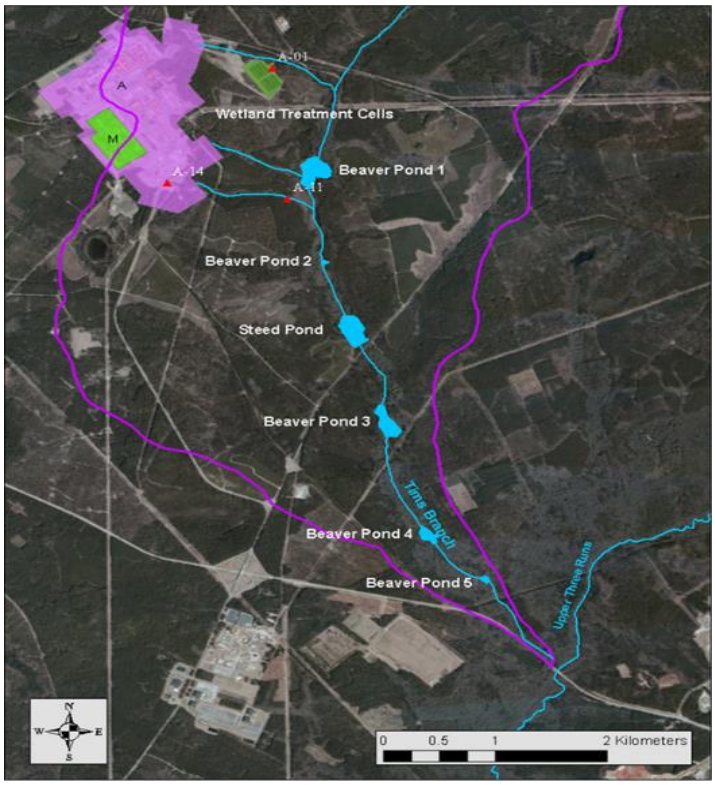

Figure 107. Tims Branch, Beaver Ponds 1 – 5, Steed Pond and the wetland treatment area in TBW. Tims Branch receives water from the A/M Area and discharges into Upper Three Runs.

There are very limited site specific studies that provide details of the hydrology and sediment transport mechanisms of Tims Branch and other streams at SRS. These studies are primarily based on experimental work and field data rather than numerical modeling approaches. Modeling hydrological processes and sediment transport mechanisms requires a detailed understanding of soil and sediment characteristics, geologic formation, topography, climate, and hydraulic properties. Numerical modeling has proven to be a cost effective tool in studying natural processes such as hydrology and fate and transport of contaminants. In the case of Tims Branch, this approach may provide insight into how sediment may become resuspended, transported and redistributed during various extreme weather scenarios and therefore help to predict the fate and transport of tin through the watershed.

FIU-ARC has developed flow and transport models, and this report presents the preliminary calibration and sensitivity analysis of the MIKE SHE overland flow model for TB watershed, as well as the process of delineation of the Tims Branch stream network for preliminary development of the MIKE 11 stream model. This integrated flow and transport model (MIKE SHE/MIKE 11/ECOLAB) will serve as an assessment tool to evaluate the effect of hydrological events on particle/sediment transport in the Tims Branch Watershed. The model includes the main components of the hydrological cycle and sediment transport: groundwater flow (saturated

and unsaturated), overland flow, precipitation, and evapotranspiration. The main objective of these modeling applications is to provide the spatiotemporal distribution of tin in the sediment of Tims Branch and to forecast the fate and transport of tin and its possible methylation during extreme hydrological events.

Subtask 3.1: Methodology

MIKE SHE Overland Flow Model Sensitivity Analysis

Numerical models are powerful assessment tools that have been widely used over the past decade. Their ability to predict the outcome of an event with a good level of certainty has made them a practical and valuable research and monitoring tool where experimental or field data are scarce. Today, numerical models are the primary tool in environmental assessment and monitoring research providing comprehensive insights for scientist and decision makers in the most convenient cost–effective way. Despite the benefits, all mathematical models are subject to uncertainty and numerical errors which may result in an overestimated or underestimated outcome in comparison to available data. Model outcome uncertainty is often a function of measurement error on the model input parameters, and grid cell size. Therefore the tendency has been to use models in a deterministic way, assuming that the input parameters represent reality in an accurate way (Christiaens and Feyen, 2002). Calibration and sensitivity analysis are two phases that are required to minimize the model uncertainty and maximize the results' reliability. Combined with real-time data, numerical models will become more influential in providing reliable results.

The primary objective of this task is to develop an integrated surface water and groundwater model to predict the fate and transport of tin in Tims Branch. The presence of tin in Tims Branch is the result of the implementation of a unique remediation technology to remove trace mercury in groundwater in the SRS A/M Area in 2007 via the addition of stannous (tin) chloride prior to air stripping in a pump and treat operation. This report describes the preliminary calibration and sensitivity analysis for the hydrological model of Tim Branch which was developed using the MIKE SHE model. The focus over the past year (FIU Performance Year 7) was to identify parameters that affect simulation results substantially, whereby small changes in their values would cause the model results to divert tremendously.

Calibration of a physically based model such as MIKE SHE is an essential and often challenging step in model development. Physically based models require a large number of initial input data and parameters that can usually be derived directly from experimental work or field measurement. Some of the data and parameters may vary spatially or temporally, and obtaining data may become challenging, and in most cases, be associated with measurement errors. Sensitivity analysis is a step prior to calibration which serves to reduce the number of parameters in the calibration process. Sensitivity analysis is a technique that determines whether changing a parameter value affects the outcome of the model. This technique is useful to identify the parameters that are significant to the model outcome, and have the greatest control on the predicted output. Applying sensitivity analysis also reduces the amount of simulations and computer time tremendously.

Several studies show the importance of sensitivity analyses prior to model calibration. Rogers et al. (1985) used sensitivity analysis to explore the most sensitive parameters that could be used for calibration of the MIKE SHE model developed for Tanllwyth watershed, Powys, Wales.

Their findings show that the model was most sensitive to surface roughness and soil hydraulic conductivity. They estimated the uncertainty of the calibration parameters for several different storms. Xevi et al. (1997) calibrated the MIKE SHE model developed for Neuenkirchen research catchment located south of Braunschweig, Germany. The sensitivity of the model to flow resistance and surface/subsurface hydraulic properties was investigated. Their results indicated that overland flow was very sensitive to changes to the flow resistance parameter, but remained unaffected by changes in vegetation parameters or specific storage coefficient.

Parameters

The MIKE SHE model includes a wide range of parameters such as hydrological, climate, hydraulic, soil, etc. Each parameter can be considered as a calibration factor. Performing a model calibration for the entire range of MIKE SHE parameters is almost impossible, as this would require a substantial amount of field data. This, in addition to the significant computer runtime that would be required, makes it impractical. Performing a sensitivity analysis will limit the number of parameters to only those that have a significant impact on the simulation results.

In this model development process, the focus was on parameters that had the greatest impact on the hydrology and characteristics of the overland flow in Tims Branch watershed. Table 41 below shows the initial parameter values used in the MIKE SHE Evapotranspiration (ET) module which were based either upon experimental/field data if available, or from the literature.

Table 41. Initial Parameter Values Used in the MIKE SHE – ET Module

Parameter	Value	Unit
Detention Storage	2.5	mm
Surface-Subsurface Leakage Coefficient	0.0001	1/sec
Reference Evapotranspiration	2.22	mm/day
Leaf Area Index	1.3 – 6.3	m2/ m2
Root Depth	0.0 – 4000	mm

Sensitivity analysis was initiated by first changing the values of the detention storage (DS) and reference evapotranspiration (RET). A series of MIKE SHE oveland flow simulations were performed for a period of 9 months from 1/1/2014 to 9/30/2014. Two peak rainfall events were selected as the point for visual comparison. The rain events occurred on 2/14/2014 and 6/1/2014 (Figure 108). No Saturated Zone (SZ) module was included in these simulations.

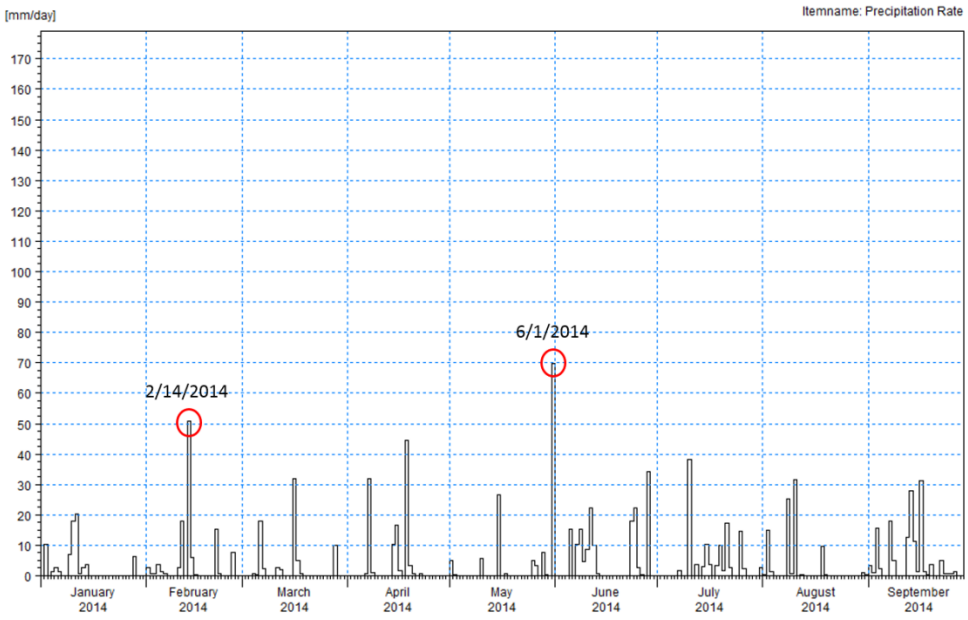

Figure 108. Rainfall events in 2014, SRS, SC. The two peak rainfall events on February and June are marked as red circles.

MIKE 11 Stream Flow Model

MIKE 11 is one of the most widely used hydrodynamic models that simulates flow behavior, water quality, and sediment transport in channels, rivers, irrigation systems, and estuaries. It implements one-dimensional simulations of river flows and water levels using the fully dynamic Saint Venant equations. This model provides flow hydrographs at any desired location in the watershed. It includes a comprehensive, user-friendly graphical interface and strong 1D, 2D, and 3D visualization capabilities. The model uses the finite difference approach and double sweep algorithm to solve the unsteady state flow equations.

This following provides details of the preliminary stages of development of a one dimensional flow model of the Tims Branch A-014 outfall tributary that can be used as a tool to simulate water depth and velocity in the stream over time and space. The model results will provide some insight of the response of the stream to any extreme hydrological event that may occur under various climate conditions. An FIU graduate student (DOE Fellow), Natalia Duque, was trained on the implementation of this model and assisted in the stream delineation and preliminary set up of this model. This research also served as the basis for her final project topic to obtain her graduate (Master's) degree.

Data Preparation

The data required for the MIKE 11 model include a topographic map of the study area, river geometry and timeseries of water level and discharge. A digital elevation model of the South Carolina area was used as a base map for delineating the channel networks using a combination of ArcGIS and MIKE 11 tools. Details of this procedure are described in Subtask 3.2 below. The channel geometry was defined by inserting computer-generated as well as measured channel cross-sections at different locations of the channel. About twenty-two cross-sections at different locations of the A-014 were used to define the geometry of the channel.

Stream Cross-Section Profiling

Having an accurate representation of a stream's cross-sections is of great significance in modeling surface water systems since open-channel flow is governed by parameters such as cross-section area, wetted perimeter, and hydraulic radius. For a precise representation of the real system, accurate cross-sections are imperative.

A data collection and sampling study was conducted at Savannah River Site in August 2016 in order to measure stream cross-sections, and collect water samples to support the Tims Branch watershed modeling effort. Sampling was conducted at approximately 20 different locations in which mean flow velocity measurements, water quality samples, and cross-section measurements were taken. Cross-sections were measured along the A-014 stream, the main tributary that flows into Tims Branch from the SRS A/M Area, and along the A-011 stream (a secondary tributary to the A-014 stream). The ground coordinates of each sampling location were recorded by a handheld GPS tracker (eTrex HC series). A TruPulse 200X Laser Rangefinder was used to measure stream width and bank slope. Due to the Laser Rangefinder's limitation in measuring areas covered by water, it was mainly used to estimate the bank slope and the width of the stream. At each sampling location, the stream geometry was manually profiled by taking several depth measurements using a measuring rod across the channel width. Figure 110 to Figure 113 illustrate how the depth measurements were taken.

The Rangefinder has Bluetooth capabilities that allow the device to connect to an application previously downloaded onto a cellphone. When a measurement is taken, the results are shown in the app (Figure 109) where notes could be added if necessary.

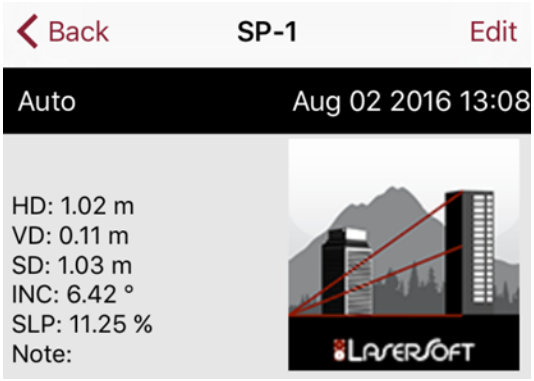

Figure 109. Measurement results visible in app downloaded onto mobile device/cellphone.

The process for measuring the cross-sections included the following steps:

- Flags were placed along the stream width to identify specific points to measure the cross-section geometry (Figure 110).
- Exact location coordinates of sample points were recoded with a GPS unit.
- The Rangefinder was placed upon a tripod on one side of the stream bank (Figure 111).
- The Rangefinder was ensured to be properly connected to the app on a phone or mobile device via Bluetooth.
- The Rangefinder was configured to use the 2-point shooting method. This method is particularly useful when measuring distances having one of the points as reference. This method also requires a clear line of sight for both shots.

- After the Rangefinder was properly set up, the observer pointed to one side of the stream for the first shot and then proceeded to aim at the other side of the stream for the second shot (Figure 111 and Figure 112).
- If there was no clear line of sight for both shots, the stream width was measured manually using a measuring tape (Figure 113).
- After the width of the stream was measured, the cross-section geometry was manually measured using a measuring rod.
- The measuring rod was placed at each flag location and the water depth and distance of the flag from the reference point (one side of the stream) were recorded.
- This procedure was repeated for each of the cross-sections.

Figure 110. Flag placement across the stream width to identify measurement points.

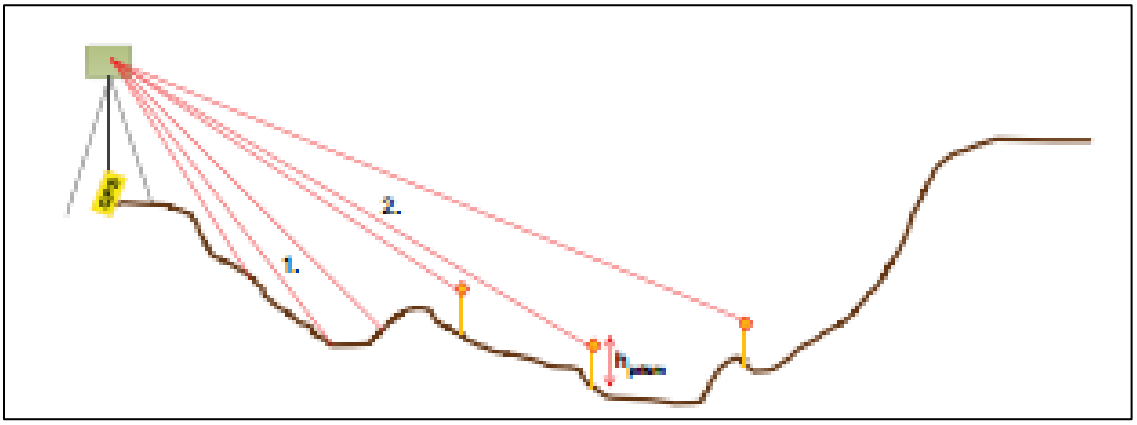

Figure 111. Schematic for using the rangefinder.

Figure 112. Aiming the rangefinder at one side of the stream.

Figure 113. Measuring stream width manually with a measuring tape.

MIKE 11 Model Setup

The initial MIKE 11 model setup required generation of the following five essential files:

- Simulation file (.sim11)
- River Network file (.nwk11)
- Cross Section file (.xns11)
- Boundary file (.bnd11)
- Hydrodynamic (HD) parameters (.hd11)

Pre-processing of the stream network data is described under Subtask 3.2 below. After the data pre-processing was completed, the model setup was initiated in MIKE 11. A folder was set up to contain all the model files: (TBW_Model). A MIKE11 simulation file (.sim11) was then created.

River Network File

The river network file includes river networks, branch connections, hydraulic structures, and catchment inflow points. The river network can be imported as a shapefile (Figure 114) while input of hydraulic structures requires technical design data of the existing structures.

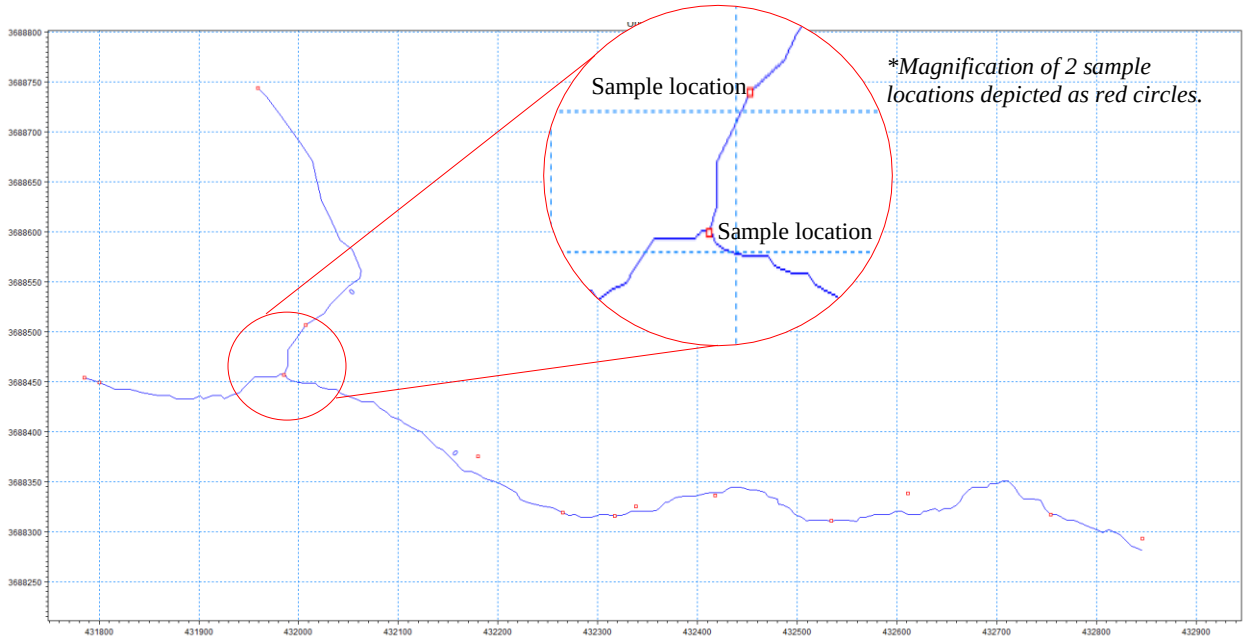

Figure 114. Stream network shapefile imported to a MIKE 11 network file. Red circles are sampling locations where the stream cross sections were measured.

MIKE 11 only recognizes the network file as a chainage file with chain numbers and ID. Therefore, the network shapefile needs to be converted into a chainage shapefile.

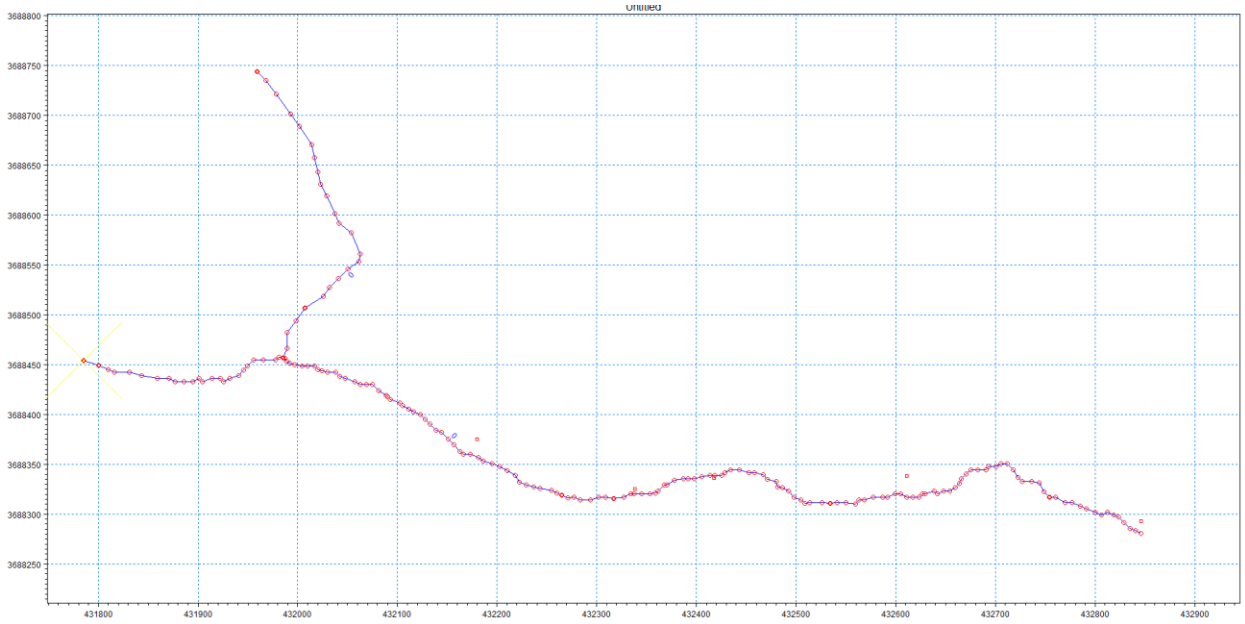

Figure 115. River network chainage file generated in MIKE 11.

First, a River Network file (.nwk11) was created, within which the workspace area was set up as described in table below:

Table 42. Geographic Coordinates of the A-014 Outfall Tributary Study Area in MIKE 11

	X	Y	units
Lower Left Corner	428638	3682527	m
Upper Right Corner	439252	3697210	m
Map Projection: NAD_1983_UTM_Zone_17N			

The shapefiles created using ArcGIS were then imported into the River Network file to serve as a base layer for digitizing the stream network in MIKE 11. Points were created along the different branches and then connected to define each branch. The network generated was then exported as a GIS shapefile.

Cross-Section File

The cross-section file was created by assigning field-measured water depth at a given location along the stream. Using ArcGIS, the existing DEM of South Carolina seen below was converted to an ASCII file.

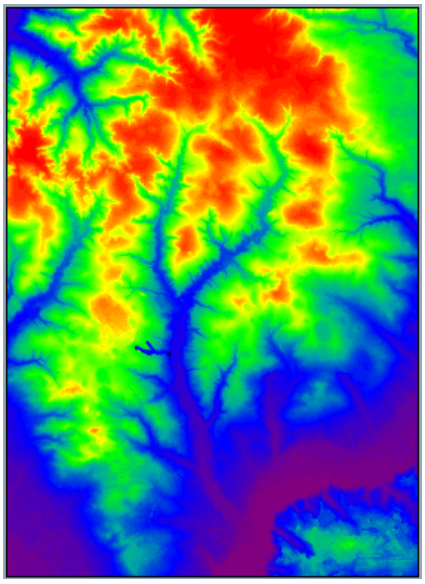

Figure 116. Digital elevation model (DEM) of South Carolina

The MIKE Zero Toolbox was then used to convert the ASCII file to a dfs2 file, which is readable in MIKE SHE and MIKE 11. In order to create a cross-section from the dfs2 grid file, a MIKE HYDRO file (.mhydro) was created. The model type was then set up as 'River' and coordinate system was specified. The Stream Network shapefile was then imported into MIKE HYDRO. In MIKE HYDRO, the DEM and the cross-section file were then specified. With the tool 'Auto generate cross-sections', cross-sections were generated every 1000 meters along Tims Branch and every 200 meters along the Outfall A014 Branch. The cross-sections were each 100 meters wide.

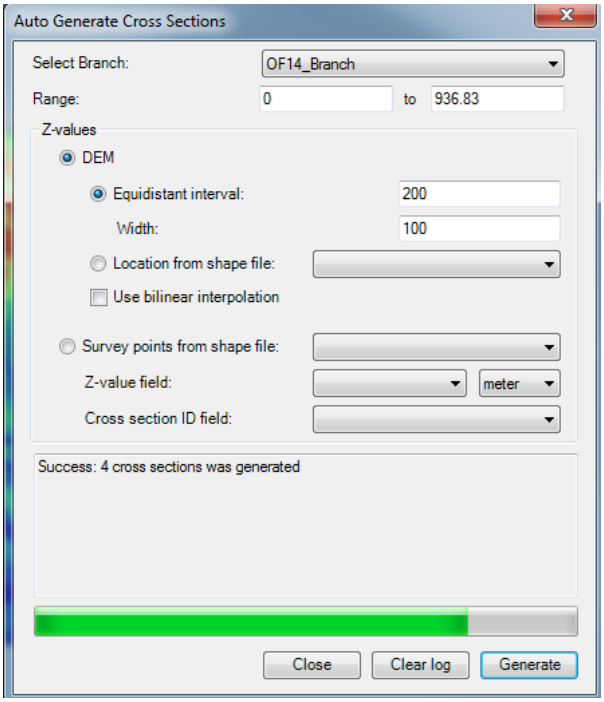

Figure 117. Screenshot of the 'Auto Generate Cross Sections' tool in MIKE HYDRO.

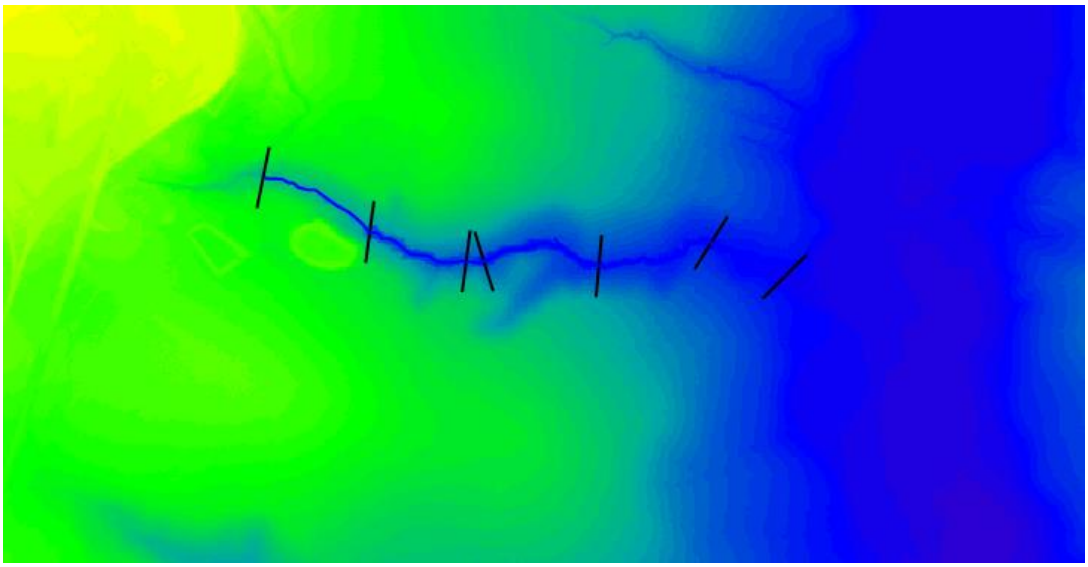

Figure 118. Cross sections generated every 200m along the A-014 outfall tributary in MIKE HYDRO.

Below (Figure 119) is an example of how the cross-sections appear when the cross-section file is opened in MIKE Zero.

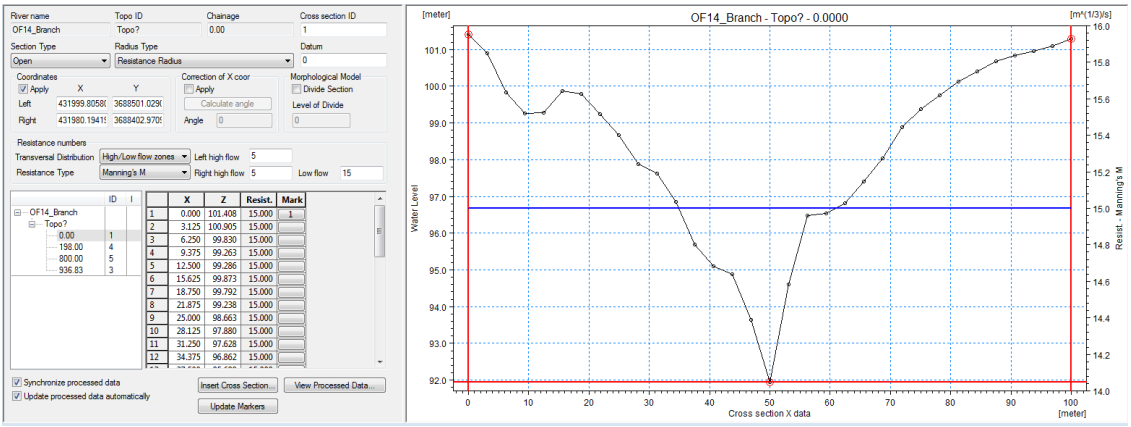

Figure 119. Sample cross section as viewed using MIKE Zero.

For all the cross-sections, the following parameters were entered:

Table 43. MIKE 11 Input Parameters

Parameters	
Transversal distribution	High/Low flow zones
Resistance type	Manning's M
Left high flow	5
Right high flow	5
Low flow	15

Markers 1, 2, and 3 were relocated to mark highest left point (1), lowest point (2), and highest right point (3).

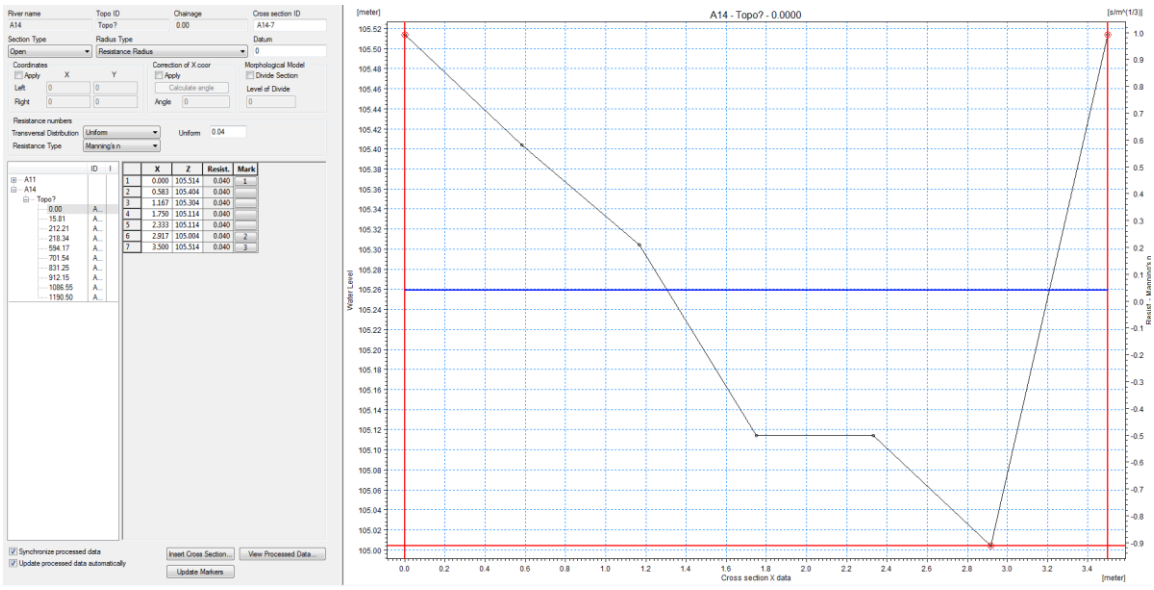

Figure 120. MIKE 11 cross-section file.

Boundary Condition File

Boundary condition files (.bnd11) were created for three locations: A-011 inflow, A-014 inflow, and A-014 outflow. A constant flow boundary condition was used for both the A-011 and A-014 inflows. Flow discharges were obtained from cross-section and field flow velocity measurements. The estimated flow discharges were 0.0294 m^3/s and 0.0386 m^3/s for A-014 and A-011 respectively. The rating curve (Q/h) boundary condition was used as the downstream boundary condition at the A-014 outflow. A theoretical rating curve was calculated based on Manning's equation:

$$Q = \frac{1}{n} A R^{2/3} S^{1/2}$$

where, Q is discharge (m^3/s), n is Manning's roughness value, A is channel cross section (m^2), R is channel hydraulic radius (m), and S is the surface friction slope. In this study, Manning's coefficient of 0.04 and the slope of 0.0294 was used to calculate the discharge rate. Figure 121 shows the Q/h rating curve for the A-014 outflow.

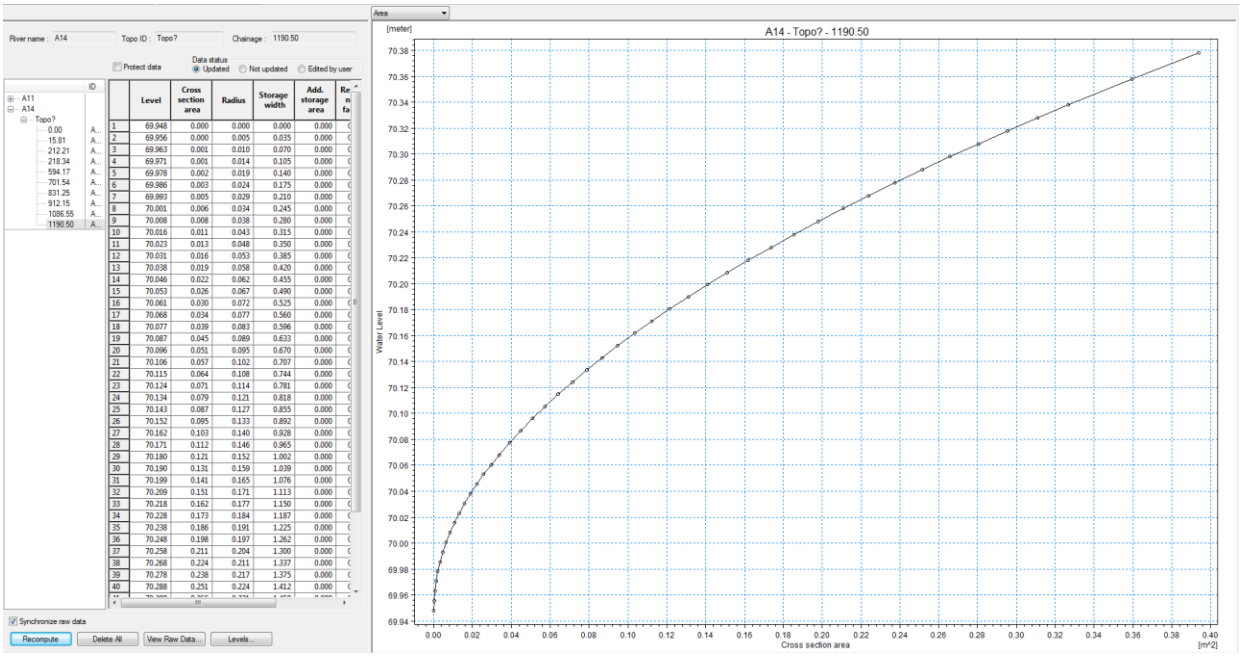

Figure 121. Q/h rating curve of A-014 outflow downstream, used as the outflow boundary condition.

Subtask 3.1: Results and Discussion

MIKE SHE Overland Flow Model Sensitivity Analysis

Detention Storage (DS)

The first sensitivity analysis was performed by changing the initial value of the detention storage (DS) in the MIKE SHE overland flow model. The initial value of DS was set to 2.5 mm. This value was adjusted by ± 5% (2.625 mm, 2.375 mm), ± 10% (2.75 mm, 2.25 mm), and ± 20% (3.0 mm, 2.0 mm). A total of 6 overland flow simulations were implemented. The results indicate that the overland flow model appears to be sensitive to the changes in DS. It also shows that the sensitivity of the model to changes in DS increases as the amount of rainfall in one single event increases. The month of February experiences a lower amount of rain, while the month of June has a higher rainfall volume. Figure 122 & Figure 123 both show the results of simulations with an increase in DS value for both rainfall events taking place on 2/14/2014 and 6/1/2014 respectively. Although the changes in overland flow volume appeared to be negligible for the rainfall event on 2/14/2014, which had less rain (Figure 122), it was apparent that an increase in the DS value increased the depth of overland flow when there was higher rainfall intensity (Figure 123).

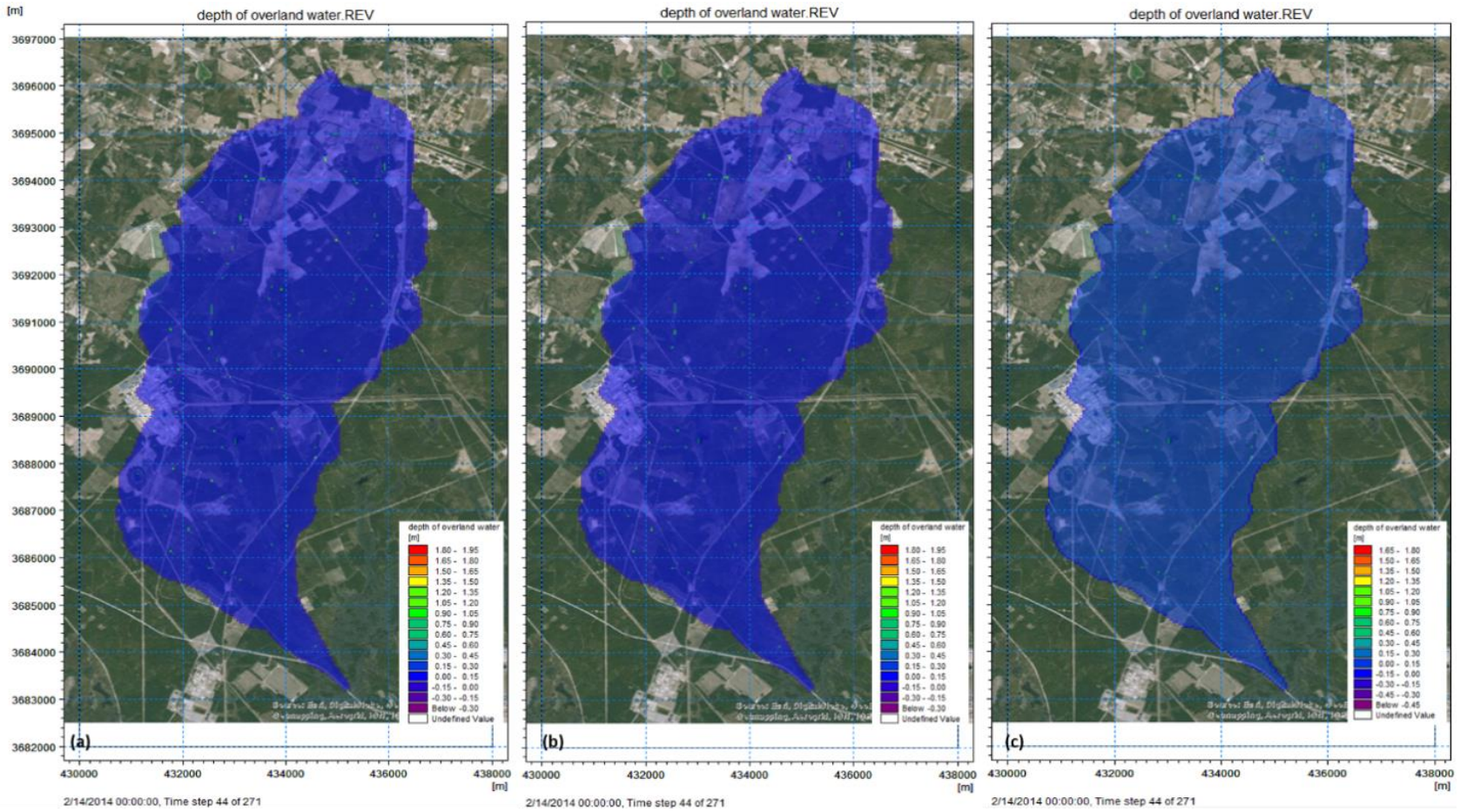

Figure 122. MIKE SHE simulations of overland flow depth for a rainfall event on 2/14/2014, with an increase in detention storage of (a) 5%, (b) 10%, and (c) 20%.

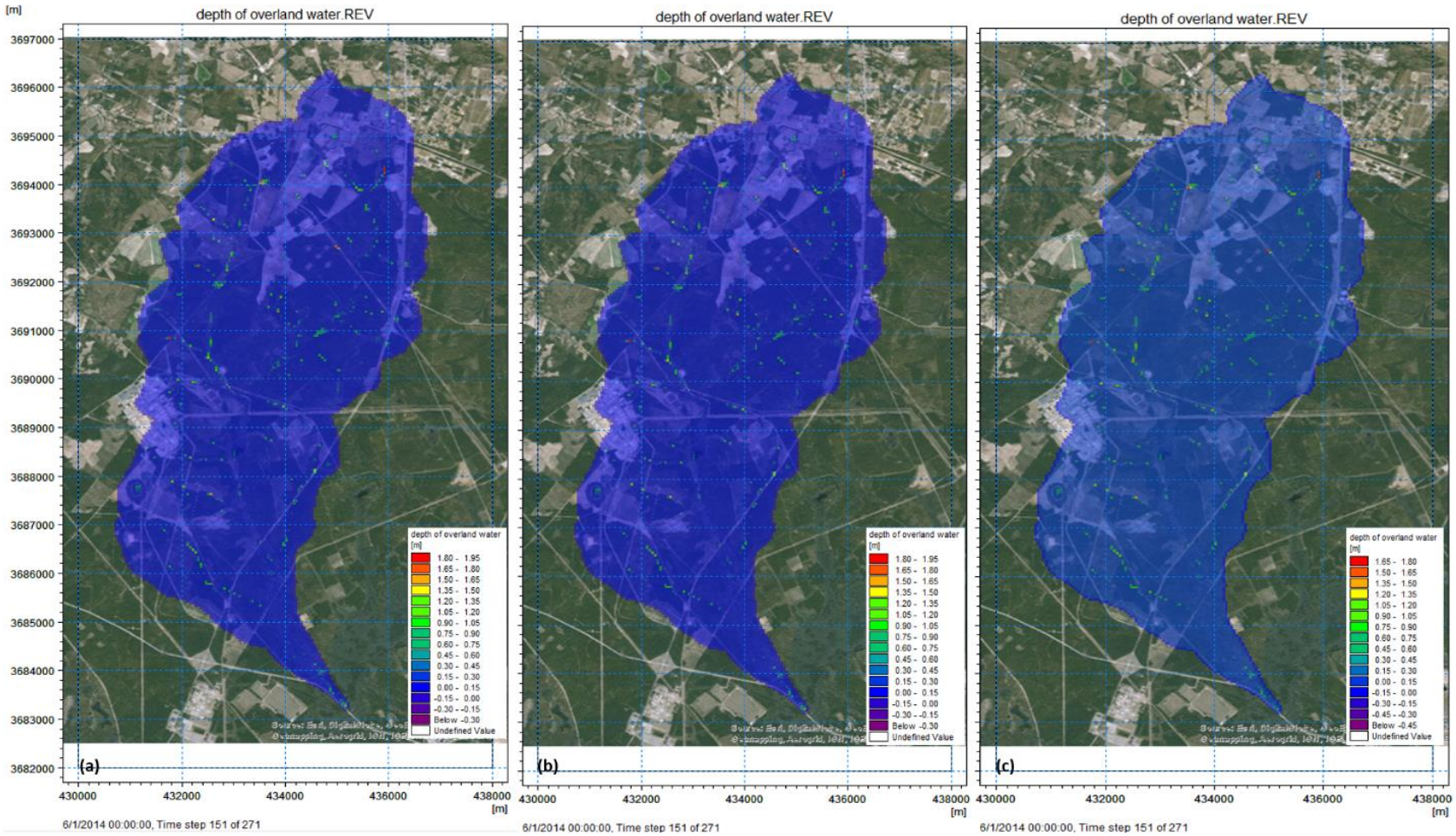

Figure 123. MIKE SHE simulations of overland flow depth for a rainfall event on 6/1/2014, with an increase in detention storage of (a) 5%, (b) 10%, and (c) 20%.

Figure 124 & Figure 125 illustrate the results of simulations for both rainfall events with decreasing the amount of DS by 5%, 10%, and 20%. It appears that a decrease in DS value may cause a noticeable change in overland flow depth for both rainfall events. This also indicates that the model is sensitive to changes in detention storage. Therefore it is important to find the timeseries of DS that is temporally and spatially distributed rather than using a uniform value that is constant over time.

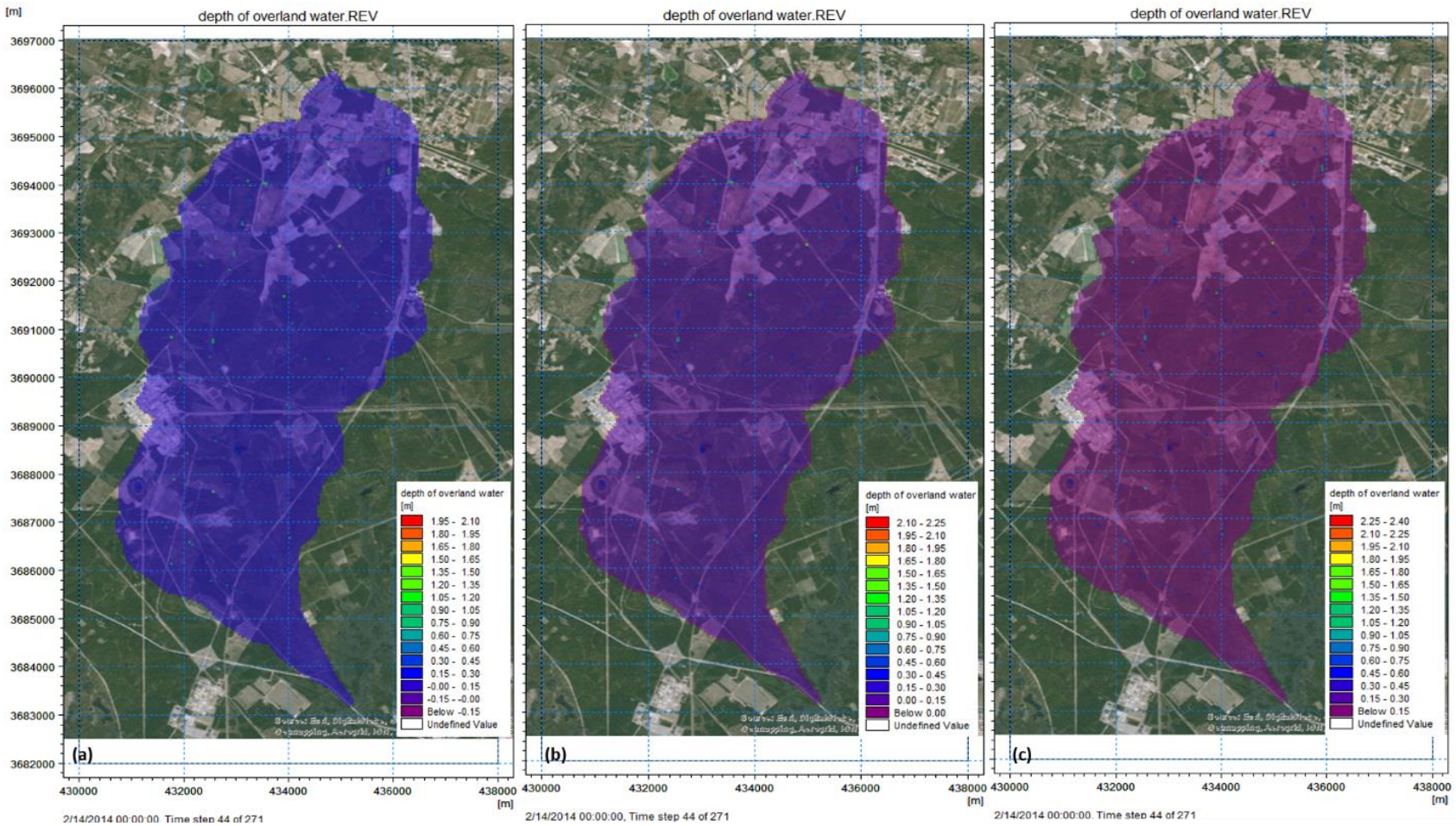

Figure 124. MIKE SHE simulations of overland flow depth for a rainfall event on 2/14/2014, with a decrease in detention storage of (a) 5%, (b) 10%, and (c) 20%. The images indicate that a decrease in DS decreases the overland flow depth.

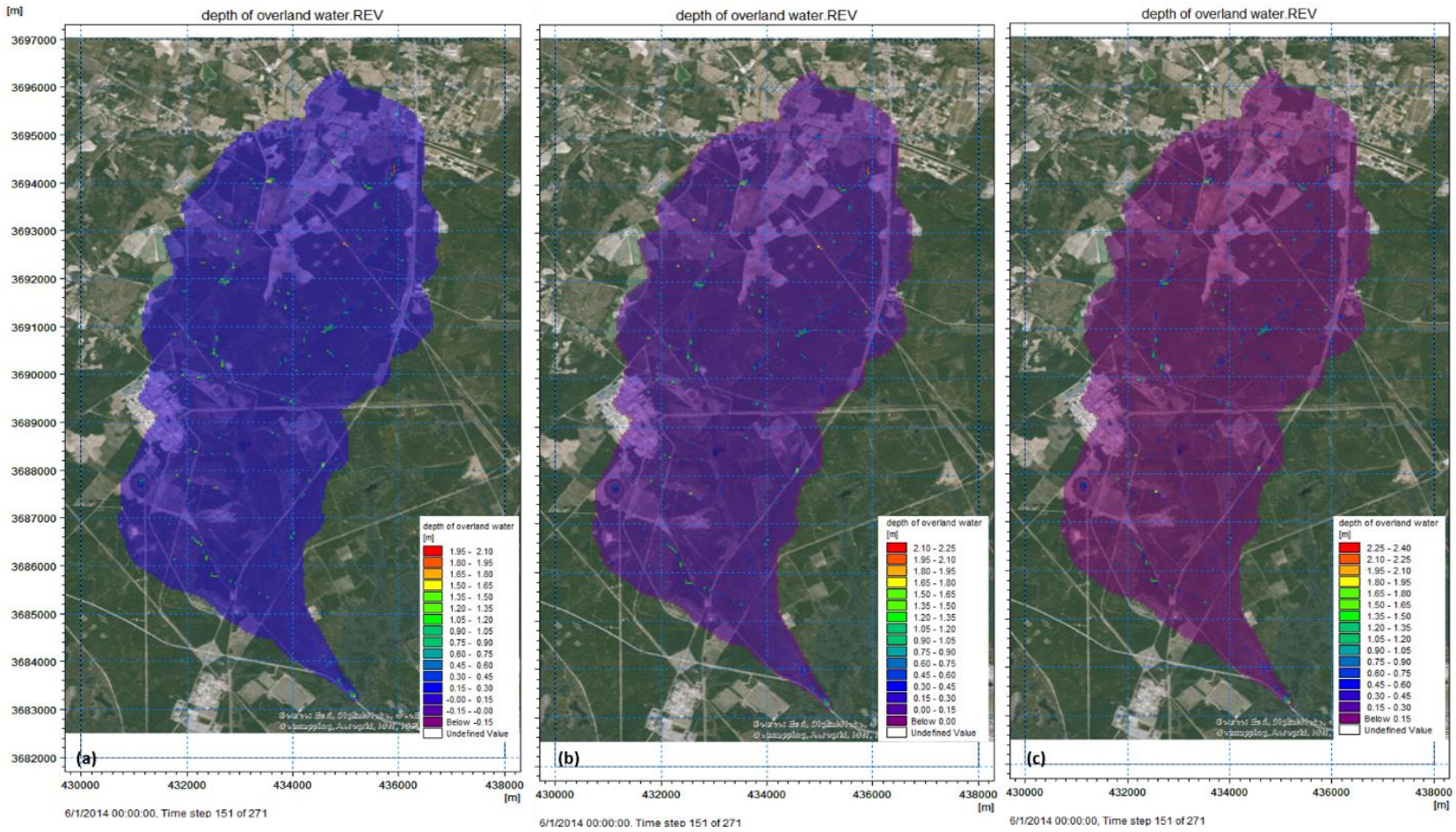

Figure 125. MIKE SHE simulations of overland flow depth for a rainfall event on 6/1/2014, with a decrease in detention storage of (a) 5%, (b) 10%, and (c) 20%. The images indicate that a decrease in DS decreases the overland flow depth.

Although the images above show visual differences with the change in DS values, the MIKE SHE overland flow simulations' numerical results for these DS values depict very little difference in overland flow depth downstream in Tims Branch, as seen in the graph in Figure 126. This series of simulations was performed for three years from 2010 to 2013. These results depict the simulated flow depth at the point downstream of Tims Branch where it connects to Upper Three Runs. These simulations were performed for values higher and lower (± 5% and ± 10%) from the initial estimated value of detention storage (2.5 mm). As mentioned above, these results indicate that the model is not sensitive to changes in detention storage value, and therefore may not be able to be used as a calibration parameter. The simulated results are overestimated as the model is still being calibrated. Graphed sensitivity analysis results for other parameters (e.g. surface-subsurface leakage coefficient) will be provided in future reports.

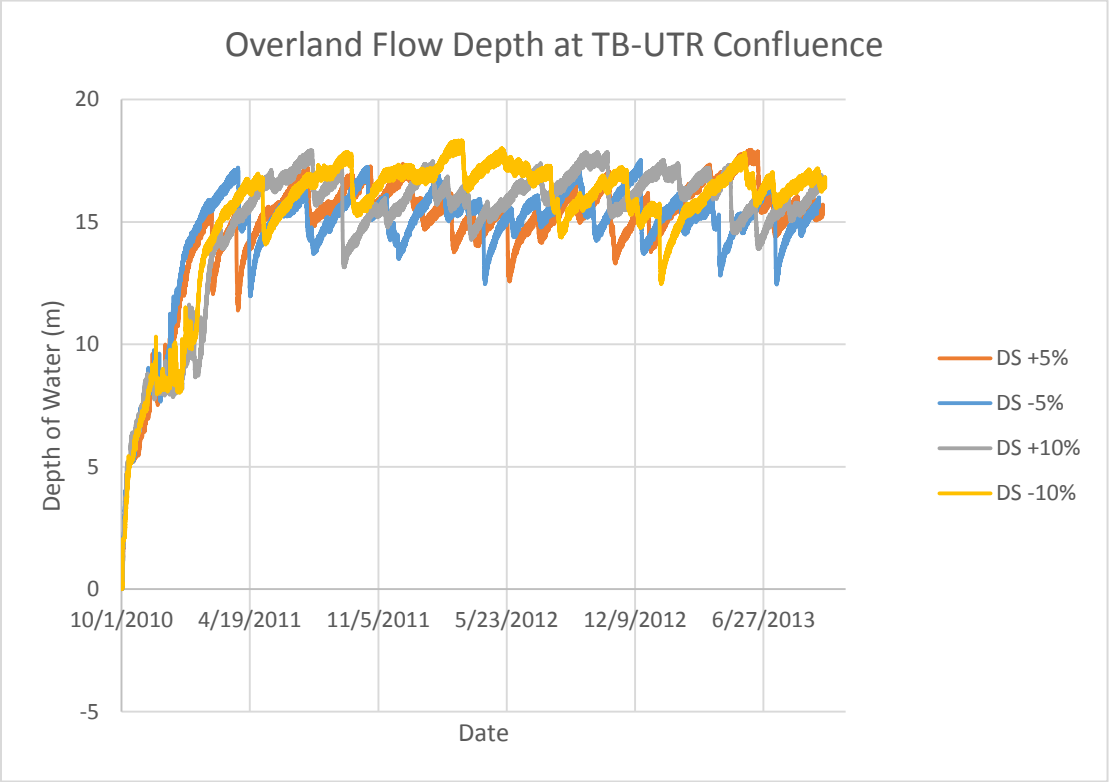

Figure 126. Overland flow depth at the Tims Branch-Upper Three Runs (TB-UTR) confluence for varying detention storage (DS) values (+/- 5%, +/- 10%) from the original estimate of DS = 2.5 mm.

Reference Evapotranspiration (RET)

The next series of sensitivity analyses were performed by changing the initial value of the reference evapotranspiration (RET) in the MIKE SHE overland flow model. The initial value of RET was set to 2.22 mm/d. This value was then adjusted by ± 5% (2.625 mm/d, 2.109 mm/d), ± 10% (2.75 mm/d, 1.998 mm/d), and ± 20% (2.664 mm/d, 1.778 mm/d). A total of 6 overland flow simulations were implemented. Figure 127 & Figure 128 show results of the overland flow depth simulations with changing RET. The results indicate that the overland flow model appears not to be sensitive to the changes in RET. Increasing the amount of RET does not show any

visible effect on the images of the simulated depth of water. Further investigation is in progress to better understand the effect of RET on the depth of water in the overland flow simulation. As the results indicate, the uniformly distributed value of 2.22 mm/d seems to adequately represent the amount of RET in the vicinity of SRS.

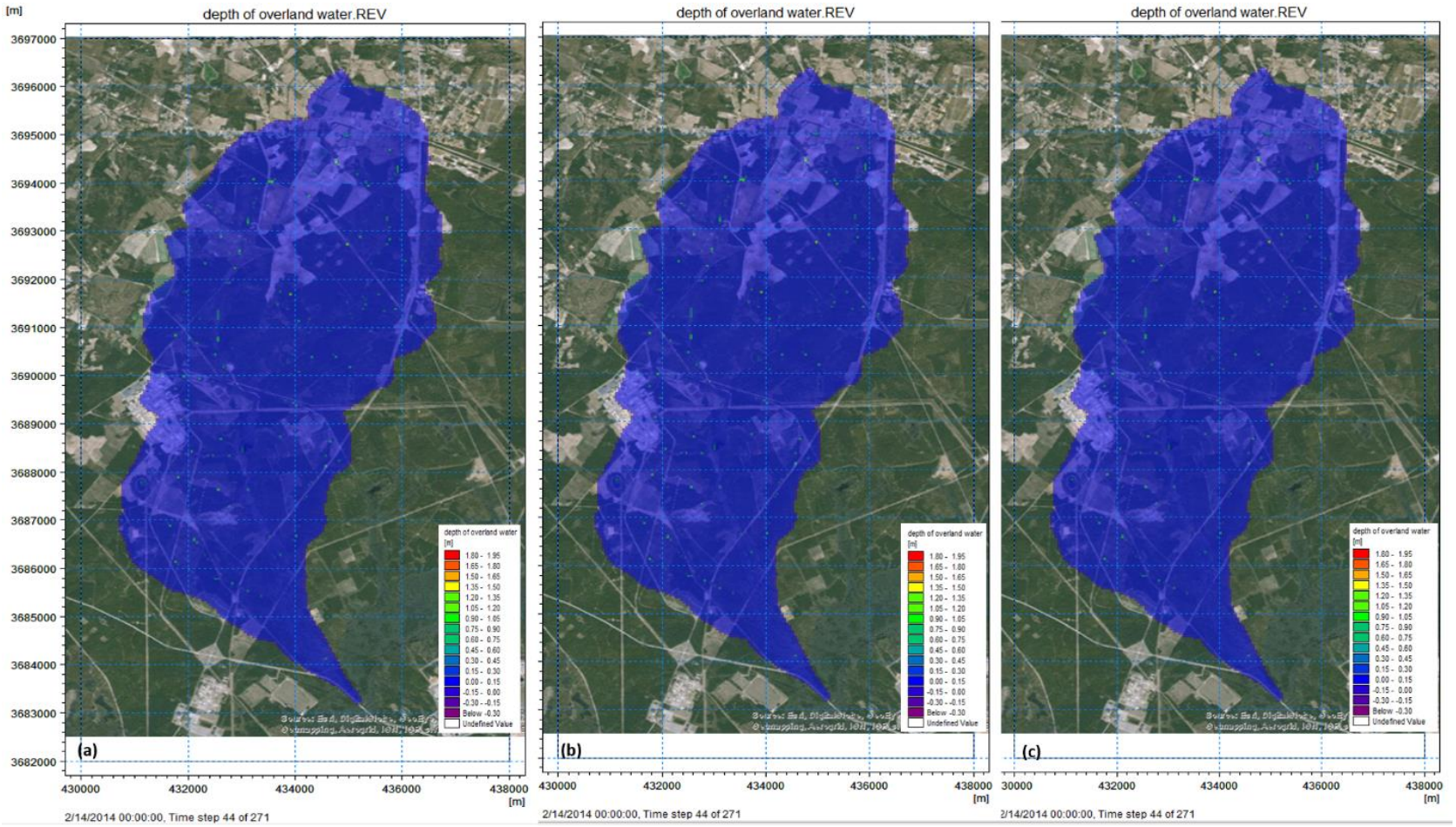

Figure 127. MIKE SHE simulations of overland flow depth for a rainfall event on 2/14/2014, with an increase in reference evapotranspiration of (a) 5%, (b) 10%, and (c) 20%. The images indicate that increasing the RET does not have any visible effect on the overland flow depth.

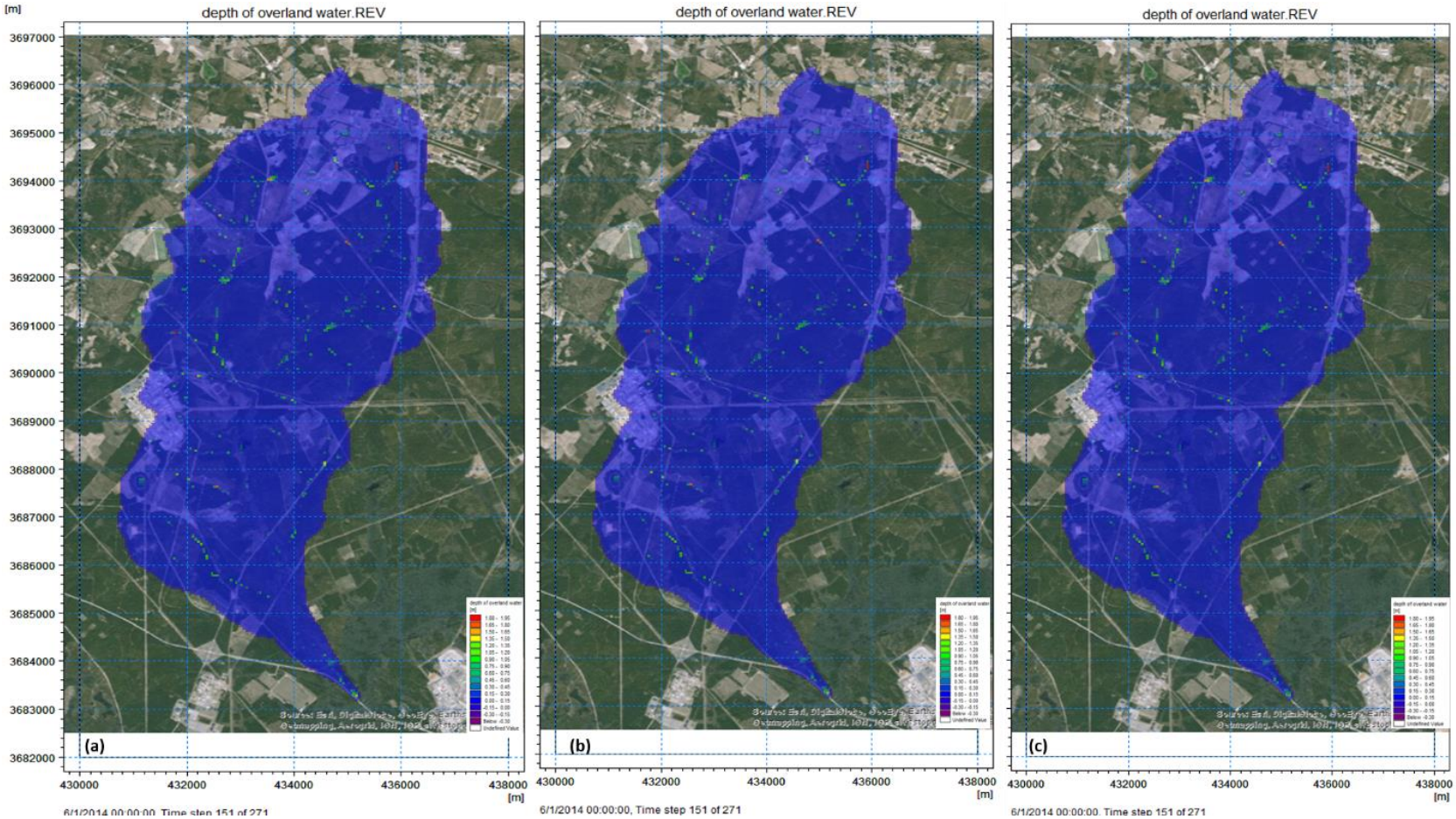

Figure 128. MIKE SHE simulations of overland flow depth for a rainfall event on 6/1/2014, with an increase in reference evapotranspiration of (a) 5%, (b) 10%, and (c) 20%. The images indicate that increasing the RET does not have any visible effect on the overland flow depth.

Leaf Area Index (LAI) and Root Depth (RD)

The current version of the MIKE SHE overland flow model includes a vegetation file that consists of average Leaf Area Index (LAI) and average Root Depth (RD) values for each vegetation class. According to (Wijesekara et al., 2014), the leaf area index (LAI) and root depth (RD) define the vegetation properties of the model domain. These components govern the precipitation interception on leaves and the evapotranspiration through roots and they both vary through time in a year. In reality, LAI and RD vary throughout the year. Seasonal fluctuations occur as vegetation growth is maximized over the summer with highest leaf and root production, and minimized during winter with lowest leaf and root growth. LAI values vary from 1 to 6 in the Tims Branch study area. Root depth values are average depths of the actual root zone of the vegetation. Forest areas are usually defined with a higher root depth which is considered a constant. Root depth values for agricultural areas begin at 0, peak when the crops are fully grown, and drop down to 0 when the crops are harvested.

To improve the model performance, a MIKE SHE vegetation file (*.etv) was generated that includes seasonal changes in both LAI and RD. LAI and RD increase as vegetation grows faster during spring and summer (the peak) while the growth slows down during fall. During winter there is no vegetation growth and therefore no increase in LAI or RD. Sample graphs which reflect seasonal changes in LAI and RD for various vegetation types are depicted in Figure 129.

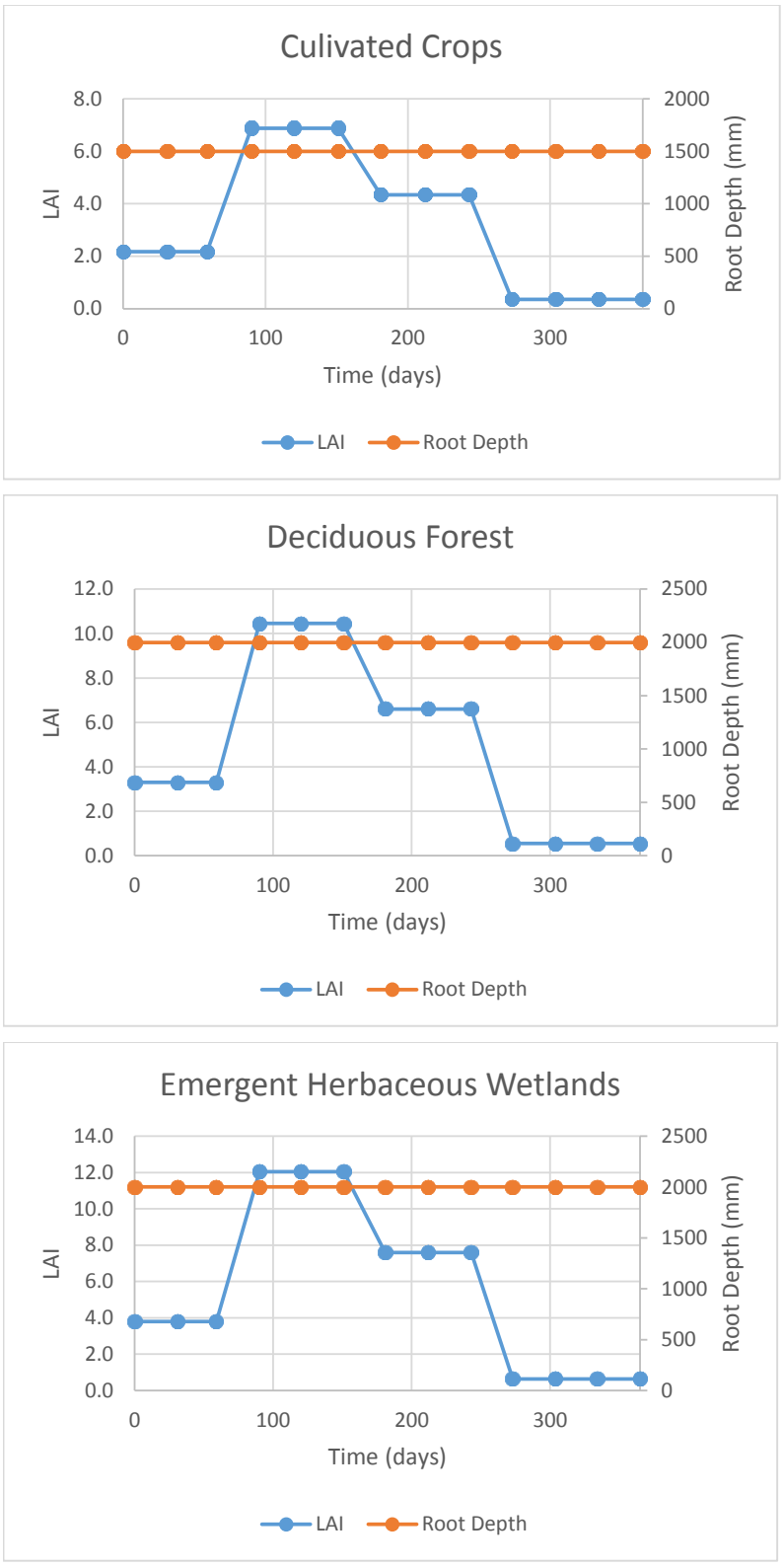

Figure 129. Graphs showing seasonal variation of LAI and RD for various vegetation types.

MIKE 11 Stream Flow Model

Figure 130 shows the preliminary simulation results of MIKE 11 stream flow model for A-014 as a natural stream without hydraulic structures. These simulations were intended to provide experimental results of stream flow at early stage of model development. Although these results are experimental with no calibration performed, they demonstrate the model functionality when further enhanced. The model output will include flow depth, profile, water level and discharge in spatial and temporal distribution.

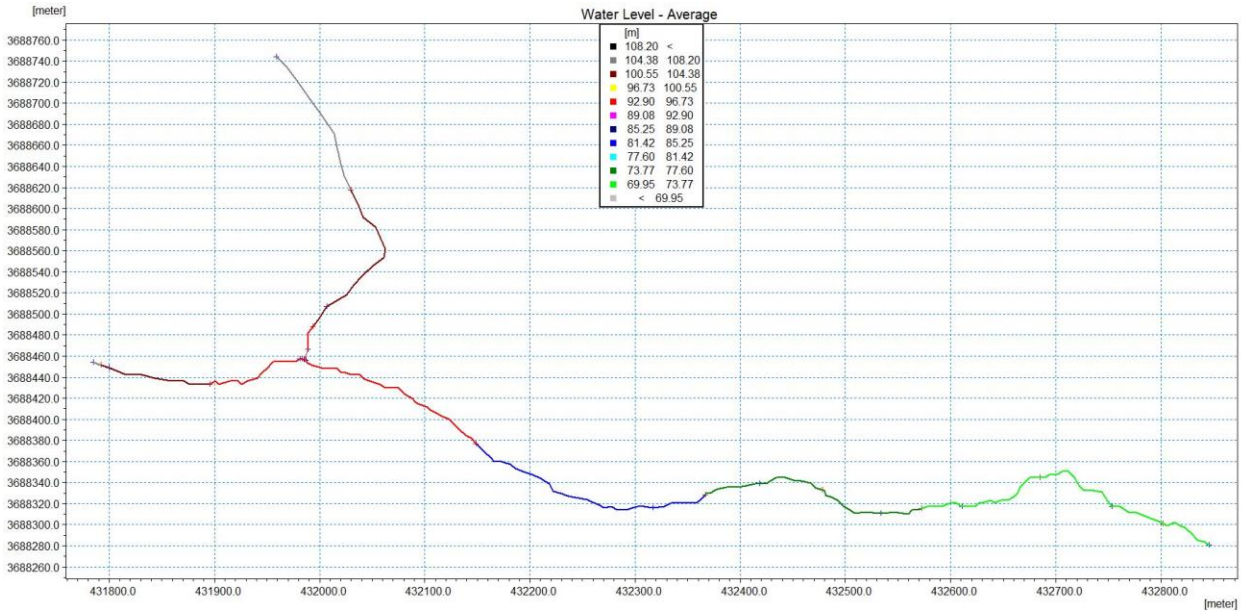

Figure 130. Simulated average water level along the A-014 outfall (OF) tributary using the MIKE 11 model.

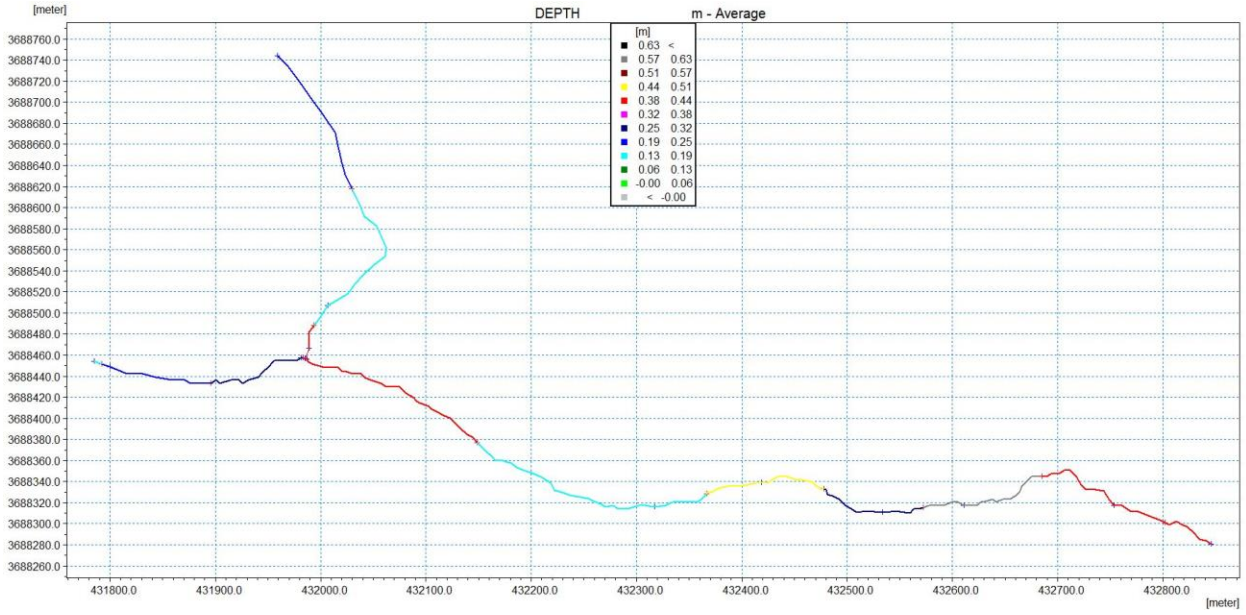

Figure 131. Simulated depth of water along the A-014 OF tributary.

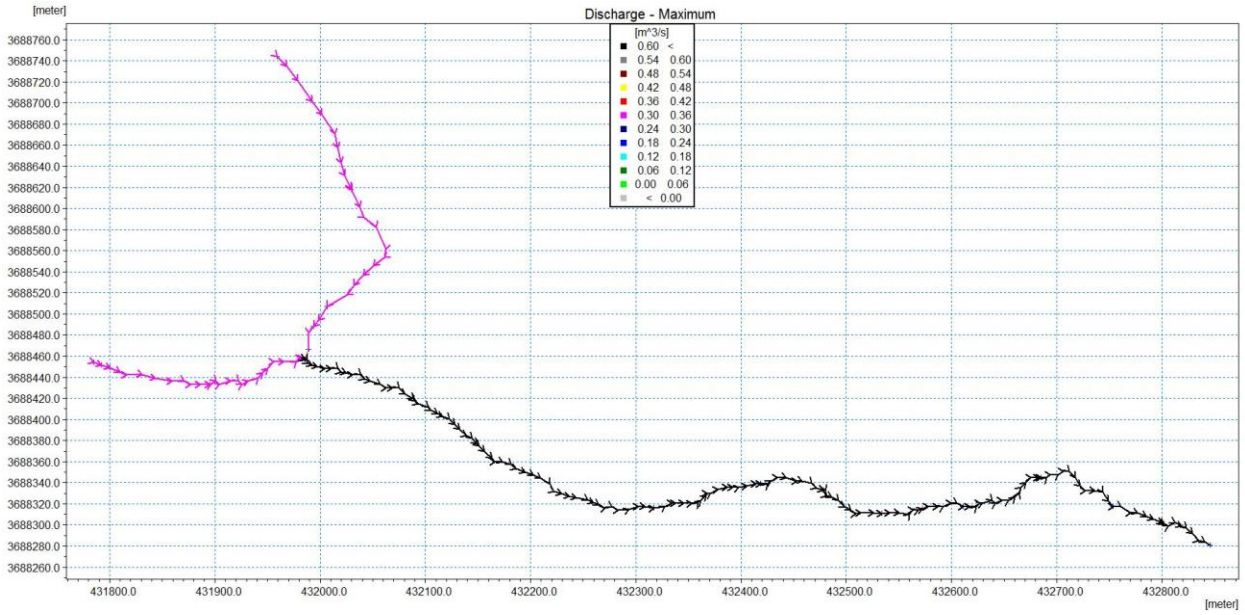

Figure 132. Maximum discharge (m^3/s) within the A-014 OF tributary based on MIKE 11 simulation.

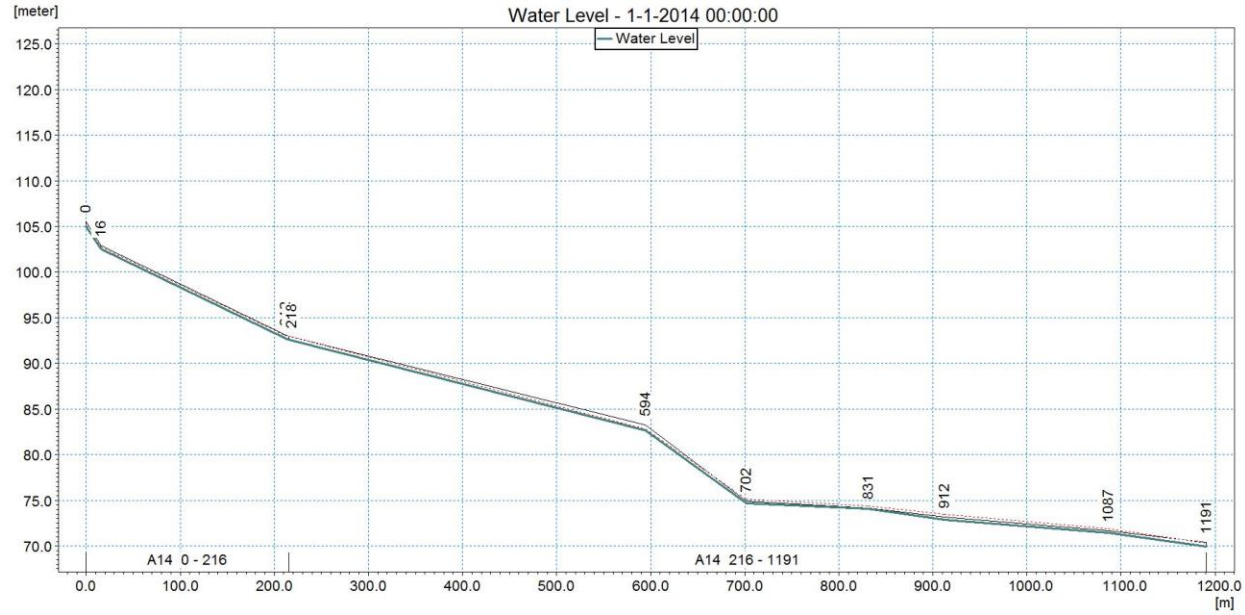

Figure 133. Simulated results of water level profile along the A-014 OF tributary.

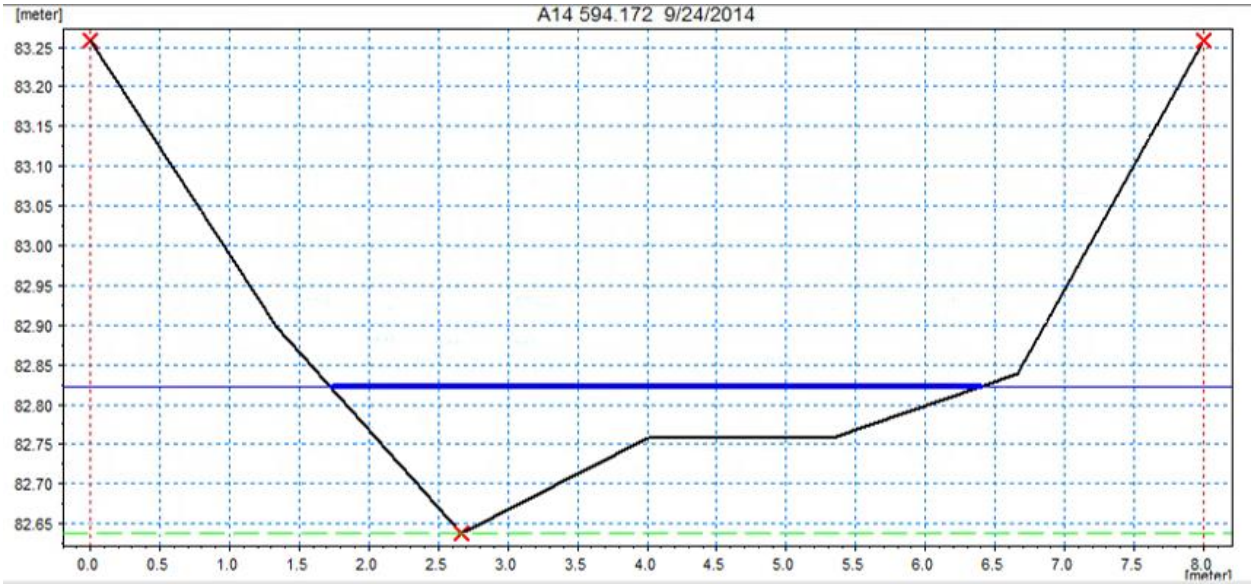

Figure 134. MIKE 11 simulated result of depth of water profile in A-014.

Subtask 3.1: Conclusion

MIKE SHE Overland Flow Model Sensitivity Analysis

The MIKE SHE overland flow model is still undergoing the calibration process. Initially, the visual simulation results seemed to indicate that the model is sensitive to all the tested parameters. In the case of detention storage, however, further analysis of the numerical results was somewhat contradictory as there was little change in overland flow depth with varying DS values. As model sensitivity is based primarily on numerical results, further in-depth analysis of the numerical results for the other tested parameters (RET, RD and LAI) is also necessary and will be conducted over the next year.

MIKE 11 Stream Flow Model

The preliminary MIKE 11 model was successfully set up. The model is a preliminary, simplified, simulation of river flow. Future work is needed to include existing hydraulic structures such as the culvert and weir. After the model development is complete, calibration and validation processes are necessary. Results analysis is facilitated by a powerful visualization component. Important water flow parameters, such as Manning's coefficient, are crucial for accurate results. When coupled with MIKE SHE, the model will be able to simulate the complete water cycle hydrology.

Subtask 3.2: Application of GIS Technologies for Hydrological Modeling Support

Subtask 3.2: Introduction

Application of GIS technology has remained a key component of the hydrological model development. ArcGIS tools have significantly reduced the time needed for data preparation and has improved overall efficiency by automating and batch processing required model-specific geospatial and timeseries data. Utilization of the ArcGIS platform has provided a basis for

management and geoprocessing of model configuration parameters, documenting process workflows, conducting geospatial analyses and visualization of model results.

Subtask 3.2: Methodology

The MIKE SHE and MIKE 11 models being developed require many of the input data parameters to be in GIS format. Over the past year, GIS tools were used to prepare and process field data collected at SRS by FIU researchers and students, converting them into model-compatible formats. A GIS point shapefile of the sample locations where water quality data as well as cross section measurements were collected was generated by importing their location coordinates from an Excel file into ArcMap. ArcGIS tools were then used to export the mapped points as a shapefile. Tabulated water quality data as well as laboratory chemical analysis results will be appended to the associated attribute table to generate a shapefile that can be used to show spatial and temporal distribution of chemicals and water quality parameters in Tims Branch.

The following provides details of the procedure employed to delineate the stream network for input into the MIKE 11 model of the A-014 outfall tributary.

Pre-processing of MIKE 11 Model Configuration Data Using ArcGIS

Prior to starting the model setup in MIKE 11, it was necessary to pre-process the required data using ArcGIS. In the existing stream network file, the streams were not accurately defined. The hydrology tool in ArcGIS was therefore used to define the streams as described below:

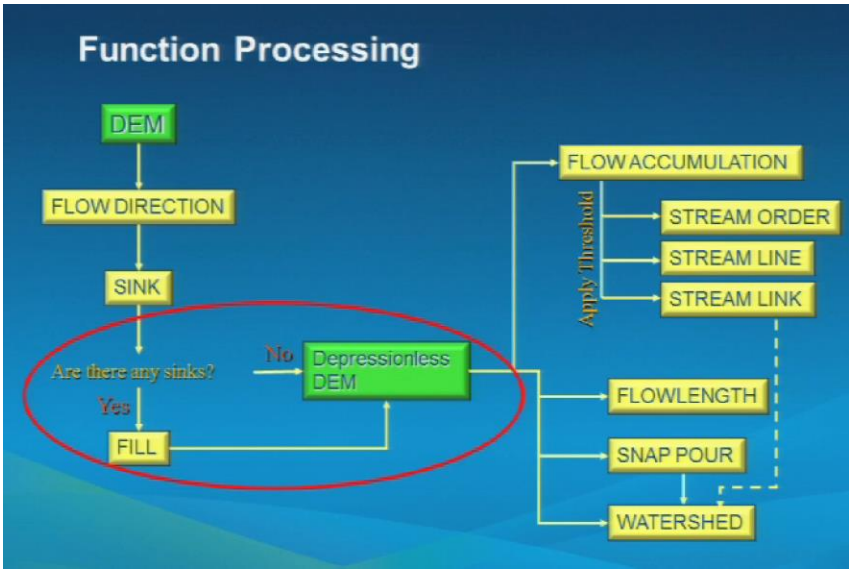

Figure 135. Stream/Watershed delineation process in ArcGIS (Source: esri.com)

- The Fill tool was used to fill low elevation cells that are surrounded by higher elevation cells; this avoids water being trapped.
- The flow direction in each cell was computed. The values in the cells of the flow direction grid indicate the direction of the steepest descent from that cell.
- The flow accumulation grid that contains the accumulated number of cells upstream of a cell was calculated for each cell in the input grid.
- The symbology for the created flow accumulation file was selected and the number of classes changed to 2.

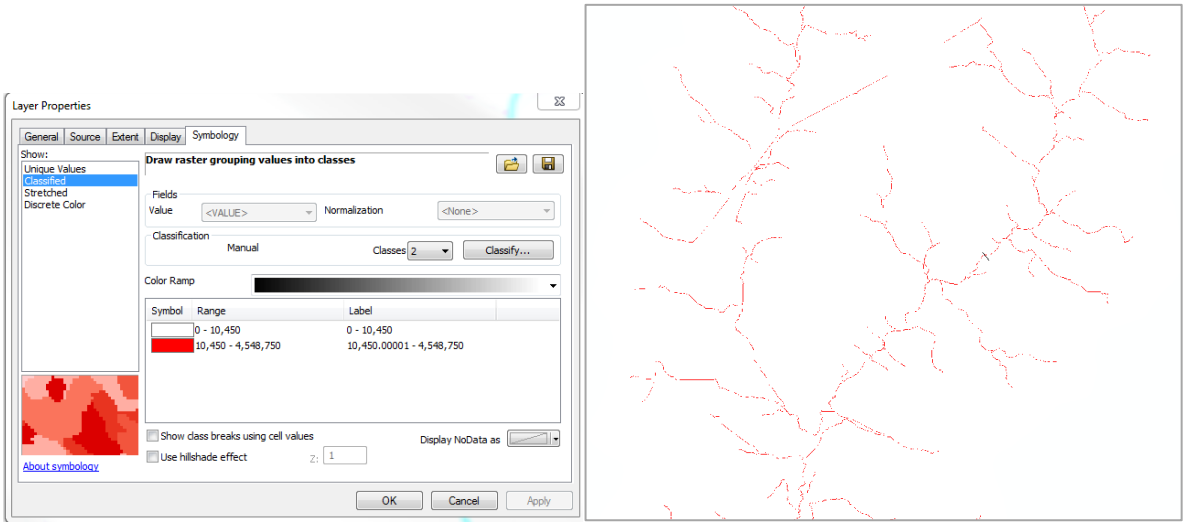

Figure 136. Screenshot of the symbology properties of the stream network grid generated in ArcMap.

- The Raster Calculator was used to create a raster file that has a value of 1 for any pixel >= 10450 and a value of 0 for any pixel below this value.

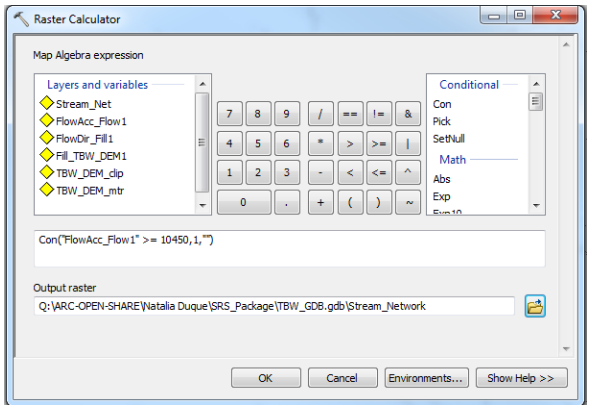

Figure 137. Screenshot of the ArcGIS Raster Calculator.

- The Raster to Polyline tool was used to convert the created file to a line shapefile.
- The resulting file contains all the streams in the network but Tims Branch is divided into small segments, so the Merge tool was used to make Tims Branch one continuous line.

Subtask 3.2: Results and Discussion

The delineated stream network shapefile of the A-014 outfall tributary seen in Figure 114 was generated as described above from data collected by FIU researchers and students at SRS in August 2016. The following images show the point shapefiles of the field sampling sites selected in June 2017 during DOE Fellow Ron Hariprashad's summer internship. Sampling sites were selected along the A-014 tributary and Tims Branch stream based on the ease of accessibility. Specifically, three sites were selected on the A-014 tributary and five were selected on Tims Branch (Table 44).

Table 44. Field Sampling Sites

Location ID	Landmark	Latitude	Longitude	Elevation (m)
Site 1	A-014 outfall	33.28711	-81.69721	
Site 2	A-014/A-011 confluence	33.29205	-81.70107	53
Site 3	Weir, culvert, riprap	33.32485	-81.71822	76
*Site 4	Wetland area above confluence of A-014 and Tims Branch	33.31727	-81.71508	72
Site 5	TIMS04 (SRR sampling site)	33.34035	-81.7177	83
Site 6	Steed Pond	33.33308	-81.73305	112
Site 7	Old train tracks	33.33175	-81.72164	88
Site 8	Old USGS sampling site	33.33186	-81.72732	104

**Site 4 is upstream of the A-014/Tims Branch confluence and is therefore the control site.*

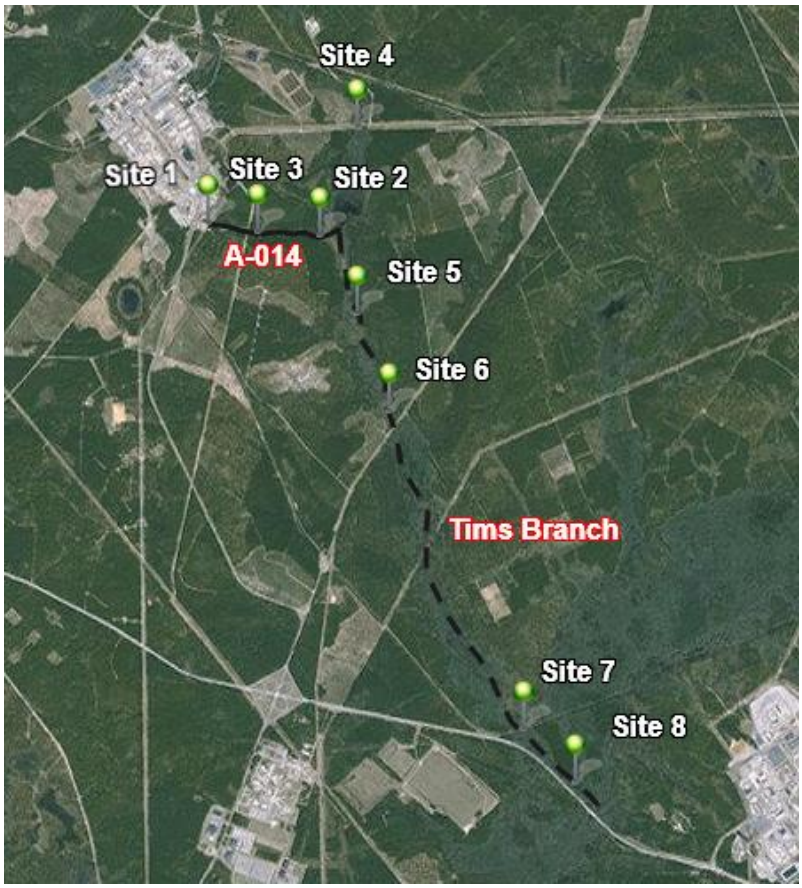

Figure 138. Sampling locations during summer 2017 internship.

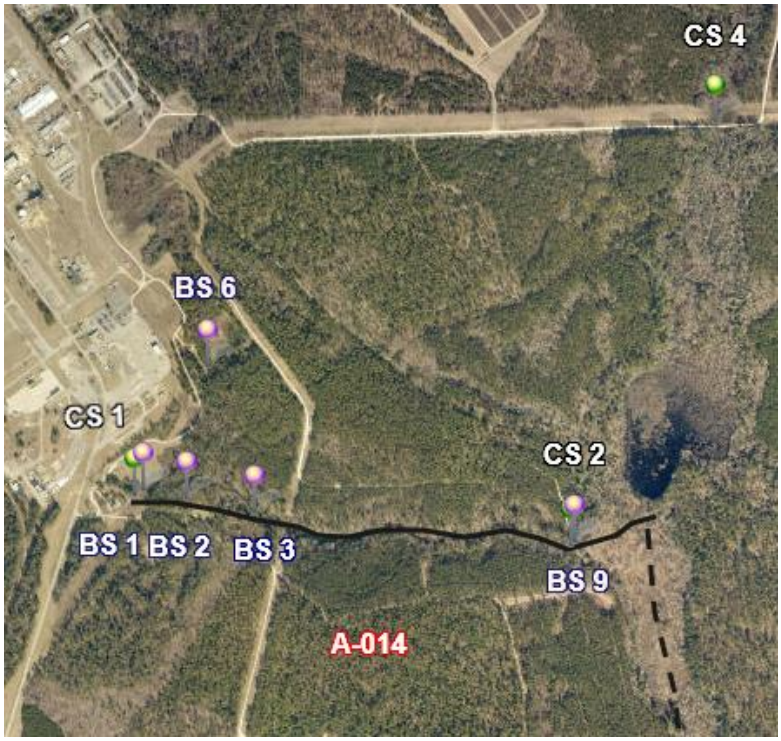

Figure 139. Biofilm sampling locations along A-014 tributary.

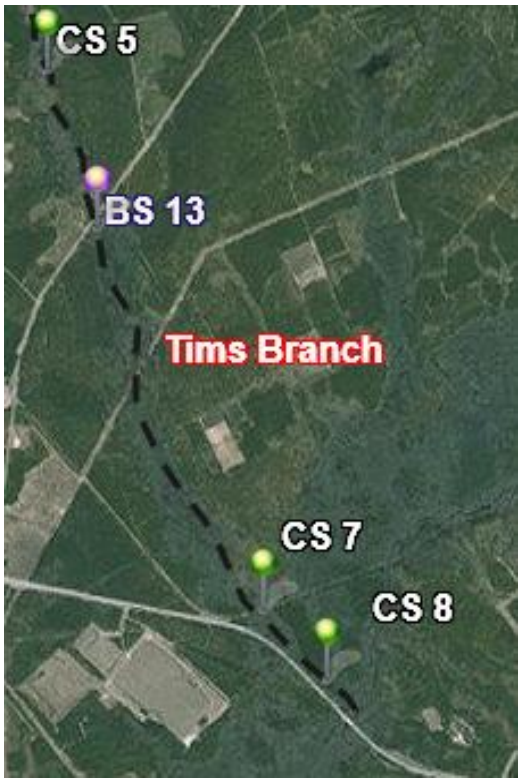

Figure 140. Biofilm sampling locations along Tims Branch.

Subtask 3.2: Conclusion

GIS technology has been continuously utilized throughout the project to support the hydrological model development. ArcGIS tools have significantly reduced the time needed for data preparation. The ArcGIS geodatabase developed by ARC researchers for SRS and the Tims Branch watershed has served as a foundation for management, storage, processing, analysis and visualization of required environmental and hydrological parameters. The SRS hydrologic geodatabase infrastructure enables linkage with other hydrologic modeling tools and applications to model hydrologic systems, and is scalable and replicable for implementation at other DOE sites. FIU graduate and undergraduate DOE Fellow students will continue to be mentored and trained on how to perform geoprocessing tasks, conduct geospatial analyses and generate maps and graphs for reporting purposes.

Subtask 3.3: Biota, Biofilm, Water and Sediment Sampling in Tims Branch Watershed

Subtask 3.3: Introduction

Calibrating a numerical model of stream flow requires real-time data of rainfall and flow velocity/depth. Such data is essential for hydrological model development for calibration and validation as the final steps to maximize model certainty in estimating overland flow depth and velocity over time in an entire watershed. It is also important to collect real-time data as part of post remediation monitoring. Conducting numerical simulations with real-time data will provide a better understanding of the system's response to clean-up activities. Collecting real-time data, however, is one of the most challenging parts of any study as it becomes cumbersome and sometimes impossible due to limited site accessibility. Tims Branch and the A-014 outfall tributary at SRS are examples where collection of field data is challenging due to various field constraints such as physical inaccessibility due to dense vegetation or other environmental conditions, or restricted areas which require site permits and adherence to specific safety protocols before they can be accessed. For this reason, in addition to sampling along Tims Branch and the A-014 outfall tributary, FIU collaborated with researchers at SRNL and SREL to mentor and train an FIU graduate student (DOE Fellow) to deploy a remote monitoring device in Tims Branch during a summer internship at SRS to assist in collecting real-time data which is essential in both model calibration and monitoring water quality and the fate and transport of contaminants in Tims Branch.

Subtask 3.3: Methodology

The first sampling and data collection exercise along Tims Branch and the A-014 outfall tributary was conducted in August 2016 by FIU researchers and graduate students. It consisted of cross section profiling and measurement of flow velocity and water quality. A second field trip was conducted in June 2017. This time, field work consisted of biofilm sampling in addition to the water quality and flow velocity measurements along A-014 and Tims Branch at the same locations where the first set of samples and data were collected. Cross section measurements were also taken along the main Tims Branch stream, particularly in northern portion where no data was previously collected. Cross section, water quality, and flow data collected in June 2017 following the same methodology as previously employed during the August 2016 exercise. Details of the field and laboratory methodologies employed can be found in previous FIU reports to DOE under this DOE-FIU Cooperative Agreement.

Water samples were taken from each site using 125 mL plastic bottles. Volumes of 125 mL were collected so enough sample was available for both an unfiltered and filtered sample. Biofilm samples were collected by gently cutting off parts of vegetation which a thin layer of biofilm covered. It was best to do this in an area where a log or some sort of "dam" laid across the stream, allowing the vegetation and their roots to float in the water. Sampling for biofilm was repeated because the first sampling trip resulted in the prolonged storage of the biofilm samples, making them unviable.

Water quality, flow, and cross-sections measurements were taken at each sampling site to be implemented in the hydrological models. Water quality data was collected at all sites. Flow measurement was not possible at Sites 4 and 5 as the water depth was too shallow to obtain a reading. Cross-sections were taken at each site except Site 4 because Tims Branch became a wetland in this area. All water and biofilm samples were analyzed at SREL and SRNL laboratories under the guidance and supervision of their researchers. Details of the lab procedures can be found in the report written by DOE Fellow, Ron Hariprashad, following his Summer 2017 internship entitled *"In-Situ Data Collection, Sampling, and Water Quality Monitoring in Tims Branch Watershed, Savannah River Site, SC"*.

Subtask 3.3: Results and Discussion

The water samples were analyzed for 15 elements in total. Six were macro-elements (Na-23, Mg-24, Al-27, K-39, Ca-44, and Fe-56) and 9 were microelements (Mn-55, Ni-60, Cu-63, Zn-66, As(2)-75, Cd-111, Pb-208, U-238, As(1)-75.

Sample names with an "A" at the end of the name were filtered samples. The marco-elements showed an increase in their concentration after being filtered. This is common because the concentration before being sampled was so minuscule that the water sample picked up some of the element from the filter's fibers. As an example, Figure 141 shows an increase in Na for each filtered sample except at Site 5, where the concentration decreases from 3.929 ppm to 3.915 ppm. Analysis results of the micro-elements are provided in Table 45.

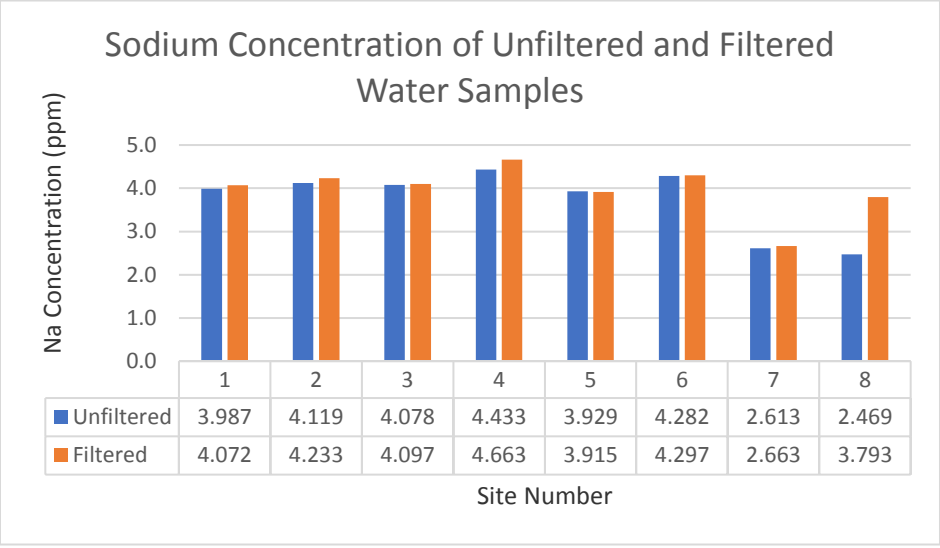

Figure 141. Na concentration in unfiltered and filtered water samples from Tims Branch and A-014 OF tributary.

Table 45. ICP-MS Reading for River Standard and Site Water Samples

Sample ID	Mn 55 (ppb)	Ni 60 (ppb)	Cu 63 (ppb)	Zn 66 (ppb)	As-2 75 (ppb)	Cd 111 (ppb)	Pb 208 (ppb)	U 238 (ppb)	As-1 75 (ppb)
River SRM Reading	40.228	25.750	89.975	59.137	7.748	4.067	13.222	26.492	7.800
River SRM CAV	40.390	25.320	85.750	55.640	8.075	3.992	12.101	25.350	8.075
Error %	0.4%	1.7%	4.7%	5.9%	4.2%	1.8%	8.5%	4.3%	3.5%
1	5.823	0.408	0.168	3.248	0.029	0.003	0.087	0.029	0.028
1A	5.380	0.457	0.088	8.678	0.036	0.008	0.076	-0.013	0.027
2	2.275	0.414	0.304	4.887	0.117	0.001	0.095	0.067	0.109
2A	1.111	0.280	0.166	10.708	0.063	-0.002	0.092	0.000	0.063
3	2.687	0.541	0.356	5.822	0.178	0.021	0.077	0.043	0.162
3A	2.077	0.388	0.200	11.803	0.061	0.034	0.093	-0.006	0.066
4	51.575	1.315	5.124	13.085	1.451	-0.002	0.725	1.893	1.480
4A	11.916	0.969	3.745	12.184	1.133	0.028	0.347	1.006	1.101
5	24.285	8.648	0.854	5.097	0.413	0.023	0.612	19.959	0.413
5A	6.175	3.988	0.315	0.022	0.228	0.008	0.041	2.369	0.223
6	92.966	19.135	0.887	1.517	1.336	0.031	0.301	9.400	1.410
6A	17.303	15.299	0.567	-0.175	0.714	0.021	0.028	4.342	0.680
7	122.218	5.072	0.220	0.701	1.434	0.004	0.227	2.715	1.464
7A	38.107	3.503	0.145	-1.140	0.653	0.009	0.005	0.937	0.648
8	92.612	4.575	0.251	0.986	1.128	0.004	0.217	2.466	1.153
8A	19.862	3.166	0.230	-0.786	0.640	0.038	0.030	0.908	0.668

Heavy metal concentrations in the unfiltered samples collected at various locations followed a similar trend. Following the concentration of U may provide insight into how the microelements are distributed throughout Tims Branch. Along the A-014 outfall tributary, U levels are below 0.1 ppb, possibly because this is a more recently created tributary generated from the outfall of treated groundwater from the M-1 air stripper, and would therefore not likely have received discharge from the A/M area since the 1950s. At the control site, Site 4, 1.893 ppb of U was observed. High levels of U are observed at Sites 5 and 6. At Site 5, 19.959 ppb of U was recorded while 9.400 ppb of U was recorded at Site 6. An unexpected higher U concentration at Site 5, which was almost twice the amount of U as Site 6 (Steed Pond) was detected. One possible explanation is Site 5 could have possibly been included in the ponding of water when the farmer's dam was still standing. Today, Site 5 is a labeled SRR sampling site, labelled TIMS04. Downstream, at Sites 7 and 8, U levels drop to 2.715 ppb and 2.466 ppb, respectively.

Biofilm samples were disaggregated and placed in the XRF sample cups. Of the eight sites visited, only six (Sites 1, 2, 4, 5, 7, and 8) had enough biofilm for drying and analysis. The same Sn standards created by Betancourt (2011) was used to analyze Sn concentration and to create a calibration curve. Sn is an extremely inert element so it was acceptable to use the same standard from six years ago.

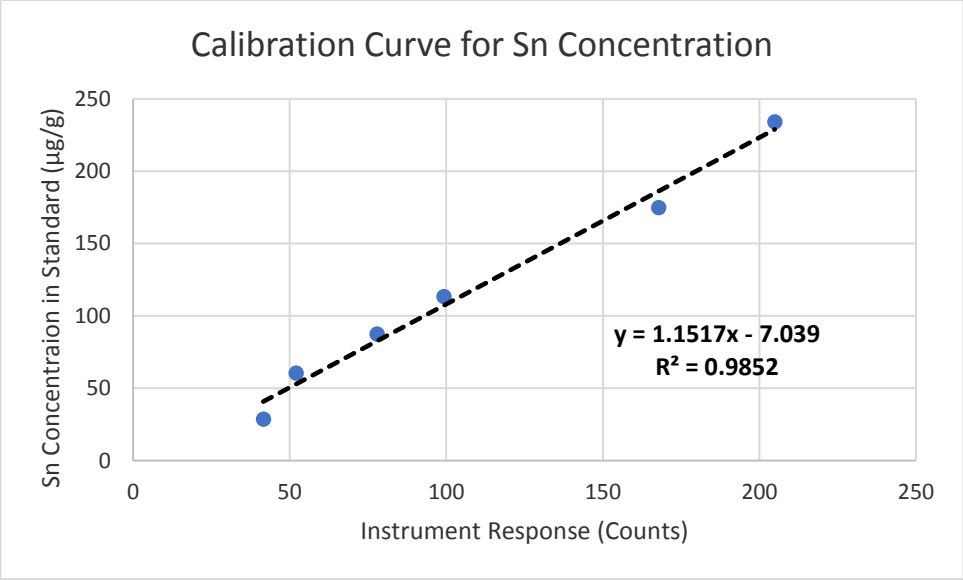

Figure 142. Calibration curve for Sn concentration on XRF

To analyze the Sn accumulation data, it was necessary to correlate our sample locations with Betancourt's sample locations from 2011.

Table 46. Comparison of Tin Concentration in Betancourt (2011) Biofilm Sampling Sites to the Current Sampling Sites

Current Site	Sn Concentration (µg/g)	Distance from A-014 Outfall	Betancourt's Site	Sn Concentration (µg/g)	Distance from A-014 Outfall
1	2,757	5	1	10,640	5
2	49	3,700	2	9,737	20
4*	8		5	2,071	750
5	0	6,700	6*	0	
7	0	23,000	9	585	3,700
8	0	25,700	13	0	10,500

***Control site**

From the data, we can see that the Sn concentrations in the biofilm between 2011 and 2017 have dropped significantly. At the A-014 outfall, Sn decreased 74.1% from 10,640 ppm to 2,756 ppm. At the A-014/A-011 confluence, Sn decreased 91.6%. Along Tims Branch, there was no detection of Sn. It is important to mention that the XRF did report values of 12 ppm for Betancourt's Sites 6 and 13, but this is effectively zero given the accuracy of the device. The Current Sites 5, 7, and 8 gave a reading of "limit of detection", or LOD; effectively zero.

The overall decrease in Sn concentration along A-014 was an unexpected result as it was assumed that the Sn would accumulate or have reached a steady-state concentration after six years. It was also interesting that there was no Sn found in the Tims Branch stream, even just downstream of the A-014/Tims Branch confluence. With the assumption that the Sn would have reached a steady-state concentration along A-014, a mass flux of Sn was expected to have carried over to Tims Branch, which does not appear to have occurred.

Further sampling of water, sediment, and biofilm at additional points along the A-014 OF tributary is required to address the question of where the Sn is fractioning. Another contribution would be results of the ongoing research into nanoparticles and their activity in the environment. The mass flux Sn from the M-1 air stripper is known, as well as the water outflow. This would therefore present an ideal case for further investigation because of the known parameters and the recent data indicating that the Sn is not accumulating in the biofilm.

Subtask 3.3: Conclusion

Cross-section profiles and stream flow data are basic input parameters required when developing a detailed river flow model that can represent the natural system with certainty. Field data collection is an important step in providing accurate data for model development, calibration, and validation.

In the recent field data collection exercise, various data such as flow velocity, depth, and suspended particle concentration were measured in Tims Branch and the A-011 and A-014 outfall tributaries. A total of 20 cross-sections were profiled. The collected water and biofilm samples were prepared and processed in SRNL and SREL laboratories to estimate the micro- and macro-element concentrations, with particular focus on U, tin, and other contaminants of concern. Sn accumulation does not appear to be occurring in biofilm along the A-014 OF tributary or the main Tims Branch stream, which is surprising as Sn is a very inert material and was expected to be bioaccumulating. Further studies on the distribution of Sn in the Tims Branch watershed is necessary, including field studies of nanoparticles in the natural environment. Continuous *in situ* data collection and performing numerical simulations will support the investigatation of the fate and transport of tin-rich sediment during heavy rainfall or storm events.

TASK 3: FUTURE WORK

FIU will continue to support SRS and DOE EM's Office Subsurface Closure goals by conducting a targeted stream-scale study in the Tims Branch ecosystem to monitor the fate and transport of sediment and contaminants in Tims Branch and examine the response of the ecosystem to innovative EM-developed remediation treatment technologies that have eliminated anthropogenic mercury sources from this watershed.

The research under this task will directly support interpretation of historical data on the trends of contaminant concentration distribution in Tims Branch, and support planning and execution of future biota sampling in this important ecosystem, particularly considering the effect of extreme hydrological events on the stream flow and pollutant transport. In addition, the SRS Area Completion Project (ACP) is currently conducting additional characterization projects in Steed Pond to develop final plans for remediation, and this work will assist in developing cost effective remediation plans. This research also fosters collaboration between the students and scientists at FIU and the scientists at the Savannah River National Laboratory and the Savannah River

Ecology Laboratory. Performing simulations of extreme storm events will provide DOE-EM/SRS with information that can assist in: (a) understanding the potential impact on flow depth and velocity in Tims Branch, (b) determining the potential for contaminant transport due to the resuspension and remobilization of sediment during such extreme events, and (c) identifying areas where sediment/contaminants might further be deposited.

During FIU Performance Year 8, the hydrology models developed by FIU in Performance Years 6 & 7 will be fully calibrated and coupled. The software used has provided the flexibility to simulate overland flow and stream flow in either a stand-alone or coupled fashion, which can provide significant results in each case. The main activities will include the following:

- Sensitivity analysis and calibration of the existing MIKE SHE overland flow model.
- Addition of existing man-made hydraulic infrastructures to the existing MIKE 11 stream flow model of the A-014 outfall tributary, followed by sensitivity analysis and calibration of the model.
- Development, sensitivity analysis and calibration of the MIKE 11 stream flow model of the main Tims Branch stream.
- Coupling of the overland flow and stream flow hydrological models and calibration of the coupled flow model.
- Scenario analysis where FIU will implement specific rainfall scenarios in each model to understand the models' behavior under various atmospheric conditions. Atmospheric scenarios will be determined based upon historical rainfall events and data provided by federal/state online databases or data provided by SRNL/SRNS.
- Data analysis and visualization using MIKE and ArcGIS tools.
- FIU, with the support of DOE Fellow graduate students, will begin the literature review and assimilation of data to initiate the development of the solute transport component of the model using MIKE ECO Lab or other solute transport models.
- A draft manuscript will be prepared based on the calibration of the MIKE SHE model of the Tims Branch watershed for submission to a relevant peer reviewed journal.

GIS technology will be continuously utilized throughout the project to support the hydrological model development. Application of GIS technology is a key component in hydrological modeling that helps to prepare data, display results and conduct further spatial analyses. The use of GIS technology has supported the preliminary development of the MIKE SHE and MIKE 11 models. In FIU Performance Year 8, ARC will continue to support hydrological model development with pre- and post-processing of data. GIS tools will support the development of the MIKE SHE/MIKE 11 model for delineation of the stream network and generation of cross-sections and profiles of the major and minor tributaries of Tims Branch. Advanced geospatial analyses will also be conducted for the Tims Branch watershed. FIU graduate and undergraduate students will be mentored and trained on how to update and query the existing geodatabase within the ArcGIS environment, perform geoprocessing tasks, conduct geospatial analyses and generate maps and graphs for reporting purposes.

FIU Performance Year 8, sampling and *in situ* data collection will be continued by FIU students (DOE Fellows) as part of a student summer internship mentored by SRNL/SREL scientists, and any additional/follow-up fieldwork will be conducted by FIU students and FIU ARC researchers in collaboration with SRNL/SREL personnel. FIU's proposed sampling and *in situ* data collection protocol will include establishing long term monitoring station(s) (stage gauge) along

Tims Branch and the A-014 outfall tributary to collect timeseries data including depth of water/discharge, water temperature, pH, turbidity, and suspended particle concentration. FIU also plans to deploy a remote monitoring system in Tims Branch. A HOBO RX3000 Remote Monitoring System was purchased by FIU and will be tested and used to train DOE Fellow students prior to its deployment at SRS. This instrument is a water level data logger which has a web-based configuration so that data is stored and managed via the internet in the HOBOlink service cloud. HOBOlink allows the user to access current and historical data and manage and control the configuration of sensors, logging rates, alarm notifications and relay activations. Other field activities have been proposed which include measurement of flow velocity in at least two locations upstream and downstream of Tims Branch and along A-014 outfall tributary; cross section profiling along the main Tims Branch stream; collection of samples (water, sediment and biofilms) from selected Tims Branch compartments and the A014 outfall tributary; analyzing biota samples for possible contaminant deposit; sediment core sampling and thickness measurement at locations along the A-014 tributary and the main Tims Branch stream as site regulations permit; and laboratory analysis of contaminant concentrations (e.g., mercury, tin and uranium) in bulk water, sediment and biota samples; SEM/EXAFS/XRD analysis of isolated particulates (particle size and morphology, mineralogy and element concentration/distribution). *In situ* field data will be used for model validation and to assess the Tims Branch ecosystem response (cleanup progress) to the implemented tin-based remediation technology.

TASK 3: ACKNOWLEDGEMENTS

Funding for this research was provided by U.S. DOE Cooperative Agreement DE-EM0000598. We would like to acknowledge and thank Dr. Brian Looney from SRNL and Dr. John Seaman from SREL for their input and consistent support and we look forward to and value their continued participation.

TASK 3: REFERENCES

http://websoilsurvey.sc.egov.usda.gov/App/WebSoilSurvey.aspx
http://oceanservice.noaa.gov/facts/lclu.html

Batson, V. L., Bertsch, P., and Herbert, B., 1996, Transport of anthropogenic uranium from sediments to surface waters during episodic storm events: Journal of Environmental Quality, v. 25, no. 5, p. 1129-1137.

Betancourt, A. (2011). Tin Distribution and Fate in Tims Branch at the Savannah River Site.

Christiaens, K., and Feyen, J., 2002, Use of sensitivity and uncertainty measures in distributed hydrological modeling with an application to the MIKE SHE model: Water Resources Research, v. 38, no. 9, p. 8-15.

Hariprashad, R. (2017). In-Situ Data Collection, Sampling, and Water Quality Monitoring in Tims Branch Watershed, Savannah River Site, SC.

Hayes, D., 1984, Uranium studies in the Tims Branch and Steed Pond system: Westinghouse Savannah River Co., Aiken, SC (United States).

Looney, B., Jackson, D., Peterson, M., Mathews, T., Southworth, G., Paller, M., Bryan, L., Eddy-Dilek, C., and Halverson, N., 2010, Assessing Potential Impacts of Stannous Chloride Based Mercury Treatment on a Receiving Stream Using Real-World Data from Tims Branch, Savannah River Site: SRS.

Mast, M. A., and Turk, J. T., 1999, Environmental characteristics and water quality of hydrologic benchmark network stations in the midwestern United States, 1963-95, US Geological Survey.

Rogers, C., Beven, K., Morris, E., and Anderson, M., 1985, Sensitivity analysis, calibration and predictive uncertainty of the Institute of Hydrology Distributed Model: Journal of Hydrology, v. 81, p. 179-191.

Varlik, B., 2013, Total Maximum Daily Load Document Tims Branch SV-324 and Upper Three Runs SV-325 Hydrologic Unit Codes 030601060501, 030601060502, 030601060503, 030601060504, 030601060505, 30601060506.

Wijesekara, G., Farjad, B., Gupta, A., Qiao, Y., Delaney, P., and Marceau, D., 2014, A Comprehensive Land-Use/Hydrological Modeling System for Scenario Simulations in the Elbow River Watershed, Alberta, Canada: Environmental Management, v. 53, no. 2, p. 357-381.

Xevi, E., Christiaens, K., Espino, A., Sewnandan, W., Mallants, D., Sorensen, H., and Feyen, J., 1997, Calibration, Validation and Sensitivity Analysis of the MIKE-SHE Model Using the Neuenkirchen Catchment as Case Study: Water Resources Management, v. 11, no. 3, p. 219-242.

TASK 5: REMEDIATION RESEARCH AND TECHNICAL SUPPORT FOR THE WASTE ISOLATION PILOT PLANT

TASK 5: EXECUTIVE SUMMARY

The following task is a collaboration begun in spring 2016 with Los Alamos National Laboratory's field office at the Carlsbad Environmental Monitoring and Research Center (LANL CEMRC) which is a part of New Mexico State University. The goal is to generate accurate sorption data for the trivalent actinides to minerals and under conditions relevant to the Waste Isolation Pilot Plant (WIPP) as previous risk assessment models are based on conservative assumptions. This task produced three oral presentations at national conferences and seven poster presentations during FIU Performance Year 7 (listed below). Notably, DOE Fellow Frances Zengotita received 3rd place for her poster presentation at the McNair conference and was competitively selected to become an FIU McNair Fellow based on her research proposal to continue this work. A progress report was also submitted in May 2017. In addition, DOE Fellow Zengotita spent ten weeks as an intern at LANL CEMRC and began a new project investigating the impact of bacteria on the transport of relevant radionuclides to the WIPP.

Oral Presentations between October 2016 and October 2017 (presenter is underlined):

The Role of Chromohalobacter on Transport of Lanthanides and Cesium in the Dolomite Mineral System, Frances E. Zengotita, Timothy M. Dittrich, Hilary P. Emerson, Michael P. Dugas, Juliet S. Swanson, and Donald T. Reed, FIU McNair Scholars Research Conference, Miami, FL, Oct. 19-20, 2017.

The Role of Ionic Strength on Sorption of Neodymium on Dolomite, Hilary P. Emerson, Timothy Dittrich, Frances Zengotita, Yelena Katsenovich, and Donald Reed, ABC Salt V Workshop, Ruidoso, NM, Mar. 24-26, 2017.

Role of Brine Chemistry and Geologic Sorption on Potential Long-Term Storage of Radioactive Waste: Experimental Evaluation of Sorption Parameters, Timothy M. Dittrich, Hilary P. Emerson, Michael P. Dugas, and Donald T. Reed, American Geophysical Union, San Francisco, CA, Dec. 16, 2016.

Poster Presentations between October 2016 and October 2017 (presenter is underlined):

The Role of Chromohalobacter on Transport of Lanthanides and Cesium in the Dolomite Mineral System, Frances E. Zengotita, Timothy M. Dittrich, Hilary P. Emerson, Michael P. Dugas, Juliet S. Swanson, and Donald T. Reed, FIU McNair Scholars Research Conference, Miami, FL, Oct. 19-20, 2017. (3rd Place Poster Award)

The Role of Ionic Strength on Sorption of Neodymium on Dolomite, Hilary P. Emerson, Frances Zengotita, Timothy Dittrich, Yelena Katsenovich and Don Reed, ACS 254th National Meeting, Washington D.C., Aug. 20-24, 2017.

Long-term Disposal of Radioactive Waste at the Waste Isolation Pilot Plant near Carlsbad, NM, Hilary P. Emerson and Frances Zengotita, Miami March for Science, Miami, FL, Apr. 22, 2017.

Role of Ionic Strength on Sorption of Neodymium on Dolomite, Frances Zengotita and Hilary P. Emerson, Life Sciences South Florida STEM, West Palm Beach, FL, Apr. 1, 2017.

Evaluating Potential Environmental Transport of Actinides from the Waste Isolation Pilot Plant, Timothy M. Dittrich, Hilary P. Emerson, Michael P. Dugas, and Donald T. Reed, ABC Salt V Workshop, Ruidoso, NM, Mar. 24-26, 2017.

Role of Ionic Strength on Sorption of Neodymium on Dolomite, Frances Zengotita and Hilary P. Emerson, Waste Management Symposia, Phoenix, AZ, Mar. 8, 2017.

Role of Ionic Strength on Sorption of Neodymium on Dolomite, Frances Zengotita and Hilary P. Emerson, FIU McNair Scholars Research Conference, Miami, FL, Oct. 19-21, 2016.

TASK 5: RESULTS AND DISCUSSION

Because a peer-reviewed publication is in process for this work, the full results will be attached as a separate appendix (Appendix B). These data highlight that the adsorption and incorporation processes of Nd to dolomite are complex. Results show that the kinetics of removal of Nd increase with increasing ionic strength (up to 5.0 M) with greater removal at greater ionic strength at 24 hours. However, at equilibrium (greater than 5 days of exposure to dolomite), similar removal is observed at variable ionic strength and confirmed by sequential additions in batch experiments. Moreover, column saturation experiments show similar breakthrough curves at 0.1 and 5.0 M ionic strength. The working hypothesis is that adsorption processes are not affected by ionic strength due to the strong chemisorption of Nd to the dolomite surface. However, incorporation processes may play a greater role with increasing ionic strength due to greater dissolution and re-precipitation caused by changes in activity with ionic strength but are not influencing column data due to the short retention time of approximately 17.5 minutes.

TASK 5: FUTURE WORK

FIU Performance Year 8 will focus on understanding ternary interactions of the trivalent and hexavalent oxidation states (Am, U, and lanthanide analogs) with relevant minerals in the presence of relevant ligands including but not limited to oxalate, EDTA, and isosaccharinic acid. These experiments are expected to significantly reduce the uncertainty in the partitioning coefficients for the actinides in the presence of dolomite under WIPP relevant conditions. There is synergy with this proposed work with our LANL collaborators through current and future studies by Reed and Yalcintas investigating redox chemistry (including radiolysis effects) and complexation of uranium in the presence of EDTA and carbonate in the absence of minerals. In addition, ongoing research by Swanson and Reed will benefit from these results as microbial communities may be impacted by and be capable of influencing the formation and degradation of cellulose degradation products like isosaccharinic acid.

TASK 5: ACKNOWLEDGEMENTS

Funding for this research was provided by U.S. DOE Cooperative Agreement DE-EM0000598. We truly appreciate Drs. Tim Dittrich, Juliet Swanson, and Don Reed for their invaluable feedback in the design of these experiments and the time given to training and hosting Hilary Emerson and Frances Zengotita as visiting scientists.

APPENDICES

The following documents are included in this report as separate attachments:

Appendix A: Florida International University, *Uranium immobilization in the presence of minerals following remediation via base treatment with ammonia gas*, draft publication for task 1.1, 2017.

Appendix B: Florida International University, *Mobility of neodymium at variable ionic strength in the presence of dolomite*, draft publication for task 5, 2017.